A Diagnostic Suite of Models for the Evaluation of Oceanic Mesoscale Eddy Parameterizations

by

S. D. Bachman

B.S., California State University, Long Beach, 2006

M.S., University of Colorado, 2008

M.S., University of Colorado, 2011

A thesis submitted to the

Faculty of the Graduate School of the

University of Colorado in partial fulfillment

of the requirements for the degree of

Doctor of Philosophy

Department of Atmospheric & Oceanic Sciences

2012

This thesis entitled:
A Diagnostic Suite of Models for the Evaluation of Oceanic Mesoscale Eddy Parameterizations
written by S. D. Bachman
has been approved for the Department of Atmospheric & Oceanic Sciences

Baylor Fox-Kemper

Dr. Frank Bryan

Date

The final copy of this thesis has been examined by the signatories, and we find that both the content and the form meet acceptable presentation standards of scholarly work in the above mentioned discipline.

Bachman, S. D. (Ph.D., Atmospheric and Oceanic Sciences)

A Diagnostic Suite of Models for the Evaluation of Oceanic Mesoscale Eddy Parameterizations

Thesis directed by Dr. Baylor Fox-Kemper

The practice of modeling geophysical fluid flows has grown tremendously in concert with recent advances in computing power. To study the climate models must simulate centuries of real time, a difficulty made worse by the need to capture fine-scale (eddy) activity. Turbulence at scales ranging from 10 km to 250 km, whose coherent structures are colloquially referred to as mesoscale eddies, is of particular interest because of its ability to transport and mix water masses, and because it dominates the oceanic kinetic energy budget. As of the writing of this dissertation, it also happens to represent the cutting edge in OGCM resolution, hence the need for skillful parameterizations. Calibration and evaluation of such parameterizations is the focus of this work.

An "eddy parameterization challenge suite" is being developed, consisting of a set of high-resolution tracer experiments designed to assist in parameterizing subgridscale processes in ocean models. In each experiment, multiple tracers are initialized in a frontal spindown simulation designed to mimic the stirring effect of mesoscale eddies. Diagnosis of an eddy transport tensor is performed by inverting a matrix of passive tracer gradients, each of which is assumed to satisfy an identical linear flux-gradient relationship. Aspects of the matrix inversion are explored, including the implications of overdetermining the linear relationship using a large number of tracers.

Two sets of simulations, featuring Eady-like and exponential stratification, allow us to investigate scaling laws and vertical structures of the eddy transport tensor. The diagnosed tensor reproduces the horizontal transport of an active tracer (buoyancy) to within $\pm 7\%$ and the vertical transport to within $\pm 12\%$. The derived scalings are shown to be close in form to the Gent and McWilliams (1990) and Redi (1982) diffusivity tensors, with a magnitude that varies in space and time. The parameterization suite is also used to evaluate an extant scheme (Ferrari et al., 2010) and to recommend improvements. We also attempt a local scaling for the along-isopycnal diffusiv-

ity and argue that it is unlikely that any such scaling can be written as a simple function of the velocity, stratification, or eddy variances.

Dedication

To my amazing wife, Marysia!

Acknowledgements

I was funded by NSF OCE 0825614 and the CIRES Graduate Student Fellowship during the course of my dissertation. I thank both agencies for their support.

First and foremost, thanks to my wife Marysia for always being supportive of me, even on those nights when I had to work late and I couldn't watch Law and Order with her. She is the best thing that ever happened in my life.

Thanks to my parents for always doing the best they could to raise me right. I hope that this dissertation makes them proud.

Thanks to my committee, for their advice, support, and for putting me through the crucible that is all of these exams. I am a better scholar because of it.

Finally, a special thanks to my advisor, Baylor Fox-Kemper, without whom this dissertation definitely would not have been possible. I could not have asked for a better advisor, mentor, colleague, and friend to help me through this.

Contents

Chapter

Tables

Table

Figures

Figure

Chapter 1

Introduction

1.1 Preliminaries

The completeness of modeling geophysical fluid flows has grown tremendously in concert with recent advances in computing power, and with this growth has come a cultural shift in the way oceanographers view the future of their field. There is now widespread acceptance that the results from a physically sound, properly calibrated numerical model can approximate observed oceanic flows quite well, and can supplement our understanding of ocean dynamics just as observational studies can. Modeling also supports the development of new analytic or diagnostic methods through evaluation by idealized models, which are far quicker and cheaper to implement than a typical research cruise. Models also helps the broader earth science community to account for the role of the ocean for problems of anthropogenic climate change and environmental impact (McWilliams, 1996).

The unfortunate paradox of oceanic general circulation models (OGCM's) is that, despite being improved substantially by advances in computing power, they are also limited by computing power. This is of course true for numerical modeling in general regardless of scientific discipline, but is a particularly onerous problem in this field. To study the climate models must simulate centuries of real time, a difficulty made worse by the need to retain fine-scale (eddy) activity in the model for accuracy reasons (Killworth, 1997). It immediately becomes apparent that some concessions must be made with regard to either spatial resolution or simulation time[1] in order to

[1] Simulation time is most often regarded as an invariant in this context for two reasons: 1) the timestep of

make such studies feasible at all.

The problem with coarse spatial resolution is that fully turbulent flow, as is found in the ocean, contains important structures and energy at scales far below what is feasible to resolve. This is the root of the so-called "turbulence closure problem", which has received extensive treatment (Mellor and Yamada, 1974, 1977, 1982) and continues to be an area of ongoing research[2] . In ocean modeling, "closing" the turbulence problem has traditionally been reduced to "parameterizing" the turbulent processes not resolved at the gridscale. The list of spatial regimes that the turbulence parameterization problem spans (the mesoscale, submesoscale, and so on down to the turbulent microscale) is expansive, with each regime certainly deserving of its own body of literature. The problem is even more complicated due to the fact that there is no abrupt scale separation between these regimes - they smoothly transition into each other, as do the energy and turbulent structures found within.

The body of literature devoted to the study of turbulence could fill a library by itself. Fortunately, the problem at hand is not to do something as bold as to solve the closure problem or to prove that the three-dimensional Navier-Stokes equations have a solution. The task here will be to analyze one particular type of turbulence, and to make progress toward properly parameterizing that turbulence in a numerical model. Therefore, for the sake of this thesis, we will focus entirely on the study of oceanic **mesoscale** turbulence. The motivation for this task is rather simple: the mesoscale contains the majority of the oceanic kinetic energy, and is not directly resolved by the state-of-the-art general circulation models we use in climate simulations. Because it is also the eddying regime with the largest spatial scale, it is a logical candidate for a parameterization study.

The parameterization of mesoscale eddies is yet in its infancy (Ferrari et al., 2008), though much theoretical and observational progress has been made in recent years (see Griffies et al. (2000) for an excellent overview of the state of ocean modelling). However, because collecting observations

fluid models can only be manipulated to a limited degree because of numerical stability, and 2) total simulation time is usually constrained by the timescales of the relevant dynamics, and cannot be reduced without changing the model physics. Because of these limitations, the spatial resolution is usually sacrificed in the name of computational feasibility.

[2] Perhaps indefinitely!

with which to compare and evaluate parameterizations is so expensive, we do not have a strong sense on how well our parameterization schemes are improving our models outside of a few numerical studies (e.g., Danabasoglu and McWilliams, 1995; Danabasoglu and Marshall, 2007; Eden et al., 2009). For this reason, a large, organized modeling study would go a long way towards refining our existing parameterizations as well as offering improvements for the next generation of schemes. This thesis describes such a study, including the methods, components, and theoretical considerations that have gone into building the models therein. These models comprise what we refer to as an "eddy parameterization challenge suite", which we will refer to continuously throughout this thesis.

In the following introductory sections, we begin by reviewing the phenomenology of mesoscale turbulence. We discuss the conditions that generate baroclinic instability and how this basic instability grows into fully nonlinear turbulence. We also review some common eddy parameterizations that populate OGCM's today, and explore the theory and physical intuition that led to their creation. In chapter 2, we discuss the matrix pseudoinversion technique that makes this research possible. Many incremental refinements were made to this technique over the course of this research, the consequences of which are also discussed here. Chapter 3 contains results from the first major component of the challenge suite, which consists of a set of models inspired by the work of Eady (1949). Chapter 4 discusses the second component of the challenge suite, consisting of a set of models inspired by Charney (1947) which allow us a much more detailed and rigorous evaluation of the parameterizations from Chapter 1. Finally, in the conclusion we discuss implications of our results for OGCM's and look to the future at the last set of models which will complete the challenge suite.

1.1.1 The Role of Mesoscale Eddies

The oceanic mesoscale corresponds to spatial scales ranging from 10 km to 250 km, over which turbulent motion typically dominates the mean circulation. Observations reveal that the eddy kinetic energy in the mesoscale can be up to 250 times that of the mean kinetic energy (Wyrtki et al., 1976; Stammer, 1997; Henning and Vallis, 2004; Grooms et al., 2011). Turbulence

at these scales, whose coherent structures are colloquially referred to as "mesoscale eddies", is of interest because of its ability to transport and mix water masses, and also because it strongly feeds back upon the general circulation and mean flow of the ocean (Stammer, 1998). Early studies of eddy effects focused largely on such interaction between eddy and mean (Rhines and Holland, 1979, 1980; Rhines and Young, 1982**b**). In the years since, many more specific examples have emerged about how eddies play a leading-order role in setting the general characteristics of the ocean circulation.

Eddy mixing has a strong effect on the ventilation rate and turnover time of water masses in the interior of the ocean, and thus affects the rate at which deep water is exposed to the atmosphere. The mixing of waters within and throughout the ocean is a strong control on the Earth's climate because it has a direct effect on the poleward transport of heat and carbon (Bryan, 1987, 1991; Gnanadesikan et al., 2003). Beyond the mixing and transport of water masses, mesoscale eddies play a central role in maintaining the vertical distribution of heat in the oceanic interior (Karsten et al., 2002; Marshall et al., 2002; Radko and Marshall, 2004), particularly in the thermocline (Henning and Vallis, 2004; Stammer et al., 2006; Greatbatch et al., 2007). Eddies have also been shown to exert a strong feedback effect in western boundary currents (Fox-Kemper, 2004; Fox-Kemper and Ferrari, 2009; Grooms et al., 2011) as well as in the ocean gyres themselves (Scott and Straub, 1998; Berloff and McWilliams, 1999; Fox-Kemper and Pedlosky, 2004**a**; Fox-Kemper, 2005).

Ship observations dating back to the early 1970s (Gill et al., 1974) and more recent global high-resolution satellite altimetry (Stammer, 1997; Stammer et al., 2006) have shown that mesoscale eddies are driven by baroclinic instability, and that the regions of strongest eddy activity coincide are also those featuring steep isopycnal gradients. As such, mesoscale eddy effects contribute importantly to the distribution of heat, salt, and passive tracers anywhere there exist strongly tilted isopycnal surfaces, such as western boundary currents and the Antarctic Circumpolar Current (ACC), and thus are crucial to determining the climate state (Shuckburgh et al., 2009).

The Southern Ocean in particular exhibits strong eddy activity due to the strong southward

tilting of isopycnals due to the thermal wind effect. This region is also unique in that most isopycnals from the ocean interior outcrop here. Eddies are thought to be of first-order importance with regard to the total poleward heat transport (de Szoeke and Levine, 1981; Nowlin Jr. and Klinck, 1986; Gordon and Owens, 1987; Gille, 2003), and their transport dominates the southern high-latitude heat budget (Stammer, 1998; Wunsch, 1999; Lee and Nurser, 2006; Gille et al., 2007). Furthermore, it has been shown that eddies affect not only the heat transport across the ACC, but also the overturning of the ACC itself (Johnson and Bryden, 1989; Henning and Vallis, 2005; Radko and Marshall, 2006) and its response to changes in wind stress (Hallberg and Gnanadesikan, 2006).

1.1.2 Baroclinic Instability

The problem of parameterizing turbulence is keyed to the fact that energy exists in a continuous spectrum all the way from the planetary scale down to the viscous scale. The scale-to-scale transfer of energy is nonlinear and nonlocal, meaning that a turbulence parameterization must attempt to represent activity within an entire **band** of spectral space. For a mesoscale parameterization, that band will correspond with the set of wavelengths ranging from 10 km to 250 km.

Insight is gained by considering the **physics** of mesoscale eddies; that is, the various forces that both drive and characterize the turbulence itself. Mesoscale eddies grow partly through the phenomenon of baroclinic instability, which grows entirely from the available potential energy of the basic horizontal gradients of buoyancy (Bretherton, 1966**a**). The simplest scenario for baroclinic instability was developed by Eady (1949) for a flow with constant buoyancy frequency and constant vertical shear[3] . However, the physical interpretation of baroclinic instability has evolved in the years since Eady's seminal paper. A wonderful description of the mechanism of baroclinic instability is discussed in Cushman-Roisin and Beckers (2011), from which the key points are discussed next.

[3] The resulting flow model, aptly named the "Eady model", is described in detail in detail in Appendix C.2. Another model of baroclinic instability from the same era was developed by Charney (1947), which inspires the model in Appendix C.3.

Mesoscale eddies fall into a broader category of turbulence known as "geostrophic eddies" because their horizontal scale is large enough that the flow within the eddy is in geostrophic balance. Given a sufficiently stratified fluid[4] , it is also appropriate to use the hydrostatic approximation in lieu of the full vertical momentum equation. Thus consider a base state using combined geostrophy and hydrostasy, so that the fluid is in thermal wind balance. Such a base state satisfies the relation

$$f \times \frac{\partial \mathbf{u}}{\partial z} = \nabla_h b, \tag{1.1}$$

where f is the Coriolis parameter, $\mathbf{u}$ is the horizontal velocity, and b is the buoyancy. This equation implies that, for a flow featuring a meridional temperature gradient[5] , a zonal flow will be established that induces sufficient Coriolis acceleration to balance the temperature gradient and maintain a **sloping** isopycnal profile. We then will have a situation where warmer (less dense) fluid and colder (denser) fluid exist at the same vertical level, which is not a state of least energy. Such a state would imply that the warmer fluid rests above the colder fluid. It would also reduce the kinetic energy of the system since the horizontal pressure gradient would be relaxed, which would require a slower geostrophic velocity. Then the state of least energy would be one with minimum combined kinetic and potential energy, and if we are to believe that all natural systems tend toward such a state, then there should exist a mechanism by which the fluid can restratify itself.[6]

Restratification toward a state of rest requires that the potential vorticity of the system be altered locally; that is, a fluid column must either be vertically stretched or squeezed to accommodate the tilting of isopycnal surfaces toward the horizontal. On an f-plane, this can be achieved through modification of relative vorticity alone[7] .

Consider the same idealized system discussed above with two layers, where thermal wind balance maintains an isopycnal surface (which we will call the "front") sloping upwards in the positive y-direction. The geostrophic velocity U that establishes this balance is directed along

[4] See Griffies (2004) for details.

[5] This is certainly a realistic scenario given the natural gradient of temperature existing from equator to the poles.

[6] By "restratify" we mean moving lighter water over denser water, reducing the potential energy of the system.

[7] In a quasigeostrophic system with $\beta = 0$, such a situation can only occur through wave instability with horizontal scale larger than the first baroclinic deformation radius. When $\beta \neq 0$, no such lower bound exists and the potential vorticity can be altered by waves at arbitrarily large wavenumber.

the front in the positive x-direction. Now suppose a meridional, cross-flow perturbation such that two parcels of fluid swap places along the sloping density surface. A graphical depiction of this displacement is shown in the boxes in Figure 1.1. For Parcel 1, whose initial position was at lower y, its fluid column in the lower layer is stretched and its column in the upper layer is squeezed. The corresponding relative vorticity for these columns becomes more cyclonic for the lower layer and more anti-cyclonic for the upper layer. For Parcel 2, whose initial position was at larger y, its fluid column in the lower layer is squeezed and its column in the upper layer is stretched. The corresponding relative vorticity for these columns becomes more anticyclonic for the lower layer and more cyclonic for the upper layer. This displacement has thus created a series of interacting vortices; these have the potential to **reinforce** the initial displacement and to coalesce into fully-developed turbulence.

Here it is appropriate to refer back to the previous statement that baroclinic instability grows entirely from the potential energy of the horizontal temperature gradient. By this we mean that a slight relaxation of the density interface serves to reduce the potential energy of the system by moving some of the denser fluid lower and simultaneously raising the warmer fluid. Conservation of energy requires that this liberated potential energy be converted to either kinetic energy or to internal energy through viscous dissipation[8] . The growth of kinetic energy by the displacement above also corresponds to the generation of vortices through the aforementioned modification of relative vorticity. Thus, the cumulative effect of this perturbation is threefold: the density surface is lowered, the strength of the motion is enhanced, and the vortices grow. The conditions have now been created for growth of turbulence by the action of the vortices pushing the density surface more and more toward the horizontal.

In the idealized situation described above, the density interface is not rigid; the displacement will cause a small deflection of the density surface. For Parcel 1, the interface will deflect in such a way as to relieve some of the upper-squeezing and lower-stretching, which corresponds to a

[8] We will ignore friction due to the large temporal and spatial scale separation between the growth of baroclinic waves and the dissipation by viscosity. Simply put, viscosity acts too slowly and at too small of scales to matter here.

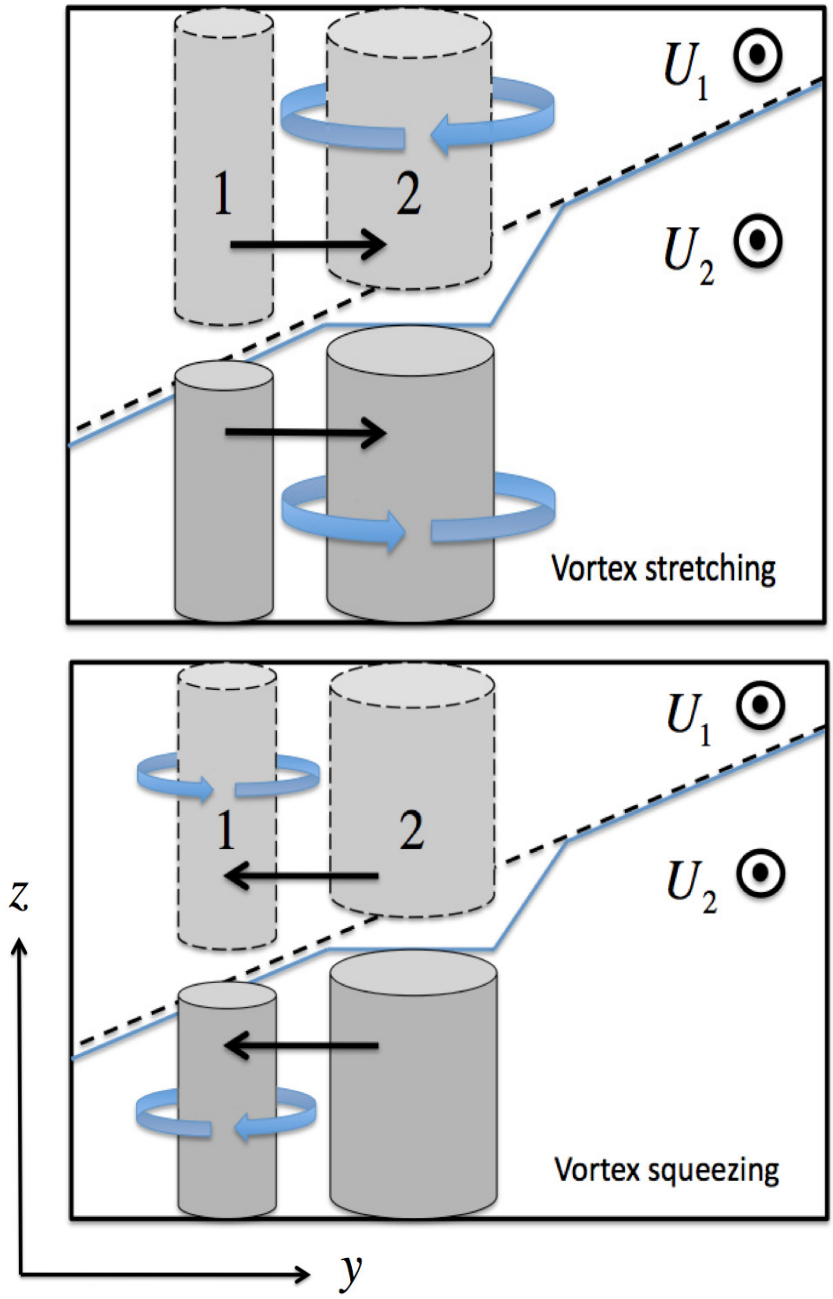

Figure 1.1: Depiction of a parcel displacement leading to baroclinic instability. a) The displacement of Parcel 1 in the positive y-direction creates vortex stretching in the lower layer, while it creates vortex squeezing the upper layer. b) The displacement of Parcel 2 creates the reverse situation - vortex stretching in the upper layer and vortex squeezing in the lower layer. The flexibility of the density interface causes some of this stretching and squeezing to be shared between the layers for each displacement. The net result is a system of interacting vortices which can mutually reinforce each other to create growing baroclinic instability.

lowering of the density interface in the direction of greater y . For Parcel 2, the deflection relieves some of the upper-stretching and lower-squeezing, **raising** the density interface in the direction of smaller y. Thus in **both** locations we have reduced the potential energy of the system by sliding some of the denser water underneath the lighter water.

Thus far we have established a basic description of the three major effects that occur with a simple fluid parcel displacement in this system. Now we shall illustrate under what conditions this simple displacement can grow and manifest into fully-turbulent flow, which we define to be a state where the nonlinear terms play an $\mathcal{O}(1)$ role in the next order after thermal wind balance.

Consider the same style of displacement along the frontal interface, where we swap the y positions of fluid parcels, except now suppose the displacement is somewhat periodic (so that we are swapping a series of fluid parcels lined up in the x direction instead of just a pair of them). This case sets up a series of alternating columns of cyclonic and anticyclonic vorticity due to the stretching and squeezing of each fluid parcel pair. The rotation induced by these alternating vorticities forces the fluid parcels lying **between** each column to move in a cross-frontal direction, leading them to be displaced in y as well. As a result, the perturbation becomes translated from the original fluid columns to the new positions which were originally between the columns. The net result of this scenario in the upper layer is a propagating Rossby wave moving in the along-front direction against the thermal wind. The net result of the same scenario in the lower layer is a Rossby wave moving with the thermal wind.

The respective phases of these waves will ultimately determine whether the disturbance grows or decays. The simplest scenario for the growth of the disturbance is when the waves in the upper and lower layers are in quadrature with each other, such that one of the waves is shifted in the direction of the mean flow for its layer. The vortical motion of the two layers will then reinforce each other, increasing the displacements in both layers simultaneously.

Further treatment of this phenomenon appears in Chapter 17 of Cushman-Roisin and Beckers (2011), who points out extra requirements on the Rossby wavelength and phase speed in order for the disturbance to be amplified. The reader is encouraged to consult that text for further details.

For this text, we close this section by remarking that mesoscale eddies are the fully-turbulent vortical structures that arise as the end result of the baroclinic instability process. Much of the work that has been written about mesoscale eddies assumes that the baroclinic waves are still linear (or equivalently, have infinitesimally small amplitude). Making this assumption allows one to linearize the governing equations and substitute a wave-like solution, from which growth rates and timescales can be inferred[9] However, by the time that the baroclinic waves grow to the point of manifesting as turbulence, the governing equations become fully nonlinear and much of the extant literature on the subject no longer applies. The focus of this dissertation, however, is on presenting and utilizing a diagnostic method for evaluating mesoscale eddy fluxes that applies even in the nonlinear regime.

In summary, the most concise description of baroclinic instability is that it is a shear instability associated with counter-propagating Rossby waves (Held, 1999). It is at this point where we jump off the subject of baroclinic instability and move into the topic of parameterizing eddies. Even though we will be considering nonlinear turbulence, baroclinic instability remains important because it informs us about how to set up the flow model in terms of grid spacing and simulation time. We will also keep the lessons from this section in mind because it is imperative that we know about the physics driving the turbulence. In fact, the most successful mesoscale eddy parameterizations to date have been built by acknowledging that baroclinic instability is the precursor to mesoscale turbulence. For now, though, we have the basic physical picture established, and we can now discuss the customary mathematical approaches to eddy parameterization.

1.2 Equations of Motion

A first step towards mathematical treatment of eddy fluxes is to describe the equation set appropriate for the analysis. The most important consideration in this regard is the scale of turbulence that one wishes to discuss - this will inform the appropriate reduction from the full

[9] The mathematical treatment for two flow models used in this research, the Eady and exponentially-stratified models, appears in Appendix C.

rotating Navier-Stokes equations down to the equation set to be used. Essentially this amounts to a scaling exercise, in that terms deemed to be unimportant[10] to the equation balance are discarded, yielding a simpler set of equations to work with.

Before we go further into the particulars of eddy-mean decomposition, we will start by presenting the basic equation set governing the motion. We now introduce the Boussinesq, hydrostatic primitive equations, a discrete version of which is solved in the numerical model used for this research. The reduction from the full Navier-Stokes equations down to the Boussinesq, hydrostatic form is motivated in detail in Chapter 2 of Vallis (2006). The most pertinent parts to this research are desribed below.

We will begin this discussion with the Navier-Stokes Equations on an f-plane using z-coordinates. For the analysis ahead we will consider this equation set to be "truth", from which all of our approximations will be sourced:

$$\frac{D\vec{\mathbf{v}}_h}{Dt} + f_0\hat{\mathbf{k}} \times \vec{\mathbf{v}}_h = -\frac{1}{\rho}\nabla_z p + \vec{\mathcal{F}}_{\dot{v}_h} \tag{1.2}$$

$$\frac{Dw}{Dt} = -\frac{1}{\rho}\frac{\partial p}{\partial z} - g + \mathcal{F}_{\dot{w}_h} \tag{1.3}$$

$$\frac{D\rho}{Dt} + \rho\nabla_z \cdot \vec{\mathbf{v}}_h + \rho\frac{\partial w}{\partial z} = 0 \tag{1.4}$$

$$\rho = \rho(\theta, S, p) \tag{1.5}$$

$$\frac{D\theta}{Dt} = \dot{\theta} \tag{1.6}$$

$$\frac{DS}{Dt} = \dot{S}. \tag{1.7}$$

The equation variables used in 1.2 - 1.7 are as follows: $\mathbf{v}_h$ is the horizontal velocity vector; f_0 is the (constant) Coriolis parameter, set to be $f_0 = 7.29 \times 10^5\, s^{-1}$ the Coriolis parameter; ρ is the density of seawater; p is the thermodynamic pressure; $\vec{\mathcal{F}}$ represents frictional and external forces; w

[10] In mathemathical terms, "small" compared to the other terms in the equation.

is the vertical velocity; g is gravity; θ is potential temperature; S is the salinity; and dotted terms represent nonconservative sources and sinks. Note that in (1.3) we are making the traditional approximation that the Coriolis acceleration in the vertical is aligned with the gravitational force, and so can be absorbed into a definition for g.

1.2.1 The Momentum Equation

The most straightforward analysis considers an unforced system, so we will set $\mathcal{F} = 0$ for simplicity. In the ocean the variations of density are small compared to the mean density, a fact which can be used to simplify the above equation set. Here we seek to ignore variations of the density ρ except where it is multipled by g; this exclusion will act to filter gravity waves from the model, consistent with the small Mach number of the ocean mean circulation (McWilliams, 1996). This simplification is known as the Boussinesq approximation, and it proceeds as follows. Define the background density of the fluid to be ρ_0, and consider the spatially varying perturbation away from this background density to be $\delta\rho$. Then the full oceanic density field can be described by

$$\rho = \rho_0 + \delta\rho(x, y, z, t), \qquad \delta\rho/\rho_0 << 1. \tag{1.8}$$

Consider a reference pressure that is in hydrostatic balance with the background density field, so that

$$p = p_0(z) + \delta p(x, y, z, t) \tag{1.9}$$

$$\frac{dp_0}{dz} = -g\rho_0. \tag{1.10}$$

Multiply (1.2) through by ρ and making use of (1.8), the inviscid momentum equation can be written

$$(\rho_0 + \delta\rho)\left(\frac{D\vec{\mathbf{v}}_h}{Dt} + f_0\hat{\mathbf{k}} \times \vec{\mathbf{v}}_h\right) = -\nabla_z \delta p - \frac{\partial}{\partial z}(p_0 + \delta p)\mathbf{k} - g(\rho_0 + \delta\rho)\mathbf{k} \tag{1.11}$$

$$= -\nabla\delta p - \frac{\partial p_0}{\partial z}\mathbf{k} - -g(\rho_0 + \delta\rho)\mathbf{k}. \tag{1.12}$$

Substituting 1.10 into 1.12 gives

$$(\rho_0 + \delta\rho)\left(\frac{D\vec{\mathbf{v}}_h}{Dt} + f_0\hat{\mathbf{k}} \times \vec{\mathbf{v}}_h\right) = -\nabla\delta p - g\delta\rho\mathbf{k}. \tag{1.13}$$

$$\tag{1.14}$$

We can finally divide through by the $\rho_0 + \delta\rho$ term, and again exploiting the smallness of $\delta\rho$, the final Boussinesq form of the momentum equation becomes

$$\frac{D\vec{\mathbf{v}}_h}{Dt} + f_0\hat{\mathbf{k}} \times \vec{\mathbf{v}}_h = -\nabla\frac{\delta p}{\rho_0} + b\mathbf{k} \tag{1.15}$$

$$b = -g\frac{\delta\rho}{\rho_0}. \tag{1.16}$$

1.2.2 The Continuity Equation

The mass continuity equation can be simplified in a manner similar to that of the momentum equation by direct substitution of 1.8 into 1.4. Using the Boussinesq assumption, then the continuity equation becomes

$$\frac{D\delta\rho}{Dt} + (\rho_0 + \delta\rho)\nabla \cdot \mathbf{v} = 0. \tag{1.17}$$

In order to make progress with this equation we must assume that time scales advectively; that is, the D/Dt term must have the same nondimensional scaling as the the nonlinear advection term $\mathbf{v} \cdot \nabla$ (U/L, where U is a characteristic velocity and L is the characteristic length scale of the motion). If this is indeed the case, then we can directly exploit the smallness of $\delta\rho$ to scale out all terms where it appears, leaving

$$\nabla \cdot \mathbf{v} = 0. \tag{1.18}$$

This final form of the continuity equation, which is identical to that for an incompressible fluid, reflects the fact that a Boussinesq fluid is incompressible to lowest order. All variations of density,

which we have assumed to be small, can be ignored except when multiplied by a large term (such as the gravity term in the momentum equation). The Boussinesq approximation becomes useful in ocean modeling precisely because the incompressibility condition eliminates sound waves, making it possible to use much larger time steps in an iterative scheme. It has become commonplace to use the Boussinesq approximation in conjunction with an accurate equation of state as the basis for an OGCM.

1.2.3 The Equation of State

Equations 1.5 - 1.7 capture the instantaneous thermodynamic state of the fluid, where the right hand sides are purposely nonspecific to allow for sources and sinks of temperature and salinity. If, however, we assume that the fluid is adiabatic[11] and that we can ignore nonlinear effects such as cabbeling, we can consider both potential temperature and salinity to be conservative properties. Then 1.6 and 1.7 become, respectively,

$$\frac{D\theta}{Dt} = 0 \qquad\qquad \frac{DS}{Dt} = 0. \tag{1.19}$$

One immediate consequence of these conservation laws becomes apparent if we consider a linear equation of state for 1.5, such that

$$\rho = \rho_0 \left[1 + \alpha(\theta - \theta_0) + \beta(S - S_0)\right], \tag{1.20}$$

where θ_0 and S_0 are reference values of potential temperature and salinity. Note that we can ignore the dependence of ρ on the pressure because of the incompressibility condition established earlier. Taking the material derivative of 1.20 and using the conservation laws of 1.19 gives the result

$$\frac{D\rho}{Dt} = 0. \tag{1.21}$$

Now we can directly substitute 1.8 to obtain

$$\frac{D\delta\rho}{Dt} = 0, \tag{1.22}$$

[11] In an adiabatic flow the First Law of Thermodynamics states that $D\theta/Dt = 0$. This is a good approximation for the ocean interior, where there is no direct input of energy by solar heating.

whereupon simple multiplication by $-g/\rho_0$ gives the conservation equation for buoyancy,

$$\frac{Db}{Dt} = 0. \tag{1.23}$$

It is worth emphasizing that 1.23 is a single approximation to a fully described **set** of equations, and is not appropriate for every application, such as when cabbeling, double diffusion, or salt fingering are active processes. However, for model simulations where a sophisticated treatment of the thermodynamics is unnecessary, the buoyancy equation is a very useful way to collapse the equation set down significantly.

1.2.4 The Hydrostatic Relation

The Boussinesq equation set, while already highly simplified, can be made even more facile by assuming hydrostasy. A proper criticism of the advantages and pitfalls of using hydrostatic balance appears in Marshall, Hill, Perelman and Adcroft (1997), from which certain points are highlighted here. Consider the vertical component of the Boussinesq momentum equation[12] (1.15),

$$\frac{Dw}{Dt} + \frac{1}{\rho_0}\frac{\partial \delta p}{\partial z} = b. \tag{1.24}$$

Assuming hydrostatic balance implies that the downward gravitational force is balanced to leading order by a pressure gradient acting upwards. In terms of scaling, this would imply that $Dw/Dt << b$ in order for the material derivative to scale out of (1.24). Then consider the following scaling argument. Here again we assume that time scales advectively; as such, we can define characteristic length and velocity scales for the motion as follows:

$$x, y \sim L \qquad z \sim H \tag{1.25}$$

$$u, v, \sim U. \tag{1.26}$$

[12] Notice that we ignore the vertical Coriolis acceleration when making the hydrostatic approximation. The missing term only becomes problematic near the equator and at small spatial scales; roughly speaking, where hydrostasy holds, so does the choice to neglect $f\hat{\mathbf{i}}$ and $f\hat{\mathbf{j}}$.

If we take the buoyancy equation (1.23) and split it into its horizontal and vertical components, so that

$$\frac{D_h b}{Dt} + N^2 w = 0, \tag{1.27}$$

a scaling for w emerges such that $w \approx bU/N^2L$. Then if we use the same scaling rules (1.25) and (1.26) on the Dw/Dt and b terms from 1.24, we find that $Dw/Dt << b$ if

$$\frac{U^2}{N^2L^2} << 1. \tag{1.28}$$

This criterion shows that the validity of the hydrostatic approximation is tied to how short the advective timescale is to the buoyancy period. In regions of heavy stratification (N^2 large), hydrostatic balance can be a good approximation even if the velocity field is weak. Another way of saying this, which is put forth in Marshall, Hill, Perelman and Adcroft (1997) and is more insightful for this research, is to consider the flow in terms of the Richardson number

$$Ri = \frac{N^2}{\left(\frac{\partial u}{\partial z}\right)^2}. \tag{1.29}$$

This nondimensional number compares the buoyancy frequency with the vertical shear, and is a measure of how well the stratification stabilizes against effects which might contribute to the growth of turbulence. Defining the aspect ratio of the motion, $\alpha = H/L$, (1.28) can be written

$$\frac{\alpha^2}{Ri} << 1. \tag{1.30}$$

As long as this condition holds, the hydrostatic approximation does as well. Then defining $\phi = \delta p/\rho_0$, a concise way of writing the vertical momentum equation in hydrostatic balance becomes

$$\frac{\partial \phi}{\partial z} = b. \tag{1.31}$$

In simulations such as the ones conducted in this research, the horizontal scale of a mesoscale eddy is of O(10-100 km), much greater than even the total fluid depth (O(3 km)). For our simulations in particular, Ri ranges from $\mathcal{O}(10^3)$ to $\mathcal{O}(10^5)$. Then hydrostatic balance is safe to employ in all the cases we will be considering, thereby completes the conversion from the full, rotating Navier-Stokes equations to the Boussinesq, hydrostatic primitive equations.

1.2.5 The Boussinesq, Hydrostatic, Primitive Equations

In summary, the full equation set we will be using is

$$\frac{D\vec{\mathbf{v}}_h}{Dt} + f_0\hat{\mathbf{k}} \times \vec{\mathbf{v}}_h = -\nabla\phi + b\mathbf{k} + \vec{\mathcal{F}}_{\dot{v}_h} \tag{1.32}$$

$$\frac{\partial\phi}{\partial z} = b \tag{1.33}$$

$$\nabla \cdot \mathbf{v} = 0 \tag{1.34}$$

$$\frac{Db}{Dt} = 0 \tag{1.35}$$

$$\frac{D\tau}{Dt} = 0. \tag{1.36}$$

The only new equation appearing here is the passive tracer equation (1.36), where the tracer τ is conserved with the flow. In practice, the only nonconservative effects in (1.35) and (1.36) are due to the numerical diffusion imposed to maintain model stability. At this point we note that the frictional term $\vec{\mathcal{F}}_{\dot{v}_h}$, which includes the effects of viscosity, will be parameterized in our model using the Smagorinsky (1963) scheme.

1.3 Eddy-Mean Decomposition

With the governing equation set in hand, we may now explore different ways of decomposing the equations into mean and eddy components. Many such decompositions exist, often yielding very similar forms for the decomposed equations, but differing slightly in their physical interpretation. Example decompositions include the Transformed Residual Mean (Andrews and McIntyre, 1976, 1978**b**; Plumb, 1979; Andrews et al., 1987; McDougall and McIntosh, 1996; Plumb and Ferrari, 2005; Eden, Greatbatch and Olbers, 2007; Eden, in press), the Generalized Lagrangian Mean (Andrews and McIntyre, 1978**a**; Dunkerton, 1980; Plumb and Mahlman, 1987; Buhler, 2009), and the Semi-Lagrangian (Isopycnal) Mean (McDougall and McIntosh, 2001; Nurser and Lee, 2004). We will explore the Transformed Residual Mean (TRM) theory in detail due to its popularity. First, however, we will define the decomposition technique that will be used throughout the rest of this text.

1.3.1 Reynolds Averaging

Small-scale fluctuations in the ocean are driven by a wide variety of physical processes and occupy a continuous spectrum of spatial and temporal scales. It is completely unfeasible to try to consider each fluctuation individually[13] , so we introduce averaging or filtering operators to partition the equations into something more tractable. Such operators form the basis for many types of numerical models (finite difference, finite element, finite volume, RANS, LES, spectral, etc.), detailed discussions of which are far beyond the scope of this text.

Generally speaking, the approach we will use in much of the forthcoming analysis will be to break the equation variables into mean[14] (denoted by a $\overline{\text{bar}}$) and perturbation (denoted with a prime$'$) components. This approach has two primary uses.

The first usage of this technique appears in linear stability analysis, where the ansatz is that the mean component is much greater than the perturbation component, allowing one to discard the nonlinear advection term. Examples are located in Appendices C.2 and C.3, where linear stability analysis is applied to obtain growth rates and timescales for Eady and exponentially-stratified instability.

The second usage of this technique is in setting up the **discretized** equation set for a parameterization. In this approach the bar represents quantities that are directly resolved in the model, and the prime indicates subgridscale quantities. The Boussinesq primitive equations are decomposed in this manner in Appendix B. From this technique, a parameterization can be formed by taking all of the prime quantities is the decomposed equations and attempting to write them in terms of bar quantities.

An equivalent, but less formal, way of describing the above decomposition is that it breaks up

[13] The closest we can feasibly come to achieving this dream is to separate all the subgridscale processes by type and attempt to produce a parameterization of each. To give an idea about the status of such a quest, mesoscale eddy parameterizations are by far the most developed of the lot, and yet the field is still considered to be in its infancy (Ferrari et al., 2008). Good luck and God Speed.

[14] Here we do not yet state what kind of averaging we are performing when taking this "mean". Conceivably, the averaging could be a spatial average, a time average, a spectral average, or otherwise. Each of these kinds of averaging has its place in the analysis ahead, so the exact type of mean we are using will be defined as it arises in the text.

the equations into their "mean" and "eddy" components. In linear stability analysis the reasons for this terminology are clear and require no additional explanation. In numerical modeling, however, the vernacular is that the "mean" part is resolved by the model and the "eddy" part is subgridscale, even if the model resolution is fine enough to actually resolve some turbulence. This is pointed out here partly as a warning so the reader does not become confused, and partly because this informal language will be used later in this text[15] .

We will focus on (arguably) the simplest operator of the lot, Reynolds Averaging, mostly as an example of the leverage we gain by performing the operation, but also to later introduce the concept of "eddy fluxes". A handy review of Reynolds Averaging (whose operation is also known as a "Reynolds decomposition") can be found in Randall (2009); the following includes a few selected highlights from that paper. Consider a flow variable $\alpha(x, y, z, t)$, and let the linear averaging operator be denoted by a $\overline{\text{bar}}$. The nature of the operator (spatial, temporal, or otherwise) need not be defined at this time, except that we necessitate that it be linear. Let all local deviations away from the average be denoted by a prime$'$, so that the full decomposition is

$$\alpha = \bar{\alpha} + \alpha'. \tag{1.37}$$

As noted in Section 1.2, colloquially we refer to the bar variable as the mean component and the prime variable as the eddy component. The averaging can be based on user preference; in some instances it is convenient to average along the spatial coordinate x (as we will do later in this text), while other applications may require averaging in t, z, etc. The only absolute requirement is that the averaging operation must satisfy the Reynolds conditions (Monin and Yaglom, 1971):

$$\overline{\alpha + \beta} = \overline{\alpha} + \overline{\beta} \tag{1.38}$$

$$\overline{c\alpha} = c\overline{\alpha}, \text{ with } c \text{ a constant} \tag{1.39}$$

$$\overline{c} = c. \tag{1.40}$$

These conditions correspond to the requirement that the operator be linear. We also impose the

[15] This terminology is more convenient than always having to use "subgridscale eddies" to refer to the quantities we are parameterizing, and using "perturbation" is no longer appropriate once the turbulence becomes nonlinear.

following rules regarding derivatives and products:

$$\overline{\frac{\partial \alpha}{\partial s}} = \frac{\partial \overline{\alpha}}{\partial s} \tag{1.41}$$

$$\overline{\alpha\bar{\beta}} = \overline{\alpha}\overline{\beta}. \tag{1.42}$$

Finally, the above requirements imply the following identities as well:

$$\bar{\bar{\alpha}} = \overline{\alpha} \tag{1.43}$$

$$\overline{\alpha'} = 0 \tag{1.44}$$

$$\overline{\bar{\alpha}\bar{\beta}} = \overline{\alpha}\overline{\beta} \tag{1.45}$$

$$\overline{\bar{\alpha}\beta'} = 0 \tag{1.46}$$

$$\overline{\frac{\partial \alpha'}{\partial s}} = 0. \tag{1.47}$$

With Reynolds Averaging defined as above, we can now present an example of where it may be used in a modeling context. The following example is known as the Reynolds Averaged Navier Stokes equations.

Consider the rotating, Boussinesq Navier Stokes equations. In vector notation, the momentum equation can be written

$$\frac{\partial \mathbf{u}}{\partial t} + \mathbf{u} \cdot \nabla \mathbf{u} + \mathbf{f} \times \mathbf{u} = -\nabla \phi + b\hat{\mathbf{k}} + \mu \nabla^2 \mathbf{u}. \tag{1.48}$$

Decomposing all of the dependent variables according to Reynolds averaging, we now have an equation written with bar variables and prime variables (not shown for space reasons). "Barring" the entire equation causes all the prime variables from the linear terms to vanish, and we now have a modified momentum equation written to solve for the mean velocity $\bar{\mathbf{u}}$:

$$\frac{\partial \bar{\mathbf{u}}}{\partial t} + \bar{\mathbf{u}} \cdot \nabla \bar{\mathbf{u}} + \mathbf{f} \times \bar{\mathbf{u}} = -\nabla \bar{\phi} + \bar{b}\hat{\mathbf{k}} + \mu \nabla^2 \bar{\mathbf{u}} - \overline{\mathbf{u}' \cdot \nabla \mathbf{u}'}. \tag{1.49}$$

Notice that nearly the entire equation is written in terms of bar quantities, except for the last term on the right hand side. This term is known as the Reynolds stress term, and represents the nonlinear interactions of small eddies with each other (not surprisingly, this term arises by Reynolds

averaging the nonlinear advection term on the left hand side). From a modeling perspective, each term in this equation could be discretized straightforwardly with the exception of the Reynolds stress term, which must be parameterized.

Parameterization of the Reynolds stresses, while certainly related to the topic of parameterizing mesoscale eddy effects in general, will not be considered further here. Instead, we will be primarily interested in parameterizing passive **tracer** transport, which turns out to be an easier problem because the tracers do not feed back upon the flow. We will return to equation 1.49 shortly in order to highlight extra considerations that must be made when building an oceanic parameterization.

1.3.2 The Transformed Residual Mean

We will begin discussing the issue of oceanic tracer transport by manipulating the Reynolds Averaged tracer equation. The framework that follows is known as the Transformed Residual Mean (or Transformed Eulerian Mean, since we are working in the Eulerian frame), and is a useful way of decomposing the tracer equation for geophysical flows that emphasizes eddy effects.

Consider the evolution of a materially conserved tracer, which in vector form is written

$$\frac{\partial \tau}{\partial t} + \mathbf{u} \cdot \nabla \tau = 0. \tag{1.50}$$

If we perform a Reynolds decomposition in the usual manner (not yet defining the context of the mean we take in the process) the mean equation is given by

$$\frac{\partial \bar{\tau}}{\partial t} + \bar{u}\frac{\partial \bar{\tau}}{\partial x} + \bar{v}\frac{\partial \bar{\tau}}{\partial y} + \bar{w}\frac{\partial \bar{\tau}}{\partial z} + \frac{\partial \overline{u'\tau'}}{\partial x} + \frac{\partial \overline{v'\tau'}}{\partial y} + \frac{\partial \overline{w'\tau'}}{\partial z} = 0,$$

or in vector form,

$$\frac{\partial \bar{\tau}}{\partial t} + \bar{\mathbf{u}} \cdot \nabla \bar{\tau} = -\nabla \cdot \overline{\mathbf{u}'\tau'} = -\nabla \cdot \mathbf{F}. \tag{1.51}$$

Here we see that, just as for the momentum equations, the evolution is written in terms of the mean tracer concentration, with one extra term representing the subgridscale fluxes. Notice that the eddy term $\nabla \cdot \overline{\mathbf{u}'\tau'}$ represents the divergence of the subgridscale fluxes - the divergence operator

will allow us an extra degree of freedom in the analysis. We have the freedom to choose what to do with this term, so we look to physical intuition to guide us.

The interior flow of the ocean is considered to be approximately adiabatic, in the sense that density is conserved following the motion and viscous dissipation is confined to the momentum equations (Gent and McWilliams, 1990). In such a model tracer mixing can only occur along isopycnal surfaces, since diapycnal motion would imply a mixing of density, violating the assumption of adiabaticity. We can use this to our advantage in the decomposition of the eddy flux term in 1.51.

We can decompose the vector field $\mathbf{F}$ into the sum of two vector fields, with one oriented along the tracer gradient and one orthogonal to it:

$$\begin{aligned}\mathbf{F} &= \mathbf{F}_\perp + \mathbf{F}_\parallel \\ &= \frac{\mathbf{F}\cdot\nabla\bar{\tau}}{|\nabla\bar{\tau}|^2}\nabla\bar{\tau} + \frac{\nabla\bar{\tau}\times\mathbf{F}}{|\nabla\bar{\tau}|^2}\times\nabla\bar{\tau}.\end{aligned}$$

The component $\mathbf{F}_\parallel$ is known as the skew flux, and using the vector identity $\nabla\cdot(A\times\nabla B) = (\nabla\times A)\cdot B$ we have

$$\begin{aligned}\nabla\cdot\mathbf{F}_\parallel &= \nabla\cdot\frac{\nabla\bar{\tau}\times\mathbf{F}}{|\nabla\bar{\tau}|^2}\times\nabla\bar{\tau} \\ &= \left(\nabla\times\frac{\nabla\bar{\tau}\times\mathbf{F}}{|\nabla\bar{\tau}|^2}\right)\cdot\nabla\bar{\tau} \\ &= \tilde{\mathbf{u}}\cdot\nabla\bar{\tau}.\end{aligned}$$

The skew flux is then equivalent to an advection by the divergence-free velocity $\tilde{u}$, which means that the skew-flux does nothing to change the distribution of the tracer $\bar{\tau}$ (for an analogy, consider how the divergence-free velocity does not change the distribution of ρ in the incompressible mass continuity equation).

With the eddy-induced velocity $\tilde{u}$, we can now define a **residual velocity** $\bar{\mathbf{u}}^* = \bar{\mathbf{u}} + \tilde{\mathbf{u}} = \bar{\mathbf{u}} + \nabla\times\psi$.

Substituting this expression into 1.51 gives

$$\begin{aligned}\frac{\partial \bar{\tau}}{\partial t} + \bar{\mathbf{u}}^* \cdot \nabla \bar{\tau} &= -\nabla \cdot \mathbf{F}^* \\ &= -\nabla \cdot (F + \bar{\tau} \nabla \times \psi) \\ &= -\nabla \cdot (F + \nabla \bar{\tau} \times \psi).\end{aligned} \tag{1.52}$$

The new function $\mathbf{F}^*$ is called the **residual flux**, and we note that no matter the choice of ψ we have $\mathbf{F}_\perp \cdot \nabla \bar{\tau} = \mathbf{F}^*_\perp \cdot \nabla \bar{\tau}$. However, $\mathbf{F}_\parallel \cdot \nabla \bar{\tau} \neq \mathbf{F}^*_\parallel \cdot \nabla \bar{\tau}$. Therefore, because the residual velocity $\bar{\mathbf{u}}^*$ already contains the skew flux on the left hand side of 1.52, the most useful choice for ψ is the one that sets the residual skew flux to zero. Then we let

$$\psi = -\mathbf{F}_\parallel = -\frac{\nabla \bar{\tau} \times \mathbf{F}}{|\nabla \bar{\tau}|^2} \times \nabla \bar{\tau},$$

so that the tracer evolution equation becomes

$$\begin{aligned}&\frac{\partial \tau}{\partial t} + \bar{\mathbf{u}}^* \cdot \nabla \bar{\tau} = -\nabla \cdot \mathbf{F}^* \\ &\bar{\mathbf{u}}^* = \bar{\mathbf{u}} + \nabla \times \psi = \bar{\mathbf{u}} - \frac{\nabla \bar{\tau} \times \mathbf{F}}{|\nabla \bar{\tau}|^2} \times \nabla \bar{\tau} \\ &\mathbf{F}^* = \frac{\mathbf{F} \cdot \nabla \bar{\tau}}{|\nabla \bar{\tau}|^2} \nabla \bar{\tau}.\end{aligned}$$

The interesting aspect of this formulation is that, because the streamfunction is a function of the tracer gradient, there will be a unique streamfunction for each different tracer. The usual approach is to assume that small-scale motions tend to advect each conserved tracer similarly, so we can choose a convenient conserved tracer such as buoyancy[16] and let its streamfunction act for all tracers.

The residual velocity can now be introduced into the momentum equation as well. Replacing $\mathbf{u}$ with $\bar{\mathbf{u}}^*$ in 1.49, the new residual momentum equation (Ferreira and Marshall, 2006) is

$$\frac{\partial \bar{\mathbf{u}}^*}{\partial t} + \bar{\mathbf{u}}^* \cdot \nabla \bar{\mathbf{u}}^* + \mathbf{f} \times \bar{\mathbf{u}}^* = -\nabla \bar{\phi} + \frac{\partial}{\partial z} (\psi \rho_0 f) + \mu \nabla^2 \bar{\mathbf{u}}^* - \overline{\mathbf{u}' \cdot \nabla \mathbf{u}'}, \tag{1.53}$$

[16] The careful reader will note that buoyancy is **not** a passive tracer and that choosing its streamfunction to represent all the passive tracers in the flow is a tenuous proposition. The dynamical consequences of such a choice are a worthy topic of research.

where we notice a new eddy stress term $\frac{\partial}{\partial z}(\psi\rho_0 f)$ on the right hand side. This term arises from our choice to decompose the eddy flux term in 1.52 the TEM style. Ferreira and Marshall interpret this term to be the stretching component of the eddy potential vorticity flux, as well as an eddy form drag resulting from the correlative of eddy pressure fluctuations and isopycnal displacements under geostrophic balance.

The residual momentum equation 1.53 lies outside the traditional presentation of Transformed Residual Mean theory; it is presented here as an example of a consequence of choosing a particular eddy decomposition method. One should have the impression of TRM as a useful analytical, **physically-motivated** approach to the tracer transport problem.

In summary, in TRM Reynolds averaging has been implemented to decompose the original tracer equation into eddy and mean components. Following this, a second round of decomposition partitions the eddy flux into components directed along and across the tracer isosurface. The end result is an equation 1.52 which is both mathematically tractable and physically meaningful, and provides a nice basis from which to attempt an eddy parameterization. Notice, however, that TRM gives no additional information about **how** to form a parameterization - the vector $\overline{\mathbf{u}'\tau'}$ still has not been related to any mean variables. We will merely move forward with the along- and across-isosurface decomposition in mind, cognizant that it and any parameterization we build should be physically consistent.

1.4 Flux-Gradient Relation

Generally speaking, most eddy parameterizations assume that eddy transport is predominantly local in the sense that the eddy term can be approximated on a point-to-point basis. There do exist a few exceptional parameterizations (Aiki et al., 2004; Ferrari et al., 2008, 2010) that rely on vertically integrated quantities to become nonlocal in the vertical, but discussion of these is beyond the scope of this thesis[17] .

[17] Indeed, a local yet physically correct eddy parameterization may not be possible, because it is widely accepted that turbulence is decidedly nonlocal and nonlinear (Tandon and Garrett, 1996). Lacking any further guidance on how to represent eddies nonlocally, local parameterizations remain far easier to justify and implement.

We will restrict our examination to local parameterizations (i.e., Gent and McWilliams, 1990; Greatbatch and Lamb, 1990; Visbeck et al., 1997; Treguier et al., 1997; Killworth, 1997), whose basic form is that of a simple diffusive operator acting on the resolved tracer gradients. The derivations in this section are based on those of Chapter 10 of Vallis (2006), who does a nice job explaining the connection between turbulent diffusion and eddy transport. The basic framework of a local eddy parameterization is as follows.

Suppose that a fluid parcel is displaced some distance l' away from its initial location, and that the parcel retains its initial properties up to this distance. Let the mean distribution of a tracer τ be denoted by $\bar{\tau}$, and let the perturbation away from this mean associated with the parcel displacement be denoted by τ'. A series expansion of τ' in terms of l' is

$$\tau' = -l' \frac{\partial \bar{\tau}}{\partial x} - \frac{1}{2} l'^2 \frac{\partial^2 \bar{\tau}}{\partial x^2} + \dots \tag{1.54}$$

Assuming that the mean gradient of τ varies on a spatial scale much longer than the parcel displacement, it is appropriate to make a first-order approximation to this series, leaving

$$\tau' = -l' \frac{\partial \bar{\tau}}{\partial x}. \tag{1.55}$$

Multiplying by the perturbation velocity u' and taking the mean gives the eddy covariance

$$\overline{u'\tau'} = \overline{u'l'} \frac{\partial \bar{\tau}}{\partial x}. \tag{1.56}$$

Following the same approach in multiple dimensions gives

$$\overline{u_i'\tau'} = -\overline{u_i'l_j'} \frac{\partial \bar{\tau}}{\partial x_j}, \tag{1.57}$$

or in vector notation,

$$\overline{\mathbf{u}'\tau'} = -\mathbf{R} \nabla \bar{\tau} \tag{1.58}$$

$$R_{ij} = \overline{u_i'l_j'}. \tag{1.59}$$

This is known as the flux-gradient relation, which links the eddy flux of a tracer with its own mean gradient. The proportionality between these two quantities is governed by the eddy mixing tensor[18]

R, which in three spatial dimensions is a dyadic, second-rank tensor. Note that the diffusivity κ associated with **R** can be directionally variable and is not the same as the molecular diffusivity; at high Peclet number the eddy diffusivity is a property of the flow and not the fluid itself.

In modeling we can consider the "prime" quantities to represent the subgridscale; that is, all the values that are not directly resolved due to resolution limitations. The "bar" quantities represent those that are directly resolved in the model. This flux-gradient relation gives an avenue by which the subgridscale quantities can be put in terms of directly resolved quantities, thereby closing the tracer transport equation.

The flux-gradient relation assumes that the bulk transport is down the mean tracer gradient, as is indicated by the negative sign on the right hand side of 1.58. The flux-gradient relation form is not, however, appropriate as a representation of momentum transfer (e.g., $\overline{v'u'} \neq -\kappa\partial\bar{u}/\partial y \neq \kappa\partial\bar{v}/\partial x$) because baroclinic eddies can, and often do, transfer momentum up the local momentum gradient (Visbeck et al., 1997). We also would not even expect the same κ to hold, since passive tracers and momentum are transported by different mechanisms. Tracer transport happens only by local movement of matter, whereas momentum transport also happens nonlocally through pressure forces and can thus be greater (McWilliams, 1996). Attempts have been made to extend tracer flux parameterizations to include momentum transport (Wardle and Marshall, 2000; Smith and McWilliams, 2003; Plumb and Ferrari, 2005; Ferreira and Marshall, 2006; Marshall et al., 2012), but there is still little knowledge of how these methods perform in OGCM's (Ferrari et al., 2008). However, it is worth noting that Grooms et al. (2011) have shown asymptotically that for the class of flows we consider in this research, the momentum fluxes tend to be secondary to b' for the momentum balance.

The approach of writing the eddy quantities in terms of the eddy mixing tensor is but one

[18] Another commonly used (and misleading) name for **R** is the "eddy diffusivity tensor". This name often shows up when oceanographers want to speak in terms of diffusivity by dividing the eddy flux by the mean gradient. Doing so is indeed a convenient way of normalizing the flux so that it has units of velocity times length, from which one can try to relate this normalized flux to eddy length and time scales (Held, 1998). However, use of the term "diffusivity tensor" is strongly discouraged unless one is referring only to the symmetric part of **R**; it will be shown later that **R** represents the sum of diffusion **and** advection.

way to decompose the tracer equation. In general, a decomposition into bar-prime form[19] requires that there be a spectral gap between the two (or more) components, so that correlations between them can be neglected. This is akin to assuming that the turbulence interacts locally in spectral space, similar to the assumptions underpinning Kolmogorov theory (Kolmogorov, 1941) and related viscous parameterizations (Smagorinsky, 1963, 1993).

Note that this approach does not tell us anything about how strong the diffusivity must be in any particular direction, other than that it must be governed by the correlation between an eddy velocity and an eddy length scale. We thus might be guided by a physical interpretation of the tensor $\mathbf{R}$. Simple reasoning might lead one to expect that, in general, the diffusion by $\mathbf{R}$ should be anisotropic. The oceans are quite thin in the sense that the horizontal dimensions of the ocean basins far exceed the ocean depth. Adding in the usually stable stratification that suppresses vertical motion, we can surmise that the horizontal diffusivities should be far greater than the vertical diffusivity[20]

In quasigeostrophic scaling we assume that the vertical buoyancy gradient $\bar{b}_z$ is much greater than the horizontal buoyancy gradient $\bar{b}_y$, and that the vertical velocity is dominated by the horizontal velocity. Inserting these assumptions into (1.57) then suggests that the horizontal diffusivity dominates the vertical diffusivity. It is because of the dominance of the horizontal diffusivity that we will focus the majority of our attention on the along-isopycnal parameterization.[21] Two parameterizations, Redi (1982) and Gent and McWilliams (1990) (hereafter GM90), have gained tremendous popularity due to their clever physical intuition and ease of implementation in models. We will begin by discussing Redi, the simpler of the two, before moving on to the more physically complex GM parameterization.

[19] Or a form with more than one eddy component, such as the mean-mesoscale-microscale idea suggested in Ferrari et al. (2008).

[20] Or, to be physically correct, the diffusivity along an isopycnal surface should be far greater than the diffusivity across it.

[21] Here we make the "small-slope" approximation, where we assume that at quasigeostrophic scales the isopycnals are nearly flat. Then in this case "horizontal" means essentially the same thing as "along-isopycnal".

1.5 The Redi Parameterization

The earliest attempt at mesoscale eddy parameterization (Bryan and Cox, 1967) represented the eddy term as a down-gradient diffusion of momentum and tracers in the horizontal and vertical directions with spatially constant diffusion coefficients.[22] This approach quickly proved inadequate, as observations dating as far back as Iselin (1939) and Montgomery (1940) first suggested that mixing in the ocean occurred along isopycnal surfaces in stably stratified parts of the ocean. Thus, it was argued (Solomon, 1971; Redi, 1982) that horizontal and vertical diffusion in the tracer equation should be replaced by diffusion along and across isopycnals. The more sophisticated of these treatments, derived by Redi, is also the one most commonly implemented in OGCMS and is detailed below.

The basic form of the Redi (1982) parameterization represents the diffusive mixing of tracers along isopycnals, with an optional extra parameter to represent diapycnal diffusion. In isopycnal coordinates, eddy effects are represented by the term $\nabla \cdot \mathbf{S}_I \cdot \nabla \tau$, where $\mathbf{S}_I$ is a second rank, positive definite tensor. It will be shown later that $\mathbf{S}_I$ is identically the symmetric part of the flux-gradient tensor $\mathbf{R}$ from Section 1.4.

Assuming the diffusivity is isotropic in the horizontal, a simple form for $\mathbf{S}_I$ is

$$\mathbf{S}_I = \mu \begin{bmatrix} 1 & 0 & 0 \\ 0 & 1 & 0 \\ 0 & 0 & \epsilon \end{bmatrix} . \tag{1.60}$$

This form is relatively simplistic, in that the isopycnal diffusivity in the $x-$ and $y-$directions is governed by μ, with $\mu\epsilon$ representing a weak (diabatic) diapycnal diffusivity[23] .

The Redi tensor is the projection of this simple, isopycnal form of $\mathbf{S}_I$ into geodesic (x, y, z) coordinates. This is achieved by rotating the isopycnal surface using two angles, α and β, embedded

[22] This representation was also used in Munk (1950), although in that case it was used to simplify an analytical problem.

[23] The ansatz here is that $\epsilon \ll 1$; Redi chose $\epsilon \approx 10^{-7}$ based on the observations of (Sarmiento and Bryan, 1982).

in a rotation matrix $\mathbf{R}$, where

$$\mathbf{R} = \begin{bmatrix} \cos\alpha\cos\beta & -\sin\alpha & -\sin\beta\cos\alpha \\ \sin\alpha\cos\beta & \cos\alpha & -\sin\beta\sin\alpha \\ \sin\beta & 0 & \cos\beta \end{bmatrix}. \tag{1.61}$$

The transformation for $\mathbf{S}_I$ to geodesic coordinates is obtained by $\mathbf{R}\cdot\mathbf{S}_I\cdot\mathbf{R}^{-1} = \mathbf{S}_g$.

In relation to the elements of $\mathbf{R}$, it can be shown that

$$\frac{\rho_x}{\rho_y} = \frac{1}{\tan\alpha} \qquad \tan\beta = \frac{(\rho_x^2+\rho_y^2)^{1/2}}{\rho_z} \tag{1.62}$$

$$\cos\alpha\tan\beta = -\frac{\rho_x}{\rho_z} \qquad \sin\alpha\tan\beta = -\frac{\rho_y}{\rho_z}. \tag{1.63}$$

Substituting into $\mathbf{R}$ and performing the coordinate transformation, the diffusivity tensor in geodesic coordinates is

$$\mathbf{S}_g = \frac{\mu}{\rho_x^2+\rho_y^2+\rho_z^2}\begin{bmatrix} \rho_z^2+\rho_y^2+\epsilon\rho_x^2 & (\epsilon-1)\rho_x\rho_y & (\epsilon-1)\rho_x\rho_z \\ (\epsilon-1)\rho_x\rho_y & \rho_z^2+\rho_x^2+\epsilon\rho_y^2 & (\epsilon-1)\rho_y\rho_z \\ (\epsilon-1)\rho_x\rho_z & (\epsilon-1)\rho_y\rho_z & \rho_x^2+\rho_y^2+\epsilon\rho_z^2 \end{bmatrix}. \tag{1.64}$$

This is the full Redi tensor form, including the small diapycnal diffusivity parameter ϵ. Note that the symmetry of $\mathbf{S}_I$ is preserved in the transformation, so that it will have positive, real eigenvalues. In both coordinate systems the Redi tensor represents a downgradient diffusive flux, so that it works to align the tracer parallel to the isopycnal direction.

The Redi tensor need only be implemented in the passive tracer equation because it does not affect the local potential density (and thus has no effect in the continuity equation or the buoyancy equation), and thus will not change the available potential energy of the system (Griffies, 1998). Because of this latter fact, we see that Redi does not attempt to replicate the phenomenology of baroclinic instability at all. When viewed in this light, it becomes clear that the Redi tensor is nothing more than a simple (albeit extremely useful) assumption that turbulence diffuses tracers along density surfaces, with no physical intuition necessary beyond that[24] .

[24] We will see in the next section that the complementary parameterization to Redi, that of Gent and McWilliams

Before moving on, it is worth mentioning a few points about how the Redi parameterization is used in practice. Implementing the Redi tensor in a z-coordinate model has proven to produce a more realistic thermocline and reduce spurious and nonphysical diapycnal fluxes (Cox, 1987; Veronis, 1975; Gough and Lin, 1995). A numerically stable implementation of this parameterization is described in Griffies et al. (1998).

One principle advantage of Redi is that its implementation in a numerical model is straightforward and requires the simple calculation of first derivatives at each point. For much of the interior of the ocean, however, it has an even simpler form if we assume that the isopycnal slopes $\nabla\rho/\rho_z$ are small (here defining "small" as being $< 1/10$, a criteria usually violated only in convective regions (Griffies, 1998). This condition is equivalent to saying $\rho_x, \rho_y \ll \rho_z$. Under this assumption, and neglecting ϵ for the moment, $\mathbf{S}_g$ simplifies to

$$\mathbf{S}_g = \mu \begin{bmatrix} 1 & 0 & -\frac{\rho_x}{\rho_z} \\ 0 & 1 & -\frac{\rho_y}{\rho_z} \\ -\frac{\rho_x}{\rho_z} & -\frac{\rho_y}{\rho_z} & \frac{\rho_x^2+\rho_y^2}{\rho_z^2} \end{bmatrix}. \tag{1.65}$$

This is known as the "small-angle approximation", and it is used often for its greatly simplified numerics. This form of the Redi tensor holds throughout the ocean interior other than in the most exceptional of circumstances. Because of this, it is the form we will carry through the rest of this text, and henceforth we will simple refer to it as $\mathbf{S}$.

1.6 The Gent-McWilliams Parameterization

As mentioned previously, the Redi parameterization is a highly successful, nearly universally used representation of eddy diffusion. It fails to tell the whole story, however, because it cannot simulate how eddies affect the thermal structure of the ocean by altering the density or buoyancy distributions. Parameterizing the buoyancy flux purely by the Redi tensor gives

$$\overline{\mathbf{u}'b'} = -\mathbf{S}_g \nabla \bar{b}, \tag{1.66}$$

(1990), is formulated specifically to mimic baroclinic instability, and requires a great deal more physical interpretation as a result.

which in two dimensions reduces to

$$\mathbf{S}_g \nabla \bar{b} = \begin{bmatrix} \mu & -\mu \frac{\bar{b}_y}{\bar{b}_z} \\ -\mu \frac{\bar{b}_y}{\bar{b}_z} & \mu \frac{\bar{b}_y^2}{\bar{b}_z^2} \end{bmatrix} \begin{bmatrix} \bar{b}_y \\ \bar{b}_z \end{bmatrix} \tag{1.67}$$

$$= \begin{bmatrix} \mu \left(\bar{b}_y - \bar{b}_y \right) \\ \mu \left(-\frac{\bar{b}_y^2}{\bar{b}_z} + \frac{\bar{b}_y^2}{\bar{b}_z} \right) \end{bmatrix} = \begin{bmatrix} 0 \\ 0 \end{bmatrix} \tag{1.68}$$

$$\overline{\mathbf{u}' b'} = 0. \tag{1.69}$$

If this were the case, then all of the eddy buoyancy flux would be along-isopycnal and would have no effect on the mean ocean stratification. which is obviously untrue. It is this shortcoming of the Redi parameterization that led Gent and McWilliams (1990) to form their seminal parameterization of mesoscale eddies.

As with Redi, the GM90 parameterization attempts to replicate eddy effects on the distribution of passive tracers, except that it is formed specifically to also affect the oceanic density field. The physical considerations for GM90 are as follows:

- The transport of passive tracers features a forward cascade of tracer variance to small scales, so the dissipation of this variance is significant no matter the tracer diffusivity.
- In adiabatic flow, tracer mixing can only occur along isopycnals, which motivates two additional criteria:
  - Mean tracer concentration is conserved along isopycnals.
  - All higher moments of passive tracer concentration decrease in time.
- Domain-averaged moments of ρ are conserved.
- The volume (in incompressible flow) between isopycnal surfaces is conserved.

The Gent-McWilliams parameterization is necessary because a purely diffusive parameterization fails to simulate the eddy flux divergence of the density. That is, using density as the tracer

in an isopycnal diffusion scheme returns a value of identically zero since there is no density gradient along isopycnal surfaces. This would imply that density is mixed by the large-scale velocity, which has been shown in numerical and observational studies to be untrue (Gent et al., 1995). A mesoscale eddy parameterization therefore requires an additional **advective** term to parameterize the eddy density flux divergence.

Consider the mass and tracer conservation equations in isopycnal coordinates:

$$\frac{\partial h_\rho}{\partial t} + \nabla_\rho \cdot (h_\rho \mathbf{u}) = 0 \tag{1.70}$$

$$\frac{\partial \tau}{\partial t} + \mathbf{u} \cdot \nabla_\rho \tau = \left(\frac{1}{h_\rho}\right) \nabla_\rho \cdot (\mu h_\rho \mathbf{J} \cdot \nabla_\rho \tau) \tag{1.71}$$

$$\mathbf{J} = \frac{1}{1 + h_x^2 + h_y^2} \begin{bmatrix} 1 + h_y^2 & -h_x h_y \\ -h_x h_y & 1 + h_x^2 \end{bmatrix}. \tag{1.72}$$

Equation 1.70 represents the conservation of isopycnal layer thickness following the flow. Equation 1.71 is a similar conservation equation for a tracer in isopycnal coordinates, except for a non-conservative term on the right side that represents Redi isoneutral diffusion. In the limit that the horizontal density gradients are small, the h_x and h_y terms can be scaled out of $\mathbf{J}$ to return the identity matrix, reducing 1.71 to a simple Fickian diffusion in isopycnal coordinates. Under Reynolds averaging, the density equation 1.70 becomes

$$\frac{\partial \bar{h}_\rho}{\partial t} + \nabla_\rho \cdot \left(\bar{h}_\rho \bar{\mathbf{u}}\right) + \overline{\nabla_\rho \cdot \left(h'_\rho \mathbf{u}'\right)} \approx 0. \tag{1.73}$$

In a fine-resolution model and in a statistically steady state (setting $\frac{\partial \bar{h}_\rho}{\partial t} = 0$), the flux divergence of the mean density field by the mean velocity is balanced by the eddy flux divergence of the density. The latter term is not directly resolved in a coarse-resolution model (since it is inherently non-eddy-resolving), and thus must be parameterized in order to achieve a sensible balance in the density equation. This term is nonconservative and is the focus of the GM90 parameterization. Defining $\nabla \cdot \mathbf{F}$ to be the analytic representation of the nonconservative term $\overline{\nabla_\rho \cdot \left(h'_\rho \mathbf{u}'\right)}$, the eddy

mixing is incorporated into 1.70 by

$$\frac{\partial \bar{h}_\rho}{\partial t} + \nabla_\rho \cdot \left(\bar{h}_\rho \mathbf{u}\right) + \nabla \cdot \mathbf{F} = 0. \tag{1.74}$$

In order to ensure along-isopycnal mixing in adiabatic flow, the "eddy-mixed" form of the tracer equation is

$$\frac{\partial \bar{\tau}}{\partial t} + \bar{\mathbf{u}} \cdot \nabla_\rho \bar{\tau} = \frac{1}{\bar{h}_\rho} \left[\nabla_\rho \cdot \left(\mu \bar{h}_\rho \mathbf{J} \cdot \nabla_\rho \bar{\tau}\right) - \mathbf{F} \cdot \nabla_\rho \bar{\tau}\right]. \tag{1.75}$$

The parameterization therefore hinges on an appropriate choice for $\mathbf{F}$. Gent and McWilliams (1990) proposed the form

$$\mathbf{F} = -\frac{\partial}{\partial \rho}(\kappa \nabla_\rho \bar{h}), \tag{1.76}$$

where the thickness diffusivity κ can be spatially varying. In the case that κ is a constant, the nonconservative term in 1.74 becomes a simple Laplacian diffusion operation.

The important physical aspects of the GM90 parameterization are as follows. When κ is positive, there is a downgradient vertical diffusion of mean momentum and a positive definite conversion of mean potential energy to eddy potential energy. The latter is meant to simulate the potential energy conversion due to baroclinic instability, a hallmark of mesoscale turbulence. Note that there is no particular specification for κ; the original authors warned that it would have to be tuned (likely by spatiotemporal dependence) in order to fit what is observed in nature.

In physical coordinates, 1.74 and 1.75 correspond to

$$\frac{D\bar{\rho}}{Dt} = \nabla_z \cdot (\kappa \nabla_z \bar{\rho}) - \frac{\partial}{\partial z}(\kappa \nabla_z \bar{\rho} \cdot \nabla_z \bar{\rho}/\bar{\rho}_z) \tag{1.77}$$

$$\frac{D\bar{\tau}}{Dt} = \nabla \cdot (\mu \mathbf{S}_g \cdot \nabla \bar{\tau}) - \nabla_z \cdot \left[\bar{\tau} \frac{\partial}{\partial z}(\kappa \nabla_z \bar{\rho}/\bar{\rho}_z) \right] + \frac{\partial}{\partial_z} \left[\bar{\tau} \nabla_z \cdot (\kappa \nabla_z \bar{\rho}/\bar{\rho}_z) \right] \tag{1.78}$$

$$\mathbf{S}_g = \frac{1}{1 + \bar{\rho}_x^2 + \bar{\rho}_y^2 + \bar{\rho}_z^2} \begin{bmatrix} \bar{\rho}_y^2 + \bar{\rho}_z^2 & -\bar{\rho}_x \bar{\rho}_y & -\bar{\rho}_x \bar{\rho}_z \\ -\bar{\rho}_x \bar{\rho}_y & \bar{\rho}_x^2 + \bar{\rho}_z^2 & -\bar{\rho}_y \bar{\rho}_z \\ -\bar{\rho}_x \bar{\rho}_z & -\bar{\rho}_y \bar{\rho}_z & \bar{\rho}_x^2 + \bar{\rho}_y^2 \end{bmatrix}. \tag{1.79}$$

Here we recognize 1.79 as the Redi diffusivity tensor without the diapycnal diffusivity ϵ. Equation 1.78 gives the full, parameterized tracer evolution equation for a coarse-resolution model, albeit in a somewhat complicated form. Griffies (1998) presented a simplifed version of this equation which is often implemented in OGCMs, and is discussed in detail in Section 1.7.

1.6.1 Advection by an Eddy-Induced Velocity

Gent et al. (1995) note that the GM90 form of the thickness flux in 1.73 is formally equivalent to advection by an eddy-induced transport velocity, given in isopycnal coordinates by

$$\mathbf{u}^* = \frac{\overline{h'_\rho \mathbf{u}'}}{\bar{h}_\rho} \tag{1.80}$$

$$= -\frac{\frac{\partial}{\partial \rho}(\kappa \nabla_\rho \bar{h})}{\bar{h}_\rho}. \tag{1.81}$$

The equivalent form in z-coordinates is

$$\mathbf{u}^*{}_h = -\frac{\partial}{\partial z}\left(\kappa \frac{\nabla \bar{\rho}}{\bar{\rho}_z}\right) \qquad\qquad w^* = \nabla \cdot \left(\kappa \frac{\nabla \bar{\rho}}{\bar{\rho}_z}\right). \tag{1.82}$$

Plumb and Mahlman (1987) diagnosed the zonally averaged tracer transports in the GFDL general circulation/transport model and used the name "effective transport velocity" for the velocity advecting the tracers. As mentioned at the beginning of the Section 1.3, there exist several different forms for this velocity, such as the residual mean (Andrews and McIntyre, 1976, 1978**b**; Plumb, 1979; Andrews et al., 1987; McDougall and McIntosh, 1996; Plumb and Ferrari, 2005; Eden, Greatbatch

and Olbers, 2007; Eden, in press), Lagrangian-mean (Andrews and McIntyre, 1978**a**; Dunkerton, 1980; Plumb and Mahlman, 1987; Buhler, 2009), and Isopycnal mean (McDougall and McIntosh, 2001; Nurser and Lee, 2004). The mathematical differences between these forms are important but subtle, and no further attention will be paid to them here[25] . We will simply refer to the GM90-related velocity as the "eddy-induced velocity" and be done with it.

Note that in 1.81 and 1.82 κ lies inside the vertical derivative, which, in accordance with the GM90 design, does not imply exact Fickian diffusion along isopycnal surfaces. The main consequence of the form 1.82 is that it results in a sign-definite sink of potential energy. Numerically it is also convenient since w^* can be evaluated as a local function of ρ. A third major consequence of this choice is discussed in Section 1.6.5.

Hereafter we are finished using eddy terms ("prime" terms in the Reynolds averaging), so we will drop the "bar" notation except when it is important to make the distinction between the mean and eddy-induced velocities.

1.6.2 Energetics

Using the GM90 parameterization, an evolution equation for potential energy, $E_p = \rho g z$, can be constructed by multiplying 1.77 by gz. Distributing gz through the derivatives, such an equation appears as

$$\frac{\partial E_p}{\partial t} + (\bar{\mathbf{u}} + \mathbf{u}^*) \cdot \nabla E_p = \nabla \cdot \left(g\rho\kappa \frac{\nabla \rho}{\rho_z} \right) + g\rho w + g\kappa \frac{\nabla \rho \cdot \nabla \rho}{\rho_z}. \tag{1.83}$$

With the convention that g is always negative, this equation reveals that the GM90 scheme provides a sign-definite sink of potential energy. This is in accordance with the design of GM90, which was to mimic the fact that baroclinic instability grows at the expense of the potential energy of the mean flow. This potential energy sink manifests itself as a reduction of isoneutral slope as the potential energy decreases. The magnitude of the along-isopycnal ("skew") flux is linked with both of these quantities, so available potential energy, skew flux, and isoneutral slope asymptote to zero

[25] For a detailed comparison between these forms, see Olbers et al. (2012) and Eden (in press).

simultaneously. The second term on the right hand side represents the transfer of this potential energy to the eddy kinetic energy, while the other terms represent an internal sink of potential energy by redistribution of the parcel down the neutral slope.

1.6.3 The Vertical Momentum Flux Analogy

Consider the planetary geostrophic momentum equation

$$f\mathbf{k}\times\bar{\mathbf{u}} = -\frac{\nabla p}{\rho_0}. \tag{1.84}$$

Adding the GM90 effective transport velocity $\mathbf{u}_h^*$ defined above, we have

$$f\mathbf{k}\times(\bar{\mathbf{u}}+\mathbf{u}_h^*) = -\frac{\nabla p}{\rho_0} + \left(\kappa f\mathbf{k}\times\frac{\nabla\rho}{\rho_z}\right)_z \tag{1.85}$$

Employing thermal wind balance

$$g\frac{\nabla\rho}{\rho_0} = -f\mathbf{k}\times\frac{\partial\mathbf{u}_h}{\partial z}, \tag{1.86}$$

equation (1.85) becomes

$$f\mathbf{k}\times(\bar{\mathbf{u}}+\mathbf{u}_h^*) = -\frac{\nabla p}{\rho_0} + \left(\frac{\kappa\rho_0 f^2}{g\rho_z}\frac{\partial\mathbf{u}_h}{\partial z}\right)_z. \tag{1.87}$$

Defining the buoyancy frequency $N^2 = -g\rho_z/\rho_0$, (1.87) reveals that GM90 is analogous to a vertical mixing of momentum with coefficient $\delta = \kappa f^2/N^2$. Greatbatch and Lamb (1990) also made an heuristic derivation of (1.87) based on the correspondence in quasi-geostrophic theory between vertical mixing of momentum and horizontal mixing of potential vorticity (Rhines and Young, 1982**a**). Tandon and Garrett (1996) noted that this is equivalent to a viscous spindown with vertical viscosity coefficient δ. The vertical momentum flux/viscosity analogy depends on the use of thermal wind balance, and therefore it is accurate to the extent that the thermal wind relation is appropriate in the above equations.

1.6.4 Form drag

In addition to representing the GM90 parameterization as a vertical momentum flux, it is also possible to draw an analogy with an eddy stress acting on isopycnal surfaces (Greatbatch, 1998). Once again employing the planetary geostrophic approximation with GM90, we have

$$f\mathbf{k}\times(\bar{\mathbf{u}}+\mathbf{u}_h^*)=-\frac{\nabla p}{\rho_0}+\left(\kappa f\mathbf{k}\times\frac{\nabla\rho}{\rho_z}\right)_z. \tag{1.88}$$

We can subtract out 1.84, the PG relation for the large-scale flow, which leaves

$$f\mathbf{k}\times\mathbf{u}_h^*=\left(\kappa f\mathbf{k}\times\frac{\nabla\rho}{\rho_z}\right)_z. \tag{1.89}$$

Here it becomes apparent that the eddy-induced velocity is an Ekman velocity, with a horizontally directed eddy stress $\kappa f\mathbf{k}\times\frac{\nabla\rho}{\rho_z}$. We can exploit this association by examining the GM90 thickness flux in isopycnal coordinates. The exact form of this flux is given by 1.80; assuming the eddies are in geostrophic and hydrostatic balance, it can be shown (Greatbatch, 1998) that

$$\mathbf{u}^*=\frac{1}{f\rho_0\bar{h}_\rho}\mathbf{k}\times\left[-\frac{\partial}{\partial\rho}\overline{p'\nabla_\rho z'}+\nabla_\rho\overline{\left(p'h'_\rho\right)}\right]. \tag{1.90}$$

Here the first term is equivalent to the vertical momentum flux in (1.87), except this version is unapproximated by GM90. Rhines and Holland (1979) refer to this term as the "form drag" exerted on the isopycnal interfaces. This term is also equivalent to the eddy stress on the right side of (1.89). The second term is equivalent to a horizontal momentum flux, which is small relative to the vertical flux term when the large-scale flow is much bigger than the eddy length scale. This would be an appropriate choice in the planetary geostrophic equations, which would then reconcile (1.90) with (1.89).

We are thus left with the conundrum of what to do when the eddy scale and the scale of the background flow are similar, as would be the case in quasigeostrophy. This situation is reconciled by noting that the eddy transport velocity $\mathbf{u}^*$ only enters in to 1.73 as the **divergence** of the eddy thickness flux, so that a purely rotational component of $\mathbf{u}^*$ makes no contribution. On an f-plane,

the horizontal momentum flux term is precisely such a rotational term, so that

$$\nabla_\rho \cdot \left[\frac{1}{f\rho_0} \mathbf{k} \times \nabla_\rho \left(\overline{p' h'_\rho} \right) \right] = 0. \tag{1.91}$$

Then even in the QG limit it is appropriate to make the association of GM90 with a form drag and with a vertical momentum flux. It must be kept in mind that if we allow f to vary with latitude, 1.90 does not hold identically. Also, eddies are not purely geostrophic and will interact with even smaller scales of turbulence. However, any such contributions from the β-effect and ageostrophic turbulence are likely to be small compared with the horizontal form drag term (Greatbatch, 1998).

1.6.5 Isopycnal Flux of Potential Vorticity

Potential vorticity is perhaps the most powerful active tracer in geophysical fluid dynamics, whose material conservation describes and constrains a wide variety of geophysical flows.[26] Both theoretical (Marshall, 1982; McWilliams and Chow, 1981; Rhines and Young, 1982**a**) and observational evidence suggests that potential vorticity is homogenized along isopycnals by mesoscale eddies (McDowell et al., 1982; Keffer, 1985; Talley, 1988; O'Dwyer and Williams, 1997). Various attempts have been made to draw upon the analogy between potential vorticity mixing and passive tracer mixing along isopycnals (Greatbatch and Lamb, 1990; Treguier et al., 1997; Killworth, 1997) to further inform GM90-style parameterizations.

We can investigate the degree to which GM90 is an appropriate choice with which to parameterize potential vorticity mixing by considering the planetary geostrophic limit, with momentum equation given by geostrophic balance

$$f\mathbf{k} \times \mathbf{u} = -\frac{\nabla p}{\rho_o}. \tag{1.92}$$

[26] The full derivation of potential vorticity conservation and its many consequences would be extraneous to this dissertation. The essential concept of potential vorticity is that we can define a scalar $q = (f + \nabla \times \mathbf{u}) \cdot \nabla\chi$ that is materially conserved following the flow, so long as the tracer χ is also conserved following the flow. In the adiabatic Boussinesq case we will let $\chi = \theta$, the potential temperature. Generally, the density ρ and buoyancy b are not suitable choices for χ due to dependence on spice; however, we will ignore this dependence and use ρ- and b-dependent definitions of q as well.

At these scales, the potential vorticity is $q = f\rho_z$, and its evolution equation is

$$\frac{\partial q}{\partial t} + (\bar{\mathbf{u}} + \mathbf{u}^*) \cdot \nabla q = \nabla \cdot [\kappa f \mathbf{K} \nabla \rho_z] + \nabla \cdot (f \kappa_z \nabla \rho) - \left(f \kappa_z \frac{\nabla \rho \cdot \nabla \rho}{\rho_z} \right)_z . \tag{1.93}$$

Here potential vorticity is being advected by the effective transport velocity and has mixing of ρ_z along isopycnals with coefficient κf. Now suppose that either κ is vertically constant, or that we choose the exact Fickian diffusion form, so that

$$\mathbf{u}^*{}_h = \kappa \frac{\partial}{\partial z} \left(\frac{\nabla \rho}{\rho_z} \right) . \tag{1.94}$$

With this choice, (23) reduces to

$$\frac{\partial q}{\partial t} + (\bar{\mathbf{u}} + \mathbf{u}^*) \cdot \nabla q = \nabla \cdot [\kappa f \mathbf{K} \nabla \rho_z] . \tag{1.95}$$

Here it becomes apparent that potential vorticity is **advected** like a tracer along isopycnals. However, it is not **diffused** like a tracer; rather, it is ρ_z that is diffused, with f in the coefficient. This is desirable because there can exist a steady, motionless solution of 1.93 with ρ independent of the horizontal coordinates, which is not possible if it were potential vorticity being mixed (Gent et al., 1995).

This demonstrates the link between the vertical flux of momentum with the horizontal mixing of potential vorticity (Rhines and Young, 1982**a**). The assumption that we made above, namely that κ is vertically constant, is critical however. As originally designed, the GM90 parameterization represents the transport of thickness along isopycnals, **not** potential vorticity. Under certain assumptions, however, these two transports become similar. For example, if we use the Boussinesq form of Ertel potential vorticity, $q = (f + \xi) \cdot \nabla b$ and assume that the buoyancy gradient is dominant, the GM90 thickness transport is roughly equivalent to potential vorticity transport. However, numerically this becomes problematic because of the vertical boundary condition - in order for $w^* = 0$ at the surface and bottom, κ must be set to zero there. Then κ must be depth-dependent, violating our original assumption. To conclude this remark, it suffices to say that the GM90 parameterization is not equivalent to a potential vorticity transport, although this does not necessarily preclude the local GM90 κ from being **dependent** on the potential vorticity.

We can make the relevance of GM90 to a potential vorticity flux parameterization more explicit by considering the Boussinesq primitive momentum equations written in Transformed Residual Mean form (Andrews, 1983, 1987; Andrews et al., 1987; Greatbatch and Lamb, 1990; Wardle and Marshall, 2000; Ferreira and Marshall, 2006; Marshall et al., 2012; Young, 2012):

$$\frac{D\mathbf{u}}{Dt} + f\mathbf{k}\times\mathbf{u} = -\nabla\phi - \nabla\cdot\mathbf{E}. \tag{1.96}$$

The 3×2 eddy stress pseudotensor $\mathbf{E}$ contains the Eliassen-Palm vectors (Andrews and McIntyre, 1976), whose divergence gives the quasigeostrophic eddy potential vorticity flux. That is,

$$\nabla\cdot\mathbf{E} = \mathbf{k}\times\overline{\mathbf{u}'\mathbf{q}'} \tag{1.97}$$

$$\mathbf{E} = \begin{pmatrix} -M+P & N \\ N & M+P \\ -S & R \end{pmatrix} \tag{1.98}$$

$$M = \frac{\overline{v'^2 - u'^2}}{2}, \qquad N = \overline{u'v'}, \qquad P = \frac{\overline{b'^2}}{2N^2} \tag{1.99}$$

$$R = \frac{f_0}{N^2}\overline{u'b'}, \qquad \text{and} \qquad S = \frac{f_0}{N^2}\overline{v'b'}. \tag{1.100}$$

Equations (1.96) - (1.100) make clear the fact that in the primitive equations the eddy potential vorticity flux belongs in the momentum equation, even though in the quasigeostrophic framework it is transported like a tracer[27] . The contributions from the buoyancy fluxes which would be parameterized by GM90 appear only in the last row of (1.98), which analytically proves that a proper parameterization for the potential vorticity fluxes would require GM90 as well as a parameterization for the Reynolds stresses. Alternatively, a parameterization could be attempted for the potential vorticity fluxes directly without either of these, though this would require a completely different conceptual and computational approach. It should be said that having a mesoscale parameterization

[27] Quasigeostrophy is the most natural framework in which to discuss potential vorticity, and is particularly useful because of the analogy between the QG potential vorticity on z surfaces and Ertel potential vorticity on isopycnal surfaces (Charney and Stern, 1962).

be in the momentum equation is at least as justifiable as having it in the thermodynamic equation for scales of Rhines or smaller (Zhao and Vallis, 2008).

The argument over whether it is better to approach a mesoscale parameterization from the potential vorticity angle or the thermodynamic angle is ongoing. Potential vorticity is a natural candidate for a diffusive parameterization because of its homogenization along isopycnal surfaces, so one might try applying the flux-gradient relation to achieve a downgradient eddy flux (Plumb and Ferrari, 2005). One odd consequence of this is that, even with horizontally flat isopycnals, the meridional gradient of potential vorticity (the β term) causes the fluxes to be nonzero. Some feel that this is natural, arguing that eddies drive the circulation toward a state of motion (Holloway, 1992; Treguier et al., 1997; Greatbatch, 1998) rather than toward a state of rest. Disagreement over this issue may be more philosophical than physical.

1.6.6 Limitations of GM90

Despite the fact that the GM90 parameterization is built upon the phenomenology of baroclinic instability, there do remain certain aspects of the phenomenology that GM90 fails to tap into.

- **The inverse cascade.**The first, and perhaps most glaring, of these deficiencies is that GM90 fails to account for strong eddy-eddy interaction (Ferrari et al., 2010). Such interaction results in an inverse energy cascade (Kraichnan, 1967), wherein eddies grow to larger length scales and can have very nonlocal effects. Presumably, this phenonemon could be captured in the diffusivity κ, but this is a separate problem and will be considered later.

- **Dissipation.** Related to the inverse cascade issue is the question of how the eddy energy is dissipated. Because GM90 does not account for the inverse energy cascade, it implicitly assumes that eddies are damped locally and adiabatically (Tandon and Garrett, 1996). This in itself implies that there must exist some mechanism by which energy is nonlinearly transferred back to smaller length scales. GM90 was not designed to account for dissipative

processes that might solve this dilemma, such as breaking internal waves, convection, and shear instability. Even so, evidence suggests that the dissipation contributed by these small-scale, three-dimensional motions is too small to balance the budget of energy and tracer fluxes (Wunsch and Ferrari, 2004). It stands to reason that there is some mechanism at intermediate scales[28] that contributes the remainder of the dissipation (McWilliams, 2003; Mahadevan, 2006). In any case, GM90 is ill-equipped to deal with this conundrum.

- **Diapycnal Mixing.** The assumption that the motion is damped locally and adiabatically precludes diapycnal mixing by eddies. However, observations indicate that the total amount of diapycnal mixing required to balance the eddy energy budget is not small (Tandon and Garrett, 1996), and that it should be accounted for in ocean models. It is possible that the adiabatic motion of the mesoscale eddies acts in series with the smaller dissipative agents listed above (internal wave breaking, etc.), and that this issue isn't the fault of GM90 but rather that these smaller processes are not present in the model.

- **Energetics.** The work of Gent et al. (1995) shows that the potential energy equation (1.83) has a sign-definite sink on the right hand side, meaning that mean potential energy is locally converted to eddy kinetic energy. It is argued by Ferrari et al. (2010) that this is an unnecessarily strong condition, and that while there should certainly be domain-averaged sink of potential energy, there is no reason to believe that mesoscale eddies are local sinks of potential energy (Wolfe et al., 2008).

- **Numerics.** Numerically implementing the GM90 parameterization also has its challenges. Equation (1.82) reveals that the eddy-induced transport is dependent on both the local isopycnal slope and a variable diffusivity κ. In regions of weak stratification, convective processes can lead to infinite isopycnal slopes, generating unreasonably large eddy transports. While interpolation schemes can handle this issue in such regions, these methods

[28] This would imply the submesoscale, which is problematic because its motions are still governed by GM90-style baroclinic instability, but are confined primarily to the diabatic mixed layer where GM90 breaks down.

are physically unsatisfying and rely on imposing some arbitrary cap on the isopycnal slope.

- **Boundary conditions.** There remain outstanding issues about how to taper the GM90 parameterization to satisfy the vertical boundary conditions. At stated previously, the condition $w^* = 0$ at $z = 0, -H$ requires either the isopycnal slope or κ be set to zero at the boundaries. There is no reason to believe that the isopycnal slope becomes zero here, so usually κ is tapered to zero through some dynamically determined boundary layer. Unfortunately, many such tapering methods are ad hoc (Griffies, 2004). One could argue that in the boundary regions GM90 **should** break down because the flow is no longer adiabatic, violating the assumptions upon which the parameterization is built. This is a perfectly reasonable argument in theory, but in practice we must still account for eddy effects at the boundaries and in the absence of a better way to do this, tapering GM90 to zero is the easiest way to proceed. It is conceivable that this problem could be addressed by a suitable diagnosis for κ, a possibility which will be explored later.

1.6.7 Concluding Remarks

Despite its limitations, GM90 remains arguably the most successful subgridscale turbulence parameterization in OGCMs in the past twenty years. Early tests showed a vast improvement in the form of more realistic circulations and tracer distributions (Danabasoglu and McWilliams, 1995; England, 1995; Robitaille and Weaver, 1995); since then, studies largely have focused more on refining the theory (Dukowicz and Smith, 1997; Greatbatch, 1998; Dukowicz and Greatbatch, 1999), implementation in models (Griffies, 1998; Griffies et al., 1998), diffusivity (Held and Larichev, 1995; Visbeck et al., 1997; Smith et al., 2002; Eden and Greatbatch, 2008), and boundary conditions (Aiki et al., 2004; Griffies, 2004; Ferrari et al., 2008, 2010) rather than on trying to supercede GM90 with a new scheme.

1.7 Advective and Diffusive Fluxes

1.7.1 Combining Parameterizations

So far two parameterizations have been presented which must be included in a non-eddy resolving model. The first, the Redi tensor, represents along-isopycnal diffusion of tracer concentration, with the possibility of adding a small diapycnal component. This tensor captures the projection of this diffusivity into geodesic coordinates. The second parameterization, the GM90 tensor, represents an eddy flux of isopycnal layer thickness. It is meant to simulate the conversion of mean potential energy to eddy kinetic energy by baroclinic eddies, and appears as an additional advective flux in both the continuity and tracer equations. Because these two parameterizations capture two unique physical processes, it is reasonable to consider using them in concert with each other.

To this point we have not made explicit how to combine these two parameterizations in the same model. It is not immediately clear from the previous sections how one should go about this - mathematically, it would be most convenient if we were able to unify the form of both parameterizations in order to compare them properly. Fortunately, there exists a way to transform the GM90 parameterization into tensor form which will now be explored using the tracer equation.

Using the flux-gradient relationship, the tracer equation in a coarse-resolution model is

$$\frac{\partial \bar{\tau}}{\partial t} + \bar{\mathbf{u}} \cdot \nabla \bar{\tau} = \nabla \cdot \mathbf{R} \nabla \bar{\tau}, \tag{1.101}$$

where $\mathbf{R}$ is the 3×3 eddy mixing tensor. One can split $\mathbf{R}$ into the sum of an antisymmetric tensor, $\mathbf{A}$, and a symmetric tensor $\mathbf{S}$ by the rule

$$\mathbf{K} = \mathbf{A} + \mathbf{S} \tag{1.102}$$

$$A_{ij} = \frac{R_{ij} - R_{ji}}{2} \tag{1.103}$$

$$S_{ij} = \frac{R_{ij} + R_{ji}}{2}. \tag{1.104}$$

If we assume downgradient isoneutral diffusion, the symmetric tensor $\mathbf{S}$ is identically the Redi

tensor, so no further discussion about its physical meaning will appear here. It will now be shown that the divergence of $\mathbf{A}$ is equivalent to advection by eddy-induced velocity.

Consider equation 1.101 after the mixing tensor has been split,

$$\frac{\partial \bar{\tau}}{\partial t} + \bar{\mathbf{u}} \cdot \nabla \bar{\tau} = -\nabla \cdot (\mathbf{A} + \mathbf{S}) \nabla \bar{\tau}. \tag{1.105}$$

In computing the right hand side, we are asked to calculate the convergence of the antisymmetric tensor dotted with the tracer gradient. In index notation, this term can be written $\nabla_i A_{ij} \nabla_j \bar{\tau}$. We can take advantage of the antisymmetry of $\mathbf{A}$ by noting that $\nabla_i \nabla_j$ is a symmetric operator, meaning that $\nabla_i \nabla_j A_{ij} = 0$. Then by application of the product rule,

$$\nabla_i A_{ij} \nabla_j \bar{\tau} = \nabla_i \nabla_j A_{ij} \bar{\tau}. \tag{1.106}$$

We can define an advective velocity $u_i^* = -\nabla_j A_{ij}$, and note that it is nondivergent through the antisymmetry of $\mathbf{A}$:

$$\nabla_i \nabla_j A_{ij} = \nabla_i u_i^* = 0. \tag{1.107}$$

Reverting back to vector notation for a moment, we now have that $\nabla \cdot \mathbf{A} \nabla \bar{\tau} = \mathbf{u}_i^* \cdot \nabla \bar{\tau}$, so the tracer equation becomes

$$\frac{\partial \bar{\tau}}{\partial t} + (\bar{\mathbf{u}} + \mathbf{u}^*) \cdot \nabla \bar{\tau} = \nabla \cdot \mathbf{S} \nabla \bar{\tau}. \tag{1.108}$$

This demonstrates that the convergence of the antisymmetric tensor $\mathbf{A}$ operating on the tracer gradient is equivalent to advection by the nondivergent velocity $\mathbf{u}^*$ [29] . This gives rise to the term **skew flux** (Griffies, 1998), referring both to the skewness of the operator $\mathbf{A}$ and the fact that the resulting flux is orthogonal to the tracer gradient. Then if we were to use density as the representative tracer, a la GM90, the resulting flux would be precisely in the along-isopycnal direction, conserving domain-integrated mass within the isopycnal layer and leaving all moments of the density distribution unaffected.

[29] Furthermore, since $\mathbf{u}^*$ is nondivergent, we can define a vector streamfunction Ψ such that $\mathbf{u}^* = \nabla \times \Psi$. This is occasionally referred to in the literature as the **overturning streamfunction**, or **Quasi-Stokes streamfunction**. This is very closely related to the ψ defined in Section 1.3.2, but additional degrees of freedom in the TEM definition do not make the two exactly equivalent.

1.7.2 Equalities Using Statistical Turbulence

In order to emphasize the connection between the tensor **A** and the eddy-induced advection even more, we now segue to a different approach performed by Dukowicz and Smith (1997). They used a stochastic model for turbulent fluid transport in order to derive the continuity and tracer equations from an alternative perspective. Assuming that turbulence acts to displace fluid parcels in a random and Markovian fashion, one can construct the Fokker-Planck equation (Gardiner, 1983), which is equivalent to 1.101 except written in terms of conditional probability density functions. Using ensemble averaging, substituting $\bar{\rho}$ and the density-weighted tracer concentration $\hat{\tau} = \overline{\rho\tau}/\bar{\rho}$ into the Fokker-Planck equation gives

$$\frac{\partial \bar{\rho}}{\partial t} + \nabla \cdot \bar{\rho} \left(\tilde{\mathbf{u}} - \frac{1}{\bar{\rho}} \nabla \cdot \mathbf{K} \bar{\rho} \right) = 0 \tag{1.109}$$

$$\frac{\partial \hat{\tau}}{\partial t} + \left(\tilde{\mathbf{u}} - \frac{1}{\bar{\rho}} \nabla \cdot \mathbf{K} \bar{\rho} \right) \cdot \nabla \hat{\tau} = \frac{1}{\bar{\rho}} \nabla \cdot \mathbf{K} \bar{\rho} \cdot \nabla \hat{\tau}, \tag{1.110}$$

where **K** is an as-yet undefined diffusivity tensor. Dukowicz and Smith use a result from Monin and Yaglom (1971) to argue that the **residual circulation** $\tilde{\mathbf{u}} = \bar{\mathbf{u}} + \nabla \cdot \mathbf{K}$ (see also Section 1.3.2). One may then take advantage of the isomorphism between the the compressible density equation in z-coordinates and the thickness equation in isopycnal coordinates, seen as

$$\frac{\partial \rho}{\partial t} + \nabla \cdot \rho \mathbf{u} = 0 \qquad \longleftrightarrow \qquad \frac{\partial h}{\partial t} + \nabla_\rho \cdot h \mathbf{u} = 0 \tag{1.111}$$

$$\frac{\partial \rho\tau}{\partial t} + \nabla \cdot \rho\tau \mathbf{u} = 0 \qquad \longleftrightarrow \qquad \frac{\partial h\tau}{\partial t} + \nabla_\rho \cdot h\tau \mathbf{u} = 0, \tag{1.112}$$

where $h = \partial z/\partial \rho$. By demonstrating the functional equivalence of these equations, they form the ensemble-averaged eddy equations in isopycnal coordinates using 1.110 and 1.111:

$$\frac{\partial \bar{h}}{\partial t} + \nabla_\rho \cdot \bar{h} \left(\tilde{\mathbf{u}} - \frac{1}{\bar{h}} \mathbf{K} \cdot \nabla_\rho \bar{h} \right) = 0 \tag{1.113}$$

$$\frac{\partial \hat{\tau}}{\partial t} + \left(\tilde{\mathbf{u}} - \frac{1}{\bar{h}} \mathbf{K} \cdot \nabla_\rho \bar{h} \right) \cdot \nabla_\rho \hat{\tau} = \frac{1}{\bar{h}} \nabla_\rho \cdot \mathbf{K} \bar{h} \cdot \nabla_\rho \hat{\tau}. \tag{1.114}$$

Here we can demonstrate the connection between Eq. 1.81 and 1.113. The eddy-induced velocities $\mathbf{u}^*$ in these equations are

$$\text{GM90:} \qquad \mathbf{u}^* = -\frac{1}{h}\frac{\partial}{\partial\rho}\mathbf{K}\cdot\nabla_\rho z \tag{1.115}$$

$$\text{Dukowicz and Smith:} \qquad \mathbf{u}^* = -\frac{1}{h}\mathbf{K}\cdot\nabla_\rho\frac{\partial z}{\partial\rho}, \tag{1.116}$$

and are functionally equivalent if $\mathbf{K}$ is independent of density (or depth). The astute reader will recognize this condition as being the same required to reconcile GM90 with downgradient potential vorticity transfer. Smith and Gent (2004) note that the Dukowicz and Smith form was developed by considering turbulence isolated within a single isopycnal layer, so in reality it cannot distinguish whether $\mathbf{K}$ is outside or inside the $\partial/\partial\rho$ operator[30] .

Dukowicz and Greatbatch (1999) later refined this result using the same statistical turbulence approach. Assuming the turbulence is approximately geostrophic[31] (valid in the planetary geostrophy case, as well as for the quasigeostrophic case when the turbulence is homogeneous), they showed that the bolus velocity is a function of the potential vorticity, so that

$$\mathbf{u}^* = \frac{1}{q}\mathbf{K}\cdot\nabla_\rho q. \tag{1.117}$$

The main consequence appears in the tracer equation, which may now be written

$$\frac{\partial\hat{\tau}}{\partial t} + \left(\tilde{\mathbf{u}} + \frac{1}{q}\mathbf{K}\cdot\nabla_\rho q\right)\cdot\nabla_\rho\hat{\tau} = \frac{1}{\bar{h}}\nabla_\rho\cdot\mathbf{K}\bar{h}\cdot\nabla_\rho\hat{\tau}. \tag{1.118}$$

The Dukowicz and Greatbatch result is yet another window in which we can see the close analogy between the GM90 thickness flux and a potential vorticity flux. It is consistent with earlier arguments by Plumb (1979) and Andrews et al. (1987) that, in general, the symmetric tensor is tracer dependent, whereas the antisymmetric part (bolus velocity) is independent of the tracer. However, it also acts as a warning: a tensor diagnosis that relies on passive tracers must initialize the tracer fields to be roughly coincident with the potential vorticity field[32] .

[30] They also note that the GM90 form is much easier to implement numerically because the boundary conditions $w^* = 0$ at $z = 0, -H$ is satisfied by tapering κ to zero. McDougall and McIntosh (2001) note that uncertainty in the boundary conditions for the Dukowicz and Smith form can lead to false overturning and incorrect poleward heat transport.

[31] The exact condition required is that f dominates ξ in the potential vorticity equation.

[32] An equivalent way of saying this is that if one seeks a tensor $\mathbf{R}$ that satisfies the flux-gradient relationship for potential vorticity (or buoyancy), and one hopes to do this by a passive tracer method, then the passive tracer fields

1.7.3 Combined Redi and GM90

In terms of forming an eddy parameterization, the key point of these derivations is as follows. To review, the symmetric Redi tensor (neglecting diapycnal diffusivity and making the small slope approximation) in z-coordinates is

$$\mathbf{S} = \mu \begin{bmatrix} 1 & 0 & -\frac{\rho_x}{\rho_z} \\ 0 & 1 & -\frac{\rho_y}{\rho_z} \\ -\frac{\rho_x}{\rho_z} & -\frac{\rho_y}{\rho_z} & \frac{\rho_x^2+\rho_y^2}{\rho_z^2} \end{bmatrix}. \tag{1.119}$$

The GM90 parameterization introduces an advection by the eddy-induced velocity $\mathbf{u}^*$, which by 1.105 and 1.108 is equivalent to the divergence of the antisymmetric tensor $\mathbf{A}$. Then the GM90 parameterization in tensor form becomes

$$\mathbf{A} = \kappa \begin{bmatrix} 0 & 0 & -\frac{\rho_x}{\rho_z} \\ 0 & 0 & -\frac{\rho_y}{\rho_z} \\ -\frac{\rho_x}{\rho_z} & -\frac{\rho_y}{\rho_z} & 0 \end{bmatrix}. \tag{1.120}$$

In the tensor framework, restoring the full mixing tensor $\mathbf{R}$ is as simple as adding the Redi and GM90 tensors together (Griffies, 1998). Combined together, $\mathbf{R}$ becomes

$$\mathbf{R} = \begin{bmatrix} \mu & 0 & -(\mu-\kappa)\frac{\rho_x}{\rho_z} \\ 0 & \mu & -(\mu-\kappa)\frac{\rho_y}{\rho_z} \\ -(\mu+\kappa)\frac{\rho_x}{\rho_z} & -(\mu+\kappa)\frac{\rho_y}{\rho_z} & \mu\frac{\rho_x^2+\rho_y^2}{\rho_z^2} \end{bmatrix}. \tag{1.121}$$

The crucial simplification comes upon inspecting the Dukowicz and Smith tracer equation 1.114, which suggests that **the Redi and GM90 diffusivities should be equal.** With this result in hand, the combined Redi and GM90 mixing tensor is

$$\mathbf{R} = \kappa \begin{bmatrix} 1 & 0 & 0 \\ 0 & 1 & 0 \\ -2\frac{\rho_x}{\rho_z} & -2\frac{\rho_y}{\rho_z} & \frac{\rho_x^2+\rho_y^2}{\rho_z^2} \end{bmatrix}. \tag{1.122}$$

must be initialized broadly similar to the potential vorticity (or buoyancy) fields.

Note that the tensor components above the diagonal all reduce to zero under this simplification. In a 3D simulation, taking a zonal average effectively reduces $\mathbf{K}_g$ to a 2×2 tensor, in which case it becomes

$$\mathbf{R} = \kappa \begin{bmatrix} 1 & 0 \\ -2\frac{\rho_y}{\rho_z} & \frac{\rho_x^2+\rho_y^2}{\rho_z^2} \end{bmatrix}. \tag{1.123}$$

1.7.4 Summary

In summary, the key results demonstrated in this section are:

(1) The antisymmetric tensor $\mathbf{A}$ represents advection by a nondivergent velocity $\mathbf{u}^*$.

(2) The stochastic model of Dukowicz and Smith (1997) arrives at a similar functional form for $\mathbf{u}^*$ as does GM90, up to placement of the $\partial/\partial\rho$ operator.

(3) The overturning streamfunction $\mathbf{\Psi}$, which arises as $\nabla \times \mathbf{\Psi} = -\nabla \cdot \mathbf{A}$ is related to the off-diagonal components of $\mathbf{R}$.

(4) The Redi and GM90 tensors can be combined to form the full eddy mixing tensor $\mathbf{R}$.

(5) The Dukowicz and Smith result greatly simplifies the form of $\mathbf{R}$ by predicting equal diffusivity coefficients, as is illustrated in Griffies (1998).

A diagnosis of $\mathbf{R}$ in an eddy-resolving model should therefore look for the following features:

(1) For the symmetric tensor, a Redi-like structure where all of the elements are proportional to each other by a factor of isopycnal slope.

(2) $R_{yz} \approx 0$, which would support the Dukowicz and Smith derivation.

(3) A diffusivity κ, which will appear as the top left element of the tensor, which is spatially variable.

It is this last point which is the main focus of this research. To this point, physical considerations have assisted us in building up the Redi and GM90 parameterizations, and as a result we have a

general tensor **structure** which we can verify in a model. The difficulty lies in the fact that κ is unknown - it is a property of the flow, not the fluid, and could conceivably be slave to many different physical parameters (velocity, stratification, rotation, etc.). To make matters even worse, the numerics of the model itself also play a role, as the local value of κ will be tied to the amount of unresolved turbulence in the model (i.e. the grid resolution). Fortunately, there does exist a body of research, both observational and theoretical, which might steer us in the right direction.

1.8 Studies on Eddy Diffusivity

1.8.1 Observational Experiments

As discussed previously, mesoscale eddy parameterizations generally cannot be validated with real ocean data due to the inherent difficulty of collecting observations. This has partly to do with the spatial and temporal scales of the eddies themselves, since they are quite large and evolve slowly. Oftentimes parameterizations are checked numerically by observing their effects on the locations of large current structures (see below). One must think carefully about how to design an experiment so that the correct parameters are being measured. For diffusivity, many different measurement techniques and inversion methods exist.

Generally estimates of κ have been calculated from observations using three main techniques (Marshall et al., 2006):[33]

- Mooring data can be used to calculate cospectra of eddy velocity and temperature, thereby giving $\overline{\mathbf{v}'T'}$ directly. If the mean gradient $\nabla\bar{T}$ is calculated as well, then one can employ the flux-gradient relationship to invert for κ. However, the time series required to calculate the cospectra are usually so short as to make interpretation difficult. Also, this technique has not been used often, so it is unclear about how general the extant statistics from this method actually are. A more serious issue lies in the use of Eulerian data to measure

[33] Sadly, Flierl and McWilliams (1977) suggest that most of our observational data is not dense enough to be statistically significant anyways! One then wonders how much stock to put into observations for informing eddy parameterizations...

Lagrangian quantities, since it can be contaminated by large nondivergent eddy fluxes that have no role in eddy-mean interaction (Marshall and Shutts, 1981).

- Floats and drifters offer another route to estimating diffusivity which is useful because they are Lagrangian in nature. They are constrained to follow particle trajectories and thus can only measure isopycnal diffusivity. One commonly used interpretation method is to measure the displacement of two floats relative to each other, from which an estimate of two-particle diffusivity can be made. The main downfall of this method is that the reported diffusivities are not straightforwardly interpretable in terms of the values that must be used in large-scale ocean models due again to the conversion from Lagrangian to Eulerian quantities. For an excellent review of Lagrangian observation techniques, see LaCasce (2008).

- Satellite altimetry allows for diffusivity estimates using the root mean square sea surface height field. This method was pioneered by Holloway (1986), after which many subsequent studies have been designed (see below). The main drawback to this method is that the results are valid only for the ocean surface, however. Also, this method only measures dimensional quantities such as eddy velocity and length scale, so it can tell us nothing about dependence on nondimensional parameters.

The following is a survey of papers that have attempted to diagnose eddy characteristics (diffusivity, cospectra, kinetic energy, etc.) through the above observational methods. This list is by no means comprehensive[34] .

- Munk (1966) wrote a seminal paper prescribing a diapycnal diffusivity of 10^{-4} m^2 s^{-1} to maintain the abyssal stratification against global upwelling associated with 25 Sv of deep water formation. In the same paper, he cites microstructure measurements and dye release experiments pointing to diffusivity on the order of 10^{-5} m^2 s^{-1} at middepth.

[34] However, most of these papers cross-reference each other, and so this is certainly a large sample of the literature on this topic.

- Whitehead Jr. and Worthington (1982) used both current meter data and geostrophic data from the northwestern Atlantic basin to calculate diapycnal diffusivities ranging from $1.0 - 3.9 \times 10^{-4}$ m^2 s^{-1}. Their geostrophic data was only reconcilable with the current meter data if they assumed that the potential temperature of the water was between 1.2 and 1.9^o C.

- Price (in Rossby et al. (1983) and McWilliams and Chow (1983)) used observations of SOFAR floats at 700 m and 1300 m depth to argue the relations $L_e = u_{rms}T_e$ and $\kappa = u_{rms}^2 T_e$, where the eddy timescale T_e is treated as a constant.

- Whitehead Jr. (1984) further evaluated the results of Whitehead Jr. and Worthington (1982) by comparing them to the data of Mantyla and Reid (1983), arguing that the two data sets are reconciled if the diapycnal diffusivity is closer to Whitehead and Worthington's geostrophic calculation of 3.9×10^{-4} m^2 s^{-1}.

- Olbers et al. (1985) developed maps of diffusivity in and below the mixed layer by inverting hydrographic observations in the North Atlantic. In the mixed layer and in strong current regions they found isopycnal diffusivities around 1.0×10^3 m^2 s^{-1} and diapycnal diffusivities of 1.0×10^{-4} m^2 s^{-1}. In the relatively quiescent region below the mixed layer each of these values tended to be an order of magnitude lower.

- Bryden and Heath (1985) used two years of time series measurements on the northern edge of the ACC to directly measure cospectra of eddy velocity and temperature. Among their findings that pertain to this research, they found that the eddies were vertically coherent at depths from 1,000 m to 5,000 m, affirming that mesoscale eddies affect the full water column.

- Krauß and Boning (1987) calculated Lagrangian eddy statistics using 113 buoys deployed in the North Atlantic, finding that the eddy diffusivity is spatially variable and linearly dependent on the RMS velocity. It is important to note that the buoys prevented them

from drawing any conclusions about the eddy statistics at depth.

- Saunders (1987) used six moorings and ten current meters to examine the flow through a gap in the East Azores Fracture Zone of the eastern Atlantic (considered important because here bottom water can be exchanged), estimating that diapycnal diffusivity ranges from $1.5 - 4.0 \times 10^{-4}$ m^2 s^{-1}.

- Keffer and Holloway (1988) used satellite altimetry to argue that a sensible way of measuring eddy heat fluxes across the ACC was to calculate eddy diffusivity first and employ the flux-gradient relationship to calculate eddy transport. They were successful in closing a long-standing problem related to heat and salt budgets in the Southern Ocean using this technique.

- Böning (1988) analyzed SOFAR floats to find a systematic depth dependence of mixing length in the North Atlantic. In contrast to the earlier paper (Krauß and Boning, 1987), he suggests that eddy diffusivity does not vary linearly with eddy kinetic energy, but that the eddy length and timescales are nonconstant and highly depth dependent. He warns that float statistics from different depth levels should be considered independent from one another.

- Barton and Hill (1989) used three hydrographic sections from the western Indian Ocean (Somali Basin) to calculate geostrophic transports through the region, noting that all water that enters the basin must be upwelled. They used a heat budget to calculate a required diapycnal diffusivity of $10.6 \pm 2.7 \times 10^{-4}$ m^2 s^{-1}.

- Poulain and Niiler (1989) released drifters into the California Current System and calculated the dispersion of single particles about the mean drift track. They found that the diffusivity tended to be proportional to the eddy kinetic energy, and tended to be about 4×10^7 cm^2 s^{-1}. They found that neither of the two diffusivity scalings $\kappa = \overline{u'^2}T$ or $\kappa = \overline{u'^2}^{1/2}L$ (Rossby et al., 1983; Krauß and Boning, 1987) was statistically superior when applied to

their dataset.

- Brink et al. (1991) used data collected from 77 drifters off the coast of California and found that eddy diffusivity increases with increasing eddy kinetic energy. They found anisotropic diffusivities in the California Current, with the diffusivity in the alongshore direction suppressed relative to the offshore component, averaging 8.0×10^7 cm^2 s^{-1}. Their analysis concluded that eddy length scale in the current could be treated as a constant.

- Davis (1991) reviewed the use of Lagrangian floats for determining eddy statistics. He cautioned that eddy length and time scales would vary with changing eddy kinetic energy, and that a tendency for diffusivity observations to follow either Rossby et al. (1983) or Krauß and Boning (1987) would depend on the relative fluctuation of L_e and T_e.

- Paduan and Niiler (1993) analyzed drifter data collected in the northeast Pacific Ocean as part of the OCEAN STORMS experiment. Data from the 47 drifters revealed that the eddy kinetic energy was four times greater than the mean kinetic energy, and showed single-particle diffusivities from 1.1×10^3 m^2 s^{-1} to 1.6×10^3 m^2 s^{-1}.

- Ledwell et al. (1993) analyzed the vertical dispersal of a patch of SF_6 in the middle of the northern Atlantic Ocean over hundreds of kilometers and a period of five months, and found a diapycnal diffusivity of 0.11 ± 0.02 cm^2 s^{-1}. The authors note that this diapycnal diffusivity is so small that it would be appropriate to neglect diapycnal processes in the stratified oceanic interior, which is consistent with the parameterization framework of GM90-Redi.

- Spall et al. (1993) used data from 32 SOFAR floats in the Mediterranean outflow region and found nonlocal and anisotropic values for the horizontal eddy diffusivity. These values were $\kappa_x, \kappa_y = 21$ and 8.4×10^6 cm^2 s^{-1} in the core of the outflow, reducing to 4.3 and 3.5×10^6 cm^2 s^{-1} the the south of the core.

- Toole et al. (1994) created profiles of diapycnal eddy diffusivity using velocity and temper-

ature microstructure data collected in the Northeast Pacific and Northeast Atlantic oceans. They found depth-invariant diapycnal diffusivities on the order of 10^{-5} m^2 s^{-1} in the ocean interior, suggesting that basin-averaged eddy dissipation may be dominated by processes near the oceanic boundaries. In this study they assumed that the diffusivity was directly related to internal wave breaking, and that dissipation/diffusivity would be enhanced in regions of high internal wave activity.

- De Madron and Weatherly (1994) used hydrographic sections as part of the South Atlantic Ventilation Experiment to estimate transports of North Atlantic Deep Water and Antarctic Bottom Water in the Brazil Basin. They utilized the method of Whitehead Jr. (1984) to find diapycnal diffusivities of heat and salt to range from $3.6 - 7.2 \times 10^{-4}$ m^2 s^{-1}.

- Kunze and Sanford (1996) find agreement with Toole et al. (1994) in that the mixing needed to close deep global water-mass budgets cannot occur over the midlatitude abyssal plains. They applied a parameterization based on internal wave theory to 114 velocity profiles taken in the Sargasso Sea, finding an average diapycnal diffusivity on the order of 10^{-5} m^2 s^{-1}.

- Polzin et al. (1996) used CTD measurements to estimate diapycnal diffusivity as high as 150×10^{-4} m^2 s^{-1} in the Romanche fracture zone of the eastern equatorial Atlantic Ocean. They note that this region was immediately downstream of a narrow sill, implicating hydraulic control as a main cause of intense vertical mixing here.

- Swenson and Niiler (1996) used five years worth (1985-1990) of mixed-layer drifting buoy trajectories in the California Current System to find horizontal diffusivities ranging from 1.1×10^7 cm^2 s^{-1} to 8.7×10^7 cm^2 s^{-1}. They were not able to distinguish whether either of the diffusivity scalings (Rossby et al., 1983; Krauß and Boning, 1987) was statistically superior when applied to their dataset.

- Roemmich et al. (1996) used a 2 years worth (1992-1994) of CTD and hydrographic data

to determine transport characteristics through the Samoan Passage of the South Pacific Ocean. They found that extraordinarily high diapycnal diffusivities of up to 10×10^{-1} m^2 s^{-1} were necessary to balance the abyssal heat budget, supporting the notion that intense mixing can occur near sills and constricted passages.

- McCarthy et al. (1997) used WOCE hydrographic data from the Ninetyeast Ridge area (Indian Ocean) to determine the diapycnal diffusivity near a sill passage. From volume transport calculations they deduced the upwelling rate, from which vertical diffusivities of 1.1×10^{-2} m^2 s^{-1} at the sill and 1.3×10^{-3} m^2 s^{-1} immediately downstream were found.

- Polzin et al. (1997) used ocean microstructure data to infer diapycnal diffusivity of approximately 1.0×10^{-5} m^2 s^{-1} above the smooth abyssal plains of the South Atlantic Ocean. However, they also deduced diapycnal diffusivity exceeding 5.0×10^{-4} m^2 s^{-1} based on mixing rates above the Mid-Atlantic Ridge, suggesting that vertical mixing is linked to the underlying bathymetry.

- Ledwell et al. (1998) looked at this same patch of SF_6 on an isopycnal surface near 300 meters depth over a period of 30 months, and found time-varying diapycnal diffusivities ranging from 0.12 ± 0.02 cm^2 s^{-1} to 0.17 ± 0.02 cm^2 s^{-1}. They also inferred an isopycnal diffusivity of 0.07 m^2 s^{-1} at scales below the submesoscale, 2 m^2 s^{-1} in the submesoscale, and 1000 m^2 s^{-1} in the mesoscale. They also measured the straining of the initial tracer patch into longer filaments, from which they deduced exponential growth of the mesoscale strain field at a rate of $3.0 \pm 0.5 \times 10^{-7}$ s^{-1}.

- Bauer et al. (1998) developed a method using 17 years of near-surface drifter observations to estimate diffusivity from the inhomogeneity of the mean flow in the tropical Pacific Ocean. Between two observation sites in the North and South Equatorial Currents, they found horizontal mesoscale diffusivities ranging from 3×10^7 cm^2 s^{-1} to 15×10^7 cm^2 s^{-1}.

- Sundermeyer and Price (1998) compared float and tracer observations from the North

Atlantic Tracer Release Experiment and found a large-scale effective meridional diffusivity of $0.7 \pm 0.4 \times 10^3$ m^2 s^{-1} and a zonal effective diffusivity of $1.5 \pm 0.7 \times 10^3$ m^2 s^{-1}. They found these values by measuring the variance of a tracer patch when the tracer field is under the influence of the mesoscale strain field.

- Stammer (1998) estimated eddy energy and eddy scales using TOPEX/POSEIDON altimeter data and concluded that numerical models must account for the high variability in eddy diffusivity. He noted that there is a qualitative agreement between the linear Eady timescale and the eddy timescales inferred from the data.

- Phillips and Rintoul (2000) used a two-year time series of mooring data to analyze eddy heat and momentum fluxes in the ACC, and found that the eddy heat flux across the Subantarctic Front was large enough to balance heat lost south of the Polar Front. They found that the eddy potential energy was an order of magnitude larger than the EKE, and contribute to the growth of low-frequency motions (mesoscale eddies). They also found that the average eddy growth timescale was on the order of one month.

- Ledwell et al. (2000) measured tracer dispersion and turbulent energy dissipation in the Brazil Basin on the flank of the Mid-Atlantic Ridge, and found diapycnal diffusivities of $2.0-4.0\times10^{-4}$ m^2 s^{-1} at mid-depth and 10×10^{-4} m^2 s^{-1} near the bottom. They suggested that mixing here was due to breaking internal waves generated by tidal currents flowing over the rough bathymetry.

- Ganachaud and Wunsch (2000) used hydrographic data from WOCE along with high-resolution current meter data to seed an inverse model, from which abyssal velocities and diffusivities were calculated. They were able to calculate dianeutral diffusivities for each ocean basin, from which globally averaged values of $3.7 \pm 0.7 \times 10^{-4}$ m^2 s^{-1} at mid-depth and $9/ \pm 2 \times 10^{-4}$ m^2 s^{-1} in the deep abyss were found.

- Im Sang Oh et al. (2000) used WOCE/TOGA drifters in the Sea of Japan and the northwest

Pacific Ocean to estimate the horizontal diffusivity using the method of Davis (1991). They found that the spatial scale of the turbulence corresponded closely with the Rossby deformation radius, and that horizontal diffusivity ranged from $1.7 - 15.1 \times 10^7$ cm^2 s^{-1}.

- LaCasce and Bower (2000) used pair statistics of subsurface floats to calculate their dispersion relative to each other, from which single particle diffusivity was calculated by taking a derivative. They found that diffusivities at spatial scales of 50 km were $2.8 \pm 0.8 \times 10^3$ m^2 s^{-1}, and increased as a function of eddy length scale to the 4/3 power.

- Webb and Suginohara (2001) attempted to reconcile theoretical and observational evidence of the diapycnal diffusivity needed to mix the North Atlantic Deep Water vertically to the thermocline. They note that a background diapycnal diffusivity of 10^{-5} m^2 s^{-1} would mean that over half of the deep water upwelling would have to occur in regions of intense mixing (i.e. over rough bathymetry).

- Lumpkin and Flament (2001) calculated Lagrangian scales and diffusivities for the central North Pacific using surface drifter trajectories. Their diffusivities were found to range from $2.3 \pm 0.2 \times 10^3$ m^2 s^{-1} to $11.9 \pm 1.3 \times 10^3$ m^2 s^{-1} and were highly anisotropic. They found that neither of the two diffusivity scalings (Rossby et al., 1983; Krauß and Boning, 1987) was statistically superior when applied to their dataset.

- Morris et al. (2001) used vertical fluxes derived from large-scale temperature and density budgets along with a hydrographic dataset from the Brazil Basin to estimate diapycnal diffusivities in the range $1.0 - 5.0 \times 10^{-4}$ m^2 s^{-1}, confirming earlier results from Hogg et al. (1982) and Whitehead Jr. (1984).

- Lumpkin et al. (2002) measured Lagrangian eddy scales using eight years of float and drifter data (1989-1997) in the northern Atlantic Ocean. Among their conclusions was that Eulerian-based diagnoses of the horizontal diffusivity do not match Lagrangian diagnoses, and should be viewed with some suspicion (the exceptional cases being when either

the Lagrangian and Eulerian time or length scales match). They determined that eddy diffusivities can be measured easily in regions where the time or length scales are constant.

- Heywood et al. (2002) used station data in the Scotia Sea to construct a heat budget for water flowing into and out of this region. From their inverse calculations they inferred an average diapycnal diffusivity of $39 \pm 10 \times 10^{-4}$ m^2 s^{-1}, a very high value compared to other studies. They offered that this may be due to rough bathymetry.

- Zhurbas et al. (2003) derived maps of horizontal diffusivity and Lagrangian scales of eddy velocity, length, and time using drifter data from the Global Drifter Program/Surface Velocity Program. They found that the eddy length scale tended to be around the Rossby deformation radius in the midlatitudes and proposed that the diffusivity scales approximately as an eddy velocity times the deformation radius. Their method found high diffusivity values ranging from 2×10^3 m^2 s^{-1} on the low end to 3×10^4 m^2 s^{-1} on the high end.

- Zhurbas et al. (2004) followed their earlier study by analyzing surface drifters in both the Pacific and Atlantic Oceans along with mean circulation patterns. They found direct relationships between enhanced diffusivity and the presence of eddy-producing, meandering mean currents. Elevated values of horizontal diffusivity ($> 1.0 \times 10^4$ m^2 s^{-1}) were found in western boundary currents and in the equatorial currents, while more quiescent regions possessed diffusivities on the order of 10^3 m^2 s^{-1}.

- Fernández et al. (2005) conducted three cruises in the northeast Atlantic basin and found that eddy-induced vertical mixing modulated nutrient availability in the surface layer. They also found that single mesoscale eddies had a large effect on nitrate concentration on seasonal timescales.

- Garabato et al. (2004) found vertical diffusivities tending around 1.0×10^{-4} m^2 s^{-1} within the Antarctic Circumpolar Current using ship-borne hydrographic and current observa-

tions, but noted that much higher values (by up to three orders of magnitude) could occur due to bottom topography.

- Marshall et al. (2006) numerically monitored the straining of tracer contours in the Southern Ocean using satellite altimetry. They used a diffusivity metric developed by Nakamura (1996), in which an area coordinate is introduced to reduce the advection-diffusion equation to a pure diffusion equation. By the use of equivalent length, this method diagnoses the irreversible mixing generated by the eddy stirring.[35] Using the Nakamura method they found diffusivities of 2×10^3 m^2 s^{-1} on the equatorward flank of the ACC and 5×10^2 m^2 s^{-1} in the jet core. They note that low and high diffusivities correspond to regions of strong and weak potential vorticity gradients, respectively.

- Garabato et al. (2007) analyzed concentrations of helium emitted from hydrothermal vents near Drake Passage, calculating diffusivity by measuring the mean-square tracer displacement relative to the center of mass. They calculated a regional-average, cross-jet isopycnal diffusivity of 1840 ± 440 m^2 s^{-1}, with a suppressed diffusivity of 360 ± 330 m^2 s^{-1} in the jet core. Diapycnal diffusivities were found to average $3.2 \pm 2.3 \times 10^{-4}$ m^2 s^{-1}.

- Sallée et al. (2008) used 10 years (1995-2005) of surface drifter observations to compute eddy length and time scales in the Southern Ocean, finding eddy diffusivities on the order of 10^4 m^2 s^{-1} in energetic western boundary currents north of the ACC core. They test a parameterization based on satellite altimetric observations, $\kappa = 1.35\sqrt{EKE}L_d$ m^2 s^{-1}, and find that it is suitable for the core of the ACC (akin to Lumpkin et al. (2002)), this region has a constant eddy length scale proportional to the Rossby radius). Away from this region they find $\kappa = 1800 \pm 1000$ m^2 s^{-1}.

- Abernathey et al. (2010) used the Nakamura (1996) technique to diagnose the effective diffusivity in the Southern Ocean with a state estimate (Mazloff, 2008) of the eddying

[35] Other papers using this diagnostic in atmospheric contexts are Haynes and Shuckburgh (2000), Shuckburgh and Haynes (2003), Allen and Nakamura (2001), and Kostrykin and Schmitz (2006).

currents. Their method differed from Marshall et al. (2006) in that they meant to analyze diffusivity at depth by seeding a three-dimensional advection-diffusion equation with more observational data than was used in the earlier paper. The values they obtained were identical to those of Marshall et al.

- Ledwell et al. (2011) conducted a tracer release experiment on a density surface near 1500 m depth in the ACC west of the Drake Passage. A diapycnal diffusivity estimate of $1.3 \pm 0.2 \times 10^{-5}$ m^2 s^{-1} was formed by averaging the tracer concentration a year later over 82 vertical profiles. They also used EKE dissipation measurements to acquire an estimate of $0.8 \pm 0.1 \times 10^{-5}$ m^2 s^{-1}. They argue that it is doubtful that internal wave breaking is strong enough at middepth to support diapycnal diffusivities on the order of 10^{-4} m^2 s^{-1}.

In the end, the observational evidence clearly suggests that eddy diffusivity has widely ranging spatial and temporal variability. It is heavily modified in areas of rough topography or dominant mean flow features such as jets, and is closely related to both eddy kinetic energy and eddy length scale. Of course, the expense and difficulty of obtaining robust observational data cannot be overlooked - if anything, the above results should give the reader the impression that even studies using the same observational method can have very different results depending on sample size, sampling region, or even just the inherent randomness of eddies.

1.8.2 Numerical Experiments

The observational studies mentioned above demonstrate why values of isopycnal diffusivity on the order of 1000 m^2 s^{-1} and diapycnal diffusivities on the order of $10^{-5} - 10^{-4}$ m^2 s^{-1} are often used in OGCM mesoscale parameterizations. Unfortunately, the observational data does not make clear how to refine the parameters beyond these base values, and nowadays such issues are often addressed with numerical models[36] . These models have the advantage that they can simulate both

[36] This has largely been due to the advent of high-power supercomputing, so many recent observational studies have also had numerical modeling components as well.

simple, idealized flows as well as realistic flows with bathymetry, wind stress, and other forcing effects involved. A survey of modeling studies regarding eddy diffusivity appears as follows:

- Visbeck et al. (1997) attempted to apply the ideas of Green (1970) and Stone (1972**a**) to develop a functional form for the GM90 diffusivity. Their form, $\kappa = \alpha \frac{M^2}{N} l^2$, uses the Eady growth time scale $T = \sqrt{Ri}/f$. They show using three model experiments that the free, nondimensional parameter α is almost constant, $\alpha \approx 0.015$. It should be said that the use of this form is quite popular in ocean modeling, having earned a permanent place in the MITgcm model's option suite.

- Treguier (1999) used a channel model of a baroclinically unstable jet to test the flux-gradient relationship of potential vorticity. She found that the flux-gradient relation held well away from the diabatic surface region, and found that the appropriate mixing coefficient for potential vorticity along isopycnals matched that of passive tracer anomalies[37] She found that mixing was strongest at mid-depth. She argues that any diffusivity to be used with GM90 must be constant in the vertical since that is most consistent with a mixing scheme based on potential vorticity, which she strongly espouses in previous work (Treguier et al., 1997).

- McClean et al. (2002) analyzed Eulerian and Lagrangian drifter data from the North Atlantic to compare with results from two eddy-resolving simulations using the POP model. From the drifter data they found that the longest eddy length scales (highest diffusivities) were correlated with regions of strong EKE, and the longest timescales (lowest diffusivities) were in quiescent regions. They found that the eddy-resolving model produced a Gulf Stream with too many meanders and a southward displacement compared to reality, but noted that this may have been caused by other model parameters. They also found that the higher-resolution model (0.28^o) produced diffusivities that were too low in relation to the drifter data, which they attributed to the model being too hydrodynamically stable.

[37] This is in support of the notion that potential vorticity is advected as a passive tracer along isopycnals.

- Smith and Gent (2004) note that using a constant coefficient with the GM90 scheme results in solutions that are either less energetic or very noisy in comparison with results using biharmonic diffusivity closures. They also cite a personal communication with Frank Bryan (2003), saying that in a suite of 0.4^o North Atlantic experiments it was found that using a large, isotropic κ with GM90 results in maximized northward heat transport but damped nearly all eddy energy (so much so that the solution was reminiscent of the solution to a non-eddy-resolving model).

- Ferreira et al. (2005) used an adjoint model based the residual-mean formulation to infer eddy stresses in a high-resolution global simulation, finding horizontal diffusivities of up to 4000 $\mathrm{m}^2\ \mathrm{s}^{-1}$ in areas of strong eddy activity. They attempt to argue a scaling for κ that depends on the buoyancy frequency N^2, noting the similarity between their inferred vertical profiles for κ and N^2 when averaged over a region north of the ACC. However, we will argue later that a more sensible scaling is based on eddy velocity rather than N^2, and that their simulations likely hid this correlation due to surface intensification of all three quantities.

- Eden (2006) attempted to estimate κ from an eddy-resolving model of the Southern Ocean by first removing the rotational component of the raw eddy fluxes. Among his findings was a strong anisotropy of the diffusivity on the flanks of the ACC, with the highest values on the equatorward side (up to 2000 $\mathrm{m}^2\ \mathrm{s}^{-1}$). He also finds a decay of the diffusivity with depth.

- Eden (2007) measured eddy length scales for the North Atlantic using both satellite altimeter products and an eddy-resolving model. He found that the EKE spectra from the altimetry data and the model were in close agreement. His findings were in agreement with other studies suggesting that eddy length scale decreases with latitude, though he suggests that eddies near the equator are more proportional in size to the Rhines scale rather than the deformation radius. He finishes by suggesting that the eddy length scale to be used in

diffusivity calculations be set proportional to the minimum of the Rossby radius and the Rhines scale.

- Eden, Greatbatch and Willebrand (2007) used output from an eddy-resolving model of the North Atlantic to estimate the diffusivity appropriate for the GM90 parameterization. They investigated the effect of removing the rotational component of the eddy fluxes, finding that whether removed or not it was possible to obtain locally negative values for the diffusivity (where eddies are acting to increase APE). They found surface diffusivities ranging from 500 $m^2\ s^{-1}$ to 2000 $m^2\ s^{-1}$, decreasing to near zero below the thermocline. Note that they invert for κ using only the horizontal flux-gradient relationship $\overline{u'b'} = \kappa \nabla \bar{b}$, meaning that in reality they are testing the Redi diffusivity, not GM90.

- Danabasoglu and Marshall (2007) set up a model experiment using POP 1.4 and found that the isopycnal diffusivity varied in the vertical proportional to N^2. They found that their experimental results corresponded more closely to observations than did control experiments that used a constant diffusivity of 800 $m^2\ s^{-1}$. They found that the vertical structure and transport of the eddy-induced velocity in the north Pacific were in excellent agreement with the observational data of Roemmich and Gilson (2001). They also noted improved southward heat transport in the low- to mid-latitudes of the Southern Hemisphere, as well as a reduced warm bias in the upper ocean.

- Eden and Greatbatch (2008) developed a new closure for diapycnal eddy diffusivity and tested it in a coarse-resolution model of the North Atlantic. They showed that the diffusivities implied by their scheme matched results from a standard vertical mixing scheme in the stratified ocean interior. They also argue that, despite being small, the implied diffusivities remain physically relevant, especially in regions of high EKE. Note that they chose to subtract out the rotational component of the vertical eddy flux, arguing that it affects the calculation of the diapycnal diffusivity.

- Eden and Greatbatch (2009) examined the effects of different eddy closure schemes in a coarse resolution OGCM. They found that all of the closures (from Visbeck et al. (1997), a constant $\kappa = 800$ m^2 s^{-1}, from Danabasoglu and Marshall (2007), and from Eden and Greatbatch (2008)) had biases compared to observations. They noted that increasing κ near the surface of the tropical ocean had the effect of simultaneously lifting the equatorial thermocline and decreasing the strength of the ACC. They found that the Eden and Greatbatch closure also moved the pathways of the Gulf Stream and the North Atlantic Current to more realistic positions. The caveat to their simulations was that their implementation of Visbeck et al. (1997) had constant diffusivity in the vertical, so the effects of that closure may have not been properly represented.

- Shuckburgh et al. (2011) used an extension of the Nakamura (1996) effective diffusivity and calculated surface lateral diffusivities in a model of the ACC. They found that air-sea damping can augment the mixed layer lateral diffusivity by up to 500 m^2 s^{-1}. More importantly, they found that the effective diffusivity can vary greatly depending on the tracer. They found diffusivities of 200 m^2 s^{-1} for salinity, 1500 m^2 s^{-1} for temperature, and 2000 m^2 s^{-1} for chlorophyll in the ACC. Analysis conducted for the area north of the ACC showed similar differences between tracer species.

The reader will notice that the numerical studies listed above are able to address problems that would be impossible with observational data, such as eddy vertical structure, the validity of the flux-gradient relationship, and optimal scaling laws for the eddy diffusivity. For the sake of diagnosing a κ that is appropriate for OGCMs, numerical methods also have the built-in advantage that their results are unambiguous - the κ diagnosed from the model is precisely the κ that should be used in a model.

Before finishing, it should be mentioned that attempting to diagnose κ for the flux-gradient relationship is not the only possible approach to the mesoscale parameterization problem. One other avenue toward prescribing the eddy diffusivity can be followed by noting that the term that

actually enters into the tracer budget is the divergence of the eddy flux. This suggests an approach to an eddy closure using a Helmholtz decomposition

$$\overline{\mathbf{u}'\tau'} = \nabla\phi + \nabla \times \psi, \tag{1.124}$$

where ϕ is a scalar potential and ψ is a vector potential. This approach was first attempted in the atmospheric context by Lau and Wallace (1979).

The Helmholtz decomposition offers two additional approaches beyond the ones mentioned previously. The first possibility is to analyze (and hopefully parameterize) the eddy flux divergence directly, ignoring the flux-gradient relationship altogether. The second possibility is to remove the rotational part of the eddy flux (which has no effect in the mean tracer budget) before attempting to diagnose κ. In the oceanic context, only a limited number of studies have attempted either of these approaches. The majority of such studies are listed below:

- Marshall and Shutts (1981) suggested mathematically that the rotational part of the eddy fluxes is responsible for balancing the flow advection from the mean field, and that the divergent part is responsible for eddy-mean interactions. They noted that the dominance of the rotational component can mask important divergent components in diagnoses of the eddy diffusivity.

- Rix and Willebrand (1996) used data from an eddy resolving simulation of the North Atlantic to estimate the diffusivity coefficient to be used with GM90. They found that extensive averaging in both space and time was needed to obtain any sort of correlation between the eddy bolus velocity and the velocity induced by the parameterization. They were unable to determine any spatial or temporal variation of κ beyond a simple estimate that it should be of order 10^7 cm^2 s^{-1}, but they note that such variation is possible and likely necessary.

- Gille and Davis (1999) used the MOM model to run an eddy-resolving, wind-forced Eady channel experiment. After averaging in the along-channel direction, they found that the

eddy flux divergences were stronger than the mean flux divergences. They found that in time-averaged evaluations the GM90 parameterization (used with the Visbeck et al. (1997) diffusivity scheme) could account for nearly half of the eddy flux divergence, but that its skill dropped when considered locally in time.

- Bryan et al. (1999) used an eddy-permitting implementation of the POP model to evaluate thickness diffusivity. They found the highest diffusivity values where eddy activity was the strongest, particularly in the ACC, western boundary currents, and equatorial regions. They found that the rotational component of the bolus velocity was significant, and warned that it is large enough to affect verification of parameterization schemes even though it may not play into the mean equations. Among the different diffusivity scalings they tested, the best results were achieved by using the deformation radius as the eddy length scales and the inverse of the Eady growth rate as the eddy time scale.

- Roberts and Marshall (2000) used an eddy-resolving model to calculate mean eddy flux divergences of temperature, isopycnal thickness, and potential vorticity over a five-year modeling period. They found no correlation between raw eddy fluxes and the mean fields, but did find small correlation once the rotational component of the fluxes was removed. They find that the fluxes are not necessarily down the mean gradients, calling into question the need for purely downgradient eddy parameterizations.

- Nakamura and Chao (2000) used output from an eddy-resolving model of the North Atlantic to diagnose the eddy diffusivity associated with the GM90 parameterization. They found that κ varies enormously according to location and that the diffusivity field was very noisy, ranging from 10 $m^2\ s^{-1}$ to 10^7 $m^2\ s^{-1}$. However, their method was very sensitive to the timescale used to filter eddy components from the mean components. They note that a model should permit negative values of κ where the mean flow erodes the isopycnal thickness

gradient[38] .

- Peterson and Greatbatch (2001) analyzed output of two eddy-resolving shallow water models to investigate the validity of downgradient eddy parameterization schemes. They found that the divergent part of the potential vorticity and thickness fluxes were directed down their respective mean gradients, but the raw fluxes did not possess this feature. They argue that the rotational parts still play an important role in setting the proper bolus velocity in the models, and should not be ignored.

- Solovev et al. (2002) compared Fickian diffusion, Green-Stone, and GM90 as possible mesoscale eddy parameterizations using a idealized ocean model. They calculated the eddy heat flux divergence directly and compared results from a fine-resolution run with those from a coarse-resolution run using the parameterization schemes. Their analysis indicated that none of the three schemes were notably superior to the others, and that they failed to produce the correct sign of the divergence in the western boundary region. They suggest that the GM90 scheme failed to do better because the mean flow kinetic energy may be an important source of eddy kinetic energy. They also suggest that tapering schemes and a convective adjustment parameterization would likely improve its performance. Follow-up tests using a coarse-resolution real ocean model again failed to single out any of the parameterizations as superior. It must be noted that they used a constant diffusivity of 1000 m^2 s^{-1} for the GM90 parameterization, which is known to poorly reproduce observed features (see above).

- Fox-Kemper et al. (2003) show that a Helmholtz decomposition of the eddy fluxes into rotational and divergent components is not unique in a bounded domain, since the rotational part $\nabla \times \psi$ is invariant under a gauge transformation $\psi = \psi + \nabla\lambda$ and the divergent part $\nabla\phi$ is invariant under addition of a constant. There is also a lack of information

[38] That is, the eddy fluxes must always act against the fluxes of the mean flow, which means they should be able to both erode and enhance the tracer gradient when necessary.

about appropriate boundary conditions. The authors also point out a subtle difference between the divergent part of the flux and the flux divergence itself, warning that an eddy parameterization should be seen as a path towards the latter.

- Eden (2006) and Eden, Greatbatch and Olbers (2007) removed rotational fluxes before their analyses, both of which were summarized above.

- Griesel et al. (2009) diagnosed the rotational and divergent components of the eddy heat flux in an eddy-resolving model of the Southern Ocean. They found that the rotational component comprises over 95% of the total flux, becoming even more dominant with longer eddy length scales. Given this dominance, their diffusivity estimates using the total flux were as high as 15000 $m^2\ s^{-1}$, but dropped below 1000 $m^2\ s^{-1}$ when only the divergent part was considered. At small scales (i.e. those where mesoscale eddy parameterizations would be necessary), the relative importance of the divergent part grows, and they found that up to 40% of the eddy heat flux divergence could be accounted for using the divergent diffusivity value at scales less than 4^o wide.

The presumed advantage of pursuing this approach is that rotational fluxes can (and do) bias analysis if the diffusivity is computed from the raw eddy fluxes Griesel et al. (2009). The presence of these rotational fluxes is precisely the reason why Marshall et al. (2006) warn that it is unclear how observational estimates of κ relate to the κ used in OGCMs. A strong argument can be made that it is indeed only the divergent part of the fluxes that are relevant for diagnosing the κ in models, since it is the divergent flux which controls the eddy-mean (subgridscale-gridscale) interaction we wish to parameterize. However, this approach has two major unavoidable difficulties that have thus far prevented it from becoming truly mainstream. The first difficulty is that the determination of the diffusivity is not unique since it is inside the divergence operator, and would require additional information to constrain to a narrow range of values. The second, even more important difficulty is that it is unclear what kind of boundary conditions are appropriate when only considering the divergent flux. It is possible that some sort of numerical diagnosis (similar to

the one performed for this thesis) would be able to shed some light on this issue, but no such study has been conducted as of yet.

In conclusion, both observational and numerical evidence make clear the fact that κ varies horizontally, vertically, and with time. So far, we know that κ should be large in areas with high eddy kinetic energy, should be large near the surface ($O(1000\ \mathrm{m}^2\ \mathrm{s}^{-1})$, and should decay with depth. However, a common approach in the modeling community is to ignore the need for spatiotemporal variations of κ unless the solutions of a particular model are improved[39] (Griffies, 2004; Danabasoglu and Marshall, 2007). This practice has arisen due to the lack of observational and numerical evidence to guide a better method. Prescriptions for κ also suffer in this respect by the lack of a method that is computationally efficient, physically justified, and has been shown to improve model solutions. Therefore, the diagnosis for κ can really be considered an open problem in ocean modeling, one which shall receive focus through the rest of this research.

[39] The presence of many other tunable model parameters can often hide the negative effects of a poorly prescribed κ. In any case, one must not use this debate as an excuse simply to ignore κ and to tune other model parameters until the simulations look right.

Chapter 2

Tracer Gradient Matrix Pseudoinversion

2.1 Introduction

The ability to diagnose the entire eddy transport tensor $\mathbf{R}$ represents a significant advance over previous studies that attempt only to diagnose a scalar diffusivity or a tensor of limited structure. However, attempting to do so in a numerical model requires extra considerations that may not be apparent at first glance. Consider the flux-gradient relationship

$$\overline{\mathbf{u}'\tau'} = -\mathbf{R}\nabla\bar{\tau}, \tag{2.1}$$

where τ denotes an arbitrary passive tracer.[1] For now, consider the case when we have only one tracer in our model. Then in three dimensions, Equation 2.1 has a 3×1 vector on the left hand side, a 3×3 matrix $\mathbf{R}$, and a 3×1 vector with the tracer gradient. This equation is perfectly fine algebraically as long as $\mathbf{R}$ is already known. However, in our simulations $\mathbf{R}$ is **unknown** and is precisely what we would like to solve for. In this case there is an obvious problem, in that the two vectors $\overline{\mathbf{u}'\tau'}$ and $\nabla\bar{\tau}$ do not provide enough constraints on the solution of $\mathbf{R}$. This is known in linear algebra as an underdetermined system, and it features an infinite set of valid solutions for $\mathbf{R}$[2] .

[1] It is often assumed that the same transport tensor applies to all passive tracers (Eden and Greatbatch, 2009). Indeed, this assumption lies at the core of our method, and gives us the ability to try to solve for $\mathbf{R}$ using multiple tracers.

[2] Note that this does not invalidate the observational studies of the previous section. The aim of those was simply to diagnose a scalar diffusivity, which could be viewed mathematically as a nondimensional constant that multiples all of the elements of $\mathbf{R}$. In those studies, no more than one tracer is necessary, but of course the results of those studies only have limited usefulness in the evaluation of eddy parameterizations.

Basic linear algebra would suggest that three tracers are required to exactly determine $\mathbf{R}$, whereby the flux-gradient relationship becomes

$$\overline{\mathbf{u}_i' \tau_\pi'} = -R_{ij} \bar{\tau}_{\pi,j}, \tag{2.2}$$

where in Einstein notation the subscript before the comma is the tracer index and the subscript after the comma is the derivative index. As long as the tracer gradient matrix is nonsingular, matrix inversion would lead to a solution for $\mathbf{R}$ of the form

$$R_{ij} = -\overline{\mathbf{u}_i' \tau_\pi'} \left[\bar{\tau}_{\pi,j}\right]^{-1}. \tag{2.3}$$

In a full 3D simulation this approach would allow for $\mathbf{R}$ to be solved locally, and presumably the structure and diffusivity constant could be analyzed as functions of space and time. However, even with the speed of modern computing running full 3D simulations is very expensive, and unfortunately is prohibitively so if ones goal is to make an entire suite of models. Therefore, for this research it is useful to **zonally average** the simulations to effectively reduce the results from 3D to 2D[3] . In zonally averaged simulations we still retain a well-defined isopycnal slope featuring isopycnal and diapycnal diffusive fluxes, so whatever results are obtained could easily be generalized back to three dimensions. However, this averaging introduces an extra layer of complexity in the calculation of $\mathbf{R}$.

The zonal averaging operation hides a large number of degrees of freedom in both the high-resolution tracer gradients and the tracer fluxes. For example, consider a channel with n points in the zonal direction. Though each of the zonally-averaged quantities $\overline{\mathbf{u}}$ and $\overline{\tau}$ has only one degree of freedom, the bar operator actually hides n degrees of freedom for each of the raw fields $\mathbf{u}$ and τ. To make this point even clearer, the zonally averaged fluxes $\overline{\mathbf{u}\tau}$ hide n^2 degrees of freedom each! This means that we are averaging over a potentially huge amount of variability - this is by design, of course, but it also introduces the problem that our solution for $\mathbf{R}$ can be contaminated by individual, powerful eddies. We can alleviate some of the problem by choosing a long channel

[3] This is a common approach in the atmospheric literature (Plumb and Mahlman, 1987) and in idealized models of the Antarctic Circumpolar Current (Plumb and Ferrari, 2005).

(large n) so that such eddies do not overwhelm our averaging operation. Still, rather than trying to smooth over the noise by letting the channel grow to unreasonable lengths (causing the simulation time to become unreasonably long), it is entirely appropriate to use a channel of modest length and **overdetermine R** using multiple tracers, whose initial profiles are set as in 2.1.2.1. With this in mind, we would now view the solutions to **R** as an approximation, and like any approximation one must consider how to maximize the accuracy of the result[4] .

The solution to this issue is to **overdetermine** Equation 2.2 by using more than three tracers, which will in effect reduce the degrees of freedom in the averaging at the expense of computation time. As with any overdetermined set of equations, we must seek to minimize the variance in the data under some error norm. A classic approach is to perform a least-squares fit to the data, thus minimizing the Euclidean 2-norm between the data and the true result. It turns out that even in the case of a matrix inversion the procedure is straightforward and readily available in most mathematical software suites, and is known as the Moore-Penrose pseudoinverse.

2.1.1 The Moore-Penrose Pseudoinverse

The Moore-Penrose pseudoinverse is a generalization of matrix inversion, useful in cases where the number of rows m is not equal to the number of columns n. In this research, the matrix of tracer gradients satisfies this property as long as more than two tracers are being used, so it is useful to illustrate the properties of the pseudoinverse to understand what the solution means.

Consider the system of linear equations implied by the flux-gradient relationship

$$\overline{u_i'\tau_\pi'} = -R_{ij}\nabla_j\bar{\tau}_\pi \qquad \nabla\bar{\tau} \in \mathbb{R}^{m\times n};\ \overline{\mathbf{u}'\tau'} \in \mathbb{R}^{m\times n};\ \mathbf{R} \in \mathbb{R}^{n\times n}. \tag{2.4}$$

The pseudoinverse of $\nabla\bar{\tau}$, which we will denote with $(\nabla\bar{\tau})^\dagger$, has the following properties that are of interest. There are three distinct cases to consider:

- When $m < n$ there exists an infinite number of solutions to (2.1). In this case, the Moore-Penrose pseudoinverse gives the solution with minimal 2-norm. That is, $||\mathbf{R}||_2 =$

[4] "Accuracy" here pertains to minimizing the error metric (2.6).

$||\overline{\mathbf{u}'\tau'}\,(\nabla\bar{\tau})^{\dagger}\,||_2 \leq ||\mathbf{x}||_2$ for all possible solutions $\mathbf{x}$. It is worth noting that the vector 2-norm is identical to the standard definition of a least-squares solution, i.e. one that minimizes the sum of squares

$$S(\nabla\bar{\tau}) = \sum_{i=1}^{m}\sum_{\pi=1}^{n}(\overline{u_i'\tau_\pi'} + R_{ij}\nabla_j\bar{\tau}_\pi)^2. \tag{2.5}$$

- When $m = n$, the pseudoinverse is equal to the true inverse as long as $\nabla\bar{\tau}$ is of full rank. This case helps to illustrate why the psuedoinverse is considered a generalization of the true matrix inverse operation.

- When $m > n$, the system is overdetermined, meaning that there are more equations constraining the solutions than there are free variables. Then the pseudoinverse will be the solution that is closest in the least-squares sense to $\mathbf{R}$. That is, $||\overline{\mathbf{u}'\tau'}\,(\nabla\bar{\tau})^{\dagger} - \mathbf{R}||_2 \leq ||\overline{\mathbf{u}'\tau'}\,(\nabla\bar{\tau})^{\dagger} - \mathbf{x}||_2$ for all possible solutions $\mathbf{x}$.

Since we are interested in having as many tracers as is computationally feasible in the domain, we will almost always be considering the case when $m > n$.

2.1.1.1 Accuracy of the Inversion

The first concern that arises regarding the use of the pseudoinverse is how accurate of an answer it gives for $\mathbf{R}$ (along with the related question of how to even measure this accuracy). We know that after zonal averaging, the fluxes and gradients of the tracer fields are used to solve for $\mathbf{R}$, and that by definition we are assuming that the same representative $\mathbf{R}$ can be used for all tracers in the flow. Then the accuracy might be measured by checking how well $\mathbf{R}$ performs in reconstructing the fluxes of some tracer that was **not involved** in the inversion, for which a reasonable choice would be the buoyancy. The measurement is taken by comparing the diagnosed buoyancy fluxes with a set of "reproduced" fluxes derived by multiplying the inverted transport tensor $\mathbf{R}$ by the buoyancy gradient. That is, the relative error is given by

$$E(\overline{u_j'b'}) = \frac{\left|\overline{u_j'b'} - R_{ji}\nabla b_i\right|}{\left|\overline{u_j'b'}\right|}, \tag{2.6}$$

and is evaluated for both v' and w' (Fig. 2.2a-b)[5] . These errors are calculated by averaging over the region defined in Section 3.2.1. Even though buoyancy fluxes and gradients are not used in calculating R_{ji} (only those of passive tracers are), the 95% confidence interval in reproducing buoyancy fluxes has less than 7% relative error for the horizontal fluxes and 12% for the vertical fluxes in the Eady regime. Thus, **even though buoyancy and buoyancy fluxes are not used to constrain the calculation of R, the buoyancy fluxes are reproduced from the mean buoyancy gradient to high accuracy**. While passive and active tracers differ in whether they affect the evolution of the flow, the comparison here is whether they differ **given the same flow**. Thus, **all** components of **R** are constrained to agree with the eddy-induced evolution of the tracers, and buoyancy advection is accurate for free. Ideally, fluxes of potential vorticity, salinity, or any other nearly-materially-conserved scalar tracers active or passive would be similarly accurate, so long as the diagnosis of **R** has converged. However, numerically buoyancy and passive tracers are **exactly conserved** by the finite-volume code used, while potential vorticity is not. Indeed, reconstructed potential vorticity fluxes are noisier than those of buoyancy (2.1), so are not used as a check on the accuracy of **R**.

Previous numerical experiments (Rix and Willebrand, 1996; Roberts and Marshall, 2000; Eden and Greatbatch, 2008) have found low correlations between the diagnosed eddy diffusivity and the actual eddy fluxes, with the distributions of diffusivity often being noisy and permitting unphysically large or even negative values. This can be due in part to the presence of a large rotational component that does not affect the dynamics, but has the potential to contaminate the diagnosis of the eddy diffusivity (Gille and Davis, 1999; Bryan et al., 1999; Eden, 2006; Griesel et al., 2009). A good diagnostic method for **R** should therefore yield both good quantitative accuracy via (2.6) as well as an excellent representation of the dynamics in the flux divergence equation

$$\nabla \cdot \overline{\mathbf{u}'b'} = -\nabla \cdot \mathbf{R} \nabla \bar{b}. \tag{2.7}$$

The latter can be compared in a fashion similar to (2.6), except now the error of the flux divergence

[5] A robust method for initializing the tracers was found by experimentation to require six tracers, initialized in orthogonal directions and orthogonal functions (see further on in this chapter for discussion).

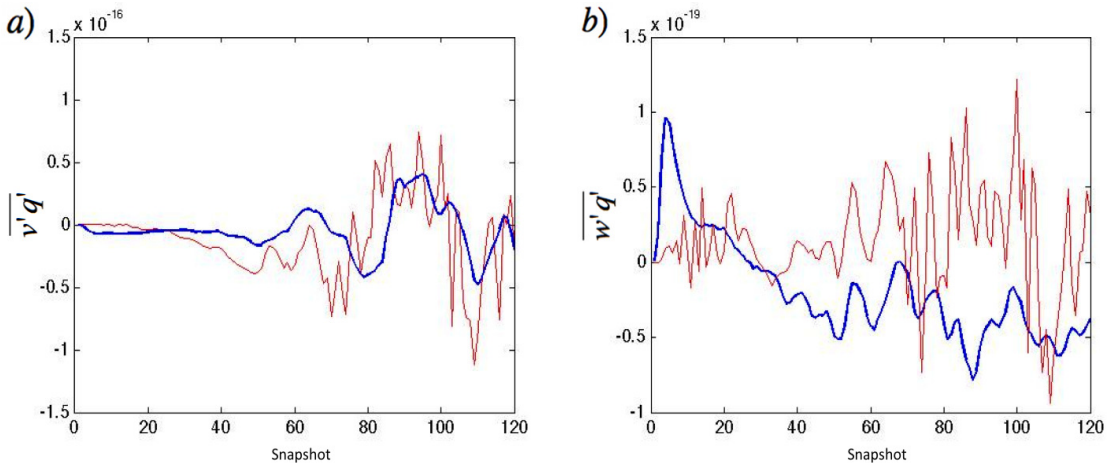

Figure 2.1: Reconstruction of the a) horizontal and b) vertical Ertel potential vorticity flux q defined in Section 1.6.5, taken at selected times (snapshots) over the course of an Eady-like simulation. Here a "snapshot" is taken to mean a fraction of the total simulation time, and is used as a nondimensional measure of the eddy growth timescale (2.1.3.4). The trend of the horizontal flux reconstruction (red line) loosely follows that of the true flux (blue line), though the noise is of the same magnitude as the signal. The noise can possibly be attributed to three factors: 1) the MITgcm does not conserve potential vorticity, 2) multiple interpolation and differentiation steps are required to project onto vorticity points, introducing noise, or 3) the passive tracer flux correlations simply do not match those of the potential vorticity. Given that potential vorticity is transported like a passive tracer along isopycnals, 3) is unlikely. However, the very small magnitude of the potential vorticity flux in the Eady problem (where the basic state $q = 0$) makes conservation of the tracer critical, so 1) is the most likely source of the noise.

is measured as

$$E(\nabla_j \overline{u_j' b'}) = \frac{\left| \nabla_j \overline{u_j' b'} + \nabla_j R_{ji} \nabla b_i \right|}{\left| \nabla_j \overline{u_j' b'} \right|}, \tag{2.8}$$

and is shown in panel c) of Fig. 2.2. The error in divergence is larger than the error in flux components, consistent with the added derivatives in (2.8) over (2.6). However, it is clear from the results based on (18) that the reproduction of fluxes by $\mathbf{R}$ also has skill in reproducing the flux divergences, not just rotational components of the fluxes.

2.1.2 Simulations Terminating in Finite Time

2.1.2.1 Tracer Initialization

The conditioning of the Moore-Penrose pseudoinverse depends on the degree to which the tracer gradients can be kept orthogonal. Such orthogonality is, of course, impossible to ensure in a freely-evolving, nonlinear flow model, as the symmetric tensor will work to align all of the tracer contours with the local isoneutral surface. For a model run of finite length, however, a clever initialization of the tracer fields might be able to maintain something close to orthogonality for as long as the simulation is running.

The most basic way to initialize a set of tracers with orthogonal gradients is to set them to be linear along each dimension of the domain. That is, impose the initial tracer fields to be

$$\tau_{2i-1}(y,z) = \frac{i\, y}{L_y} \qquad \tau_{2i}(y,z) = \frac{i\, z}{H}. \tag{2.9}$$

This method does not do very well in reconstructing the buoyancy flux $\overline{\mathbf{u}' b'}$, being particularly likely to give a noise reconstruction (Fig. 2.3). A more complex set of tracer fields is therefore required, which readily allows for more than three tracers to be uniquely initialized. Bratseth (1998) initialized the tracers to be products of Chebyshev polynomials because of their wavelike characteristics on the interval $[-1, 1]$, and because higher-order polynomials would effectively sample smaller eddies. Loosely following his approach, the tracer fields in this research are initialized sinusoidally. That is, the tracer concentrations at time $t = 0$ satisfy

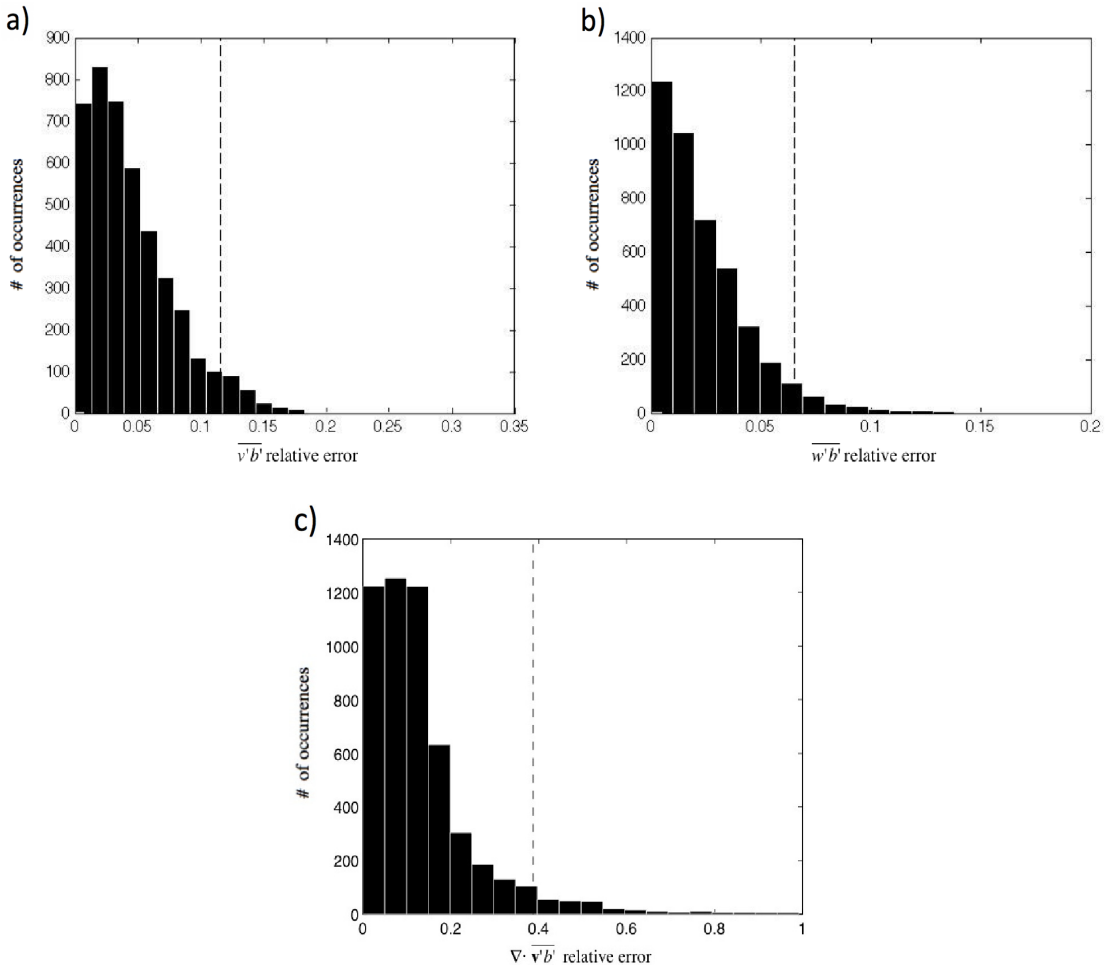

Figure 2.2: (a-b) The relative error in reconstructing the horizontal and vertical buoyancy fluxes in the Eady-like model, spanning all snapshots taken from all 69 simulations. Higher relative errors tend to occur at lower values of Ri. c) The relative error in reconstructing the eddy flux divergence. The dashed vertical lines in all panels indicate the 95% confidence interval.

$$\tau_{2i-1}(y,z) = \sin\left(i\frac{\pi y}{L_y}\right) \qquad \tau_{2i}(y,z) = \sin\left(i\frac{\pi z}{H}\right). \tag{2.10}$$

These tracer fields are qualitatively similar to Chebyshev polynomials in their obvious wave-like characteristics, but also because both sets of functions are orthogonal on a closed subset of $\mathbb{R}$. A set of tracers initialized with the gravest wavenumbers $i = \{1, 2, 3\}$ (Fig. 2.4) was found to produce the best results. Initializing the tracers in this way maintained misalignment of the tracer gradients until the simulation stopping criterion was reached. This misalignment was measured by the accuracy to which the reconstructed buoyancy fluxes approximated the actual buoyancy fluxes. Initializing the tracers sinusoidally led to no significant degradation of this approximation by the time the front had slumped to the lateral wall.

There is some subtlety in choosing how many tracers to implement. Using a large number of tracers, which by (2.10) initializes sine functions of high wavenumber, tends to accentuate progressively smaller eddies. Because the buoyancy is affected primarily by the largest eddies, such sampling suffers a loss of accuracy with respect to reconstructing the buoyancy fluxes (Fig. 2.5). Ensemble averaging over all possible sets of n tracers did show an improvement in accuracy as more tracers were used; however, the postprocessing time increased substantially and no ensemble was as accurate as simply using a modest number of tracers at low wavenumber. Six tracers were determined to be sufficient for a good approximation of the buoyancy fluxes.

The choice of six tracers is motivated by the desire to strike a balance between having enough tracer correlations for a strong least-squares fit and not losing accuracy due to having too many. Tracer fields with small initial gradient are used with the understanding that we want the eddy correlations of the buoyancy field and the tracer fields to match - that is, we want the tracer fields to correlate well with the largest eddies, just like the buoyancy does.[6] This approach minimizes

[6] Buoyancy traditionally plays an important role in quasigeostrophic (QG) and surface quasigeostrophic dynamics, as it is fundamentally connected to the QG streamfunction ($\partial\psi/\partial z = b$). In these frameworks, the boundary conditions on b specify potential vorticity sheets at $z = 0, -H$ (Bretherton, 1966**b**), and can be used to understand the baroclinic instability mechanism in the Eady (1949) problem. As the oceanic mesoscale is appropriate for QG scaling, we expect that the buoyancy will play a governing role in the dynamical evolution of the flow, making it an excellent tracer to "seek" with our pseudoinversion method.

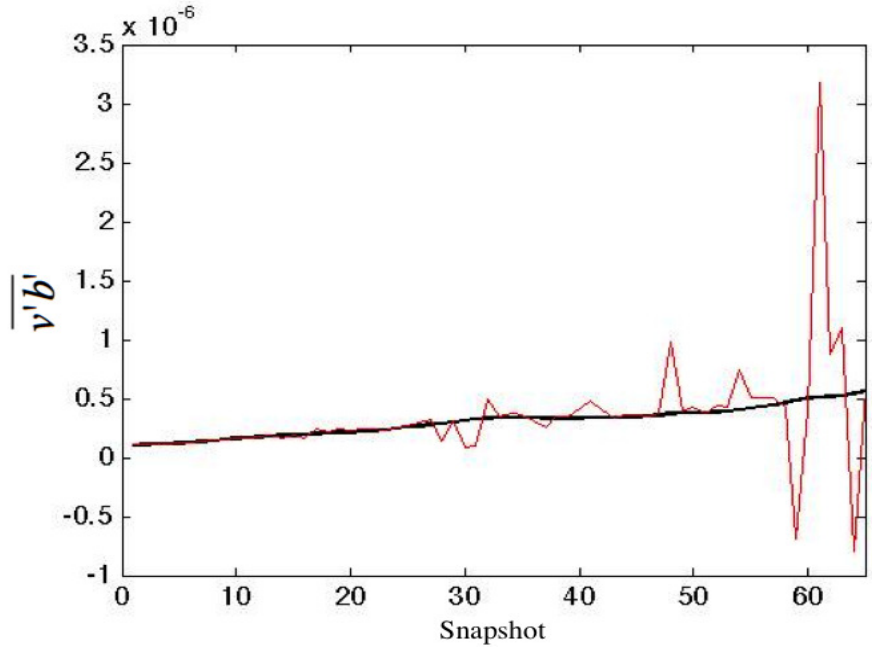

Figure 2.3: Horizontal buoyancy flux $\overline{v'b'}$ (solid black line) versus its reconstruction (red line) using the flux-gradient relationship (2.3) and tracers initialized as in (2.9), produced with data from a sample Eady-like run. Tracer fields initialized in this way produce accurate reconstructions in the early stages of the run, but they become subject to noise as the tracer gradients become collinear. The gradients of the initial tracer fields are so similar that this tends to happen long before the run is completed.

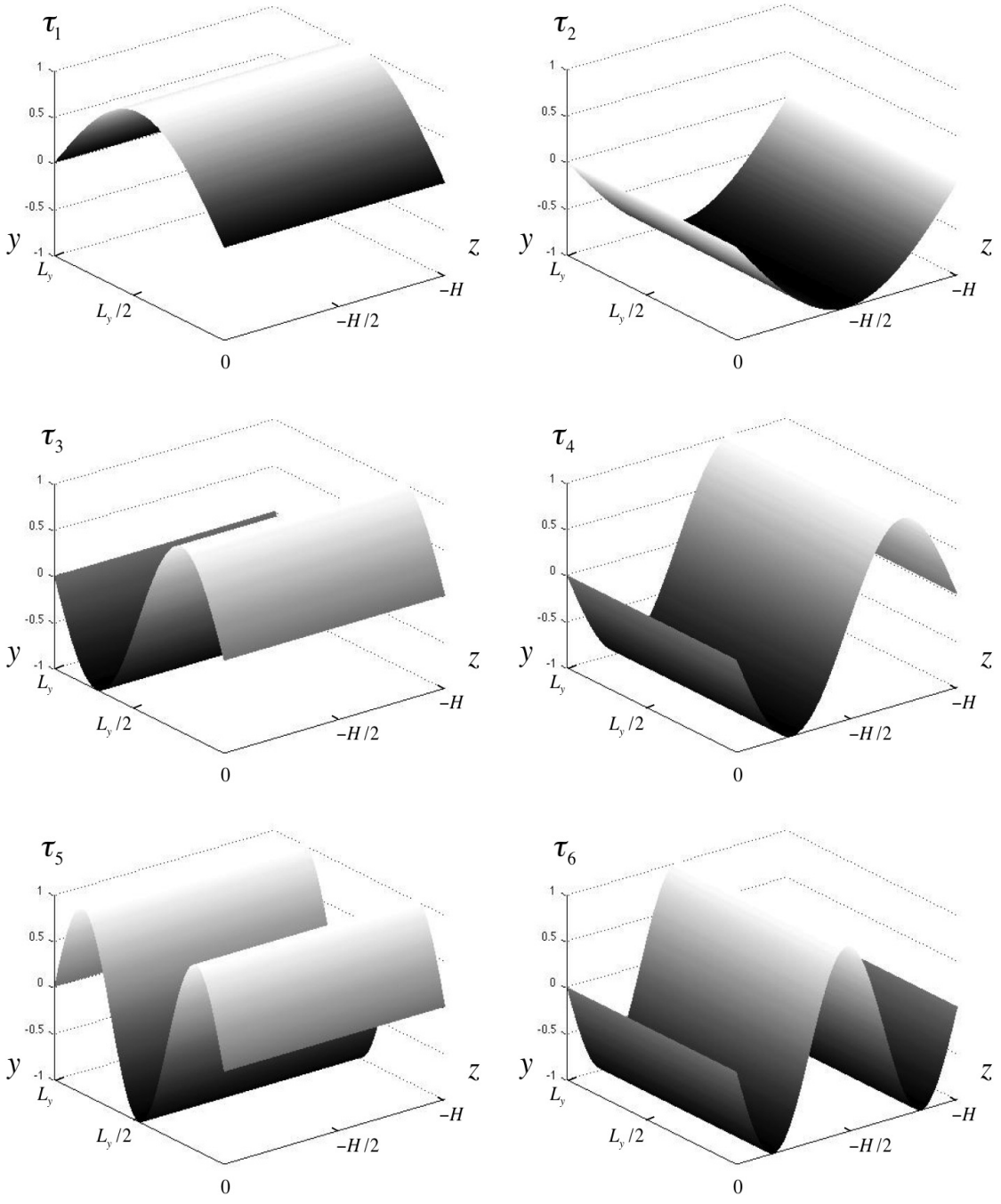

Figure 2.4: Initialization of tracer fields in y and z. All fields were constant in the zonal direction.

the reconstruction error in the domain-averaged sense, since broadly speaking the largest eddies are the dominant influence in a fully turbulent flow. However, this is not guaranteed to minimize the error **locally**, since small but powerful eddy features can show a poor correlation with these large-scale tracers.[7]

If we wanted to maximize the capability of the tracer reconstruction, we could initialize a large number of tracers and perform the reconstruction using each possible combination of six tracers[8] . In doing so we would try to find the exact combination of tracers that minimizes the reconstruction error at each point, saving the values of each tensor element each time the reconstruction is improved. If the goal really is to reproduce the buoyancy flux as accurately as possible, one could think of this approach as pushing the linear algebra of the pseudoinversion as far as it will go. The cost, of course, is an increase in processing time by a factor of $\frac{(n/2)!}{3!((n/2)-3)!}$, the number of extra tracer set combinations analyzed. Figures 2.6 and 2.7 show the outcome of using every combination of 32 tracers versus the standard six sinusoidal tracers described above. With the increase in processing time, however, this calculation went from taking 4 seconds per snapshot to 4×560 seconds ≈ 37 minutes. For a simulation with 100 snapshots the postprocessing would go from taking 6 minutes to nearly three days, a prohibitive amount of time. Fortunately, the tensor reconstruction remains very accurate even without having to go to these lengths, but there may be some applications where extreme accuracy is desired and would be worth the extra processing time.

2.1.3 Simulations Running Indefinitely

The symmetric operator $\mathbf{S}$ acts to align all of the tracer contours with the local isoneutral surface, so for long-duration model runs the Moore-Penrose pseudoinverse will slowly break down no matter how the tracers are initialized. A more sophisticated solution must then be used to maintain

[7] Note that using a particular set of tracers to maximize the accuracy of the reconstruction by (2.6) does not imply that a different $\mathbf{R}$ is needed for different metrics. The tensor $\mathbf{R}$ is a property of the flow, not of the tracers used.

[8] These would be initialized in complementary sets of two, so each sinusoid varying in y would be attached to its counterpart of the same wavenumber varying in z. Then really this is about choosing all possible combinations of **three** sets of tracers.

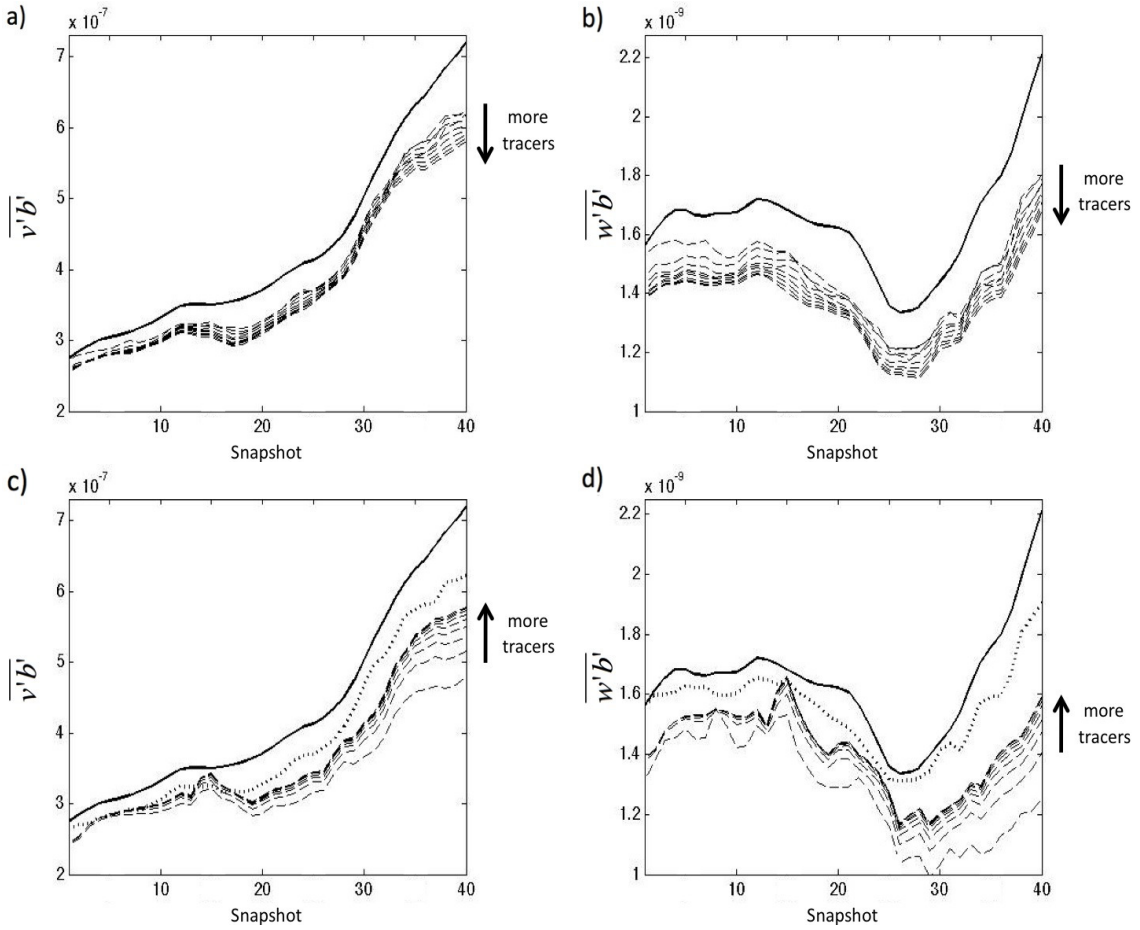

Figure 2.5: (a-b) Example of a time series reconstruction of a) $\overline{v'b'}$ and b) $\overline{w'b'}$ during one simulation, using $\{6, 8, 10, \ldots, 20\}$ tracers initialized using (2.10). The solid black line is the true value of the flux, while the dashed lines are the reconstructions. The reconstruction for both fluxes becomes less accurate as more tracers are used. (c-d) The same time series reconstruction using an ensemble average over all possible sets of n tracers out of 20 total. In this case the reconstructions become more accurate at reproducing the buoyancy flux as more tracers are used, but none are as accurate as using six tracers initialized at lowest wavenumber (dotted line).

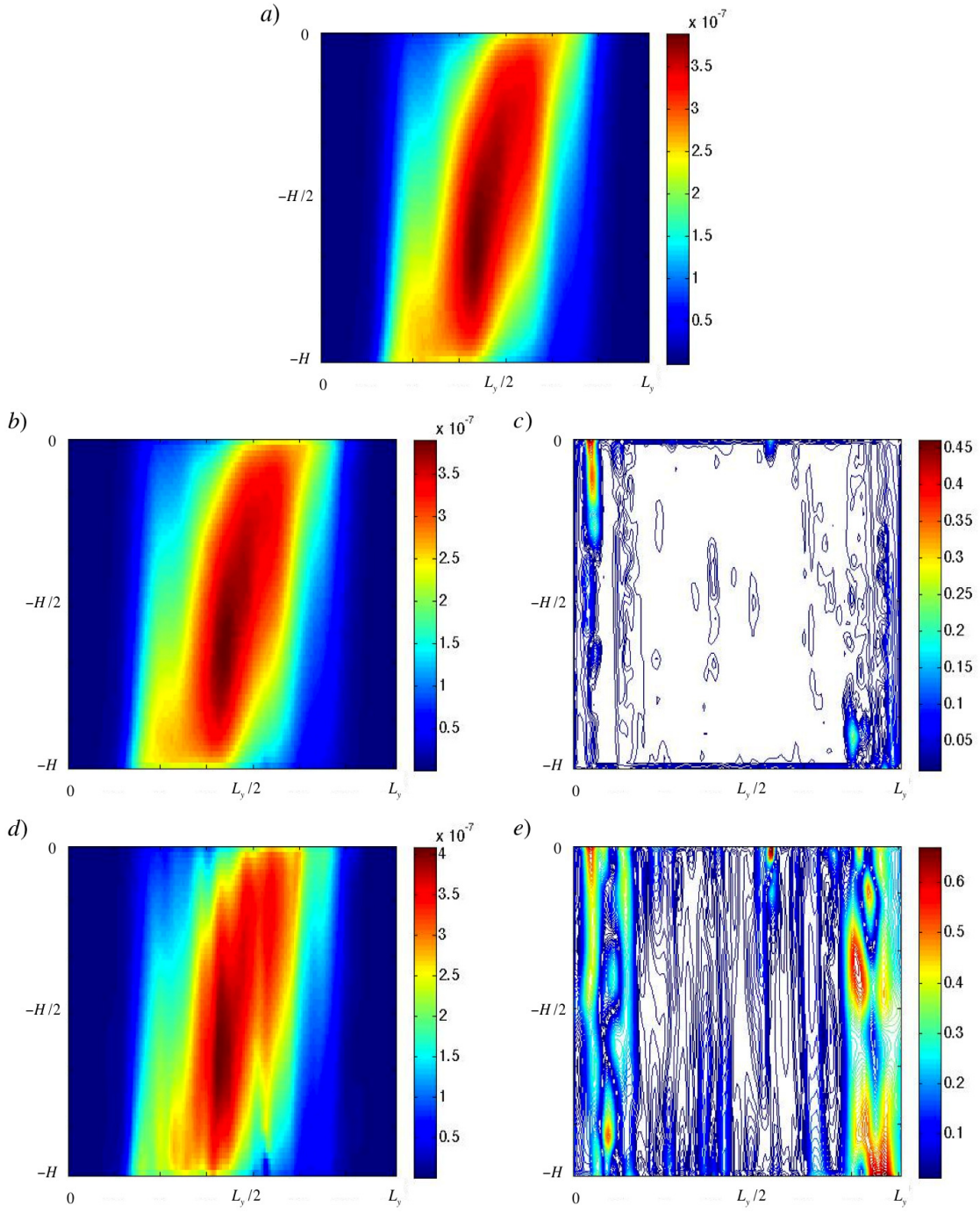

Figure 2.6: Zonally-averaged snapshots from a sample Eady-like run. a) True horizontal buoyancy flux $\overline{v'b'}$. b) Best possible reconstruction of $\overline{v'b'}$ using (2.3) and every possible combination of three pairs of tracers. The best reconstruction across all combinations is stored locally at every point, and each such optimal reconstruction is shown here. c) Local relative error of the reconstruction in b). The average relative error across all eddying points is ±1.7%. d) Reconstruction of $\overline{v'b'}$ using six tracers, using the fields shown in Fig. 2.4. e) Local relative error of the reconstruction in d). The average relative error across all eddying points is ±11.8%.

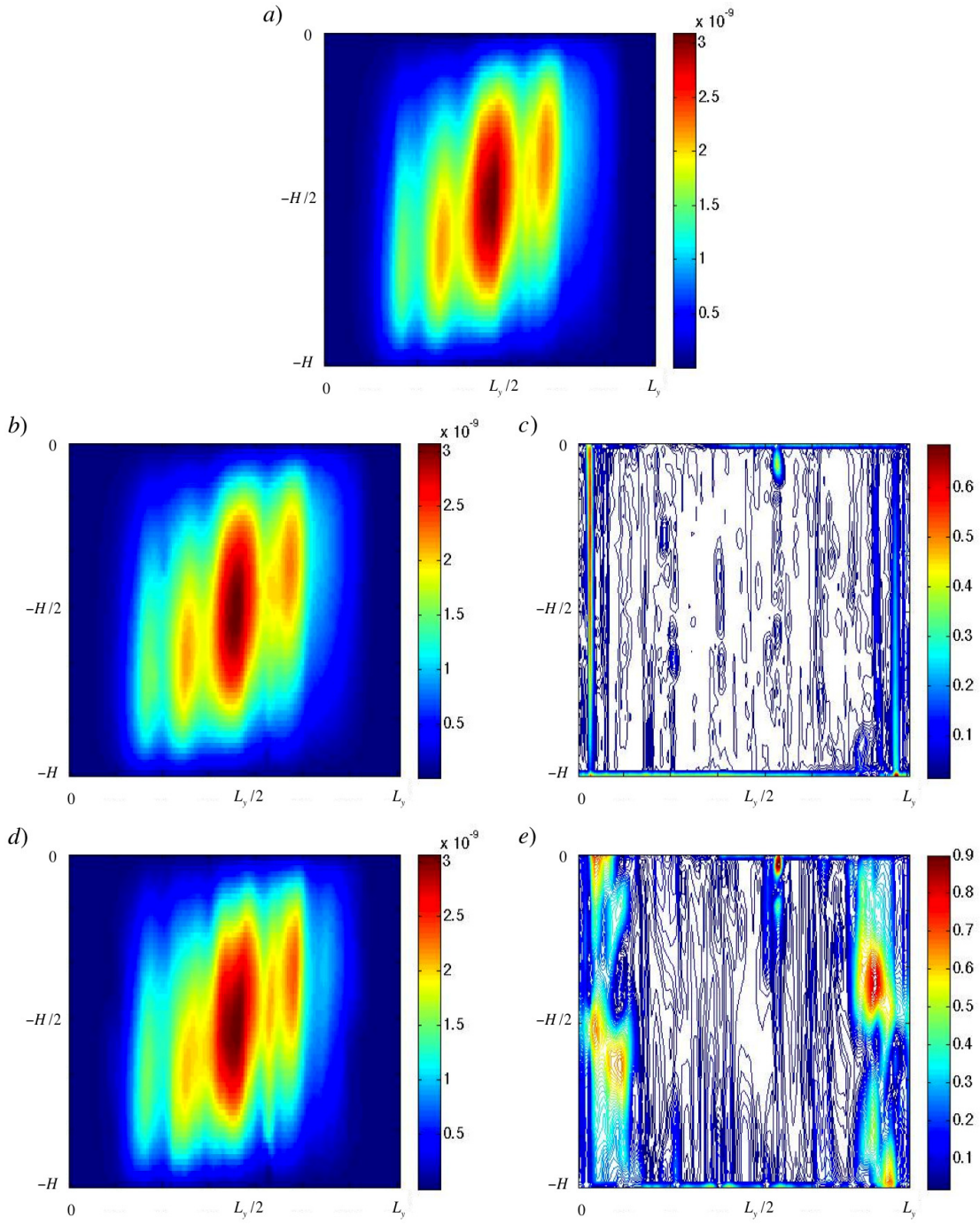

Figure 2.7: Zonally-averaged snapshots from a sample Eady-like run. a) True vertical buoyancy flux $\overline{w'b'}$. b) Best possible reconstruction of $\overline{w'b'}$ using (2.3) and every possible combination of three pairs of tracers. The best reconstruction across all combinations is stored locally at every point, and each such optimal reconstruction is shown here. c) Local relative error of the reconstruction in b). The average relative error across all eddying points is ±3.6%. d) Reconstruction of $\overline{w'b'}$ using six tracers, using the fields shown in Fig. 2.4. e) Local relative error of the reconstruction in d). The average relative error across all eddying points is ±13.6%.

misalignment of the tracer gradients. One such possibility is to slowly restore each grouping of tracers back to their initial configuration.

In this approach, each tracer pair is set to be weakly relaxed back to its initial state at a rate proportional to the eddy growth time scale from linear theory[9] . This approach still allows for **S** to progressively homogenize the tracer fields, but the differing rates at which the tracers are strained will keep them misaligned relative to each other. Unfortunately, this has the additional effect of making each tracer nonconservative. If we write the tracer conservation equation to be

$$\frac{D\tau}{Dt} = -\lambda\tau, \tag{2.11}$$

where λ is the relaxation time scale and the magnitude of the tracer sink is proportional to the tracer concentration itself, then the diffusive tensor **S** takes the form (Plumb and Mahlman, 1987)

$$\mathbf{S} = \begin{bmatrix} \frac{\partial}{\partial t}(\frac{1}{2}\overline{\eta^2}) + \lambda\overline{\eta^2} & \frac{\partial}{\partial t}(\frac{1}{2}\overline{\eta\zeta}) + \lambda\overline{\eta\zeta} \\ \frac{\partial}{\partial t}(\frac{1}{2}\overline{\eta\zeta}) + \lambda\overline{\eta\zeta} & \frac{\partial}{\partial t}(\frac{1}{2}\overline{\zeta^2}) + \lambda\overline{\zeta^2} \end{bmatrix}. \tag{2.12}$$

If we were to solve for **S** using the standard pseudoinversion (2.3), our solution would be contaminated by the tracer sink and we would obtain a suboptimal result. If we intend to use this method, we should seek out how to minimize the effect of the restoring on our result.

2.1.3.1 Effect on Tracer Variance

The above clearly demonstrates the effect that tracer restoring has on the diffusive tensor **S**, but what of its effects on the tracer variance and on the inversion for **R**? Consider the tracer conservation equation

$$\frac{D\tau}{Dt} = F, \tag{2.13}$$

where F represents sources and sinks. Under the standard rules for Reynolds decomposition, the tracer variance equation can be written

$$\frac{\partial}{\partial t}\left(\frac{\overline{\tau'^2}}{2}\right) + \bar{\mathbf{u}} \cdot \nabla\left(\frac{\overline{\tau'^2}}{2}\right) + \overline{\mathbf{u}' \cdot \nabla\left(\frac{\tau'^2}{2}\right)} + \overline{\mathbf{u}'\tau'} \cdot \nabla\bar{\tau} = \overline{F'\tau'}. \tag{2.14}$$

[9] This is obviously not the only way to set the restoring rate, but since the goal is to "undo" some of the turbulent flux, it is intuitive to relate it to the rate at which the turbulence is actually evolving.

If we define the mean of the Lagrangian evolution of tracer variance to be

$$\frac{D}{Dt}\left(\overline{\frac{\tau'^2}{2}}\right) \equiv \frac{\partial}{\partial t}\left(\overline{\frac{\tau'^2}{2}}\right) + \bar{\mathbf{u}} \cdot \nabla\left(\overline{\frac{\tau'^2}{2}}\right) + \overline{\mathbf{u}' \cdot \nabla\left(\frac{\tau'^2}{2}\right)}, \tag{2.15}$$

we have that

$$\overline{\mathbf{u}'\tau'} \cdot \nabla\bar{\tau} = -\frac{D}{Dt}\left(\overline{\frac{\tau'^2}{2}}\right) + \overline{F'\tau'}. \tag{2.16}$$

For spinup problems, Wilson and Williams (2006) note that tracer variance is initially zero and increases with time, so the $\frac{D}{Dt}$ term will be greater than zero. For a tracer source of the form $\frac{D\tau}{Dt} = \lambda\tau$, the above equation becomes

$$\overline{\mathbf{u}'\tau'} \cdot \nabla\bar{\tau} = -\frac{D}{Dt}\left(\overline{\frac{\tau'^2}{2}}\right) + \lambda\overline{\tau'^2}, \tag{2.17}$$

and so the tracer flux becomes less downgradient than for an unrestored tracer. Similarly, for a tracer sink $\frac{D\tau}{Dt} = -\lambda\tau$ we have

$$\overline{\mathbf{u}'\tau'} \cdot \nabla\bar{\tau} = -\frac{D}{Dt}\left(\overline{\frac{\tau'^2}{2}}\right) - \lambda\overline{\tau'^2}, \tag{2.18}$$

and the flux is more downgradient than for an unrestored tracer. Thus, a tracer sink will have a tendency to diffuse the original tracer gradient faster, and a source will diffuse it slower (or even sharpen it!). Of course, neither a pure source or sink is very useful for a simulation running for centuries of model time, nor does it necessarily help us in keeping the tracer gradients misaligned. To this end, the best compromise is to initialize the tracers so that their gradients are misaligned, and then to restore back to the initial profiles. Then the tracer equation becomes

$$\frac{D\tau}{Dt} = -\lambda(\tau - \tau_0), \tag{2.19}$$

where τ_0 is the local tracer value at time $t = 0$. This method was employed by Fox-Kemper et al. (2012) in their global diagnosis of $\mathbf{R}$.

Unfortunately, restoring back to a nonzero value means that we do not know at any given location or time whether there is a tracer source or sink! For all practical purposes, it doesn't matter, as this method works well in keeping the gradients misaligned (Fox-Kemper et al., 2012).

Unfortunately, it can have a significant effect on the least-squares inversion for $\mathbf{R}$, and the exact consequences are difficult to predict a priori. The effect of the restoring is felt by both the tracer flux and the tracer gradient, manifesting as a change in magnitude of both quantities.

In any case, if our goal is to match the eddy correlations of the passive tracers to that of the buoyancy, the restoring has a deleterious effect. In the models, we generally observe that restored tracers obeying (2.19) tend to underestimate the value of the buoyancy flux compared to unrestored tracers (Fig. 2.8).

2.1.3.2 The Minimum-Variance Solution

With the understanding that tracer restoring will lead to an irreversible loss of tracer variance, how might we account for this as we seek to solve for $\mathbf{R}$? It turns out that we can incorporate the effects of the restoring into the tensor itself and look for solutions not only to $\mathbf{R}$, but also to the restoration tensor $\mathbf{D}$ (defined below). This has the added benefit that $\mathbf{D}$ contains direct information about the eddy displacements, so we would gain additional information about the eddy behavior that otherwise would be unavailable.

As shown above, with a weak tracer sink the diffusive tensor will take the form

$$\mathbf{S}_{restoring} = \begin{bmatrix} \frac{\partial}{\partial t}(\frac{1}{2}\overline{\eta^2}) + \lambda\overline{\eta^2} & \frac{\partial}{\partial t}(\frac{1}{2}\overline{\eta\zeta}) + \lambda\overline{\eta\zeta} \\ \frac{\partial}{\partial t}(\frac{1}{2}\overline{\eta\zeta}) + \lambda\overline{\eta\zeta} & \frac{\partial}{\partial t}(\frac{1}{2}\overline{\zeta^2}) + \lambda\overline{\zeta^2} \end{bmatrix} \tag{2.20}$$

$$= \mathbf{S} + \lambda\mathbf{D}. \tag{2.21}$$

If we treat λ as the restoring rate in an infinite-time simulation, the flux-gradient relation

$$\overline{u_i'\tau_\pi'} = -(A_{ij} + S_{ij})\nabla_j\bar{\tau}_\pi \tag{2.22}$$

instead becomes

$$\overline{u_i'\tau_\pi'} = -\left[A_{ij} + \left(\frac{1}{2}\frac{\partial}{\partial t} + \lambda_\pi\right)M_{ij}\right]\nabla_j\bar{\tau}_\pi. \tag{2.23}$$

We would like to find the elements of $\mathbf{A}$ and $\mathbf{S} = \frac{1}{2}\frac{\partial}{\partial t}\mathbf{M}$ through some kind of matrix inversion or least-squares solution, but using tracer restoring introduces the problem of having extra terms

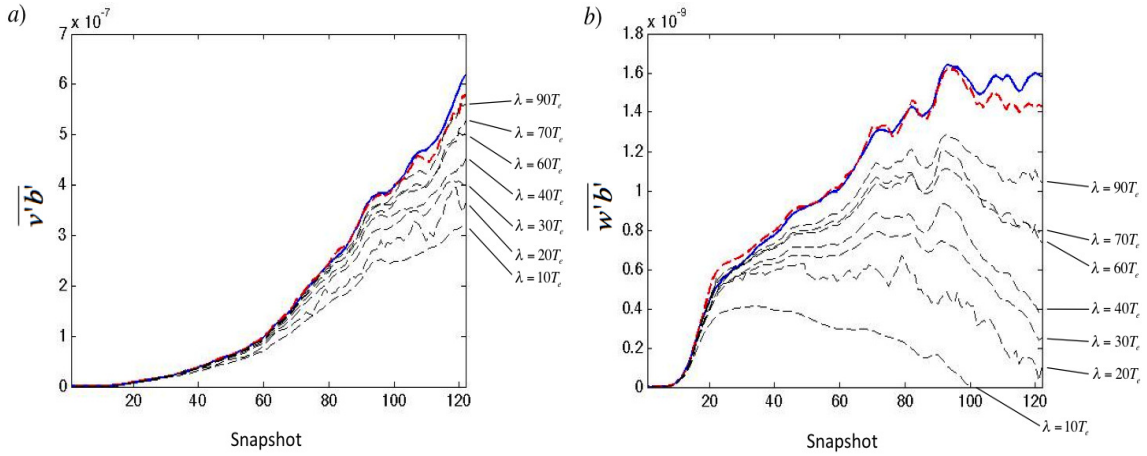

Figure 2.8: a) Horizontal and b) vertical buoyancy flux reconstructions (dashed black lines) from a sample Eady-like simulation. The restoring timescale λ for each set of tracers is set to be a multiple of T_e, the growth timescale of the fastest growing linear mode (Appendix C.2). The tracers are restored back to their initial values locally, tending to result in an underestimation of the true buoyancy flux (blue line). Longer restoring timescales asymptote to the reconstruction using no restoring (red line). The effect of the restoring is manifested stronger in the vertical fluxes, suppressing them completely after some time for $\lambda < 20T_e$ (panel b).

proportional to λ_π in the equation. One approach is to take advantage of the fact that the operator on the symmetric part of the tensor is linear, and so we can seek the solution to a linear system of the form

$$\mathbf{E}\mathbf{x} + \mathbf{n} = \mathbf{y}, \tag{2.24}$$

where we have

$$\mathbf{E} = \begin{bmatrix} \bar{\tau}_{1,y} & \bar{\tau}_{1,z} & 0 & 0 & \lambda_1\bar{\tau}_{1,y} & \lambda_1\bar{\tau}_{1,z} & 0 & 0 \\ 0 & 0 & \bar{\tau}_{1,y} & \bar{\tau}_{1,z} & 0 & 0 & \lambda_1\bar{\tau}_{1,y} & \lambda_1\bar{\tau}_{1,z} \\ \bar{\tau}_{2,y} & \bar{\tau}_{2,z} & 0 & 0 & \lambda_2\bar{\tau}_{2,y} & \lambda_2\bar{\tau}_{2,z} & 0 & 0 \\ 0 & 0 & \bar{\tau}_{2,y} & \bar{\tau}_{2,z} & 0 & 0 & \lambda_1\bar{\tau}_{2,y} & \lambda_2\bar{\tau}_{2,z} \\ \vdots & & & & \ddots & & & \vdots \\ \bar{\tau}_{m,y} & \bar{\tau}_{m,z} & 0 & 0 & \lambda_m\bar{\tau}_{m,y} & \lambda_m\bar{\tau}_{m,z} & 0 & 0 \\ 0 & 0 & \bar{\tau}_{m,y} & \bar{\tau}_{m,z} & 0 & 0 & \lambda_m\bar{\tau}_{m,y} & \lambda_m\bar{\tau}_{m,z} \end{bmatrix} \tag{2.25}$$

$$\mathbf{x} = \begin{bmatrix} R_{11} \\ R_{12} \\ R_{21} \\ R_{22} \\ D_{11} \\ D_{12} \\ D_{21} \\ D_{22} \end{bmatrix} \qquad \mathbf{n} = \begin{bmatrix} n_1 \\ n_2 \\ n_3 \\ n_4 \\ \vdots \\ n_{2m-1} \\ n_{2m} \end{bmatrix} \qquad \mathbf{y} = \begin{bmatrix} \overline{v'\tau'_1} \\ \overline{w'\tau'_1} \\ \overline{v'\tau'_2} \\ \overline{w'\tau'_2} \\ \vdots \\ \overline{v'\tau'_m} \\ \overline{w'\tau'_m} \end{bmatrix}$$

Here $\mathbf{E}$ as an $M \times N$ matrix, and will be an overdetermined system as long as $M > N$. This would suggest that we seek some sort of least-squares solution to the system.

The most direct way would be to simply solve the system by taking the Moore-Penrose pseudoinverse of $\mathbf{E}$. This has the advantage that the solution will be guaranteed to exist and be

unique, and that computing it is simple and accurate. This is not necessarily the best choice, however, for reasons explained below.

The linear system (2.24) is formulated by assuming small-amplitude displacements and steady turbulence (Plumb, 1979; Matsuno, 1980; Pyle and Rogers, 1980; Danielsen, 1981; Plumb and Mahlman, 1987), and just like any turbulence argument relying on linear theory, it cannot be expected to hold in a fully-turbulent, nonlinear regime. However, this does not preclude us from at least **trying** to solve (2.24) and seeing how the solution behaves, which unfortunately brings us to the more practical issue of the numerics.

The assumption of a "weak tracer sink" requires that λ be small, or equivalently, the terms in $\mathbf{E}$ multiplied by λ are small compared to rest. This inherently means that the λ terms will barely be felt by the pseudoinversion, which sets us up for a situation where the effect of the restoring will not be reflected in our solution. It turns out that this is the best-case scenario, for there is an intrinsic problem in the way the pseudoinverse is handled numerically that can make (2.24) not solvable at all.

The Moore-Penrose pseudoinverse requires the singular value decomposition (SVD) $\mathbf{E} = U\Sigma V^*$, where U and V are unitary matrices and the $*$ indicates the conjugate transpose. The matrix Σ is a diagonal matrix consisting of the singular values of $\mathbf{E}$, which will tell us about how suitable the system is for solution by inversion. Using the SVD, the pseudoinverse is simply $\mathbf{E}^+ = V\Sigma^+U^*$, where the $^+$ operation takes the reciprocal of each non-zero element on the diagonal of Σ and leave all the zeros in place. This highlights why taking the pseudoinverse is not a continuous operation, and why it might be a poor choice for us to use: if the original matrix $\mathbf{E}$ has a singular value 0, then modifying $\mathbf{E}$ slightly might turn this zero into a tiny positive number. This will then affect the pseudoinverse dramatically since we then would take the reciprocal of a tiny number.

Another way of looking at this problem is through the conditioning of our linear system. The pseudoinverse can be used to define the condition number for the matrix $\mathbf{E}$,

$$\mathrm{cond}(\mathbf{E}) = ||\mathbf{E}||||\mathbf{E}^{-1}||. \tag{2.26}$$

A large condition number means that the problem of finding least-squares solutions to the system is ill-conditioned. This means that the solution will be highly sensitive to small changes in the argument, and has a high potential for inaccuracy. Using the Euclidean 2-norm, the condition number takes the alternate form

$$\text{cond}(\mathbf{E}) = \frac{\sigma_{max}(\mathbf{E})}{\sigma_{min}(\mathbf{E})}, \tag{2.27}$$

where the σ are the singular values of $\mathbf{E}$. In our case this becomes problematic, because the restoring terms in $\mathbf{E}$ (those involving λ) are very small compared to the pure tracer gradient terms, yet the fact that they are nonzero is fundamental to the solution. With such disparity between the magnitudes of the terms, it is very possible that we will be left with an ill-conditioned problem. This suggests that we look for some sort of weighted least-squares solution (or preconditioning) for our system.

The ordinary least-squares solution assumes that each variable has identical variance, which is obviously incorrect in our case. Furthermore, it assumes that $E(\mathbf{n}) = 0$ and that $Cov(n_i, n_j) = 0$. We should not assume that each of the noise terms in our system is independent; rather, each of the fluxes **should** vary together since they are all part of the same flow field. Then rather than trying to solve the system $\mathbf{Ex} + \mathbf{n} = \mathbf{y}$ directly as above, we can attempt to find a least-squares solution by treating the tracer sink as the noise. First, we must transform y and $\mathbf{E}$ so that the residuals are all about the same magnitude. To do this, let us form a covariance matrix out of the the elements of $\mathbf{n}$, which we will write as

$$\mathbf{V} = \begin{bmatrix} \sigma_1^2 & Cov(n_1, n_2) & \dots & Cov(n_1, n_{2m}) \\ Cov(n_1, n_2) & \sigma_2^2 & & \vdots \\ & \ddots & \ddots & \\ \vdots & & & Cov(n_1, n_{2m-1}) \\ Cov(n_1, n_{2m}) & \dots & Cov(n_1, n_{2m-1}) & \sigma_{2m}^2 \\ , & & & \end{bmatrix}, \tag{2.28}$$

where σ_i^2 is the variance[10] . Defining $W = V^{-1}$, we must now try to minimize

$$\mathcal{S}(\hat{x}) = \sum_{i=1}^{2m} \sum_{j=1}^{2m} W_{ij}(y_i - E_i\hat{x})(y_j - E_j\hat{x}). \tag{2.29}$$

If we write our solution in the form $\mathbf{E}\hat{\mathbf{x}} = \hat{\mathbf{y}}$, we can minimize the variance by setting the derivatives of the sums of squares with respect to each parameter x_j equal to zero (Wunsch, 1996):

$$\frac{\partial}{\partial \hat{x}_j}[(\mathbf{y} - \mathbf{E}\hat{\mathbf{x}})^T \mathbf{W}(\mathbf{y} - \mathbf{E}\hat{\mathbf{x}})] = 0. \tag{2.30}$$

The solution to this system is then

$$\hat{\mathbf{x}} = (\mathbf{E'WE})^{-\mathbf{1}}\mathbf{E'Wy}. \tag{2.31}$$

To apply this method to our problem, we now must decide what to choose as our $\mathbf{E}$, $\mathbf{x}$, $\mathbf{n}$, and $\mathbf{y}$. Here we will revert back to the form for $\mathbf{E}$ and $\mathbf{x}$ that comprises our regular pseudoinversion

[10] Note that we have not yet defined the exact quantity that $\mathbf{n}$ should be; for now we assert that it must be related to the influence of λ in the flux-gradient relationship for $\overline{\mathbf{u}'\tau'}$, and that the covariance should be taken across points in the along-channel direction.

problem, so that

$$\mathbf{E} = \begin{bmatrix} \bar{\tau}_{1,y} & \bar{\tau}_{1,z} & 0 & 0 \\ 0 & 0 & \bar{\tau}_{1,y} & \bar{\tau}_{1,z} \\ \bar{\tau}_{2,y} & \bar{\tau}_{2,z} & 0 & 0 \\ 0 & 0 & \bar{\tau}_{2,y} & \bar{\tau}_{2,z} \\ \vdots & & \ddots & \vdots \\ \bar{\tau}_{m,y} & \bar{\tau}_{m,z} & 0 & 0 \\ 0 & 0 & \bar{\tau}_{m,y} & \bar{\tau}_{m,z} \end{bmatrix} \quad \mathbf{x} = \begin{bmatrix} R_{11} \\ R_{12} \\ R_{21} \\ R_{22} \end{bmatrix} \quad \mathbf{n} = \begin{bmatrix} n_1 \\ n_2 \\ n_3 \\ n_4 \\ \vdots \\ n_{2m-1} \\ n_{2m} \end{bmatrix} \quad \mathbf{y} = \begin{bmatrix} \overline{v'\tau'_1} \\ \overline{w'\tau'_1} \\ \overline{v'\tau'_2} \\ \overline{w'\tau'_2} \\ \vdots \\ \overline{v'\tau'_m} \\ \overline{w'\tau'_m} \end{bmatrix}, \quad (2.32)$$

where we still have yet to choose $\mathbf{n}$.

During the calibration of the Eady-like runs we performed a few experiments where we tried different choices for $\mathbf{n}$, the most successful of which was an estimate of the local flux sink $-\lambda u_i(\tau_\pi - \tau_{\pi,0})$ (Appendix B). Filling out the covariance matrix (2.28) using the along-channel fluxes of each tracer (so at each yz point there would be a different matrix $\mathbf{V}$), the results tended to be slightly improved over solving a system $\mathbf{Ex} = \mathbf{y}$ without considering $\mathbf{n}$ at all (not shown).[11] However, this method incurred a significant increase in computation time and data storage, and was not worth pursuing further after the emergence of the much cheaper, more accurate method discussed next.

2.1.3.3 Exploiting Linearity

In lieu of trying to numerically solve (2.32), a much simpler trick can be used that significantly improves the model results without almost any additional computation required. This trick takes advantage of the linearity of the flux-gradient relationship and restoring operator, which written in full is

$$\overline{\mathbf{u}'\tau'} = -(\mathbf{A} + \mathbf{S} + \lambda\mathbf{D})\nabla\bar{\tau}. \quad (2.33)$$

[11] By improved, we mean that the reproduced buoyancy flux was closer to the true value (Section 2.1.1.1).

We can take advantage of our multiple restoring timescales to eliminate **D** through simple linear algebra. For example, supposing we had one set of tracers with restoring timescale λ_1 (denoted with subscript $_{(1)}$), and another set with restoring timescale λ_2 (denoted with subscript $_{(2)}$), we could write their flux-gradient relationships separately as

$$\overline{u_i'\tau_{\pi}'}_{(1)} = -(A_{ij} + S_{ij} + \lambda_1 D_{ij})\nabla_j \bar{\tau}_{\pi} \tag{2.34}$$

$$\overline{u_i'\tau_{\pi}'}_{(2)} = -(A_{ij} + S_{ij} + \lambda_2 D_{ij})\nabla_j \bar{\tau}_{\pi}. \tag{2.35}$$

Supposing that the transport tensor $\mathbf{R} = \mathbf{A} + \mathbf{S}$ is the same for all passive tracers[12] and relating the restoring timescales $\lambda_2 = c\lambda_1$, we have

$$\overline{u_i'\tau_{\pi}'}_{(1)} = -(A_{ij} + S_{ij} + \lambda_1 D_{ij})\nabla_j \bar{\tau}_{\pi} \tag{2.36}$$

$$\overline{u_i'\tau_{\pi}'}_{(2)} = -(A_{ij} + S_{ij} + c\lambda_1 D_{ij})\nabla_j \bar{\tau}_{\pi}. \tag{2.37}$$

Simple linear algebra eliminates the **D** term, so that

$$\overline{u_i'\tau_{\pi}'}_{(2)} - c\overline{u_i'\tau_{\pi}'}_{(1)} = -(1-c)(A_{ij} + S_{ij})\nabla_j \bar{\tau}_{\pi}. \tag{2.38}$$

leaving the "true" solution for $\mathbf{R} = \mathbf{A} + \mathbf{S}$ to be determined by the modified flux-gradient relationship

$$\frac{\overline{u_i'\tau_{\pi}'}_{(2)} - c\overline{u_i'\tau_{\pi}'}_{(1)}}{1-c} = -(A_{ij} + S_{ij})\nabla_j \bar{\tau}_{\pi}. \tag{2.39}$$

Simplistic as this may seem, this method does an excellent job in removing the effects of the restoring (Fig. 2.9). It still does not absolve the modeler from choosing the initial tracer fields and setting each λ wisely (2.1.3.4), but it has the capability of significantly improving the flux reconstructions in any simulation where restoring is necessary.

2.1.3.4 Constraints on λ

Restoring the tracers back toward their initial state creates an irreversible sink of tracer variance, but this is a necessary cost for keep the tracer gradients misaligned. A more pressing

[12] This assumption underlies this entire research! If this were not true, the whole notion of solving for **R** using a suite of passive tracers would be without merit.

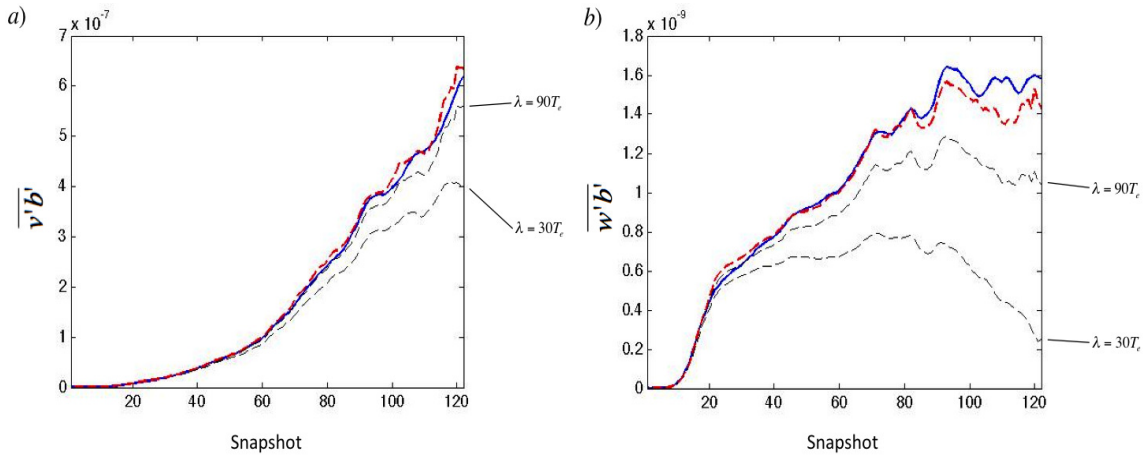

Figure 2.9: a) Horizontal and b) vertical buoyancy flux reconstructions using the modified flux-gradient relationship (2.39), for the same Eady-like simulation as in Fig. 2.8. Two distinct sets of tracers using restoring timescales $\lambda = 30T_e$ and $\lambda = 90T_e$ (dashed black lines) poorly reproduce the true buoyancy flux (blue line) when used alone, but using the linearity of 2.33 to eliminate $\mathbf{D}$ improves the reconstruction significantly (dashed red line).

issue is of how strong the restoring can be before it affects the physics of the tensor. Because the modeler has control over the magnitude of each λ_i, it is possible to set them to be so large as to make **S** an **antidiffusive** operator, featuring negative eigenvalues. This will occur if the time scale of the eddies is slower than the rate of restoration, so that the effects of the eddies become secondary to the effect of the restoring.

To investigate this possibility, we must first define an eddy turnover time. For eddy effects defined in terms of the parcel displacement (ξ, η, ζ), the horizontal eddy turnover time is determined by assuming a wavelike velocity perturbation

$$v' = a \sin(kx - \omega t), \tag{2.40}$$

from which we have

$$\eta = \int v' \, dt \tag{2.41}$$

$$= \frac{a}{\omega} \cos(kx - \omega t). \tag{2.42}$$

The mean eddy variance in terms of the energy density spectrum then becomes

$$\overline{\eta^2} = \sum_k c^2 k^2 E(k) \tag{2.43}$$

$$\overline{v'\eta} = \sqrt{\sum_k c^2 k^2 E(k)} \sqrt{\sum_k E(k)}, \tag{2.44}$$

from which the eddy turnover time is defined by

$$T_e = \frac{\overline{\eta^2}}{\overline{v'\eta}} = \frac{\sqrt{\sum_k c^2 k^2 E(k)}}{\sqrt{\sum_k E(k)}}. \tag{2.45}$$

What then does this imply about how large we can make λ? By symmetry, **S** can be made purely diagonal by a local coordinate rotation to its principle axes, in which case the diagonal components are precisely the eigenvalues of the matrix. Downgradient diffusion is therefore ensured if $S_{yy} \geq 0$, $S_{zz} \geq 0$, and $S_{yz}^2 \leq S_{yy} S_{zz}$. Assuming the eddies act predominantly in the horizontal, the first

condition is the most relevant, and this implies that

$$\overline{v'\eta} - \lambda\overline{\eta^2} \geq 0 \tag{2.46}$$

$$\lambda \leq \frac{\overline{v'\eta}}{\overline{\eta^2}} = \frac{1}{T_e} \tag{2.47}$$

$$\lambda T_e \leq 1 \tag{2.48}$$

As long as this condition is satisfied, $\mathbf{S}$ is guaranteed to have positive eigenvalues and thus represent true eddy-induced diffusion. The only question that remains is of how this constraint would play out in an OGCM, where the eddy kinetic energy is transferred upscale through an inverse cascade. At some point, it is certainly possible that the eddy turnover time would grow to the point at which the condition $\lambda T_e \leq 1$ would be violated. Fortunately, in the real ocean (and in properly calibrated OGCM's) the inverse cascade is arrested by some combination of frictional effects and upon reaching the Rhines scale (Held and Larichev, 1995; Danilov and Gurarie, 2002, 2004; Scott and Wang, 2005; Sukoriansky et al., 2007), where some of the eddy kinetic energy becomes lost to the excitation of Rossby waves. Therefore, it is plausible that each λ could be chosen small enough to satisfy $\lambda T_e \leq 1$ through the duration of the model run, while being different enough from one another that the tracer gradients are sufficiently misaligned.[13]

2.1.4 Summary

In this section we have defined the pseudoinverse technique that forms the backbone of this research, and we have explored many ways to ensure that it is both robust and accurate. The method is sensitive to both the number of tracers used and the way they are initialized in the model, but both of these can be set to maximize the accuracy by the metric defined in Section 2.1.1.1.

Note also that the pseudoinverse is applicable whenever a "least-squares approach" is needed

[13] Fox-Kemper and Bryan (in preparation) performed a global diagnosis of $\mathbf{R}$ by running the POP model at 0.1° for 23 years of simulated time (with annual forcing as in Large and Yeager (2004)). During their simulation they used nine tracers and chose distinct restoring timescales for each set of three: six months, one year, and no restoring. The pseudoinversion method worked well when a mixture of these timescales were used, but failed if only one timescale was used for all of the tracers.

- it does not necessarily have to be used only with a flux-gradient relation. Different or more complex parameterization forms might make good use of the pseudoinverse, but these are beyond the scope of this thesis.[14] For now, we will consider using this method only as applied to the simple flux-gradient relation for passive tracer transport.

2.2 Rotational Fluxes

Inspection of the mean tracer equation (1.51) reveals that the eddy tracer flux appears inside of a divergence operator. Physically, this means that despite all eddy fluxes presumed to be going on inside each grid box, it is only the net tracer quantity passing through the boundaries of the box that will affect the local mean tracer budget. However, this divergence operator can also hide important dynamical details of the eddy fluxes that we must consider before we can evaluate parameterizations with our suite of models.

Most importantly, the presence of the divergence calls into question whether the flux-gradient relationship (2.1) tells us the whole story of the eddy fluxes. Equation (2.1) tells us that the parcel displacements that carry around the tracers can be described in terms of an eddy diffusivity tensor $\mathbf{R}$ acting inside the grid box, and that for all the eddy activity we imagine might happen below the gridscale, the mean tracer gradient is the only connection the subgridscale tracer fluxes have with the numerical model. Indeed, the flux-gradient relationship is a very simplistic representation of subgridscale eddy fluxes: the net effect of all the subgridscale eddies is simply to transport some quantity of tracer up- or down-gradient, adding an extra tracer flux on top of that induced by the mean flow.

If we were to proceed with only the flux-gradient relationship, we would essentially be assuming that all subgridscale eddy activity is fluxing the tracer in a way that should be represented in a parameterization. But what if there are eddies that **shouldn't** be represented in the parameterization, such as those that are circulating entirely within the grid box? We would say that these

[14] Parameterizations of momentum fluxes, for example, do not necessarily follow downgradient transport, and are complicated by nonlocal pressure effects and the presence of the Coriolis force.

eddies are purely rotational - that is, they are circulating along a path that lies entirely within the area covered by the averaging. Just like any rotational flux, they would also be intrinsically nondivergent, so they would not have any effect in the mean tracer equation.

The idea of a rotational flux contaminating our flux diagnosis at least must be considered before we move forward. For this section we will write the rotational flux as the curl of some vector θ, with the new flux-gradient relationship given by

$$\overline{\mathbf{u}'\tau'} = -\mathbf{R}\nabla\bar{\tau} + \nabla \times \theta, \tag{2.49}$$

and we will examine whether it is possible to diagnose our eddy fluxes with this extra term present.

2.2.1 Formulation in TEM Theory

The presence of the rotational term in (2.49) complicates how we interpret the eddy fluxes being read from our numerical model. In the research performed for this thesis, the eddy fluxes are obtained via zonal averaging, using the identity

$$\overline{\mathbf{u}'\tau'} = \overline{\mathbf{u}\tau} - \bar{\mathbf{u}}\bar{\tau}. \tag{2.50}$$

The formulation of (2.49) suggests that the raw eddy flux read from the model is **not** the quantity we actually want to fit to with a parameterization. In order to manipulate (2.49) into a form where the pseudoinversion from earlier in this chapter can be used, we must first subtract off the rotational component from the raw eddy fluxes. Of course, this requires some prescription of how this rotational flux appears in terms of coarse-grid quantities.

An analytical description of the rotational flux was presented in Eden, Greatbatch and Olbers (2007), and is summarized below. The main result of this paper was to unify several different treatments of Transformed Eulerian Mean theory (Section 1.3.2), and to show that the tracer moment equations could be used to write a closure for the turbulent tracer fluxes. Consider again the flux-gradient relationship with a rotational flux added on, so that

$$\overline{\mathbf{u}'\tau'} = \mathbf{F} = -\mathbf{R}\nabla\bar{\tau} + \nabla \times \theta, . \tag{2.51}$$

Following TEM theory, we decompose the eddy flux into its components along and across the tracer contours, which we call, respectively,

$$\mathbf{F}_{\parallel} = \frac{\mathbf{n} \times \mathbf{F}}{|\nabla \bar{\tau}|^2} \times \mathbf{n} \qquad \mathbf{F}_{\perp} = \left(\frac{\mathbf{n} \cdot \mathbf{F}}{|\nabla \bar{\tau}|^2} \right) \mathbf{n}. \tag{2.52}$$

Here we are taking the normal vector to the tracer isosurface $\mathbf{n} = \nabla \bar{\tau} / |\nabla \bar{\tau}|$, and the usual Euclidean vector norm $|\nabla \bar{\tau}| = \sqrt{\bar{\tau}_x^2 + \bar{\tau}_y^2 + \bar{\tau}_z^2}$. If we define the diapycnal diffusivity

$$K = \frac{\mathbf{n} \cdot \mathbf{F}}{|\nabla \bar{\tau}|} \tag{2.53}$$

and the overturning streamfunction

$$\Psi = \frac{\mathbf{n} \times \mathbf{F}}{|\nabla \bar{\tau}|}, \tag{2.54}$$

the TEM projection of (2.51) becomes

$$\overline{\mathbf{u}' \tau'} = \mathbf{F} = -K \nabla \bar{\tau} + \Psi \times \nabla \bar{\tau} + \nabla \times \theta, . \tag{2.55}$$

Vector multiplication allows us to solve explicitly for both K and Ψ, which in terms of the rotational flux become

$$K = - |\nabla \bar{\tau}|^{-1} \left(\frac{\nabla \bar{\tau} \cdot \mathbf{F}}{|\nabla \bar{\tau}|} + \frac{\partial \theta}{\partial s} \right) \tag{2.56}$$

and

$$\Psi = - |\nabla \bar{\tau}|^{-1} \left(\frac{\nabla \bar{\tau} \times \mathbf{F}}{|\nabla \bar{\tau}|} - \frac{\partial \theta}{\partial n} \right), \tag{2.57}$$

where we are defining the along- and across-isopycnal derivatives to be $\partial / \partial s = (\nabla \bar{\tau} / |\nabla \bar{\tau}|) \cdot \nabla \times (\ )$ and $\partial / \partial n = -(\nabla \bar{\tau} / |\nabla \bar{\tau}|) \times \nabla \times (\ )$. Further leverage over these equations comes by analyzing the budgets of higher tracer moments. Consider, for example, the tracer variance equation

$$\frac{\partial \overline{\phi_2}}{\partial t} + \overline{\mathbf{u}' \tau'} \cdot \nabla \bar{\tau} + \bar{\mathbf{u}} \cdot \nabla \overline{\phi_2} + \nabla \cdot \overline{\mathbf{u}' \phi_2} = 0, \tag{2.58}$$

where we are writing $\phi_2 = \overline{\tau'^2 / 2}$. Assuming incompressibility, we can rearrange the variance advection terms so that the tracer variance is advected by the full velocity, so that (2.58) now

appears as

$$\frac{\partial\overline{\phi_2}}{\partial t} + \overline{\mathbf{u}'\tau'} \cdot \nabla\bar{\tau} + \nabla \cdot \overline{\mathbf{u}\phi_2} = 0. \tag{2.59}$$

Now we can seek a TEM projection of the variance flux $\overline{\mathbf{u}\phi_2}$ in the same fashion as we did in (2.55) - that is, we look for a skew flux (with streamfunction now called Ψ_2), a diapycnal diffusivity K_2, and a rotational flux with kernel θ_2. This TEM decomposition appears as

$$\overline{\mathbf{u}\phi_2} = -K_2\nabla\bar{\tau} + \Psi_2 \times \nabla\bar{\tau} + \nabla \times \theta_2, \tag{2.60}$$

and as with (2.53) and (2.54), we can solve explicitly for K_2 and Ψ_2:

$$K_2 = -\left|\nabla\bar{\tau}\right|^{-1}\left(\frac{\nabla\bar{\tau}\cdot\overline{\mathbf{u}\phi_2}}{\left|\nabla\bar{\tau}\right|} + \frac{\partial\theta_2}{\partial s}\right) \tag{2.61}$$

$$\tag{2.62}$$

$$\Psi_2 = -\left|\nabla\bar{\tau}\right|^{-1}\left(\frac{\nabla\bar{\tau}\times\overline{\mathbf{u}\phi_2}}{\left|\nabla\bar{\tau}\right|} - \frac{\partial\theta_2}{\partial n}\right). \tag{2.63}$$

Now by substituting (2.53), (2.54), (2.68) and (2.70) into (2.59), the TEM form of (2.59) becomes

$$\frac{\partial\overline{\phi_2}}{\partial t} + \nabla \times (\theta - \Psi_2) \cdot \nabla\bar{\tau} + K\left|\nabla\bar{\tau}\right|^2 + \nabla \cdot K_2\nabla\bar{\tau} = 0. \tag{2.64}$$

Many previous authors have offered that the rotational flux should act to cancel advection of the tracer variance, or equivalently, it should exist to localize production and dissipation of higher tracer moments (Marshall and Shutts, 1981; McDougall and McIntosh, 1996; Medvedev and Greatbatch, 2004; Eden, Greatbatch and Olbers, 2007). If this were the case, one could simply choose $\theta = \Psi_2$ in (2.64), which by (2.70) would leave us with the relation

$$\theta = -\left|\nabla\bar{\tau}\right|^{-1}\left(\frac{\nabla\bar{\tau}\times\overline{\mathbf{u}\phi_2}}{\left|\nabla\bar{\tau}\right|} - \frac{\partial\theta_2}{\partial n}\right). \tag{2.65}$$

Unfortunately, now we are left to specify θ_2. The form of (2.65), along with the use of the variance equation that led to it, suggest that we might find an iterative relation for all the θ by looking to higher moments. To make this concrete, consider the nth tracer moment equation

$$\frac{\partial\overline{\phi_n}}{\partial t} + (n-1)\overline{\mathbf{u}\phi_{n-1}} \cdot \nabla\bar{\tau} + \nabla \cdot \overline{\mathbf{u}\phi_n} + n\bar{\phi}_{n-1}\frac{\partial\overline{\mathbf{u}'\tau'}}{\partial t}, \tag{2.66}$$

where $\phi_n = \overline{\tau'^n/n}$. Performing a TEM decomposition for the tracer moment flux term, we again have

$$\overline{\mathbf{u}\phi_n} = -K_n \nabla\bar{\tau} + \Psi_n \times \nabla\bar{\tau} + \nabla \times \theta_n, \tag{2.67}$$

where solving explicitly for K_n and Ψ_n leaves us with

$$K_n = -\left|\nabla\bar{\tau}\right|^{-1} \left(\frac{\nabla\bar{\tau} \cdot \overline{\mathbf{u}\phi_n}}{\left|\nabla\bar{\tau}\right|} + \frac{\partial\theta_n}{\partial s} \right) \tag{2.68}$$

$$\tag{2.69}$$

$$\Psi_n = -\left|\nabla\bar{\tau}\right|^{-1} \left(\frac{\nabla\bar{\tau} \times \overline{\mathbf{u}\phi_n}}{\left|\nabla\bar{\tau}\right|} - \frac{\partial\theta_n}{\partial n} \right). \tag{2.70}$$

Substituting into (2.66) once again leaves us with the general form

$$\frac{\partial\overline{\phi_n}}{\partial t} + \nabla \times ((n-1)\theta_{n-1} - \Psi_n) \cdot \nabla\bar{\tau} + (n-1)K_{n-1}\left|\nabla\bar{\tau}\right|^2 + \nabla \cdot K_n \nabla\bar{\tau} + (n-1)\overline{\phi_{n-1}}\frac{\partial\bar{\tau}}{\partial t} = 0. \tag{2.71}$$

Eden, Greatbatch and Olbers (2007) use an argument from Marshall and Shutts (1981) that the rotational flux should serve to localize the generation and dissipation of the tracer moments, choosing

$$(n-1)\theta_{n-1} = \Psi_n = \left|\nabla\bar{\tau}\right|^{-1} \left(\frac{\nabla\bar{\tau} \times \overline{\mathbf{u}\phi_n}}{\left|\nabla\bar{\tau}\right|} - \frac{\partial\theta_n}{\partial n} \right). \tag{2.72}$$

Defining the along-isopycnal tracer moment flux to be $\mathbf{J}_n = \nabla\bar{\tau} \times \overline{\mathbf{u}\phi_n} / \left|\nabla\bar{\tau}\right|$, we have established the iterative relation shown in Eden, Greatbatch and Olbers (2007), who present a solution for θ as

$$\theta\left|\nabla\bar{\tau}\right| = \mathbf{J}_2 - \frac{\partial}{\partial n}\left(\frac{1}{2}\frac{\mathbf{J}_3}{\left|\nabla\bar{\tau}\right|} - \frac{\partial}{\partial n}\left(\frac{1}{3}\frac{\mathbf{J}_4}{\left|\nabla\bar{\tau}\right|} - \ldots \right. \right. \tag{2.73}$$

$$\tag{2.74}$$

$$= \mathbf{J}_2 - \frac{1}{2\left|\nabla\bar{\tau}\right|}\frac{\partial}{\partial n}\mathbf{J}_3 + \frac{1}{3!\left|\nabla\bar{\tau}\right|^2}\frac{\partial^2}{\partial n^2}\mathbf{J}_4 - \ldots \tag{2.75}$$

$$\tag{2.76}$$

$$= \sum_{m=2}^{\infty} \frac{(-1)^m \left(\frac{\partial}{\partial n}\right)^{m-2} \mathbf{J}_m}{(m-1)!\left|\nabla\bar{\tau}\right|^{m-2}}. \tag{2.77}$$

Note that θ is a three-dimensional vector. We shall henceforth refer to the x-, y-, and z-components of θ as $\theta_{(1)}$, $\theta_{(2)}$, and $\theta_{(3)}$, respectively, so as not to confuse subscripts with partial derivatives or terms of a series.

2.2.2 Series Divergence in Frontogenesis

One issue that was not adequately addressed in Eden, Greatbatch and Olbers (2007) was whether the series in (2.77) produces physically realistic fluxes in a realistic flow setting. There are two obvious issues that would leave one to wonder: 1) there are extra factors of $|\nabla\bar{\tau}|$ in the denominator that do not arise from projecting the fluxes onto the surface normal vector $\mathbf{n} = \nabla\bar{\tau}/|\nabla\bar{\tau}|$, and 2) the derivatives of higher tracer moments in the higher order terms have the potential to grow as the spatial scale is reduced.

Indeed, Figure (2.10) demonstrates that there are locations even in a standard Eady-like model where the terms in (2.77) yield unphysical fluxes. Comparison of panels (a-c) with the series components in panels (d-i) indicate that these fluxes are localized in regions adjacent to active surface frontogenesis, where we would expect an ageostrophic secondary circulation (hereafter ASC) to develop (Hoskins and Bretherton, 1972). Here we will pursue an analytical example of how an ASC in a simple flow setting can cause (2.77) to yield an unreliable result.

Let us take buoyancy as the tracer of interest, and let the averaging be a zonal average. Assume a weakly baroclinic, stably stratified flow with $\bar{b}_z = N^2 > 0$ and $\bar{b}_y = M^2 << \bar{b}_z$. Under these assumptions we define the gradient operator $\nabla = (0, \partial/\partial y, \partial/\partial z)$. Employing semi-geostrophic scaling (Hoskins, 1975), the magnitude of the buoyancy gradient $\left|\nabla\bar{b}\right| = \sqrt{\bar{b}_y^2 + \bar{b}_z^2} \approx \bar{b}_z$, and the along-isopycnal projection of the tracer moment flux is

$$\frac{\nabla\bar{b} \times \overline{\mathbf{u}\phi_m}}{\left|\nabla\bar{b}\right|} = \frac{1}{\left|\nabla\bar{b}\right|}\begin{bmatrix} \overline{w\phi_m}\bar{b}_y - \overline{v\phi_m}\bar{b}_z \\ \overline{u\phi_m}\bar{b}_z \\ -\overline{u\phi_m}\bar{b}_y \end{bmatrix} \approx \frac{1}{\left|\nabla\bar{b}\right|}\begin{bmatrix} -\overline{v\phi_m}\bar{b}_z \\ \overline{u\phi_m}\bar{b}_z \\ 0 \end{bmatrix} \approx \begin{bmatrix} -\overline{v\phi_m} \\ \overline{u\phi_m} \\ 0 \end{bmatrix}. \tag{2.78}$$

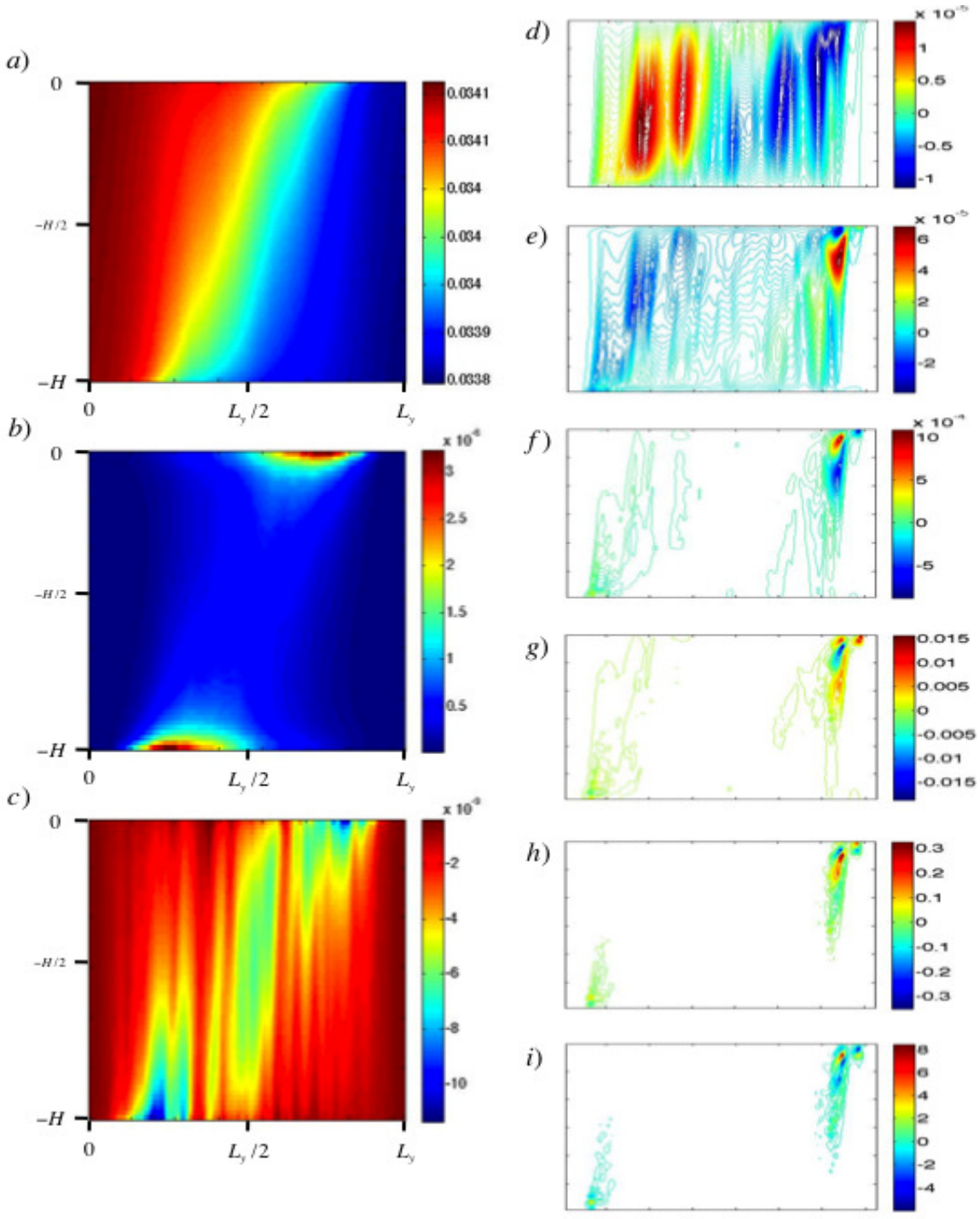

Figure 2.10: Snapshot from a zonally-averaged Eady-like run demonstrating the growth of the terms in the series (2.77). a) Mean buoyancy field. The green coloration marks the center of the main front. b) $\bar{b}_z = N^2$, and c) $\bar{b}_y = M^2$. In both panels boundary layer frontogenesis is evident at the leading edge of the main front. d-i) Terms a_2 through a_7 of (2.77). The unphysical growth of these terms is magnified in regions below/above the surface/bottom frontogenesis layer, which we attribute to an ageostrophic secondary circulation.

The across-isopycnal derivative $\partial/\partial n$ reduces to

$$\frac{\partial}{\partial n} = \mathbf{n}\cdot\nabla = \frac{\bar{b}_y\frac{\partial}{\partial y} + \bar{b}_z\frac{\partial}{\partial z}}{\left|\nabla\bar{b}\right|} \tag{2.79}$$

$$\approx \frac{\bar{b}_z\frac{\partial}{\partial z}}{\bar{b}_z} \tag{2.80}$$

$$= \frac{\partial}{\partial z}, \tag{2.81}$$

and so the mth term of the series (2.77) is approximately

$$a_m = \frac{(-1)^m\left(\frac{\partial}{\partial z}\right)^{m-2}\begin{bmatrix}-\overline{v\phi_m}\\ \overline{u\phi_m}\\ 0\end{bmatrix}}{(m-1)!\left(\bar{b}_z\right)^{m-1}} \tag{2.82}$$

Without loss of generality, we will focus our attention on the x-term involving $\overline{v\phi_m}$. Generally speaking, we cannot estimate the magnitude of $\overline{v\phi_m}$ for an arbitrary flow, but we **can** make an estimate of its vertical derivative under certain assumptions. As Figure (2.10) shows that (2.77) fails in regions where we would expect a strong ASC, we will now pursue such an estimate of $d\overline{v\phi_m}/dz$ using the mathematical framework of frontogenesis. Consider the Boussinesq semi-geostrophic momentum and buoyancy equations (Hoskins and Draghici, 1977; Hoskins et al., 1978)

$$\frac{\partial u_g}{\partial t} + u_g\frac{\partial u_g}{\partial x} + v_g\frac{\partial u_g}{\partial y} + w_a\frac{\partial u_g}{\partial z} - \left(f - \frac{\partial u_g}{\partial y}\right)v_a + = 0 \tag{2.83}$$

$$\frac{\partial b}{\partial t} + u_g\frac{\partial b}{\partial x} + v_g\frac{\partial b}{\partial y} + v_a\frac{\partial b}{\partial y} + w_a\frac{\partial b}{\partial z} = 0, \tag{2.84}$$

where the $\mathbf{u}_g$ are horizontal geostrophic velocities satisfying $f\mathbf{k}\times\mathbf{u}_g = \nabla b$ and thermal wind balance $f\times\frac{\partial\mathbf{u}_g}{\partial z} = \nabla b$, and $\mathbf{u}_a$ are ageostrophic velocities. In semigeostrophic scaling, we have a nondivergent total velocity ($\nabla\cdot\mathbf{u} = 0$) and a nondivergent geostrophic velocity ($\nabla\cdot\mathbf{u}_g = 0$), so by extension the ageostrophic velocity is also nondivergent ($\nabla\cdot\mathbf{u}_a = 0$). We can thus define an ageostrophic streamfunction ψ satisfying $\partial\psi/\partial z = v_a$ and $-\partial\psi/\partial y = w_a$ by taking $f\partial/\partial z$ of (2.83) and $\partial/\partial y$ of (2.84). Adding the two resulting equations together (taking the geostrophic

nondivergence $\nabla \cdot \mathbf{u}_g$ along the way) results in the Eliassen-Sawyer equation (Eliassen, 1951; Sawyer and Sawyer, 1956; Thomas and Lee, 2005),

$$\left[\left(f^2 - f\frac{\partial u_g}{\partial y}\right)\frac{\partial^2}{\partial z^2} + 2f^2\left(\frac{\partial b}{\partial y}\right)^2\frac{\partial^2}{\partial y \partial z} + \frac{\partial b}{\partial z}\frac{\partial^2}{\partial y^2}\right]\psi = 2\left(\frac{\partial b}{\partial y}\frac{\partial v_g}{\partial y} + \frac{\partial b}{\partial x}\frac{\partial u_g}{\partial y}\right). \tag{2.85}$$

We pursue this equation for a reason - it describes the evolution of an ASC in response to surface frontogenesis by the geostrophic flow, which was observed in Figure (2.10) where the series components (2.77) grew unphysically large. Assuming semigeostrophic scaling (Thomas and Ferrari, 2008), an approximate form of the Eliassen-Sawyer equation can be written

$$\left[f^2\frac{\partial^2}{\partial z^2} + \frac{\partial b}{\partial z}\frac{\partial^2}{\partial y^2}\right]\psi = 2\left(\frac{\partial b}{\partial y}\frac{\partial v_g}{\partial y} + \frac{\partial b}{\partial x}\frac{\partial u_g}{\partial y}\right). \tag{2.86}$$

Our goal is to reduce the this equation to a linear form, from which we can look for a solution for ψ using standard methods (Gilbarg and Trudinger, 2001). First we would like to separate the contributions of the turbulence and the background stratification in b, so we perform the usual Reynolds decomposition $b = \bar{b} + b'$,[15] giving us

$$\left[f^2\frac{\partial^2}{\partial z^2} + \frac{\partial(\bar{b}+b')}{\partial z}\frac{\partial^2}{\partial y^2}\right]\psi = 2\left(\frac{\partial(\bar{b}+b')}{\partial y}\frac{\partial v_g}{\partial y} + \frac{\partial(\bar{b}+b')}{\partial x}\frac{\partial u_g}{\partial y}\right). \tag{2.87}$$

Assuming that we have $|\bar{b}| >> |b'|$, we can scale out the b' terms in (2.87). Letting the bar operator be a zonal averaging, this reduces (2.87) to

$$f^2\frac{\partial^2\psi}{\partial z^2} + \frac{\partial\bar{b}}{\partial z}\frac{\partial^2\psi}{\partial y^2} = 2\left(\frac{\partial\bar{b}}{\partial y}\frac{\partial v_g}{\partial y}\right). \tag{2.88}$$

We cannot generally predict the lateral structure of the right side of (2.88) in a nonlinear simulation, so we will simply let it be purely a function of y (call it $g(y)$). For now we will let the y direction be unbounded[16] , allowing us to take the integral Fourier transform. Beginning with (2.88) rewritten as

$$\frac{f^2}{N^2}\frac{\partial^2\psi}{\partial z^2} + \frac{\partial^2\psi}{\partial y^2} = g(y), \tag{2.89}$$

[15] We cannot make the same assumption on the velocity field, since in fully developed turbulence $\mathbf{u}'$ is of the same order as $\bar{\mathbf{u}}$ (Section 3.1.3, Fig. 3.2).

[16] This derivation can also be performed on a bounded interval without changing the form of the final answer. The boundary conditions do not affect the answer, so to keep the math succinct they will be neglected.

we multiply both sides of this equation by e^{-ily} to give

$$\frac{f^2}{N^2}\frac{\partial^2\psi}{\partial z^2}e^{-ily} + \frac{\partial^2\psi}{\partial y^2}e^{-ily} = g(y)e^{-ily}. \tag{2.90}$$

Integrating over y from $-\infty$ to ∞,

$$\int_{-\infty}^{\infty}\frac{f^2}{N^2}\frac{\partial^2\psi}{\partial z^2}e^{-ily}\,dy + \int_{-\infty}^{\infty}\frac{\partial^2\psi}{\partial y^2}e^{-ily}\,dy = \int_{-\infty}^{\infty}g(y)e^{-ily}\,dy. \tag{2.91}$$

Define the Fourier transform $\hat{g} = \int_{-\infty}^{\infty} g(y)e^{-ily}$. Then

$$\frac{f^2}{N^2}\frac{\partial^2\hat{\psi}}{\partial z^2} + -l^2\hat{\psi} = \hat{g} \tag{2.92}$$

$$\frac{\partial^2\hat{\psi}}{\partial z^2} - \frac{N^2l^2}{f^2}\hat{\psi} = \frac{N^2}{f^2}\hat{g} \tag{2.93}$$

The homogeneous solution to this equation is

$$\hat{\psi}_h = c_1e^{-\frac{Nl}{f}z} + c_2e^{\frac{Nl}{f}z}, \tag{2.94}$$

where for $z < 0$ we discard the former. The particular solution is

$$\hat{\psi}_p = -\frac{1}{l^2}\hat{g}, \tag{2.95}$$

and so the full solution is

$$\hat{\psi} = ce^{\frac{Nl}{f}z} - \frac{1}{l^2}\hat{g}. \tag{2.96}$$

Taking the inverse Fourier transform gives us

$$\psi = \Re\left[\int_{-\infty}^{\infty} ce^{\frac{Nl}{f}z}e^{ily}\,dl\right] - \int_{-\infty}^{\infty}\int_{-\infty}^{\infty} g(y)\,dl\,dl, \tag{2.97}$$

where the constant c is a function of the boundary conditions and of $f(y)$. Differentiating ψ with respect to z gives us the ageostrophic meridional velocity

$$v = \frac{\partial\psi}{\partial z} = \Re\left[\int_{-\infty}^{\infty} c\frac{Nl}{f}e^{\frac{Nl}{f}z}e^{ily}\,dl\right]. \tag{2.98}$$

Inserting this expression into our approximation for a_m yields

$$a_m = \frac{(-1)^m\left(\frac{\partial}{\partial z}\right)^{m-2}\overline{\Re\left(\int_{-\infty}^{\infty} c\frac{Nl}{f}e^{\frac{Nl}{f}z}e^{ily}\,dl\right)\phi_m}}{(m-1)!\left(\bar{b}_z\right)^{m-1}}, \tag{2.99}$$

and so the full series for $\theta_{(1)}$ is

$$\theta_{(1)} = \sum_{m=2}^{\infty} \frac{(-1)^m \left(\frac{\partial}{\partial z}\right)^{m-2} \overline{\Re\left(\int_{-\infty}^{\infty} c\frac{Nl}{f} e^{\frac{Nl}{f}z} e^{ily}\, dl\right) b'^m}}{m!\left(\bar{b}_z\right)^{m-1}} \tag{2.100}$$

We would like to know what the contribution of the rotational flux will be to the total meridional eddy buoyancy flux $\overline{v'b'}$, so we take the curl of this term (which under zonal averaging reduces to taking $\partial/\partial z$, whereupon it moves to the y-component of the rotational flux). Doing so yields

$$[\nabla \times \theta]_{(2)} = \sum_{m=2}^{\infty} \frac{(-1)^m \left(\frac{\partial}{\partial z}\right)^{m-1} \overline{\Re\left(\int_{-\infty}^{\infty} c\frac{Nl}{f} e^{\frac{Nl}{f}z} e^{ily}\, dl\right) b'^m}}{m!\left(\bar{b}_z\right)^{m-1}} \tag{2.101}$$

Rearranging the summation and the integral gives us the new form

$$[\nabla \times \theta]_{(2)} = \Re \int_{-\infty}^{\infty} c \sum_{m=1}^{\infty} \frac{(-1)^m \left(\frac{\partial}{\partial z}\right)^{m-1} \overline{\frac{Nl}{f} e^{\frac{Nl}{f}z} e^{ily} b'^m}}{m!\left(\bar{b}_z\right)^{m-1}}\, dl. \tag{2.102}$$

We can pull the exponential terms from beneath the overbar because it represents an average in x (whereas the terms are functions of y and z), which leaves us

$$[\nabla \times \theta]_{(2)} = \Re \int_{-\infty}^{\infty} c e^{\frac{Nl}{f}z} e^{ily} N^2 \sum_{m=2}^{\infty} \frac{(-1)^m \left(\frac{l}{f}\right)^m \overline{b'^m}}{m! N^m}\, dl \tag{2.103}$$

To extend the series index to zero, we add and subtract the $m = 0$ and $m = 1$ terms to get

$$[\nabla \times \theta]_{(2)} = \Re \int_{-\infty}^{\infty} c e^{\frac{Nl}{f}z} e^{ily} N^2 \left(-1 + \frac{l\overline{b'}}{fN} + \sum_{m=0}^{\infty} \frac{(-1)^m \left(\frac{l}{f}\right)^m \overline{b'^m}}{m! N^m}\right) dl \tag{2.104}$$

$$\tag{2.105}$$

$$= \Re \int_{-\infty}^{\infty} c e^{\frac{Nl}{f}z} e^{ily} N^2 \left(-1 + \sum_{m=0}^{\infty} \frac{(-1)^m \left(\frac{l}{f}\right)^m \overline{b'^m}}{m! N^m}\right) dl \tag{2.106}$$

By the identity

$$\overline{e^x} = \sum_{m=0}^{\infty} \frac{\overline{x^m}}{m!}, \tag{2.107}$$

we now have

$$[\nabla \times \theta]_{(2)} = \Re \int_{-\infty}^{\infty} c e^{\frac{Nl}{f}z} e^{ily} N^2 \left(-1 + \overline{e^{-\Phi}}\right) dl \tag{2.108}$$

$$\tag{2.109}$$

$$\Phi = \frac{lb'}{fN} \tag{2.110}$$

The real part of this expression will be determined by the character of c:

- If c is real, a cosine will appear in the integral.
- If c is purely complex, a sine will appear in the integral.
- For c with nonzero real and imaginary parts, we will be left with both a sine and cosine term.

None of these choices will affect the final argument, so without loss of generality suppose c is real. Evaluating the integral in (2.108) directly is possible, but cumbersome in its current form. For simplicity, let $y = 0$ and $z = 0$ (we could have shifted our coordinate system to put this point directly in the center of the below-front ASC anyways without changing the derivation). Then (2.108) reduces to

$$[\nabla \times \theta]_{(2)} = \int_{-\infty}^{\infty} cN^2 \left(-1 + \overline{e^{-\Phi}}\right) \, dl, \tag{2.111}$$

with the integral evaluating to

$$[\nabla \times \theta]_{(2)} = -cN^2 l - c\overline{\frac{N^3 f}{b'} e^{-\Phi}} \Bigg|_{-\infty}^{\infty} \tag{2.112}$$

This quantity will be detemined by local correlations of l and b' across a set of scales extending down to the viscous scale, where the tracer moments would be dissipated. Shy of speculating about what happens to b' as $l \to \infty$, we can restrict ourselves to a finite set of wavenumbers and examine the size of this term in a particular scenario. Given that we have already chosen the Eady problem as the setup for this example, let us truncate the sum at the first baroclinic deformation radius $L_d = NH/f$, so that

$$[\nabla \times \theta]_{(2)} = -cN^2 l - c\overline{\frac{N^3 f}{b'} e^{-\Phi}} \Bigg|_{-L_d}^{L_d} \tag{2.113}$$

$$= -c\frac{N^3 H}{f} - c\frac{N^3 f}{b'}\overline{e^{-\Omega}} + c\frac{N^3 f}{b'}\overline{e^{\Omega}} \tag{2.114}$$

$$\Omega = \frac{H}{f^2 b'} \tag{2.115}$$

For $b' = \mathcal{O}(10^-3)$ and typical ocean values $N \approx 10^{-2}$ s^{-1}, $f = 7.29 \times 10^{-5}$ s^{-1}, and $H = \mathcal{O}(10^3)$ m, the first and third terms will give unphysically large results (the exponent $\Omega = \mathcal{O}(10^{14})$, making the third term essentially infinite; for comparison, the true value of $\overline{v'b'}$ from Figure 2.10 is $\mathcal{O}(10^{-5})$ m^2 s^{-3}).

We have thus designed a simple analytical example, which is meant to approximate the conditions present in the model in Figure 2.10, to suggest that the rotational flux derivation of Eden, Greatbatch and Olbers (2007) is likely to lead to unphysical values of the rotational gauge in areas of strong ageostrophic secondary circulation. It is possible that this may occur in other flow scenarios as well.[17] Certainly it is discouraging that this should occur in a "well-behaved", idealized flow with no grossly unrealistic features.

Note that in our derivation the choice of zonal average was made only to simplify our calculations; we could have chosen another averaging operator at much greater mathematical difficulty. Buoyancy was used as our example tracer because its distribution is closely linked with the dynamics of the flow field, allowing us to gain some handle over the vertical structure of its fluxes. It is also useful because in a stably stratified, unsteady flow we do not expect the buoyancy gradient to vanish (nor have we assumed that it does), so we do not rely on a "divide by zero" argument to show that the rotational flux formula is unphysical[18] .

With the numerical evidence of Figure 2.10 and the mathematical arguments above, we conclude that the rotational flux formula (2.77) is unphysical, and therefore unreliable. With no other argument available to specify how the rotational flux should appear, it is fruitless to pursue a decomposition of the form (2.51) any further. Then for the remainder of this research, we will fit our transport tensor scalings to the raw eddy fluxes extracted from the model, with no further discussion of rotational gauges.

[17] Unfortunately, shy of exploring other special cases, it is difficult (if not impossible) to generalize the mathematical analysis to more complex flow scenarios. This is not be necessary though, as this counterexample demonstrates the inadequacy of the Eden, Greatbatch and Olbers (2007) formulation.

[18] What to do in cases of zero gradient is still a concern, though.

Chapter 3

Challenge Suite I - Eady-like Models

3.1 Eddy Diffusivity - Mathematics and Theory

Fundamentally, this research deals with verifying and validating what we know, or **what we think we know**, about how to construct a mesoscale eddy parameterization. The body of work that has contributed to the evolution of eddy parameterizations has generally dealt with either physical arguments about the dynamical behavior of mesoscale eddies[1] , the value of the diffusivity coefficient, or the effects of the parameterization in coarse-resolution models. Up until now, however, it has not been possible to check whether the Redi plus GM90 (Griffies, 1998) parameterization is even correct in the first place! Beyond simply saying that simulation results are improved, how do we really know that the tensor structure is correct?

One can begin a proper diagnosis of the eddy stirring tensor with a simple dimensional analysis exercise on the eddy tracer flux term $\overline{\mathbf{u}'\tau'}$. Let us assume for the time being that the tracer of interest is buoyancy, so it will have an active feedback on the flow. The reason for using buoyancy is due to the implicit assumption of both Redi and GM90 that the oceanic thermal structure is what constrains the eddy motions[2] , so it is conceivable that a diffusivity tensor that works for buoyancy fluxes might be the same one to use for passive tracers. Then with buoyancy as our choice, we first note that the eddy buoyancy flux term has the dimensions of a length squared

[1] These go hand-in-hand with arguments what a mesoscale parameterization should look like. It is an open and highly controversial question about whether the stirring should be slave to buoyancy or potential vorticity - your stance on the subject will determine what you believe the advective part of the stirring tensor will look like and how it will vary in the vertical (see Section 1.6).

[2] A similar case could be made for potential vorticity, hence the controversy.

divided by a timescale cubed. The choice for how to fill in these dimensional pieces is not so clear, however.

Let us consider the vertical eddy flux for the moment, so the term we are interested in is $\overline{w'b'}$. At first glance, it would appear that a logical scaling for $\overline{w'b'}$ would be to use the eddy root-mean-square velocity $\sqrt{\overline{v'^2}}$ as the scaling for the v' contribution. However, this leaves the b' component isolated, and with no clear reasoning about how the buoyancy perturbation would relate to coarse-grid quantities, we are again stuck.

Fox-Kemper et al. (2008) (hereafter FFH) instead chose to use kinematic arguments to scale for this term, noting that $\overline{w'b'}$ is functionally equivalent to the rate of potential energy extraction by the baroclinic eddies. They proceeded by assessing the rate of potential energy release that would occur if two fluid parcels were exchanged over a decorrelation distance $(\Delta y, \Delta z)$ in a time Δt, so that

$$\frac{\Delta PE}{\Delta t} \propto \frac{-\Delta z(\Delta y M^2 + \Delta z N^2)}{\Delta t}. \tag{3.1}$$

They assumed that the relevant eddy time scale was advective, so that $\Delta t \propto \Delta y / v'$. They then substituted for the eddy velocity v' by showing numerically that it scaled with the initial mean thermal wind, so $v' \propto M^2 H / f$. They made the assumption that the vertical decorrelation distance Δz scaled with the fluid depth H[3] . Lastly, they employed the well-known idea that fluid exchange in baroclinic instability has to occur at a shallower slope than the mean isopycnals for there to be potential energy extraction, so that $\Delta z / \Delta y = (1/C) M^2 / N^2$. By substituting all of these relations into (3.1, a set of scalings emerged for both the horizontal and vertical buoyancy fluxes, appearing as

$$\overline{v'b'} = -(C-1)\frac{N^2 M^2 H^2}{|f|} \tag{3.2}$$

$$\overline{w'b'} = -\frac{(C-1)}{C}\frac{M^4 H^2}{|f|} \tag{3.3}$$

[3] This scaling depended on the true vertical excursion scale, $\sqrt{\overline{b'^2}}/N^2$, asymptoting to a constant fraction of the total fluid depth. Their calculation used only the maximum of this excursion scale in z, so it is unclear how well this scaling holds up when averaged in z. The research performed for this thesis suggest that this scaling does not hold for the latter averaging method (not shown).

It is easily seen that both scalings are dimensionally consistent and suggest that the ratio of the fluxes is proportional to the isopycnal slope (as in one of the founding assumptions). This analysis can be extended to scale for the elements of the stirring tensor by using the flux-gradient relationship, so

$$\begin{bmatrix} \overline{v'b'} \\ \overline{w'b'} \end{bmatrix} = \begin{bmatrix} R_{yy} & R_{yz} \\ R_{zy} & R_{zz} \end{bmatrix} \begin{bmatrix} \bar{b}_y \\ \bar{b}_z \end{bmatrix} \propto \begin{bmatrix} \frac{N^2H^2M^2}{|f|} \\ \frac{M^4H^2}{|f|} \end{bmatrix}, \tag{3.4}$$

$$R_{yy}\bar{b}_y + R_{yz}\bar{b}_z \propto \frac{N^2H^2M^2}{|f|}, \tag{3.5}$$

$$R_{zy}\bar{b}_y + R_{zz}\bar{b}_z \propto \frac{M^4H^2}{|f|}, \tag{3.6}$$

$$\begin{bmatrix} R_{yy} & R_{yz} \\ R_{zy} & R_{zz} \end{bmatrix} \propto \begin{bmatrix} \frac{N^2H^2}{|f|} & \frac{M^2H^2}{|f|} \\ \frac{M^2H^2}{|f|} & \frac{M^4H^2}{N^2|f|} \end{bmatrix}. \tag{3.7}$$

Another choice would be to do the reverse of the procedure above: scale for the elements of the stirring tensor directly, extending those scalings to obtain the fluxes afterwards. This offers the advantage that we can think of our scalings in terms of diffusivities rather than fluxes, for which a large body of literature already exists (see Section 1.8). In the end, regardless of which direction one wishes to proceed in the scaling formulations, both answers should match at least conceptually.

Any discussion of eddy diffusivity inevitably comes back to the flux-gradient relationship, since that it the primary assumption linking the ensemble-averaged eddy fluxes to the coarse-grained tracer gradient. The diffusivity governs the proportionality between these quantities, but it is useful to view the diffusivity through the framework of the flux-gradient relationship to see what sort of insight one might obtain. In this sense it is important to recall that the flux-gradient relationship is based on the notion of a mixing length, or the distance a fluid parcel is displaced before its properties become so well mixed as to be indistinguishable from the background flow, and that oceanographers generally assume that such mixing length scales with the eddy scale (Holloway, 1986; Salmon, 1998; Stammer, 1998; Klocher et al., 2012, in press). This assumption is discussed more critically below.

Invoking a mixing length argument for the diffusivity scaling leaves us only to consider eddy kinetic energy (EKE) as the other piece of the puzzle, since that is the only way to be consistent dimensionally. First, we can consider a scaling to be based on the (Lagrangian) supposition that

$$\text{Mixing Length} \times \sqrt{\text{EKE}} = \kappa \tag{3.8}$$

The notion that the mixing length and diffusivity scale with eddy kinetic energy dates back to the original work by (Prandtl, 1935). Indeed, various authors (Stammer, 1998; Marshall et al., 2006; Sallée et al., 2008; Abernathey et al., 2010; Ferrari and Nikurashin, 2010) have found a connection between the eddy kinetic energy and eddy diffusivity, though not without caveats. Griesel et al. (2009) argue that the EKE is only loosely correlated with the diffusivity if one looks at the vertical structure of the two quantities, suggesting a more complex relationship perhaps involving other factors. This loose correlation has also led to different explanations about how to view areas of strong EKE in terms of mixing strength. There has been even more dispute over the effects of strong eddy activity when superimposed on a strong mean flow. Recent studies (Marshall et al., 2006; Shuckburgh et al., 2009; Abernathey et al., 2010; Ferrari and Nikurashin, 2010) have suggested that the strong mean flow of jets, for example, tend to suppress mixing and thus lower the eddy diffusivity[4] .

So research suggests that the EKE connection in (3.8) has been verified, despite being somewhat tenuous[5] . So what of the mixing length part of the equation? Namely, how does one go about choosing an appropriate mixing length to plug into (3.8)? Firstly, it is important to note that the mixing length and the eddy length scale (the subject of many observational studies from Section 1.8) are **not** identical, either physically or conceptually. The mixing length refers to a distance a parcel can be transported before irreversible mixing makes the parcel indistinguishable from its surroundings, whereas the eddy length scale refers to the physical size of the turbulent flow. However, for simplicity it is often assumed that these length scales are proportional to one

[4] Linear theory (Green, 1970; Marshall, 1982; Killworth, 1997) predicts the eddy diffusivity to be proportional to $EKE/(u-c)^2$, where u is the mean velocity and c is the baroclinic wave speed.

[5] "Anisotropic" might be a better word.

another and are thus used interchangeably[6] . We will proceed under this assumption, using the term "eddy length scale" to refer to that part of the diffusivity pertaining to displacement distance.

Now we return to the question of how to choose an appropriate eddy length to plug into (3.8)? Any argument over how to choose an appropriate eddy length scale for an OGCM is invariably complicated by the presence of the inverse cascade of eddy kinetic energy. This inverse cascade represents the tendency of geostrophic turbulence to transfer energy to larger scales in both the horizontal and the vertical, and is a consequence of the analogy between quasigeostrophic flow and two-dimensional flow (Charney, 1971). Observations show an inverse spectral flux of energy from the deformation scale up to an arrest wavelength on the order of hundreds of kilometers which decreases with latitude but does not scale closely with the deformation scale (Chelton et al., 1998; Scott and Wang, 2005; Schlösser and Eden, 2007; Tulloch et al., 2009). It is theorized that the inverse cascade can be arrested by Rossby waves (Rhines, 1975), stratification (Fu and Flierl, 1980; Smith and Vallis, 2001), or by dissipation (Arbic and Flierl, 2004; Thompson and Young, 2006), but the exact mechanism is as of yet unclear. Arguments for the termination mechanism notwithstanding, the ansatz often made is that the lateral transport of tracers is dominated by the largest eddies (Howells, 1960; Haine and Marshall, 1998; Spall, 2000; Larichev and Held, 1995; Schneider and Walker, 2006; Fox-Kemper et al., 2008).

One possibility is to use the statistical moments of the spectra to "measure" the energy-containing scales (Stammer, 1997; Scott and Wang, 2005; Tulloch et al., 2011). However, even if such measurements are made, none of this information about eddy scales would be available in a coarse OGCM run. Lacking turbulence statistics, a single length scale will have to suffice, and regardless of which length scale we choose, we must proceed with the understanding that some other factor(s) should be present to adjust for the inverse cascade. An obvious choice is to begin with a scale that we know is ubiquitous in baroclinic instability, the Rossby deformation radius.

[6] To be more precise, the mixing length arises alongside a gradient, in the sense that the perturbation of a tracer quantity is equal to its mixing length multiplied by the change in tracer concentration as it traverses that length (the gradient). The eddy length scale, however, is not related to tracer concentration whatsoever. The notion that mixing length and eddy length are synonymous becomes very shaky when the tracer gradient is tight, such as in fronts or across eddy filaments.

In linear theory, the deformation radius is the eddy vertical scale H normalized by the Prandtl ratio N/f. The deformation radius appears as a crucial dimension in linear baroclinic instability, with unstable modes appearing near this scale. Because of its role as the characteristic scale of quasigeostrophic turbulence, it has been argued that the deformation radius should play the role of mixing length in eddy diffusivity calculations (Stone, 1972**a**; Stammer, 1998).

However, due to the presence of the inverse cascade, even more arguments exist that the deformation radius is not the appropriate choice for this role[7] . In nonlinear calculations, the zone of eddy activity quickly expands past the deformation radius. Green (1970) argues that a more suitable choice of length scale is the baroclinic zone width, which here is N^2H/M^2, since the horizontal scale of the eddies is limited by the availability of mean potential energy (APE).

Given that the majority of the eddy kinetic energy (EKE) is trapped in a wavenumber range between the deformation radius and the time-evolving front width, it is convenient to choose one of these length scales and rely on nondimensional parameters to reconcile the difference (see Appendix D). Hereafter the assumed horizontal eddy length scale will be the baroclinic zone width, with a focus on using a power of Ri to improve the approximation. The front width, N^2H/M^2 is larger than the deformation radius by a factor of $\sqrt{Ri}$, so it is reasonable to expect that a good scaling for δy might involve a power of Ri between -0.5 and 0. Finally, we must remember that in three dimensions the eddies will have a vertical aspect as well. For now we shall consider the simple case of a fluid with constant stratification; in this case the eddies extend the full depth of the water column, so the vertical eddy length scale is chosen be proportional to the full fluid depth H.

With the eddy kinetic energy and length scale arguments in place, we can now consider how these pieces fit into a scaling of the full transport tensor $\mathbf{R}$. Rather than proceed with scaling for each element of $\mathbf{R}$ directly, however, we will first divide $\mathbf{R}$ into its symmetric and antisymmetric parts ($\mathbf{S}$ and $\mathbf{A}$, respectively). Recalling from Section 1.7 that these parts correspond to diffusion

[7] Indeed, observational evidence (Stammer, 1997; Chelton et al., 2007) has shown that the deformation scale correlates poorly with the eddy spatial scale, particularly in the Antarctic Circumpolar Current (Larichev and Held, 1995; Smith, 2007; Fox-Kemper et al., 2008). In particular, it must be emphasized that the deformation radius, in conjunction with the Eady time scale $T = Ri/f$, arises from **linear** theory and should not necessarily be expected to retain its importance in a nonlinear turbulence problem.

and advection, we should consider their contribution separately and reason through their respective scaling arguments as such.

3.1.1 Diffusive Tensor Scaling

A purely diffusive tensor can be cast in terms of autocorrelation and cross-correlation functions of Lagrangian parcel displacements (Taylor, 1921; Plumb, 1979; Plumb and Mahlman, 1987). Defining the horizontal and vertical displacements (η, ξ), this tensor is written

$$\mathbf{S} = \begin{bmatrix} \frac{\partial}{\partial t}\left(\frac{1}{2}\overline{\eta^2}\right) & \frac{\partial}{\partial t}\left(\frac{1}{2}\overline{\eta\xi}\right) \\ \frac{\partial}{\partial t}\left(\frac{1}{2}\overline{\xi\eta}\right) & \frac{\partial}{\partial t}\left(\frac{1}{2}\overline{\xi^2}\right) \end{bmatrix}. \tag{3.9}$$

It is appropriate to approximate $\frac{\partial}{\partial t}\left(\frac{1}{2}\overline{\eta^2}\right) = \overline{v'\eta}$ by either of the expressions $\overline{v'^2}\delta t$ or $\sqrt{\overline{v'^2}}\delta y$, where $\overline{v'^2}$ is the Eulerian RMS eddy velocity and $(\delta t, \delta y)$ are the eddy time and length scales, respectively. Since we are equipped with these scales from the discussion above,

$$\eta \sim \delta y \propto \frac{N^2 H}{M^2}, \qquad \frac{\partial \eta}{\partial t} \sim \frac{\delta y}{\delta t} \propto \sqrt{\overline{v'^2}}, \tag{3.10}$$

$$\xi \sim \delta z \propto H, \qquad \frac{\partial \xi}{\partial t} \sim \frac{\delta z}{\delta t} \propto \sqrt{\overline{w'^2}}, \tag{3.11}$$

and we can directly substitute in to $\mathbf{S}$ to obtain a scaling for the full diffusive tensor. This appears as

$$\mathbf{S} \propto \begin{bmatrix} \frac{N^2 H}{M^2}\left(\sqrt{\overline{v'^2}}\right) & \frac{H}{M^2}\left(\sqrt{\overline{v'^2}}M^2 + \sqrt{\overline{w'^2}}N^2\right) \\ \frac{H}{M^2}\left(\sqrt{\overline{v'^2}}M^2 + \sqrt{\overline{w'^2}}N^2\right) & H\left(\sqrt{\overline{w'^2}}\right) \end{bmatrix}., \tag{3.12}$$

where elementwise we have

$$S_{yy} = \frac{\partial}{\partial t}\left(\frac{1}{2}\overline{\eta^2}\right) \propto \frac{N^2 H}{M^2}\left(\sqrt{\overline{v'^2}}\right), \tag{3.13}$$

$$S_{yz} = S_{zy} = \frac{1}{2}\left(\overline{\eta\frac{\partial \xi}{\partial t}} + \overline{\xi\frac{\partial \eta}{\partial t}}\right) \propto \frac{H}{M^2}\left(\sqrt{\overline{v'^2}}M^2 + \sqrt{\overline{w'^2}}N^2\right), \tag{3.14}$$

$$S_{zz} = \frac{\partial}{\partial t}\left(\frac{1}{2}\overline{\xi^2}\right) \propto H\left(\sqrt{\overline{w'^2}}\right), \tag{3.15}$$

3.1.2 Advective Tensor Scaling

We can form a dimensional scaling argument for the antisymmetric tensor $\mathbf{A}$ by following the logic laid out in FFH. Recall from Section 1.7.1 that the divergence of $\mathbf{A}$ is equivalent to advection by an eddy-induced velocity $u^\dagger$, which due to its nondivergence is equal to the the curl of a streamfunction Ψ. Through this tangled web of derivatives, we found that the elements of Ψ land in the off-diagonal elements of $\mathbf{A}$. Fortunately, in two dimensions the relationship between Ψ and $\mathbf{A}$ is quite simple, and reduces to

$$\mathbf{A} = \begin{bmatrix} 0 & \psi \\ -\psi & 0 \end{bmatrix}. \tag{3.16}$$

This enables us to describe the scaling for $\mathbf{A}$ through a single element, ψ. FFH focuses on formulating a ψ such that the vertical buoyancy flux and extraction rate of APE are captured. They form a scaling law for $\overline{w'b'}$ by considering an exchange of fluid parcels over a decorrelation distance $(\Delta y, \Delta z)$ in time Δt, so that

$$\overline{v'b'} \propto \frac{\Delta y(\Delta y M^2 + \Delta z N^2)}{\Delta t}, \overline{w'b'} \propto \frac{\Delta z(\Delta y M^2 + \Delta z N^2)}{\Delta t}. \tag{3.17}$$

This approach is appropriate for scaling ψ only, since isoneutral diffusion does not affect the APE of the system (Griffies, 1998). Making the same substitutions as in (3.10) and (3.11), the dimensional scalings for the advective fluxes are

$$\overline{v'b'}_s \propto \frac{N^2 H}{M^2}\left(\sqrt{v'^2}M^2 + \sqrt{w'^2}N^2\right) \tag{3.18}$$

$$\overline{w'b'}_s \propto H\left(\sqrt{v'^2}M^2 + \sqrt{w'^2}N^2\right), \tag{3.19}$$

where henceforth the subscript s will indicate a scaling. Division by the buoyancy gradient recovers for us the scalings for ψ that we seek; that is, division of $\overline{v'b'}_s$ by N^2 and division of $\overline{w'b'}_s$ by M^2 leaves us with

$$\psi \propto \frac{H}{M^2}\left(\sqrt{v'^2}M^2 + \sqrt{w'^2}N^2\right). \tag{3.20}$$

3.1.3 Transport Tensor Scaling

We can recombine the scalings for both **S** and **A** to obtain the scaling for the full transport tensor **R**. In two dimensions this tensor is written

$$\mathbf{R} = \mathbf{S} + \mathbf{A} = \begin{bmatrix} \frac{\partial}{\partial t}\left(\frac{1}{2}\overline{\eta^2}\right) & \frac{\partial}{\partial t}\left(\frac{1}{2}\overline{\eta\xi}\right) \\ \frac{\partial}{\partial t}\left(\frac{1}{2}\overline{\xi\eta}\right) & \frac{\partial}{\partial t}\left(\frac{1}{2}\overline{\xi^2}\right) \end{bmatrix} + \begin{bmatrix} 0 & \psi \\ -\psi & 0 \end{bmatrix}. \tag{3.21}$$

If we assume that the scalings for **S** and **A** share the same coefficients for their common elements (akin to the Dukowicz and Smith (1997) argument that the Redi and GM coefficients should be equal on an isopycnal surface), then the scaling for **R** takes the form

$$\mathbf{R} \propto \begin{bmatrix} \frac{N^2 H}{M^2}\left(\sqrt{v'^2}\right) & 0 \\ \frac{H}{M^2}\left(\sqrt{v'^2}M^2 + \sqrt{w'^2}N^2\right) & H\left(\sqrt{w'^2}\right) \end{bmatrix}, \tag{3.22}$$

$$\overline{v'b'} \propto N^2 H\left(\sqrt{v'^2}\right). \tag{3.23}$$

$$\overline{w'b'} \propto H\left(\sqrt{v'^2}M^2 + 2\sqrt{w'^2}N^2\right). \tag{3.24}$$

The same logic provides the scalings here and in FFH, except here it is not assumed that the horizontal eddy velocity scales as the mean thermal wind velocity. Fig. 3.2 shows the time-evolving ratio of eddy to mean velocity varies during simulations and according to the initial Richardson number. Likewise, Fig. 3.2b shows that the eddy velocity slope differs from the isopycnal slope and with Richardson number. Therefore, EKE and Ri contain **distinct** information about the instantaneous state of the turbulence in a way that a naive scaling using only M^2 and N^2 does not. Using eddy velocity statistics in conjunction with powers of Ri lends accuracy to the scalings, but to realize this extra accuracy in a model requires successful parameterization of the EKE. Some authors have proposed prognostic methods for EKE (Eden and Greatbatch, 2008; Eden, 2010**b**), and such approaches are common in engineering applications (Pope, 2000). Later we will return to this point with suggestions about how to incorporate these scaling ideas into a model depending on which diagnostics are available, and the implications that each has on the robustness of a parameterization.

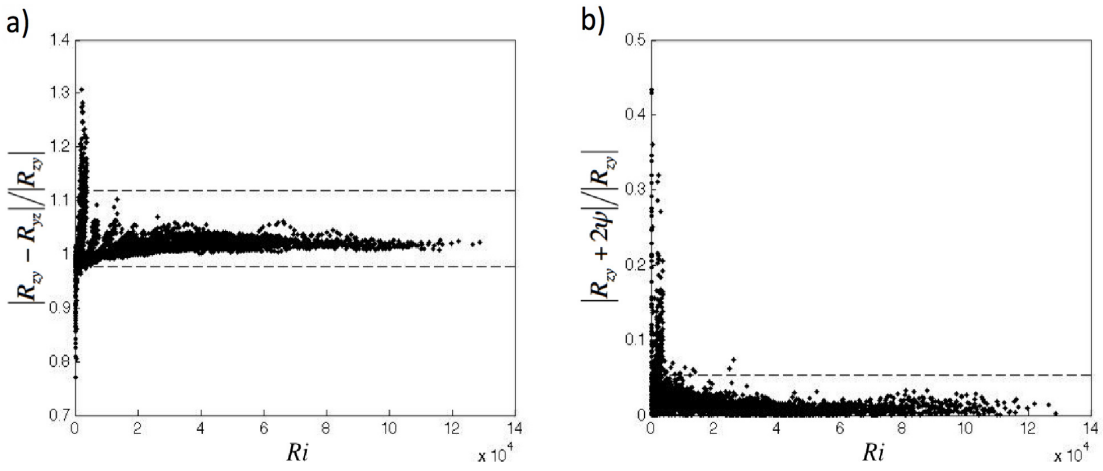

Figure 3.1: a) Comparison of R_{yz} and R_{zy}, confirming that R_{yz} is essentially equal to zero relative to R_{zy}. b) The equality suggested in Dukowicz and Smith (1997), $\psi = \kappa S$, is true to within 6%. in all snapshots except at small Ri. Dashed lines indicate the 95% confidence intervals.

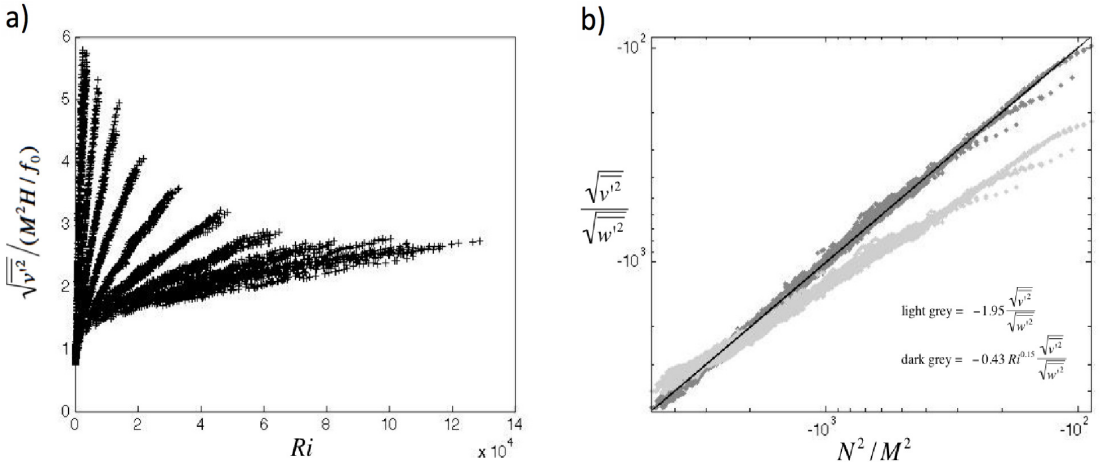

Figure 3.2: a) The horizontal RMS eddy velocity divided by the mean thermal wind. The degree to which a parameterization would suffer from approximating the eddy velocity with the mean velocity depends on the initial conditions. b) $\frac{\sqrt{v'^2}}{\sqrt{w'^2}} / \frac{N^2}{M^2} \propto Ri^{-0.15}$.

A lingering uncertainty about the scalings in (3.22) remains about whether it is appropriate to scale the $_{yz}$ term to zero. In reality, it may not be the case that GM and Redi coefficients exactly equal one another[8] , but with no further information to guide us, we will assume that the scaling for all the off-diagonal component of $\mathbf{S}$ and ψ is nonetheless the same. To confirm, it suffices to show that either R_{zy} dominates R_{yz}, or that $R_{zy} \approx -2\psi$. Fig. 3.1 shows that indeed the R_{yz} component is quite small and that the relationship between ψ and $\kappa_1\mathbf{S}$ is as predicted by GM, Redi, and Dukowicz and Smith (1997). Below, the scaling for tensor element R_{yz} is taken to be the same as for R_{zy}, only the leading coefficient is found to be near zero. The results from the models support this point except at small Richardson numbers (< 2500), when we anticipate greater vertical excursions due to coherent vortices crossing the density surfaces (McDougall, 1987).

3.2 Transport Tensor Diagnosis

The scalings (3.22) - (3.24) form the basis for the scaling laws sought in the model runs, anticipating that a nondimensional numerical constant and potentially small powers of Ri or Ro will be necessary to optimize them. Now that the scaling for the transport tensor is in place, we can design a suite of experiments to refine and optimize each of them. Done properly, this requires a large ensemble of model "challenges", in which we can explore how the eddies behave across all manner of flow profiles.

The initial intent for the eddy parameterization challenge suite was for it to be divided into three parts. The first part, based on the Eady (1949) problem (Appendix C.2) was to act as the simplest possible model for which baroclinic instability can be realized. The second part, featuring stratification that decreased exponentially with depth down to a prescribed minimum value at the bottom surface, was to be an intermediate step that would be a better approximation to the real ocean. The third part was to use a self-organizing map to extract "canonical" stratification and shear profiles from an eddy-resolving global model, and to use those profiles as our initial conditions. Each successive part represents an increase in complexity, but provides us with more information

[8] This will be analyzed in greater detail when we discuss vertical structures in Chapter 4.

about how the diffusivity is affected in ever more realistic flows. Here we begin with a discussion of the Eady model, with the objective that it will provide a straightforward test of the tracer inversion method as well as a basic set of scalings for $\mathbf{R}$. The results and derivations from this section are drawn from (Bachman and Fox-Kemper, submitted for review), the full transcript of which can be found in Appendix A.

3.2.1 Methodology

The simulations comprising the eddy parameterization challenge suite are run using Massachusetts Institute of Technology general circulation model (hereafter MITgcm) (Marshall, Adcroft, Hill, Perelman and Heisey, 1997). The hydrostatic, Boussinesq primitive equations (Section 1.2.5) are solved to simulate a zonally reentrant channel on the f-plane, with a temperature front oriented in the cross-channel direction. In this set of simulations, the density gradient is constant in z and y inside the front, akin to the Eady model. The use of the Eady model on the f-plane is simpler for the purpose of this research than β-plane models used in previous studies (Eden, 2010**a**, 2011), in that it has one fewer parameters and does not form jets.

The velocity fields are initialized in geostrophic balance, to minimize ageostrophic waves. Stratification (N^2), rotation (f), and front dimension (L_f) and velocity (U) are set according to the desired nondimensional parameters: Rossby ($Ro = U/fL_f$) and Richardson ($Ri = N^2/(\partial U/\partial z)^2 \approx N^2 f^2/|\nabla \bar{b}|^2$) numbers. Sixty-nine simulations are performed spanning a range of these parameters. Each simulation depicts the baroclinic spindown of the temperature front. A few inertial periods after the beginning of the model run the alongfront geostrophic shear goes baroclinically unstable[9] . Restratification will begin as the instabilities reach finite amplitude and begin to slump the isopycnals, akin to FFH. The eddies grow out of the frontal region and will spread meridionally throughout the domain (Fig 3.3). The simulation is stopped just before the buoyancy perturbation of the front reaches the lateral walls in order to prevent sidewall boundary effects[10] .

[9] An initial Richardson number greater than one precludes other instabilities, e.g. symmetric.

[10] The stopping criteria for a given run was satisfied when the front slumped far enough so that the leading edges of it nearly reached the lateral boundary. This criteria was tracked at each snapshot by calculating the buoyancy perturbation, $\hat{b} = \bar{b} - \bar{b}_y$. The value of $\hat{b}$ at the center of the front was defined to be identically zero at the start of

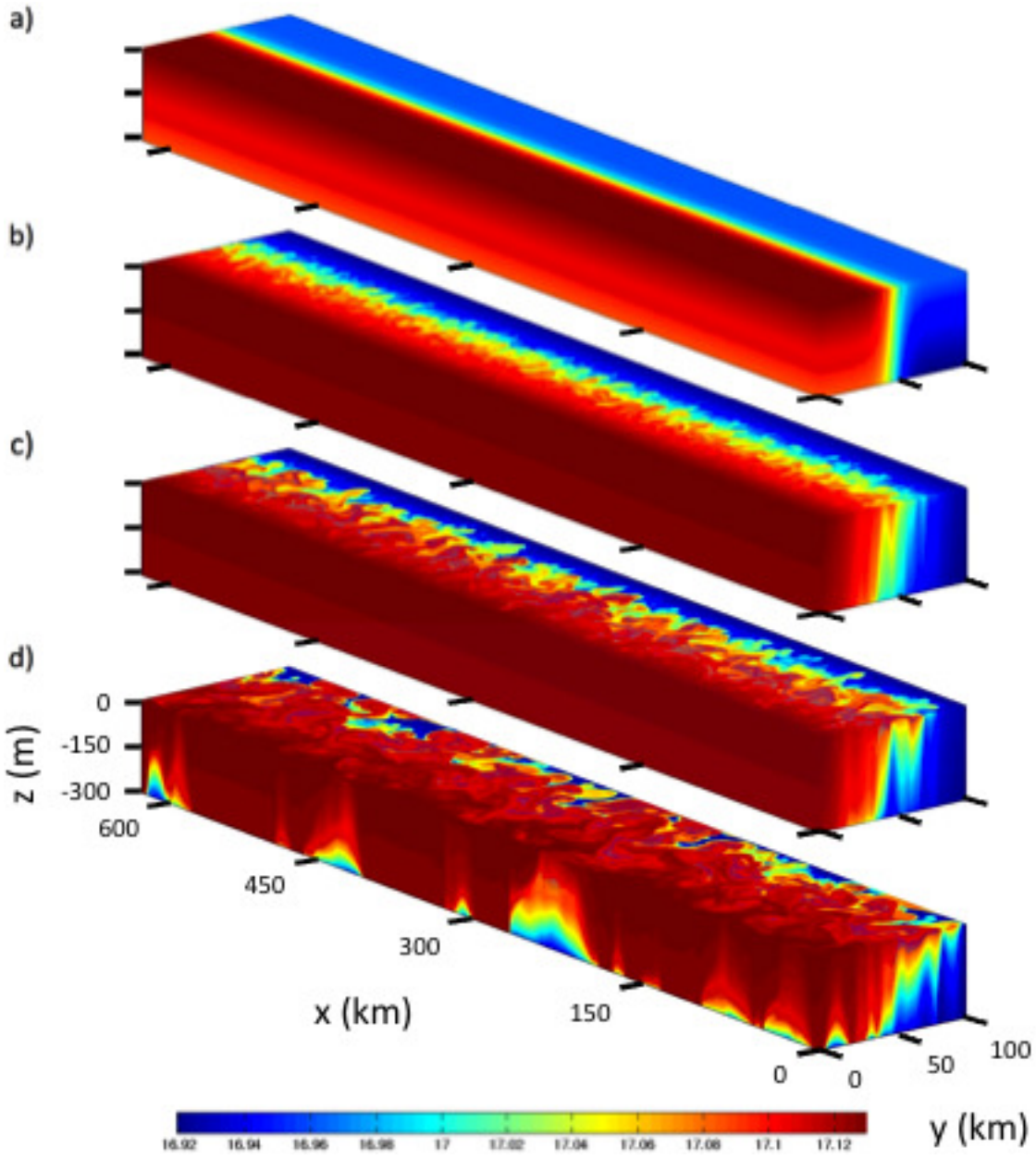

Figure 3.3: Potential temperature during a typical frontal spindown simulation. Baroclinic instability causes the front to slump towards the horizontal, releasing potential energy in the process. The eddies grow from this potential energy release as the front slumps from its initial configutation (a), through a fully nonlinear turbulent state (b-c), until the simulation is complete (d).

A new approach taken in this research is the use of transient snapshots in the collection of the eddy statistics. Despite the ever-changing nature of the ocean, an equilibrated eddy field is more commonly used (Lee et al., 1997; Eden, 2010**a**, 2011) to test eddy parameterizations than snapshots. However, in reaching equilibrium, the eddy fluxes are often constrained to reach a balance by satisfying viscous integral budgets or by balancing production and dissipation. Such balances depend explicitly and sensitively on unknown subgrid parameters and drag coefficients (Fox-Kemper and Pedlosky, 2004**b**; Thompson and Young, 2007). The transient simulations used in this research may not be representative of all situations that occur in the ocean, but they are not strongly dependent on poorly-known subgrid parameters.

Following the methods of FFH, statistics are gathered at each snapshot after the vertical eddy kinetic energy saturates. The criteria used for this saturation was that the domain-averaged vertical eddy kinetic energy did not change by more than 3% of its value at the previous snapshot. This criteria is essentially a proxy to ensure that the eddies have reached finite amplitude and that the eddy interactions have become saturated by nonlinearity. The time interval for each snapshot was chosen empirically based on the initial stratification so that each model run would generate about one hundred snapshots before completion. At each time snapshot the velocity, temperature, and tracer fields are zonally averaged and written to file (Fig. 3.4). One iteration of an unweighted, sliding-average smoothing algorithm is applied to all fields to reduce biases in the averaging from transient, powerful eddies and internal waves. Finite differencing is used to create the tracer gradient matrices, and the inversion for the transport tensor $\mathbf{R}$ is carried out using the method described in Chapter 2. Thus, in each run a time series of values is generated for each element of the transport tensor at each point in the zonally averaged field. Variability in these time series arises from the presence of internal gravity waves as well as temporal fluctuations in the eddy statistics, neither of which significantly affect the results of this research.

We have the freedom to choose the grid resolution in our models, giving us the flexibility to

the run, so the frontal passage at any location was imminent when $\hat{b}$ began to approach zero there. The runs were halted when $\hat{b}$ became zero at a point ten gridpoints from the edge of the domain and along the bottom boundary.

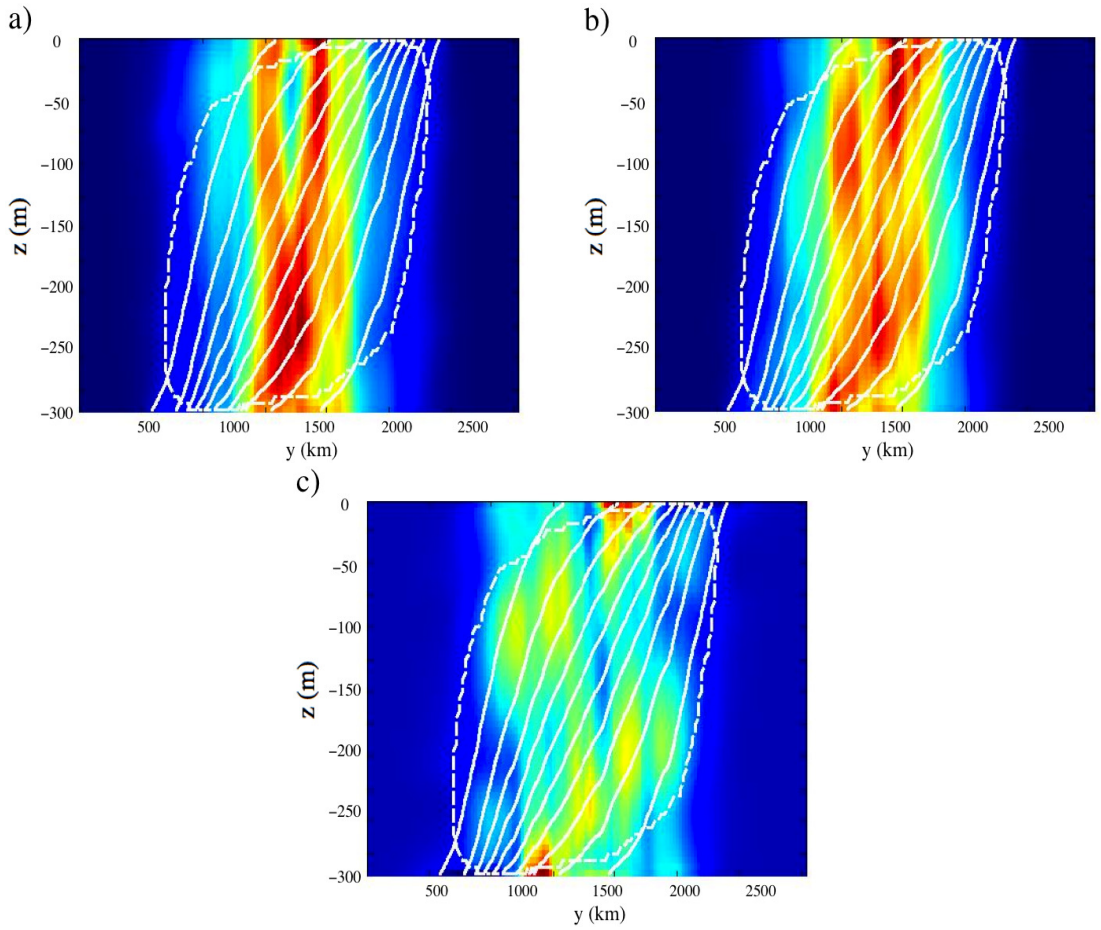

Figure 3.4: Example snapshots during a typical simulation, taken after x-averaging. Shown here are mean isopycnals (solid white lines) and eddying region (enclosed within the dashed white line). The colored backgrounds represent fields for a) R_{yy}, b) R_{zy}, and c) R_{zz}.

choose between better resolution of the eddies or faster completion time for the simulations. For the Eady model, we choose the grid resolution to be the Rossby radius of deformation. Theory predicts that the deformation radius is a dividing line for the existence (for shorter wavelengths) and the non-existence[11] (for longer wavelengths) of a region in the fluid where a growing disturbance imparts energy to the basic temperature distribution (Green, 1960; Bretherton, 1966**b**). For wavelengths larger than the deformation radius it is predicted that baroclinic instability will grow by extracting available potential energy from the mean flow and converting it to eddy kinetic energy. The inverse cascade of energy to larger scales suggests that energy will be quickly transferred away from the gridscale into more fully resolved features, so that it is not necessary to over-resolve our simulations by choosing a grid resolution smaller than the deformation radius. The front width is automatically scaled so that at least ten deformation radii lie within the front. This essentially guarantees that the effects of barotropic instability will be avoided, and that several gridpoints will be available to resolve each mesoscale eddy.

The nonlinear transfer of energy upscale from the deformation radius guarantees that the contribution of the smallest eddies will be negligible to the total flux at each point. Therefore, increasing the resolution below the deformation radius would increase the computation time while yielding essentially the same result. Coarsening the resolution slightly results in a similar situation, where the local resolved flux is largely unchanged. However, we would like to ensure that we capture the fastest growing linear mode, which in the Eady problem is only slightly larger than the deformation radius. Coarsening the resolution to the point where this mode is not resolved results in a substantial increase in the model spinup time, as slower-growing modes would now dominate the early phase of the simulations. Therefore, we can consider making the gridscale equal to the deformation radius to be a happy medium, where we are ensured of a true "eddy-resolving" solution without wasting computation time.

To be fair in the informing of an eddy parameterization, pointwise values of the transport

[11] It must be noted that the classical setup for the Eady problem takes the planetary vorticity gradient $\beta = 0$. In cases where $\beta > 0$, the flow is baroclinically unstable to disturbances of all wavelengths. However, we predict that the beta effect in the ocean is too small at the mesoscale to matter much, so we let $\beta = 0$ for all simulations.

tensor are not as useful as domain-averaged values, since the entire domain in these fine-resolution runs is **ipso facto** below the grid scale of a non-eddy-resolving model. Care must be taken in how one chooses to average these quantities, however. Averaging over the entire basin is the most realistic method for the sake of a parameterization, in that the horizontal grid is fixed in time. However, this leads to inconsistencies between quantities that are nonzero over the whole domain (such as M^2 and N^2) and those that are nonzero only in the "eddying region" (such as the tensor components and tracer fluxes). At any given timestep the eddies will be most active in those parts of the domain experiencing potential energy release; these quantities quickly taper to zero as one travels horizontally away from the center of the front, or vertically towards the top or bottom boundaries. The chosen solution was to average over those points of the domain where the vertical buoyancy flux $\overline{w'b'}$ is greater than 10% of its global maximum value. All averaging operations in this paper are taken over this region. In this way, the averaging only includes regions undergoing significant PE release, the overall area of which grows as energy cascades to graver scales.

These runs used free slip boundary conditions along the lateral and bottom boundaries. The strain-tension form of the viscous terms in the primitive equations was used, with the Laplacian Smagorinsky (1963, 1993) viscosity was set to be $\nu = (\Delta x/\pi)^2 \sqrt{(\nabla_k u_i + \nabla_i u_k)(\nabla_k u_i + \nabla_i u_k)/4}$. Implicit numerical diffusion and implicit viscosity were both used.

3.2.2 Results

In the introduction to this thesis we stated that the goal of the parameterization challenge suite was to develop a set of scalings for $\mathbf{R}$ that would help to evaluate and refine extant and future eddy parameterizations. With the pseudoinversion method of Chapter 2 and the dimensional scalings of Section 3.1.3, the necessary pieces to pursue this goal are now in place. So far, we have been able to argue that the scalings for $\mathbf{R}$ can be based on physical reasoning, but with the simulation results in hand both empiricism and data analysis now represent the way forward.

As noted previously, dimensional scalings for each of the diffusivities do not rule out the possibility of dependence on nondimensional parameters. In particular, the nondimensionaliza-

tion of the Boussinesq, hydrostatic primitive equations (Appendix D.1.1) reveals that the Rossby and Richardson numbers are relevant in this problem. Note that in the nondimensionalization we omitted the viscous term in the momentum equation, which precludes us from considering nondimensional parameters having to deal with the Reynolds stresses, such as the Reynolds and Peclet numbers. This was done by design, since at the oceanic mesoscale these numbers are dynamically unimportant due to small viscosity and molecular diffusivity, and are therefore not included in this analysis.

The first question we must ask is how important is rotation to the eddy spindown problem? FFH suggest that the Rossby number inside the front becomes irrelevant as soon as the eddies expand beyond the front width in the horizontal, which occurs not long after finite amplitude is achieved (Green, 1970). The results from these models results agree with this claim (not shown). This is fortuitous, since the problem of diagnosing a time-evolving Rossby number in a moving front is conceptually quite difficult. However, the Richardson number, which describes the overall stability of the flow by measuring the relative importance of stratification and shear, is central to the problem. It can be used to properly scale the buoyancy fluxes and elements of the transport tensor. Fig. 3.5 shows the dimensional scalings of 3.1.3 compared to the diagnosed values of each tensor element. The leading constant and power of Richardson number on each term are obtained by performing a logarithmic least-squares fit of the dimensional scalings to the true values of each element.

The least-squares fit gives some insight as to how important the EKE and Richardson numbers are to this problem. The fits to each element are performed spanning over three orders of magnitude, providing a parameter space that is plenty large enough for an incorrect scaling to go astray. This is evident when looking at both the dark grey and light grey clouds in Fig. 3.5, which represent scalings without the Richardson number and EKE contributions, respectively. The Richardson number is necessary to keep the vertical fluxes in check (bottom row). In particular, the negative exponent on the Richardson number ensures that these fluxes are not too large as the stratification becomes stronger. The consequence of not having the Ri contribution can be seen by the dark grey points

Quantity	Optimized (3.22) with Ri	Optimized (3.22) without Ri
$R_{yy,s}$	$(0.35 \pm 0.10) Ri^{-0.18 \pm 0.06} \frac{N^2 H}{M^2} \left(\sqrt{v'^2} \right)$	$(0.07 \pm 0.05) \frac{N^2 H}{M^2} \left(\sqrt{v'^2} \right)$
$R_{yz,s}$	$(0.002 \pm 0.01) \frac{H}{M^2} \left(\sqrt{v'^2} M^2 + \sqrt{w'^2} N^2 \right)$	$(0.002 \pm 0.01) \frac{H}{M^2} \left(\sqrt{v'^2} M^2 + \sqrt{w'^2} N^2 \right)$
$R_{zy,s}$	$(0.33 \pm 0.08) Ri^{-0.32 \pm 0.10} \frac{H}{M^2} \left(\sqrt{v'^2} M^2 + \sqrt{w'^2} N^2 \right)$	$(0.03 \pm 0.07) \frac{H}{M^2} \left(\sqrt{v'^2} M^2 + \sqrt{w'^2} N^2 \right)$
$R_{zz,s}$	$(0.32 \pm 0.03) Ri^{-0.35 \pm 0.03} H \left(\sqrt{w'^2} \right)$	$(0.03 \pm 0.08) H \left(\sqrt{w'^2} \right)$

Table 3.1: Empirical optimized tensor element scalings with eddy statistics corresponding to Fig. 3.5, Fig. 3.6, and (3.22), with 95% confidence intervals. Note that the reported error of the component diagnosis is ±28% from the $R_{yy,s}$ leading coefficient uncertainty. Note also that based on the observed scatter there is no dependence on Ri for $R_{yz,s}$, and so we fix the exponent on Ri to be zero for that scaling.

trending above the solid black line (the true value). On the other hand, the EKE contribution has a significant effect on both the horizontal and vertical fluxes. Even though the scatter of the light grey points remains centered around the true fluxes, it is easy to see that the actual trend lines are going **across** the true fluxes, not along them[12] One can conclude that without the EKE involved in a diffusivity scaling there is no real scaling relation to be had at all; that is, the correlation of $\mathbf{R}$ with the scalings in (3.22) depends fully on the use of $\sqrt{\overline{v'^2}}$ and $\sqrt{\overline{w'^2}}$.

3.2.2.1 Deviation from Redi

The tensor scaling (3.22) specifies a form that the transport tensor should have if it were to match the GM-Redi parameterization form. However, it is possible for this form to be satisfied and still not exactly match either GM or Redi specifically. The reason for pointing this caveat out is that the symmetric part of the diagnosed tensor does not exactly agree with the Redi isoneutral diffusion tensor. The true form of Redi in 2D under the small angle approximation is

$$\mathbf{S}_{Redi} \propto \begin{bmatrix} \kappa_1 & \kappa_1 \mathcal{S} \\ \kappa_1 \mathcal{S} & \kappa_1 \mathcal{S}^2 \end{bmatrix}, \tag{3.25}$$

where κ_1 is the along-isopycnal diffusivity and $\mathcal{S} = \left| M^2 / N^2 \right|$ is the absolute value of the local isopycnal slope. The S_{yy} component obtained from the model results tends to be a factor of 3 too large (Fig. 3.7), so that

[12] This is also apparent in both plots of Fig. 3.6.

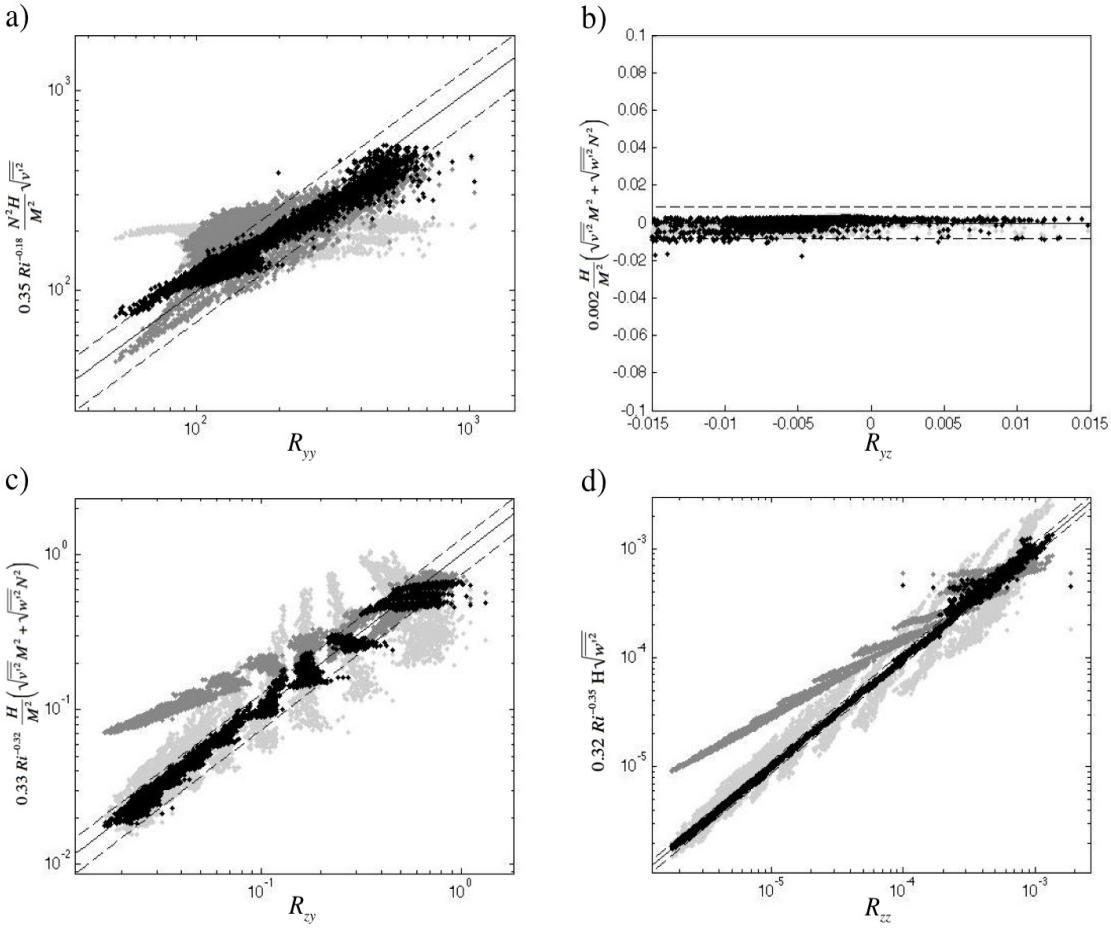

Figure 3.5: Diagnosed tensor components versus those parametrically scaled. a) $R_{yy,s}$, b) $R_{yz,s}$, c) $R_{zy,s}$, d) $R_{zz,s}$. In all panels black shows (3.22) with an empirical Ri correction, dark grey shows (3.22) without an empirical Ri correction, and light grey shows FFH scalings (3.7). Scalings are given in Tables 3.1-3.2. Dashed lines indicate 95% confidence intervals.

Quantity	Optimized FFH form with Ri	Optimized FFH form without Ri
$R_{yy,s}$	$(0.77 \pm 0.75) Ri^{-0.18\pm0.18} \frac{N^2H^2}{\lvert f\rvert}$	$(0.17 \pm 0.48) \frac{N^2H^2}{\lvert f\rvert}$
$R_{yz,s}$	$(0.01 \pm 0.09) \frac{M^2H^2}{\lvert f\rvert}$	$(0.01 \pm 0.09) \frac{M^2H^2}{\lvert f\rvert}$
$R_{zy,s}$	$(0.85 \pm 0.77) Ri^{-0.22\pm0.23} \frac{M^2H^2}{\lvert f\rvert}$	$(0.17 \pm 0.68) \frac{M^2H^2}{\lvert f\rvert}$
$R_{zz,s}$	$(0.30 \pm 0.21) Ri^{-0.20\pm0.14} \frac{M^4H^2}{N^2\lvert f\rvert}$	$(0.06 \pm 0.07) \frac{M^4H^2}{N^2\lvert f\rvert}$

Table 3.2: Empirical optimized tensor element scalings without eddy statistics, i.e., following FFH, corresponding to Fig. 3.5, Fig. 3.6, and (3.7), with 95% confidence intervals. Note that the $R_{zy,s}$ agrees with the FFH estimate of $0.06 - 0.06M^2H^2/|f|$ if GM and Redi coefficients are the same so that $R_{zy,s} = 2\psi$. Note also that the coefficient for the FFH scaling is uncertain beyond $\pm 97\%$.

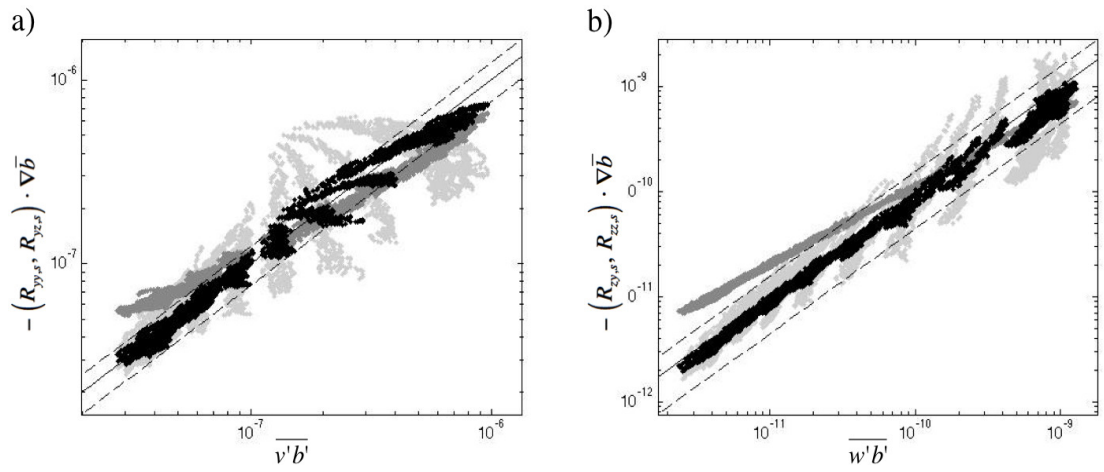

Figure 3.6: Reconstructions of a) $\overline{v'b'}$ and b) $\overline{w'b'}$ using the tensor scalings from Fig. 3.5 and Table 3.1-3.2. The solid lines indicate the true values of each flux. Black indicates reconstructions from the scalings from (3.22), with a power of Ri. 95% of the black data points are contained in the region bounded by the dashed lines. Dark grey indicates reconstructions from the scalings from (3.22), without a power of Ri; light grey indicates reconstructions from the FFH scalings (3.7) with a power of Ri.

$$\mathbf{S} \approx \begin{bmatrix} 3\kappa_1 & \kappa_1\mathcal{S} \\ \kappa_1\mathcal{S} & \kappa_1\mathcal{S}^2 \end{bmatrix} \tag{3.26}$$

The theory behind the form of Redi is sound and only relies on the well-known fact that oceanic transport tends to occur along neutral surfaces, so how could our diagnosed tensor not match it? It turns out that the time dependence of the spin-down problem can be used to understand both the excess of S_{yy} and the small diapycnal diffusivity κ_2. Consider the buoyancy variance equation

$$\frac{D\left(\frac{1}{2}\overline{b'^2}\right)}{Dt} = -\overline{\mathbf{u}'b'} \cdot \nabla\bar{b} - \overline{\mathbf{u}' \cdot \nabla\left(\frac{1}{2}\overline{b'^2}\right)} \tag{3.27}$$

Assuming the term on the far right is small[13] and using the preceding nondimensionalization and scaling results, as well as a proportionality for the flux direction compared to the isopycnal slope direction (not shown),

$$\overline{v'b'} \cdot \nabla\bar{b} \propto N^2M^2H\sqrt{\overline{v'^2}}, \quad \overline{w'b'} \cdot \nabla\bar{b} \propto N^2M^2H\sqrt{\overline{v'^2}}Ri^{-0.09}, \tag{3.28}$$

the resulting scaled buoyancy variance budget is unable to be exactly along isopycnals for all Ri. The $\overline{w'b'}$ term's contribution to the variance decreases relative to the $\overline{v'b'}$ term as Ri increases. For the range of Ri in our simulations (from 136 to 128,760), the relative contribution of the $\overline{w'b'}$ term is from 1.6 to 2.9 times smaller, with a mean of 2.5. This is close to the excess of S_{yy} over Redi of 2.8.

The above argument can explain away the largeness of the $_{yy}$ term, but how does it relate to the presence of a nonzero diapycnal diffusivity κ_2? After all, it is often argued that κ_2 should be zero in steady, adiabatic situations (McDougall and McIntosh, 1996). In such situations the Redi flux should also be exactly along the isopycnals, matching the form of (3.25). The solutions here are nearly adiabatic, but they are not steady as both eddy variance and isopycnal slope evolve during the course of each simulation. The buoyancy flux clearly has some diapycnal flux, presumably

[13] "Small" here being relative to the double-correlation terms. Quite simply, the argument is that multiplying three perturbation (prime) quantities should be smaller than multiplying two of them.

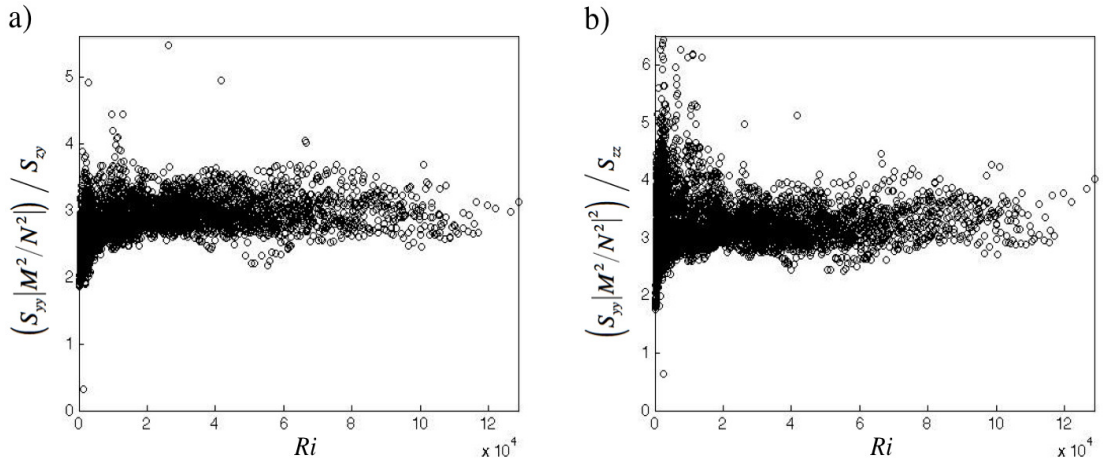

Figure 3.7: The ratio between S_{yy} multiplied by isopycnal slope and the offdiagonal elements of **S**. The Redi form of **S** would have that this ratio would be equal to one in both plots, which is not the case here. The observed ratio is greater than expected in comparison to the Redi along-isopyncal scaling by a factor of 3 on average. Thus, the eigenvectors of S are oriented at a slightly shallower angle than the isopycnal slope.

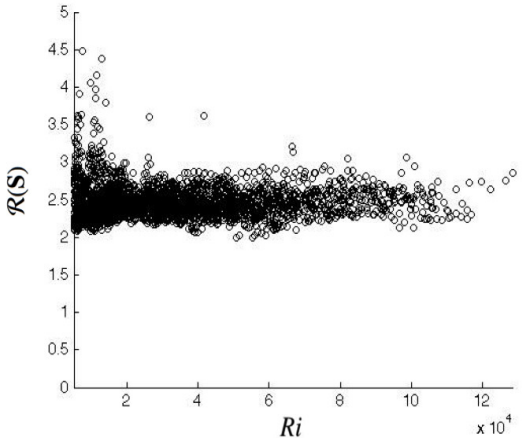

Figure 3.8: The ratio $\mathcal{R}(\mathbf{S})$ between the isopycnal slope and the slope of the diffusive flux. $\mathcal{R}(\mathbf{S})$ is above the value of 2 predicted by linear theory across the full range of Ri in the simulations.

associated with the neglected triple correlation and time dependence of eddy variance, since the terms on the right hand side do not balance exactly.

Linear theory suggests that the diffusive flux should be oriented at half the isopycnal slope to maximize potential energy extraction (Haine and Marshall, 1998). However, this result cannot be expected to hold precisely in a nonlinear, time-evolving simulation set. The model results suggest that the ratio of the isopycnal slope to the diffusive flux slope, calculated as

$$\mathcal{R}(\mathbf{S}) = \frac{\langle \mathcal{S} \rangle}{\left\langle \frac{S_{zy}M^2 + S_{zz}N^2}{S_{yy}M^2 + S_{yz}N^2} \right\rangle}, \tag{3.29}$$

remains consistently close to 2.5 across the full spectrum of Richardson numbers in the simulations (Fig. 3.8). Here the angle brackets indicate an average over the eddying region defined previously. This value is consistent with the above finding that the growth of eddy variance is responsible for the small diapycnal component of the diffusive flux. It also suggests that the excessively large value of S_{yy} can largely be attributed to the flux being directed below the true isopycnal slope.

3.2.2.2 Parameterization Options for an OGCM

Many current OGCM's use a combination of the GM and Redi tensors in calculating diffusivities. The diffusivities are often set to be equal to each other (Griffies, 1998) for numerical convenience, leaving a full mixing tensor of the form

$$\mathbf{R} = \mathbf{S} + \mathbf{A} \approx \begin{bmatrix} \kappa_1 & 0 \\ 2\kappa_1 \mathcal{S} & \kappa_1 \mathcal{S}^2 \end{bmatrix}. \tag{3.30}$$

Note that in the GM-Redi formulation κ_1 is described fully by the R_{yy} tensor element. All other elements are obtained by multiplying this value by some power of the isopycnal slope.

A modeler wishing to use the GM-Redi parameterization needs only to have a form for κ_1 to proceed. As we have shown, there are multiple options one can use for κ_1, and each of these has its own set of consequences in terms of accuracy and ease of implementation. However, one does not have stick with the GM-Redi paradigm, as one could try to take advantage of the buoyancy variance budget (3.27) to come up with an even more accurate parameterization. Among the options discussed so far, the most obvious ones are to: 1) use the "best" diagnosed $\mathbf{R}$ suggested by these model results, which would require some prescription of $\sqrt{v'^2}$ and $\sqrt{w'^2}$; 2) use a GM-Redi optimized version of these results, wherein a modeler could simply plug in a choice for κ calibrated from these results; 3) use an FFH-style κ_1, which would not require calculating $\sqrt{v'^2}$ or $\sqrt{w'^2}$; or 4) use a GM-Redi optimized version with an FFH-style κ_1. These options, with their corresponding relative errors as defined in (3.31), are shown in Table 3.3, with

$$E(\overline{\mathbf{u}'b'}) = \frac{\left|\overline{\mathbf{u}'b'} - \widetilde{\overline{\mathbf{u}'b'}}\right|}{\left|\overline{\mathbf{u}'b'}\right|} \tag{3.31}$$

Option 1 is clearly optimal insofar as accuracy is concerned, but a GM-Redi diffusivity using the κ_1 from option 2 is a good alternative. Any FFH-style implementations carry with them a nontrivial loss of accuracy, but the diagnostics required for these would be readily available in an OGCM.

Option	$E(\overline{\mathbf{u}'b'})$	$\kappa_{GM/Redi}$
1	0.188	Table 3.1, second column, or (3.32)
2	0.270	GM/Redi with $\kappa_1 = 0.32Ri^{-0.31}\frac{N^2H}{M^4}\left(\sqrt{\overline{v'^2}}M^2 + \sqrt{\overline{w'^2}}N^2\right)$, or (3.34)
3	0.551	Table 3.2, second column, or (3.33)
4	0.703	GM/Redi with $\kappa_1 = 0.58Ri^{-0.22}\frac{N^2H^2}{\lvert f\rvert}$, or (3.35)

Table 3.3: The relative errors based on different approximations to the scalings for $\mathbf{R}$. These errors are calculated by averaging over the region defined in Section 3.2.1.

In summary, the optimal full tensor, which uses the RMS eddy velocities $\sqrt{\overline{v'^2}}$ and $\sqrt{\overline{w'^2}}$, is

$$\mathbf{R} \propto \begin{bmatrix} 0.35Ri^{-0.18}\frac{N^2H}{M^2}\left(\sqrt{\overline{v'^2}}\right) & 0 \\ 0.33Ri^{-0.32}\frac{H}{M^2}\left(\sqrt{\overline{v'^2}}M^2 + \sqrt{\overline{w'^2}}N^2\right) & 0.32Ri^{-0.35}H\left(\sqrt{\overline{w'^2}}\right) \end{bmatrix} \tag{3.32}$$

The best FFH-style full tensor, which uses only the buoyancy gradients, is

$$\mathbf{R} \propto \begin{bmatrix} 0.77Ri^{-0.18}\frac{N^2H^2}{\lvert f\rvert} & 0 \\ 0.85Ri^{-0.22}\frac{M^2H^2}{\lvert f\rvert} & 0.30Ri^{-0.20}\frac{M^4H^2}{N^2\lvert f\rvert} \end{bmatrix} \tag{3.33}$$

For codes using the GM/Redi tensor, the optimal choice for the diffusivity is given by

$$\kappa_1 = 0.32Ri^{-0.31}\frac{N^2H}{M^4}\left(\sqrt{\overline{v'^2}}M^2 + \sqrt{\overline{w'^2}}N^2\right). \tag{3.34}$$

If the eddy velocities required for this κ_1 are not available, a good alternative is

$$\kappa_1 = 0.58Ri^{-0.22}\frac{N^2H^2}{\lvert f\rvert}. \tag{3.35}$$

Our prognosis for κ_1 is quite different than the values often used in IPCC-class models (Eden et al., 2009), and it is useful to compare them directly. Shy of using a global model to facilitate this comparison, to which we do not have access or funding at this time, we can list them side-by-side

and compare their formulations. The choices are:

$\kappa_1 = 800\ \mathrm{m}^2\ \mathrm{s}^{-1}$ (Danabasoglu, 2004)

$\kappa_1 = \alpha \frac{fL^2}{Ri^{1/2}}$ (Visbeck et al., 1997)

$\kappa_1 = 4000 \frac{N^2}{\max\{N^2\}}$ (Ferreira et al., 2005; Danabasoglu and Marshall, 2007)

$\kappa_1 = c \left(\min \left\{ \frac{\int_{-h}^{0} N/\pi \, dz}{|f|}, \sqrt{\frac{\int_{-h}^{0} N/\pi \, dz}{2\beta}}, \sqrt{v'\beta^{-1}} \right\} \right)^2 \frac{|\nabla_h \bar{b}|}{N}$ (Eden and Greatbatch, 2008)

$\kappa_1 = 0.32 Ri^{-0.31} \frac{N^2 H}{M^4} \left(\sqrt{\overline{v'^2}} M^2 + \sqrt{\overline{w'^2}} N^2 \right)$

Note that κ_1 is to be constant in the vertical for the first and second choices; the third has a vertical structure proportional to the vertical structure of N^2; the fourth is defined locally in both the horizontal and the vertical. The fifth choice, which is the value of κ_1 diagnosed in the research here, conceivably could be constant in the vertical or local in the vertical, depending on how one specifies the velocity variances. A study on the effects of our recommended κ_1 in a global model would be very interesting.

3.2.3 Summary

In this chapter we have presented the first component of the eddy parameterization challenge suite, consisting of a set of models featuring Eady-like stratification and shear. During this process we have developed scalings theories for each of the elements of $\mathbf{R}$ that we can test using the matrix pseudoinversion method (Chapter 2). The pseudoinversion has been shown to yield scalings for $\mathbf{R}$ that hold to within $\sim 10\%$, allowing us to evaluate the skill of GM90-Redi to a high degree of accuracy. We have also compared extant scalings (e.g. FFH) to the new ones from this research, suggesting a large loss of accuracy when the eddy velocity $\sqrt{\overline{\mathbf{u}'^2}}$ is not used.

Note, however, that the way we have performed the averaging in this study does not lend itself well to a local diagnosis of the diffusivity tensor. Barotropization and nonlocal eddy effects affect the local eddy transport both in y and in z, which is why we must press onto more complex

flow scenarios. The scalings here do not apply to every conceivable dynamical regime found in the ocean. Uneven bathymetry, boundary currents, jets, fronts, and other features complicate the growth and life cycle of the eddies. Even though we cannot possibly model all (or even many) of these, it is still important to keep them in mind as possible causes why our scalings may break down.

The next step will be to examine these same scalings in a more complex flow scenario. Namely, we will now move to simulations featuring exponential stratification, which is meant as an idealized, crude approximation to what occurs in the real ocean. With the next suite of models we will examine the vertical structure of κ_1 and ψ more in detail, and hopefully find a more local basis for our scalings of $\mathbf{R}$.[14]

[14] Hereafter we will only be concerned with the along-isopycnal diffusivity, and so for ease of notation we will refer to κ_1 simply as κ.

Chapter 4

Challenge Suite II - Exponentially-Stratified Models

4.1 Eddy Flux Vertical Structures

The Eady-like simulations from Chapter 3 have provided a simple testbed for the tracer gradient pseudoinversion, and have confirmed that the pseudoinversion can tell us important information about how to scale the eddy transport tensor $\mathbf{R}$. However, the simplicity of the Eady-like models is a double-edged sword - their simplicity has given us a solid set of scalings to start with, but such simple stratification cannot tell us how these scalings should vary in z. We should not expect that the inverse cascade of energy will always be strong enough to induce a nearly barotropic eddy field, especially considering how variable the stratification can be in the real ocean. Therefore, parameterizing the vertical structure of the eddy transport could be considered just as important as finding generalized scaling laws in the first place, for the vertical structure is what differentiates eddy behavior in the mixed layer, thermocline, and the weakly stratified abyss. Climate models have also been shown to be sensitive to how eddy fluxes are tapered in the boundary layers (Gough and Welch, 1994; Griffies et al., 2005; Gnanadesikan et al., 2007; Ferrari et al., 2008), adding extra motivation to address the vertical structure problem carefully.

One of the main challenges in finding the vertical structure of the eddy transport is due to the diabatic nature of the boundary layers. The original GM90 scheme is locally determined in z - that is, a unique value for the GM90 streamfunction Ψ (or equivalently, the bolus velocity $\mathbf{u}^*$) exists at each level in the vertical, with no transition scheme as the boundaries are approached. Unfortunately, the diabaticity in the boundary layers causes the GM90 scheme to break down, partly due to

vigorous small-scale turbulence that the scheme is not equipped to handle, and partly because the geostrophic motions are constrained to follow the boundary despite the isopycnal surfaces intersecting the boundary (Ferrari et al., 2008). As a result, GM90 tends to overestimate tracer transport in the boundary layers in comparison to observations and eddy-resolving experiments (Griffies, 2004). GM90 also is forced to interact directly with other boundary layer parameterizations (Price, 1981; Price et al., 1986; Large et al., 1994; Thomas, 2005) and does not properly represent restratification by submesoscale eddies in the surface mixed layer (FFH), suggesting that we need improvements to the basic scheme.

Diagnosing the vertical structure of the GM90 streamfunction alone is very challenging problem, but an additional difficulty is present when the Redi scheme is added. The core issue with GM90 in the boundary layers is that the vertical bolus velocity

$$w^* = \nabla \cdot \left(\kappa \frac{\nabla \bar{\rho}}{\bar{\rho}_z} \right). \tag{4.1}$$

must vanish at the ocean surface. Assuming the Dukowicz and Smith (1997, hereafter DS97) prediction of equal diffusivities for Redi and GM90, this suggests that either κ or the isopycnal slope $\frac{\nabla \bar{\rho}}{\bar{\rho}_z}$ must go to zero as we approach the surface. However, as isopycnal layers are known to outcrop at the surface and therefore their slopes cannot be zero,[1] this requires that $\kappa = 0$, contrary to observations (Robbins et al., 2000; Price, 2001; Danabasoglu et al., 2008) and violating evidence that mesoscale fluxes dominate the tracer budgets even in the mixed layer (Phillips and Rintoul, 2000; Weller et al., 2004; Marshall et al., 2005; Kuo et al., 2005). Part of this issue can be attributed to the GM90 scheme not being appropriate for the diabatic boundary layers where small-scale processes drive strong diapycnal eddy fluxes, but nevertheless the breakdown of the Dukowicz and Smith result is still something we must anticipate in our diagnosis.[2]

[1] In fact, they can actually become infinitely steep due to small-scale mixing and surface forcing!

[2] From a TEM perspective (Section 1.3.2), a parameterization could specify that the along-boundary residual velocity and flux be nonzero while the across-boundary components be zero (Treguier et al., 1997). Ferrari et al. (2008) showed that such a scheme is possible by adding an appropriate gauge to the residual velocity.

4.1.1 Previous Work

It has been shown in Section 1.7 that the transport tensor $\mathbf{R}$ can be described entirely in terms of its advective (antisymmetric) and diffusive (symmetric) components (Griffies, 1998). In reviewing existing work on the vertical structure, we can thus focus separately on the antisymmetric (GM90) streamfunction ψ and the diffusivity coefficient κ. More research has been done with regard to tapering ψ in the boundary layers and in regions of weak stratification ($N^2 \approx 0$), so we begin our discussion there.

Early attempts to transition the GM90 streamfunction into the boundary layers relied on the use of tapering functions. Although these proved very effective at reducing isopycnal diffusion and eddy transport in the boundary layers, they tended to result in an unphysically strong peak in eddy velocity at the mixed layer base, followed by an abrupt transition to zero in the mixed layer itself (Gerdes et al., 1991; Danabasoglu and McWilliams, 1995; Large et al., 1997; Ferreira and Marshall, 2006). Aside from an ill-conceived effort by Aiki et al. (2004) and an unpublished attempt by Killworth and Nurser (2006) to taper ψ via a differential operator, little progress was made on this topic between the late 1990's and the late 2000's.

A renewed effort began when Ferrari et al. (2008) developed a scheme to transition from the adiabatic interior to the boundary layer through the use of matching conditions. Danabasoglu et al. (2008) implemented this scheme in the Community Climate System Model Version 3 (CCSM3), showing it was superior to using tapering functions to achieve the transition. Among the effects of the Ferrari et al. scheme was the elimination of unphysical, shallow, and strong surface circulations and a better representation of heat transport through the surface layer. It also reduced a deep cold potential temperature bias from the tapered runs. Finally, it also allowed a higher maximum isopycnal slope than basic GM90 without inordinate numerical difficulties.

The Ferrari et al. (2008) concept was extended in Ferrari et al. (2010, hereafter FGNV10) to account for the full water column without having to rely on matching conditions. They relied on the dominance of low baroclinic modes in oceanic tracer transport to argue that one could

base a parameterization on a truncated series of linear, baroclinic modes. Their proposed scheme took the form of a second-order ordinary differential equation in z that was to be solved in every ocean column, and whose solution was essentially the basic GM90 transport modified by the depth-integrated stratification. As of the writing of this thesis, this scheme stands as the cutting edge in boundary layer tapering methods, but thus far its skill has been only minimally evaluated. Its only published test was performed by the authors using a nonlinear Eady simulation very similar to our own from Chapter 3; however, as we have seen, the simplistic stratification of such a model is inadequate to truly test the limitations of its skill. The exponentially-stratified models from this chapter provide an excellent set of tests for their parameterization.

Much research, both observational and numerical, has gone into attempting to scale for κ (Section 1.8), but only a few previous studies have attempted to deduce its vertical structure (Danabasoglu and McWilliams, 1995; Jochum, 1997; Eden, 2006; Eden, Greatbatch and Willebrand, 2007; Eden et al., 2009). These studies have each found magnitudes of κ consistent with the observations and models in Section 1.8, ranging up to 5000 $\mathrm{m}^2\ \mathrm{s}^{-1}$ and decaying roughly exponentially in z. Some authors (Ferreira et al., 2005; Danabasoglu and Marshall, 2007) have investigated having κ proportional to N^2, noting that their vertical profiles are very similar. Our results from Section 3.2.2 do not rule out this possibility; however, we note that N^2 appeared in our scalings as an artifact of the length scale we chose (baroclinic zone width $= N^2H/M^2$), not because of a direct kinematic argument. This is another idea we can investigate with the exponentially stratified models.

4.1.2 Methodology

As in the simulations from Chapter 3, we use the MITgcm to numerically integrate the hydrostatic, Boussinesq equations. The set of exponentially-stratified models are initialized as follows. We again employ a zonally reentrant channel on the f-plane, with a temperature front oriented in the cross-channel direction. The background density gradient in these runs is constant

in y and decays exponentially in z according to

$$N^2(z) = N_0^2 e^{-\frac{1}{\lambda}z}. \tag{4.2}$$

The stratification, rotation, front dimension, and velocity are now set according to the parameters N_0^2, representing the surface stratification, and λ, which represents the e-folding scale of N^2 as the depth increases.[3] The mean velocity fields are again initialized in thermal wind balance so that the background shear is constant in z.

Each simulation depicts the baroclinic spindown of the temperature front, which due to the variable stratification proceeds at different rates at different z-levels. A few inertial periods after the beginning of the model run the alongfront geostrophic shear goes baroclinically unstable. Restratification will begin as the instabilities reach finite amplitude and begin to slump the isopycnals, akin to FFH. The eddies grow out of the frontal region and will spread meridionally throughout the domain (Fig 3.3). We generally expect that the turbulent growth rate and restratification will occur faster in the abyssal layer due to its lower stratification, as is predicted by linear theory (Stone, 1972**a**).

Due to the longer integration time required for these models, six simulations have been chosen which span the range of N_0^2 and λ we wish to investigate. More simulations will be completed to "fill in the gaps" as this research progresses, but we take these six to be representative of all possible flow scenarios we will investigate. Unlike in the Eady-like simulations, the rate of frontal slumping now varies in z, with the front in the less-stratified abyss slumping faster than near the surface. Because we still do not want sidewall boundary effects to contaminate our results, the simulations are stopped just before the buoyancy perturbation of the front reaches the wall in the abyssal layer. Again we track the buoyancy perturbation $\hat{b} = \bar{b} - \bar{b}_y$ to check for frontal passage, stopping the simulations when $\hat{b} = 0$ at the wall.

As in Section 3.2.1, we continue to gather data by taking transient snapshots at different times during the simulations. Previously, we began collecting snapshots when the domain-averaged

[3] With our findings from Chapter 3 that *Ro* is no longer relevant once the eddies expand beyond the initial front width, we no longer will be checking this parameter.

vertical eddy kinetic energy (EKE) did not change by more than 3% of its value at the previous snapshot. Because the spinup time varies in z in these models, we now begin collecting snapshots once the vertical eddy kinetic energy did not change by more than 3% of its value at the previous snapshot **at every point in** z. This criteria is essentially a proxy to ensure that the eddies have reached finite amplitude and that the eddy interactions have become saturated by nonlinearity. At each time snapshot the velocity, temperature, and tracer fields are zonally averaged and written to file. One iteration of a 2D Gaussian smoothing algorithm is applied to all fields to reduce biases in the averaging from transient, powerful eddies and internal waves. Second-order finite differencing is used to create the tracer gradient matrices, and the inversion for the transport tensor $\mathbf{R}$ is carried out using the method described in Section 2.1.2.1. Thus, in each run a time series of values is generated for each element of the transport tensor at each point in the zonally averaged field. Variability in these time series arises from the presence of internal gravity waves as well as temporal fluctuations in the eddy statistics, neither of which significantly affect the results of this research.

Extracting domain-averaged values as in Chapter 3 is no longer useful, since we now want to scale for $\mathbf{R}$ at each z-level. We still would like to make our scalings based only on the eddying parts of the domain, however. At any given timestep the eddies will be most active in those parts of the domain experiencing potential energy release; these quantities quickly taper to zero as one travels horizontally away from the center of the front, but they also change vertically as one moves through layers with different N^2. The chosen solution was to average over columns of the domain where the vertical buoyancy flux $\overline{w'b'}$ at mid-depth ($z = -H/2$) is greater than 10% of its maximum value at that level. All averaging operations in this paper are taken over this region. In this way, the averaging only includes regions undergoing significant PE release, while still allowing us to evaluate the effects of the variable stratification.

Unlike the Eady model, exponential stratification has no short-wave cutoff, meaning that the initial state is baroclinically unstable at all wavelengths (Charney, 1947; Kuo, 1952; Burger, 1962; Miles, 1964). Because there is no longer an obvious length scale to guide our choice of grid resolution, our next best option is to capture the fastest growing modes and rely on the inverse

energy cascade to spin up the model to a fully-turbulent state. Therefore, we now choose our grid resolution via a numerical solver for the quasigeostrophic linear modes (Appendix C.4), and we set it to be three times the wavelength of the fastest growing mode. This resolution minimizes the influence of barotropic instability while still allowing several gridpoints to resolve each mesoscale eddy. Choosing the resolution in this way also ensures that the model spinup will proceed as fast as possible without wasting computation time on resolving small eddies with minimal contributions to the tracer fluxes.

All other simulation parameters, such as viscosity and numerical advection schemes, are set as described in Chapter 3.

4.1.3 Pseudoinversion: A Different Approach

As mentioned before, one of the strengths of this research is that we are able to diagnose the full transport tensor $\mathbf{R}$ element by element for the first time. Unlike previous research (Aiki et al., 2004; Ferrari et al., 2008, 2010), we are not limited to prescribing only the stirring effect of the eddies in the vertical - we can also examine the vertical structure of κ along with ψ, which by the DS97 result (Section 1.7.2) would determine the entire transport tensor. One of the secondary advantages of examining κ is that, if we are able to describe its vertical structure, we might immediately conquer one of the main difficulties of the GM90 scheme - namely, that it must be interpolated through regions of weak stratification where the neutral slope becomes infinite.

There are two likely options for how to extend the results of Section 3.2.2 to this set of simulations. Option 1 would be to proceed in the same manner as for the Eady-like results, where the vertical structure of each variable is inverted before the logarithmic least-squares fit is performed. Essentially this makes each field constant in the vertical (and in the horizontal, since lateral variations are fairly small), so averaging over an "eddy activity region" gives a robust quantity to fit to. The problem with this approach was that it took advantage of the unique nature of the Eady-like runs, where the stratification was fairly constant in the vertical and allowed us to define quantities like a "domain-averaged Richardson number". We made use of such domain-

averaged quantities when we found the scalings in Section 3.2.2.

Though those scalings told us there is a nontrivial dependence of κ upon the overall stability of the water column (which is captured in Ri), they are not applicable to this set of models. The reason for this is that the results from Section 3.2.2 relied on averaging in both the horizontal and vertical, which was possible because variations in the eddy strength were small both in y and z. That method no longer applies due to the exponential stratification near the surface - in the deep layer with relatively constant stratification, we expect results qualitatively similar to those from the Eady-like models. However, the eddy strength tapers off quickly as one moves upward, to a point where in some strongly stratified cases there is no eddy activity at all. Figure 4.1 shows a comparison of κ diagnosed in an exponentially-stratified run with the scaling given in (3.34), highlighting how unsuitable the previous diagnosis is in these models. In all, this set of models makes the domain-averaging approach ill-conceived, and suggests we look to some other way to diagnose the diffusivity at each snapshot.[4]

The second option, which is the one we will pursue, involves scaling the diffusivity at each vertical level, making our scaling laws **local in z**. The high accuracy of the pseudoinversion from the Eady-like runs, where the domain-averaged relative error was $\pm 7\%$ for the horizontal flux and $\pm 12\%$ for the vertical flux, was possible because the pseudoinversion held on a local basis, suggesting that a local scaling would be appropriate for these runs as well. This would also be advantageous when incorporating these results into an OGCM, since no extra calculations such as vertical baroclinic modes would be necessary (FGNV10).

Scaling the diffusivity locally in z is quite difficult due to the variable stratification, which presents a new challenge for the pseudoinversion method. Unlike the Eady-like runs, the buoyancy field is not everywhere governed by large eddies, so using only six tracers initialized as low-wavenumber sinusoids will no longer yield such accurate correlations. In particular, the buoyancy

[4] Option 1 would also be difficult to apply in a true OGCM. The notion of a Richardson number averaged over an entire water column is strange, and fails to account for surface-trapped modes or other cases where the eddy activity is confined to a particular layer. This is to say nothing of more complicated features like topography, jets, lateral boundaries, etc.

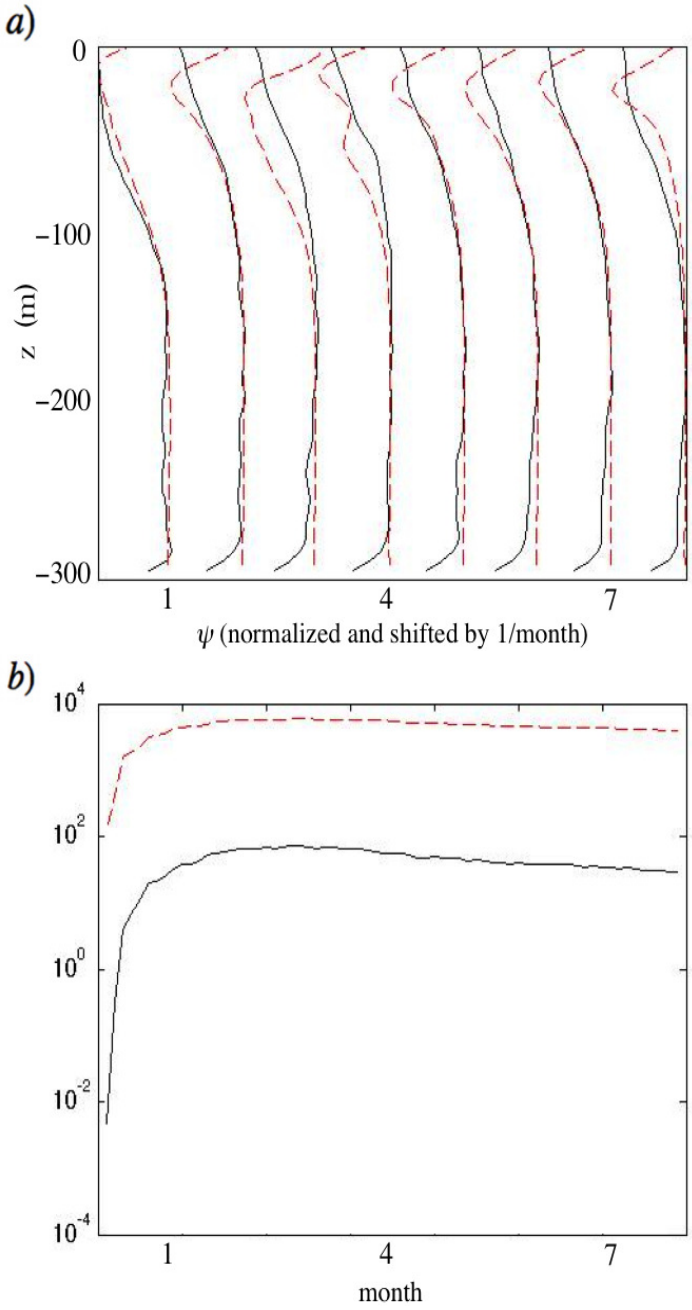

Figure 4.1: a) Normalized vertical structures of κ from a sample exponentially-stratified run, showing a comparison of the diagnosis by the pseudoinversion method (black line) and the value for κ prescribed by the Eady-like scaling (3.34). The vertical structures roughly match in the deeper, unstratified layer, but show strong differences in the surface layer. b) Domain-averaged values of κ, collected via the same averaging method used in Chapter 3. Using the scaling from the Eady-like diagnosis would overestimate the true value of κ in this run by over two orders of magnitude, confirming that a different approach is necessary.

fluxes in the highly-stratified surface layer cannot be reproduced by such tracer fields (not shown). However, we can still resort to the costly but extremely accurate method described in Section 2.1.2.1, where we initialize a large number of tracers and search for the combination that minimizes the reconstruction error at each point. Even though the accuracy of the reconstruction still decreases as the surface is approached, this method is able to reproduce the buoyancy fluxes to within $\approx 10\%$ through the full depth of the water column[5] , which we consider to be sufficient for describing $\mathbf{R}$ and its components.

Before proceeding to the research itself, it is important to remember that the models used in this section are still highly simplified. We purposely neglect surface layer processes (Thomas, 2005; Thomas et al., 2008; Thomas and Ferrari, 2008) that might contribute to the vertical profile of κ and GM90, as well as irregular topography that might induce strong diapycnal mixing in the unstratified abyss (Toole et al., 1994; Kunze and Sanford, 1996). As in Chapter 3, here we will focus more on empiricism than on derivation; our energy will be spent evaluating the FGNV10 scheme for determining ψ, as well as refining our earlier scaling for κ. We begin with a brief discussion about the modal decomposition of FGNV10, and how the vertical structure of κ plays a critical role in the skill of that scheme.

4.2 Vertical Structure of ψ

4.2.1 Vertical Baroclinic Modes

In the Eady-like simulations we took advantage of the near-constant stratification by dividing each field by its vertical structure before performing the scaling analysis. Such an approach was suitable for those runs, since we anticipated simple vertical structures for κ, ψ, and $\overline{\mathbf{u}'b'}$ consistent with linear theory (Stone, 1972**a**,**b**). Unfortunately, the Eady-like stratification profiles are unable to tell us how the eddy fluxes react to varying stratification, especially through the near-surface pycnocline. We expect a much stronger suppression of the vertical fluxes than the horizontal fluxes

[5] The pseudoinversion fails where the eddies are weak or nonexistent, as is the case outside of the baroclinic zone and at the free surface where N^2 is largest. This is why we average in y only over the width of the baroclinic zone, as this is the only region where we truly have information about the eddy transport.

through this layer, making the exponentially-stratified simulations better suited to illuminate the skill of the FGNV10 scheme.

The boundary value problem proposed in FGNV10 is inspired by the tendency of geostrophic turbulence toward a low-mode vertical structure. Indeed, they found that in an idealized Eady problem, the vertical structure of their ψ exactly matched those from Fox-Kemper et al. (2008), the linear theory of Stone (1972**a**), and our results (Fig. 4.2). However, the Eady-like stratification is not a very stringent test of their scheme, as the constant N^2 allows the vertical eddy kinetic energy to quickly (inverse) cascade to the first baroclinic mode. More will be revealed about the skill of their scheme in simulations where the inverse cascade is arrested, which we expect to occur in the exponentially-stratified simulations.

Since no theory currently exists for how to prescribe nonlinear baroclinic modes, the FGNV10 scheme relies on the idea that mesoscale eddy energy will (inverse) cascade towards grave **linear** baroclinic modes whether we use the quasigeostrophic or primitive equation set. They chose to represent ψ in terms of the linear primitive equation baroclinic modes S_m (Gill, 1982; Philander, 1990), which solve the boundary value problem

$$\frac{d^2 S_m}{dz^2} + \left(\frac{N}{c_m}\right)^2 S_m = 0 \tag{4.3}$$

$$S_m(0) = S_m(-H) = 0. \tag{4.4}$$

Without a priori knowing the baroclinic wave speeds c_m, one can solve the eigenvalue problem (4.3) to obtain them; alternatively, a WKB-approximated baroclinic wave speed c_M (Chelton et al., 1998) is

$$c_M \approx (M\pi)^{-1} \int_{-H}^{0} N \, dz. \tag{4.5}$$

The FGNV10 scheme relies on using these baroclinic modes as a basis on which to project the streamfunction ψ, so that it can be written

$$\psi = \sum_{m=1}^{\infty} S_m(z)\psi_m(x, y, t). \tag{4.6}$$

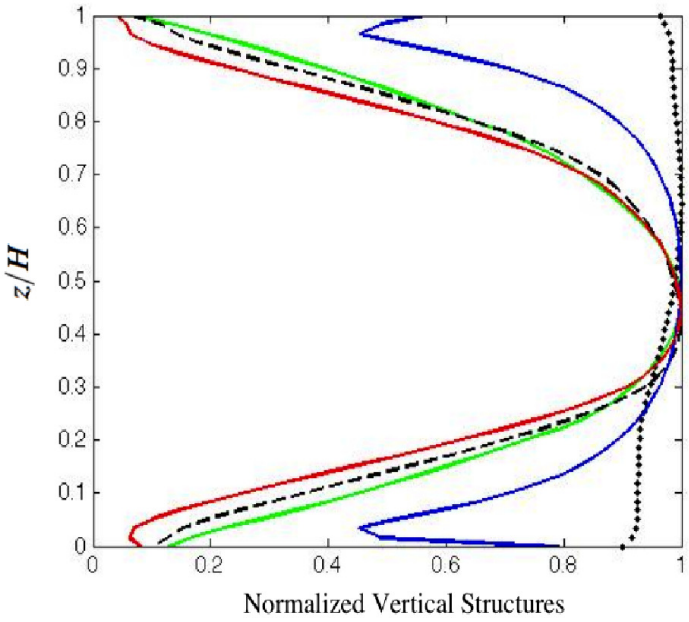

Figure 4.2: Vertical structures of ψ (green), κ (isopycnal eddy diffusivity, black dotted line), κ_d (diapycnal eddy diffusivity, black dashed line), isopycnal slope (blue), and κ multiplied by isopycnal slope (red), averaged over all time snapshots and all runs. Each is normalized to have a maximum value of 1. The vertical structure of κ matches that of $\overline{v'b'}$ and the vertical structure of ψ matches that of $\overline{w'b'}$. The DS97 result predicts $\psi = \kappa\mathcal{S}$ everywhere, which we observe by the similarity of the green and red lines.

The coefficients ψ_m are determined by the orthogonality condition

$$\frac{1}{g}\int_{-H}^{0} N^2 S_m S_n \, dz = \delta_{mn}, \tag{4.7}$$

and so are given by

$$\psi_m = \frac{1}{g}\int_{-H}^{0} N^2 \psi S_m \, dz. \tag{4.8}$$

The core idea of FGNV10 is to take advantage of the elliptic character of (4.3) to introduce a smoothing operator that weights the structure of ψ according to the local stratification. They pose the boundary value problem

$$\left(c^2 \frac{d^2}{dz^2} - N^2\right) \psi_F = \kappa \nabla_h b \tag{4.9}$$

$$\psi_F(0) = \psi_F(-H) = 0$$

for each vertical column, where we have introduced the subscript F to indicate the parameterized streamfunction. The claimed advantages of FGNV10 are that it provides a means for satisfying the natural vertical boundary conditions on ψ, interpolating through regions of low N^2, and reducing to the regular GM90 ψ when $c^2 \to 0$. Perhaps the most critical aspect of FGNV10 is that it acts as a low-pass modal filter, taking advantage of the tendency of geostrophic turbulence toward low baroclinic modes. This can be seen by rewriting the modal expansion

$$\psi = \sum_{m=1}^{\infty} S_m(z)\psi_m(x, y, t) \tag{4.10}$$

in the rescaled form

$$\tilde{\psi} = \sum_{m=1}^{\infty} S_m(z)\tilde{\psi}_m(x, y, t), \tag{4.11}$$

where $\tilde{\psi}_m = \psi_m/(1 + (c/c_m)^2)$. Because the baroclinic wave speeds c_m monotonically decrease as m increases, the expansion coefficients ψ_m are damped at higher mode numbers. A more suggestive

form makes use of the WKB approximation (4.5) to set $c = c_M$, yielding

$$\tilde{\psi}_m = \frac{\psi_m}{1 + (\frac{m}{M})^2}, \tag{4.12}$$

where m is the mode number in (4.6) and M is the chosen mode number in (4.5). Choosing higher mode wave speeds M thus has the effect of damping the expansion coefficients less, by a factor that decreases with m^2. Thus the solutions of the FGNV10 are very sensitive to the wave speed in (4.5), making a wise choice for M critical to the success of the scheme (Fig. 4.3).

The authors of the Ferrari et al. paper decline to recommend a specific choice for M, only pointing out that choosing $M > 1$ would still allow low modes to dominate the transport while not damping the magnitude of the solution too much. To determine a good choice for M, we can first check whether their assumption of low-mode dominance is correct. We can do this by taking the ψ diagnosed from the models and projecting it onto the linear baroclinic modes satisfying (4.3) using a numerical solver. Figure 4.4 shows a comparison of this projection in an Eady-like simulation and an exponentially-stratified simulation. As expected, after the early spinup phase the Eady-like simulation ψ is dominated entirely by the first baroclinic mode, consistent with linear theory. In the exponential simulation, the tendency of ψ over the course of the simulation is toward graver modes, with the structure ultimately being arrested at a combination of the first 9 modes.

We should be able to calibrate the FGNV10 scheme to approximate ψ skillfully in both the Eady-like and exponentially-stratified settings, and according to (4.9) we have two degrees of freedom to work with: the choice of M and a local scaling for κ. For the moment we will focus our attention on κ. Both the stochastic theory from DS97 and the results from Chapter 3 suggest that the diffusivity associated with the GM90 streamfunction should be the same as for the symmetric Redi tensor, meaning that the κ we want in the FGNV10 scheme is the same κ that we diagnose from the symmetric tensor $\mathbf{S}$. Therefore, we will use the κ diagnosed from the models (which is equivalent to S_{yy}, per the Redi parameterization) in the right hand side of (4.9), so that later we can decide if there is a systematic way to choose M that will give a good representation of ψ.

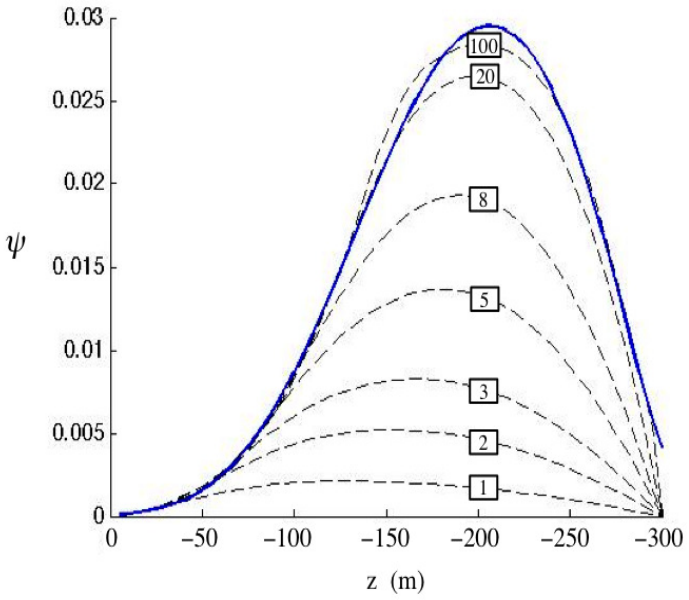

Figure 4.3: Vertical structures of ψ_F (dotted black lines), as predicted by (4.9) for one snapshot of a sample exponentially-stratified simulation. Values of M used in the WKB approximation (4.5) are shown in the black boxes. Lower values of M strongly damp the coefficients of the modal expansion (4.11), systematically underestimating the true value of ψ (blue line).

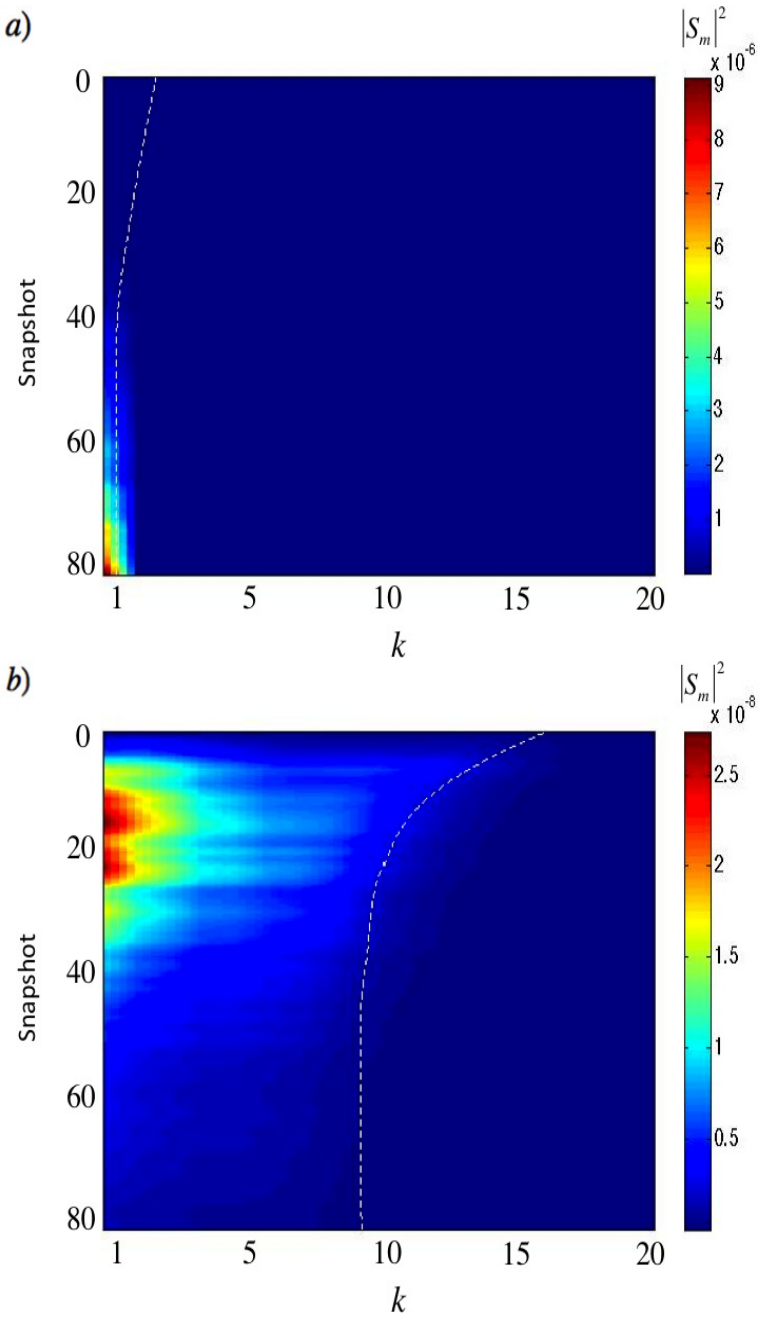

Figure 4.4: Hovmöller diagram showing the power spectra of ψ evolving over the course of sample a) Eady-like and b) exponentially-stratified simulations. White dashed lines indicate the wavenumber at which 95% of the power is contained in graver modes. After initial spinup, the power in the Eady-like simulation quickly cascades to the first baroclinic mode, which is the vertical structure predicted by linear theory (Stone, 1972**a**). Conversely, the inverse cascade is arrested in the exponentially-stratified simulation at $k = 9$. The total power decays with time in this simulation, as eddy momentum is lost to form drag as the eddies in the abyssal layer work to spin up the highly stratified surface layer.

4.2.2 Adjustment of S_{yy}

If the form of the symmetric tensor **S** exactly matched that of the Redi tensor, the along-isopycnal diffusivity would be identified as $\kappa = S_{yy}$. However, the results from Section 3.2.2.1 show that the **S** we recover from the models is not Redi due primarily to S_{yy} being too large. Therefore, we must consider whether it is acceptable to use S_{yy} as a proxy for κ, or how we might transform our results to recover the "true" κ.

In 3.2.2.1 it was shown that the excess of S_{yy} was caused by the growth of tracer variance and diapycnal fluxes, so that it is impossible to close the tracer variance budget with exactly along-isopycnal tracer fluxes. It was also suggested that this is related to the slope of the eddy buoyancy flux being less than that of the isopycnal slope $\mathcal{S}$, which is associated with the mean potential energy release in baroclinic turbulence. Unfortunately, the pseudoinversion method used to evaluate the Eady-like models[6] was not accurate enough to confirm this relationship. However, with the improved pseudoinversion from Section 2.1.2.1 we now confirm that the excess of S_{yy} given by

$$\xi_1 = S_{yy}\mathcal{S} \,/\, S_{yz}, \tag{4.13}$$

the ratio of $\mathcal{S}$ to the buoyancy flux slope $S_d = \mathbf{R}\nabla\bar{b}$

$$\xi_2 = \mathcal{S} \,/\, S_d, \tag{4.14}$$

and excess of ψ over $\kappa\mathcal{S}$ (contrary to the prediction of DS97)

$$\xi_3 = \psi \,/\, S_{yy}\mathcal{S}, \tag{4.15}$$

are all closely related. Also, because we have changed our averaging method so that we are no longer averaging in z, we can show that these quantities are related locally in the vertical (Fig. 4.5).

Because each of Redi, GM90, and FGNV10 are meant for parameterizing eddies in adiabatic flows, we must adjust the values of S_{yy} to be consistent with the adiabatic theory. If S_{yy} is too

[6] These required only six tracers, initialized sinusoidally at low wavenumber.

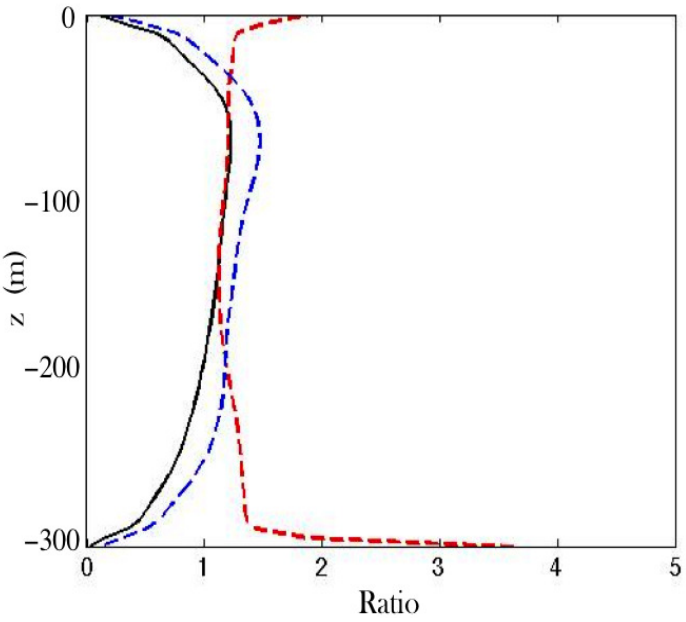

Figure 4.5: Ratios of the eddy flux slope, excessively large S_{yy}, and deviation from the DS97 prediction that $\psi = \kappa \mathcal{S}$. Plots are averaged over all snapshots during a sample Eady-like simulation. The convergence of the ratios ξ_3/ξ_1 (black line), ξ_3/ξ_2 (blue dashed line), and ξ_1/ξ_2 (red dashed line) to one in the adiabatic interior suggests that we can recover the "true" isopycnal diffusivity κ by dividing S_{yy} by one of $\{\xi_1, \xi_2, \xi_3\}$. By DS97, this κ is to be used in the GM90 parameterization, and by extension in the FGNV10 boundary value problem (4.9).

large, this implies that the diffusion is not exactly in the along-isopycnal direction, and there will be a resulting diapycnal flux. While we do expect for a diapycnal flux to be present when the buoyancy variance is growing, if we were to use S_{yy} as our isopycnal diffusivity straight from the model output we would not be using the correct value for GM90 or on the right hand side of (4.9).

Therefore, the connection between each of $\{\xi_1, \xi_2, \xi_3\}$ offers us a way to recover the "true" isopycnal diffusivity despite having an S_{yy} that is too large to fit the Redi tensor form. This is critical, because in the exponential simulations we are faced with a potentially complicated situation where $\mathcal{S}/\mathcal{S}_d$ varies in z. We thus must make a decision on whether to scale κ and ψ based on the raw values from the model (where the growth of tracer variance forces κ to have a diapycnal component), or based on rescaled values that would make these quantities consistent with DS97. We choose the latter for practical reasons:

- GM90-Redi is ubiquitous in modern OGCM's and has been shown to hold in our simulations, minus the diapycnal fluxes. Our results would be much more accessible were we to keep these parameterizations in place and scale our results to them, rather than to specify $\mathbf{R}$ element by element.

- GM90-Redi are both appropriate for equilibriated, adiabatic flows, neither of which is satisfied here but can be closely approximated by correcting for $\mathcal{S}/\mathcal{S}_d$. A diabatic (diapycnal) component can be added to Redi later, if desired.

- If we were to proceed with the uncorrected output, estimation of the slope parameter $\mathcal{S}/\mathcal{S}_d$ would require a parameterization of its own.

To this end, we will transform the raw model output to an "adiabatic" form by locally dividing S_{yy} by $\mathcal{S}/\mathcal{S}_d$. In this sense the "true" isopycnal diffusivity κ will be recovered, and will match both DS97 and the Griffies (1998) tensor form for $\mathbf{R}$. Using this "true" κ, we reduce one degree of freedom in the calibration of FGNV10, and now can focus completely on specifying c.

4.2.3 Choosing the Baroclinic Wave Speed

Now that we have confirmed that an adjusted value of S_{yy} can be used as the diffusivity in FGNV10, we can return to the problem of choosing the correct baroclinic wave speed c. In particular, the WKB form of c given by (4.5) reduces this problem to choosing M so that the "low-pass filter" aspect of FGNV10 does not produce a misestimate of ψ. We will show in the following section that no choice for M can simultaneously replicate both the Eady-like an exponentially-stratified vertical structures of ψ; instead, we will recommend a setting for c that will still taper ψ_F to zero at the boundaries and allow us not to worry about a choice for M.

We first point out that there is not an obvious choice for M even in an idealized flow where we know the modal structure beforehand. For example, it would be intuitive to choose $M = 1$ for an Eady-like simulation, as all of the power is concentrated in the first baroclinic mode. According to (4.12), though, the FGNV10 scheme would underestimate the magnitude of the stirring by half, and indeed we find that this is the case (Fig. 4.6). That choosing $M = 1$, which we know a priori to match the modal structure of the solution, is known to give the wrong answer should be considered a deficiency of the scheme.

This deficiency remains present even for an exponentially-stratified case where we know at what wavenumber the inverse energy cascade is arrested. Consider the flow in Figure 4.4b, where the inverse cascade is halted at $k = 9$. The vertical structures of ψ and ψ_F from the same simulation, which are shown in in Figure 4.3), indicate that choosing $k = 9$ would underestimate the magnitude of ψ by about 1/3. In fact, Figure 4.3) suggests that the only way that FGNV10 can approximate the correct magnitude of ψ is for M to be chosen extremely large.

It is clear that the choice of M strongly affects the accuracy of the scheme, and that we should expect $\psi_F < \psi$ when M is small. Because ψ_F is able to match the vertical structure of ψ well, one might ask why we cannot simply let M be large so that the damping is minimized (for example, let $M = 100$ as in Figure 4.3)? The authors of FGNV10 suggest that there are numerical reasons not to do this - the vertical resolution must satisfy $\Delta z < c/N$ to ensure numerical stability,

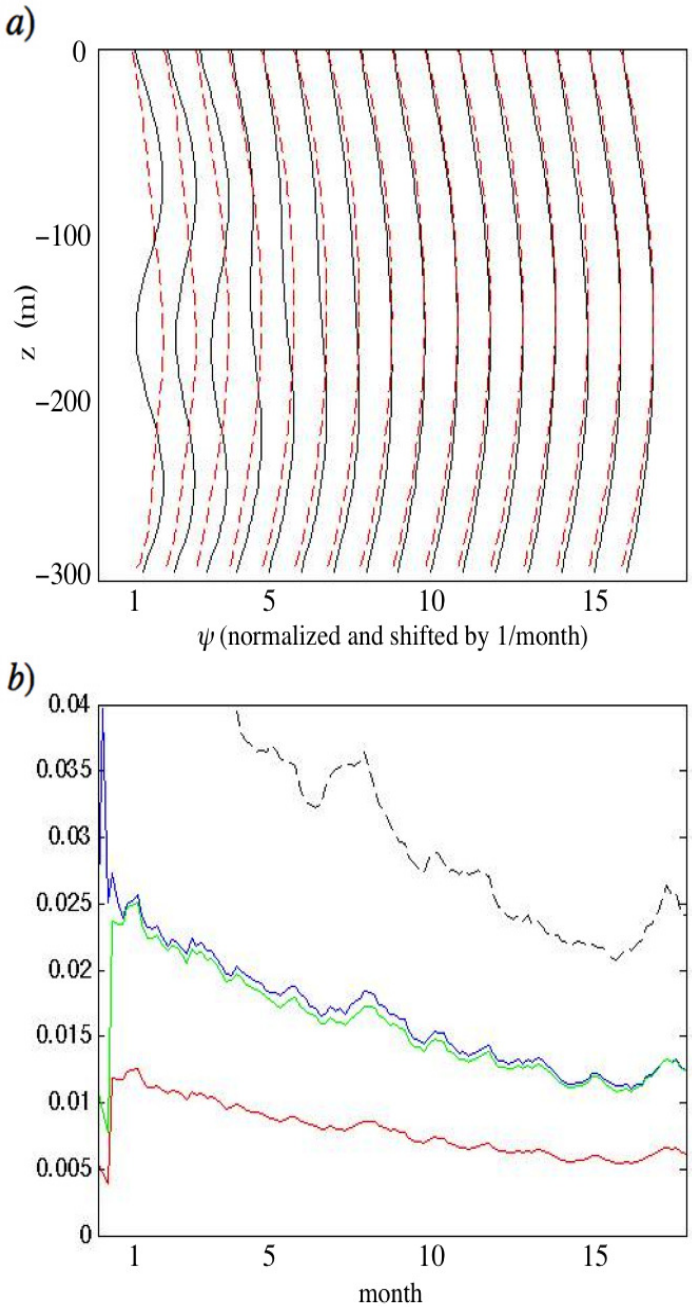

Figure 4.6: a) Normalized vertical structures of ψ (black lines) and the parameterized ψ_F (dotted red lines), plotted at various times during a sample Eady-like simulation. After the initial spinup the normalized vertical structure is well-approximated by FGNV10, and is consistent with the first baroclinic modal structure predicted in Fig. 4.4. b) Choosing $M = 1$ reduces the amplitude of S_1, the first coefficient of the series expansion (4.6), by half. Because all of the power is in the first baroclinic mode, this causes the predicted maximum value of ψ_F (red line) to be exactly half of its true value (blue line), which is confirmed by multiplying ψ_F by 2 (green line). The dotted black line represents ψ_F using S_{yy} as the GM90 diffusivity coefficient instead of "correcting" for κ (see Section 4.2.2).

placing a limit on how small one can allow c to be. It also would undermine one of the main purposes of the scheme, which is to preferentially weight the grave modes and thus capture the tendency of mesoscale eddy energy toward larger scales. Lastly, the authors of FGNV10 point out that choosing M large can cause complications in conjunction with the WKB-approximated c_M, as it is a function of the **depth-averaged** N.

Fortunately, there exist numerical methods which are stable regardless of the choice of M, and we would like to recommend one in particular to overcome the limitations on M. Consider discretizing d^2/dz^2 using the second-order central difference operator

$$\frac{d^2\psi}{dz^2} \approx \frac{\psi_{i+1} - 2\psi_i + \psi_{i-1}}{\Delta z^2} + \mathcal{O}(\Delta z^2), \tag{4.16}$$

and form a tridiagonal matrix for the left hand side of (4.9). The discretized version of (4.9) then becomes

$$\begin{bmatrix} 1 & 0 & 0 & \dots & 0 & 0 \\ \frac{-c^2}{\Delta z^2} & \frac{-c^2}{\Delta z^2} - N^2_{z=-\Delta z} & \frac{-c^2}{\Delta z^2} & 0 & \dots & 0 \\ 0 & \frac{-c^2}{\Delta z^2} & \frac{-c^2}{\Delta z^2} - N^2_{z=-2\Delta z} & \frac{-c^2}{\Delta z^2} & \dots & 0 \\ \vdots & \ddots & \ddots & \ddots & & \vdots \\ 0 & \dots & 0 & \frac{-c^2}{\Delta z^2} & \frac{-c^2}{\Delta z^2} - N^2_{z=-H} & \frac{-c^2}{\Delta z^2} \\ 0 & & \dots & & 0 & 1 \end{bmatrix} \begin{bmatrix} \psi_{z=0} \\ \psi_{z=-\Delta z} \\ \psi_{z=-2\Delta z} \\ \vdots \\ \psi_{z=-H+\Delta z} \\ \psi_{z=-H} \end{bmatrix} = \begin{bmatrix} 0 \\ (\kappa M^2)_{z=-\Delta z} \\ (\kappa M^2)_{z=-2\Delta z} \\ \vdots \\ (\kappa M^2)_{z=-H+\Delta z} \\ 0 \end{bmatrix}. \tag{4.17}$$

The $n \times n$ tridiagonal matrix on the left side of (4.17) is guaranteed to be diagonally dominant (satisfying the condition $|A_{ii}| \geq \Sigma\, |A_{ij}|$ for $j = 1, 2, \dots, n$) as long as $N^2 > 0$, which we take to be true for the stably stratified flows we are interested in. Solving for ψ via the Thomas algorithm (Thomas, 1949; Ryaben'kii and Tsynkov, 2006), which is designed specifically for such diagonally-dominant tridiagonal matrices, is guaranteed to be numerically stable and fast ($\mathcal{O}(n)$ operations). Because we used central differences, the convergence to ψ_F is $\mathcal{O}(\Delta z^2)$.

The unconditional stability of the above algorithm allows us to relax the condition on Δz so that we no longer need to worry about the scheme failing and crashing a simulation (although it is still beneficial to choose Δz as small as is feasible for accuracy reasons). Furthermore, it allows

us to suggest an improvement to FGNV10 - allow the magnitude of c^2 to vary in the vertical so that it converges to GM90 in the interior of the flow while still smoothly meeting the boundary conditions $\psi(0) = \psi(-H) = 0$.[7] For now, we recommend setting $c^2 = c_1^2 \mu(z)$, where c_1 is the WKB-approximated first baroclinic wave speed ($M = 1$ in equation (4.5)) and the structure function

$$\mu(z) = \frac{2e^{-H/2\lambda} \sinh(z/\lambda) \sinh(H/2\lambda) - 2e^{z/2\lambda} \sinh(H/\lambda) \sinh(z/2\lambda)}{\sinh(H/\lambda)} \tag{4.18}$$

$$\lambda = \mathcal{M}H/\pi. \tag{4.19}$$

Figure 4.7 shows the effect of incorporating this depth-dependent form of c^2. Note that the length-scale λ determines how quickly μ transitions from one at the boundaries to zero in the interior, which is itself controlled by the choice of $\mathcal{M}$ here.[8]

The above recommendations on how to set c^2 will continue to be updated as this research progresses. We chose the structure function (4.18) because we required a function that is nearly zero in the interior and that tapers to one at the vertical boundaries. The form of (4.18) has the added advantage that one can specify how quickly the tapering occurs by changing the value of $\mathcal{M}$. However, we admit that it is completely possible that a simpler form could be used. We make no claim that the form of (4.18) is the optimal choice, but it is easy to implement and provides a good starting point for further study. For now, it has provided us with a numerically stable means of transitioning ψ from zero at the boundaries to the GM90 solution in the interior, with no loss of amplitude due to unnecessary filtering. It is yet unclear whether this filtering (or equivalently, the weighting of the grave baroclinic mode components of ψ) is truly necessary, for the inverse cascade of eddy energy could be captured just as effectively by our scaling for κ. For now though, it suffices to say that we have proposed an improvement to the FGNV10 scheme without altering it in any major way, and we can now focus our attention on how to scale κ.

[7] Setting c^2 to be small everywhere will match ψ well in the interior but can result in a "kink" in ψ_F as the scheme abruptly transitions to meet the boundary conditons.

[8] A quick and easy recommendation would be to let $\mathcal{M} = 10$, although this matter will be considered further before these results are published in a journal. Also note that (4.18) is the analytical solution to (4.9) with constant density gradients and constant κ, as in the setup to the Eady problem.

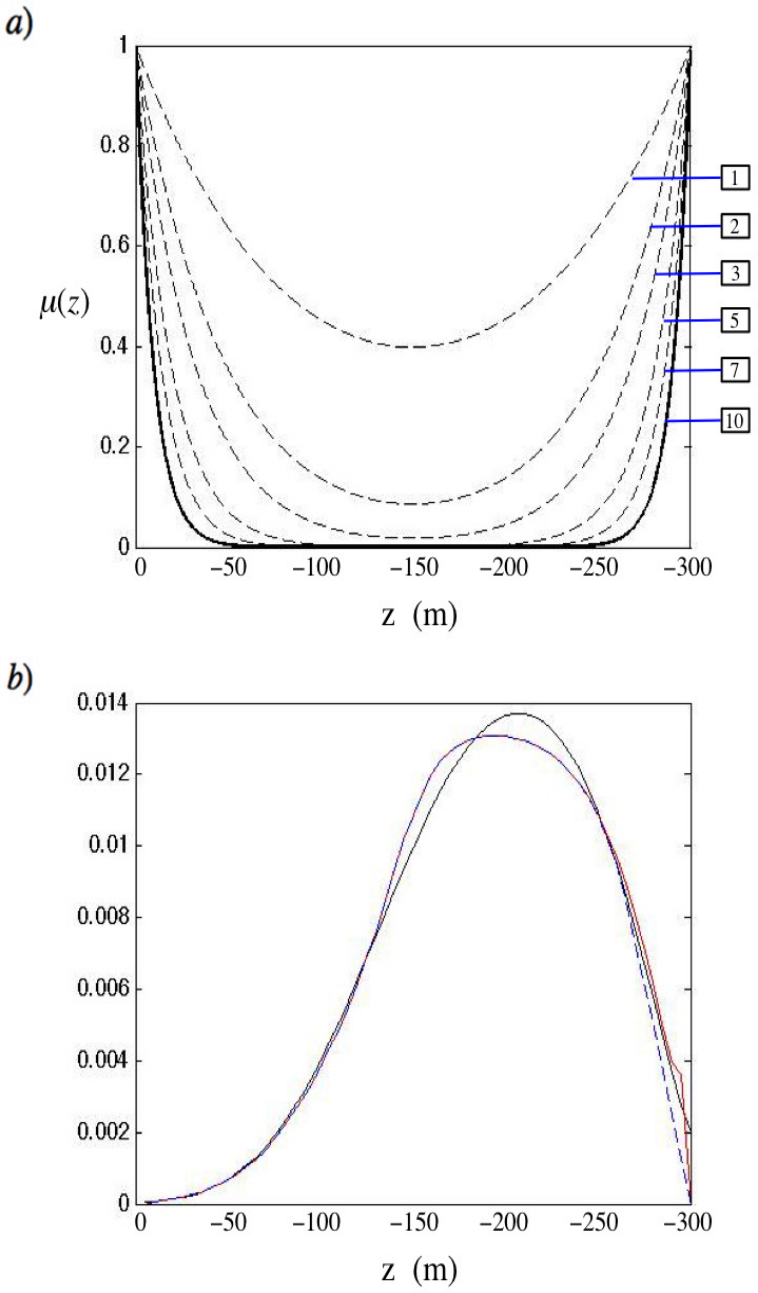

Figure 4.7: a) Magnitude and structure of μ as a function of $\mathcal{M}$, plotted as a function of depth. Choices of $\mathcal{M}$ are labeled in the black boxes. We find that setting $\mathcal{M} = 10$ is sufficient to smoothly meet the boundary conditions of ψ while approximating the true ψ well in the interior. b) Vertical structures of ψ (black line), ψ_F using a depth-independent c^2 with $M = 1000$ (red line), and ψ_F using a depth-dependent c^2 with $\mathcal{M} = 10$. The solution with depth-dependent c^2 is free of the "kink" near $z = -300$ m which is apparent on the red line. That the true solution of ψ does not converge to identically zero at the bottom boundary is an artifact of the smoothing algorithm used to eliminate noise (see Section 4.1.2).

4.3 Vertical Structure of κ

As mentioned previously, the skill of FGNV10 relies heavily on the local prescription of κ, which by DS97 is the diffusivity coefficient for both the Redi and GM90 parameterizations. The authors of FGNV10 did not devote any attention toward such a prescription, and in fact used a naive setting for κ (setting it to be constant in z) for many of their examples. The focus of this section will be on how to scale κ locally, with which we could describe the entire eddy transport tensor $\mathbf{R}$ as well as its boundary conditions.

We showed in Chapter 3 that we can scale for κ in the domain-averaged sense in the Eady-like simulations, but pursuing a local scaling in z is a much more difficult task. κ depends both non-trivially and **nonlocally** on unknown parameters - it is affected by the inverse cascade just as is ψ, and we should not necessarily expect any local scaling to be as accurate as those from Chapter 3. As we did previously (Section 3.1.3), we can begin with kinematic arguments to point us in the right direction.

A simple approach would be to take advantage of the form of $\mathbf{R}$ proposed in DS97 and Griffies (1998), by which

$$\overline{v'b'} \approx \kappa M^2. \tag{4.20}$$

We can make an approximation to the term on the left by using the individual eddy variances, so that

$$\overline{v'b'} \approx \sqrt{\overline{v'^2}}\sqrt{\overline{b'^2}} \approx \kappa M^2, \tag{4.21}$$

and by extension

$$\kappa \approx \frac{\sqrt{\overline{v'^2}}\sqrt{\overline{b'^2}}}{M^2}. \tag{4.22}$$

The physical justification is as follows. $\sqrt{\overline{v'^2}}$ is the same eddy velocity that we argued for in the scalings from Section 3.1.3, which we are using as a proxy for the Lagrangian eddy velocity by assuming the Stokes Drift is negligibly small. Then $\sqrt{\overline{b'^2}}/M^2$ must represent the missing "eddy length scale", but where does it come from?

We can see this by first considering the vertical excursion scale $\sqrt{\overline{b'^2}}/N^2$, which represents the maximum distance in the vertical a parcel can travel against the buoyancy gradient before all of its kinetic energy is converted into potential energy. Because κ is the along-isopycnal diffusivity, the relation between the vertical excursion and the corresponding horizontal excursion should be proportional to $1/\mathcal{S}$, the reciprocal of the isopycnal slope. Then the horizontal excursion scale becomes $(\sqrt{\overline{b'^2}}/N^2)(N^2/M^2) = \sqrt{\overline{b'^2}}/M^2$, which we take to be synonymous with the eddy length scale in (4.22).

Because the length scale $\sqrt{\overline{b'^2}}/M^2$ is sourced from a vertical parcel displacement argument, we can assume that it will be affected by the mean stratification. Additionally, the non-local nature of the inverse energy cascade means that the eddy length scale will not necessarily have a local relationship with any of the eddy variance fields either. Then as in Chapter 3, we will attempt to improve (4.22) by checking for dependencies on nondimensional parameters. In particular, we will expect some dependence on the gradient Richardson number as well as a new parameter $\mathcal{E} = \overline{v'^2}N^2/\overline{b'^2}$, which describes the ratio of eddy kinetic energy to eddy potential energy.[9]

Figure 4.8 shows the best-fitting scaling to κ from a set of simulations consisting of six exponentially-stratified runs and six Eady-like runs, which we find to be

$$\kappa_s = (0.01 \pm 0.02)\, Ri^{0.25}\, \mathcal{E}^{0.1} \sqrt{\overline{v'^2}} \sqrt{\overline{b'^2}}/M^2. \tag{4.23}$$

These were chosen so that they span the relevant parameter space of their respective profiles (so the Eady-like runs span a range of Ri, while the exponentially-stratified runs span a range of N_0^2 and decay scale λ). The vertical structure of κ_s from the Eady-like simulations is well-represented by this scaling; however, the vertical structure in the exponential profiles bears a complex relationship with the eddy field and mean stratification that cannot be captured by powers of Ri or $\mathcal{E}$. Other nondimensional parameters believed to be relevant, such as the isopycnal slope ($\mathcal{S}$) or buoyancy flux slope (S_d), were tested for inclusion but did not improve the scaling.

The above scaling for κ_s confirms that the simple form in (4.22) has some skill in representing

[9] It is anticipated that $\mathcal{E}$ will be able to represent some of the time-evolving, upscale energy transfer in a way that Ri cannot.

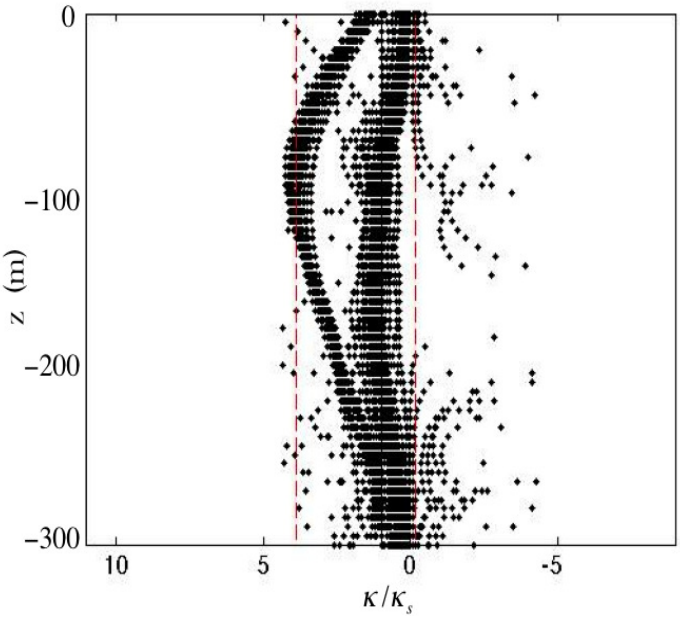

Figure 4.8: Vertical profile of κ/κ_s. Black dots indicate values of κ_s collected locally in z, for snapshots from six exponentilly-stratified simulations and six Eady-like simulations. The solid black line lies at $\kappa/\kappa_s = 1$, which corresponds to the mean of κ_s. Red dotted lines indicate the 95% confidence interval, which is also used to define the error in the definition of κ_s. The scaling does a better job of capturing the vertical structure in the Eady-like simulations (right clustering of points) than for the exponentially-stratified simulations (left clustering of points), but the remaining vertical structure cannot be represented by a simple function of Ri, $\mathcal{E}$, or others such as isopycnal slope ($\mathcal{S}$) or buoyancy flux slope (S_d) (not shown).

the along-isopycnal diffusivity. However, it also strongly suggests that the eddy variance fields play an important role in setting the appropriate value for κ_s. Based on the results here and in Chapter 3, it is the author's opinion that it is highly doubtful that a skillful parameterization can be developed deterministically with only coarse-grid variables. However, we shall still seek to improve upon the results we do have, because improvements made here can help to influence the course of more sophisticated research sometime later.

4.4 Concluding Remarks

The work in this chapter has suggested some shortcomings of the recent FGNV10 scheme, and in particular we have emphasized that in its original form the scheme is unlikely to give an accurate estimate of the eddy-induced advection. This is due primarily to the presence of the filter coefficient c^2, which strongly damps the coefficients of the series expansion (4.6) and causes the scheme to underestimate the true advective flux. While it is possible to choose c^2 so that the eddy streamfunction ψ is of the right magnitude, there currently does not exist a way to choose it without prior knowledge of the eddy field.

It is the opinion of the author that the use of a second-order operator to smoothly transition ψ to zero at the boundaries is a clever idea and one that should be kept. We have offered an improvement to the FGNV10 by recommending a depth-dependent filter coefficient that will smoothly transition from zero at the boundaries to the undamped GM90 solution in the interior. Possible improvements beyond this may come by adding another term to the boundary-value problem (4.9) or removing the "filtering" aspect of the scheme altogether, but exploration of these ideas will be left to future work.

Our evaluation of the FGNV10 scheme highlights the main role of the eddy parameterization challenge suite, which is to help us evaluate and improve extant parameterizations in a systematic way. It should be emphasized that the objective is not purely to criticize these parameterizations, but to offer suggestions about why the schemes fail and to help focus attention on where improvements might be found. Doing so requires our own methodology to evolve as well - we noted earlier in

this chapter that the tools used in Chapter 3 are insufficient for the more ambitious research in this chapter, and so we had to find a way to improve the accuracy of the pseudoinversion method. As our objectives become more specific and goals more challenging, we anticipate needing to continue to adjust and adapt in such a fashion.

There is still much work to be done to diagnose a vertical structure parameterization for use in OGCM's, and indeed we consider the findings in this chapter to be just the beginning. The obvious next objectives for this research will be to find a scaling for κ that will improve upon that posed in Figure 4.8, or to show that the vertical structure problem can be solved more straightforwardly using only coarse-grid quantities. Both of these objectives will require the eddy parameterization challenge suite to grow substantially before we can decide the best way to proceed. This research is ongoing, and due to the high computational cost, will continue to be for some time into the future.

To conclude this section, we offer a thought: even though in their current form our scalings are unsuitable for inclusion into an OGCM, they should not necessarily be viewed as insufficient or inadequate. Rather, they should encourage work on less-understood ideas such as stochastic parameterization, wherein we might be able to better represent the subgridscale fluxes without having to explicitly define a scaling law at every point. Such ideas are beyond the scope of this thesis and the eddy parameterization challenge suite, but will provide many avenues to pursue in the near future.

Chapter 5

Conclusion

5.1 Present Results

The field of mesoscale eddy parameterization is still very new to the scene of ocean modeling, and despite the tremendous amount of work over the past three decades that has gone into improving parameterizations, it continues to evolve from year to year. In this dissertation, we have reexamined many parts of contemporary parameterization schemes that modelers have always assumed to be true, but have never been confirmed so.

Prior to this work, the GM90 and Redi parameterizations were often used in OGCM's based on their proven track record of improving the realism of ocean simulations (Danabasoglu and McWilliams, 1995). However, the modeling community still lacked two important pieces: 1) was the combined form suggested by Dukowicz and Smith (1997) the correct one to use, especially with the ongoing uncertainty about rotational gauges, and 2) what is the correct scaling for the diffusivity coefficient κ?

The research presented in this dissertation is focused on answering both of these questions using a matrix pseudoinversion technique. Prior work (Smith and Gent, 2004) has acknowledged the anisotropy of the eddy transport tensor $\mathbf{R}$, but until now no method has been implemented that is able to determine the magnitude of the anisotropy uniquely[1] . The pseudoinversion is able

[1] This is not to say that our work finds a unique solution for the elements of $\mathbf{R}$ - it does not, due to the uncertainty inherent in the averaging operation. However, we emphasize that previous authors have relied on only one tracer to back out the diffusivity, which results in an underdetermined system with infinite solutions. If one takes the combined GM90-Redi form of Griffies (1998) to be correct, using only one tracer to determine the horizontal flux is fine; it is much more powerful though to be able to solve for the full flux vector $\overline{\mathbf{u}'\tau'}$, which is possible with our method.

to determine all of the tensor elements simultaneously using a linear flux-gradient relationship and a least-squares fit to the tracer fluxes, giving us unprecedented information about the structure of **R** and how to best implement it in OGCM's.

Much work has gone into the calibration of the pseudoinversion method (Chapter 2), specifically regarding how to maintain misalignment of the tracer gradients over the course of a simulation. In simulations terminating in finite time, such as the ones performed here, the accuracy of the method is maximized by initializing the tracers wisely. We found that initializing them in a sinusoidal pattern, akin to the Chebyshev polynomial approach of Bratseth (1998), made for an accurate pseudoinversion from start to finish. For simulations running indefinitely, slowly restoring the tracer fields to a prescribed set of values made the pseudoinversion possible, but resulted in a degraded solution. We explored several different ways to account for this restoring and propose a simple modification to the flux-gradient relationship that will improve the tensor diagnosis (Section 2.1.3). Finally, per the request of a reviewer, we attempted to account for rotational fluxes in our diagnosis. In doing so, we uncovered a flawed eddy flux closure in a previous paper on the topic (Eden, Greatbatch and Olbers, 2007), and formulated a simple scenario where this closure would fail. In lieu of this discovery, we did not pursue the rotational flux piece again.

One of the reasons we spent so much effort exploring the pseudoinversion was because it requires careful calibration to produce confident results. The method is very sensitive to the setting of the initial tracer fields, and a poor choice of these leads to degraded, and in some cases unusable, solutions. The challenge with making this method reproduce a particular eddy flux (in our case the buoyancy flux) is to initialize the tracer fields in such a way that the averaged correlations match those of the tracer of interest. This is both flow-dependent and tracer-dependent.

In our Eady-like examples, the flow dependence was removed because there were no significant potential vorticity gradients in the domain. Because the buoyancy fluxes in this case were driven primarily by the largest eddies, we were able to match the fluxes by using slowly-varying sinusoidal tracers. The exponentially-stratified runs proved not to be so simple, as large potential vorticity gradients near the surface made the buoyancy flux correlate with finer-scale eddies. We were forced

to use a large suite of tracers, varying on progressively finer scales, and try to locally "match" the buoyancy flux to a set of tracers that best reproduced the correlation.

The difficulty with the exponentially-stratified runs highlights the principle shortcoming of the pseudoinversion. Because of the nonlinearity of the flow, it is difficult to anticipate beforehand how the tracers should be initialized to match the buoyancy flux correlations. In this research we are holding ourselves to a very strict standard - we want to reproduce the buoyancy flux to within $\sim 10\%$ so that we can confidently scale for $\mathbf{R}$, κ, ψ, etc. In more complex flows, we have no choice but to try a large number of tracers and search for the combination of four or six that best reproduces the buoyancy flux. This in turn leads to a massive increase in computational cost relative to the simple Eady-like runs[2] as we must test each combination. We note that this is the reason why parts of Chapter 4 are presented as a "proof-of-concept"; many more runs will have to be completed before this work is submitted for publication, but the high computational cost will make this a long-term project.

The pseudoinversion has been incorporated into an eddy parameterization challenge suite, which is a set of model simulations designed specifically to study baroclinic turbulence in a variety of flow regimes. The results from the challenge suite are meant to support those diagnosed from the global model of Fox-Kemper et al. (2012). In the first set of models (Chapter 3), we were able to show that the pseudoinversion yields a tensor that can reproduce the flux of an active tracer (buoyancy) to within $\approx 10\%$, which is nearly an order of magnitude more accurate than previous work (Fox-Kemper et al., 2008). We also presented scaling laws for each of the tensor elements that hold even in a transient simulation, so that we do not have to run the model to a turbulent steady state where other unknown parameters (viscosity, friction, etc.) can contaminate our solution.

In the second set of models (Chapter 4), we used a more accurate pseudoinversion procedure to study the vertical structures of the diffusivity κ and advective streamfunction ψ. We criticized certain points of the recent Ferrari et al. (2010) scheme for parameterizing ψ and offered two improvements: a modified filter coefficient c^2 that smoothly transitions from the boundary layer

[2] By about two orders of magnitude!

to the interior without damping the solution, and a local scaling for the along-isopycnal diffusivity. We found that the vertical structures of κ from the Eady-like and exponentially-stratified models could not be reconciled using only exponents of the gradient Richardson number or eddy kinetic-to-potential energy ratio, but suggested that this should encourage us to look past deterministic parameterizations and into more novel approaches.

5.2 Toward the Future

In the future, the third (and possibly final) component of the challenge suite will be developed, consisting of stratification profiles extracted from an eddy-resolving global simulation. Plans are already in place for these profiles to be extracted using a self-organizing map, so that we can categorize each profile based on the region of the ocean it represents. This final component will provide the most difficult test for our pseudoinversion and vertical structure methods, as the presence of a true (or even double) thermocline at shallow- to intermediate depths will demand a local, very accurate inversion for $\mathbf{R}$. It will also tell us more about how suitable our scalings will be and the skill we can expect them to have when incorporated into an OGCM.

Perhaps the most important result from this research supports what earlier observational papers have claimed (Krauß and Boning, 1987; Poulain and Niiler, 1989; Sallée et al., 2008) - there is an important connection between eddy kinetic energy and isopycnal diffusivity. Though dimensional analysis certainly suggests this to be the case, previous authors (Fox-Kemper et al., 2008) have attempted to skirt the issue by writing the diffusivity totally as a function of the buoyancy gradient. Though this idea would be far easier to implement in practice, we have shown that it would give up to an order of magnitude more error in the diffusivity calculation (Section 3.2.2), and does not scale with the time-evolving eddy field.

Some may view our connection between diffusivity and eddy kinetic energy to be unsatisfactory, since it essentially passes one parameterization problem onto another. No parameterizations for the subgridscale eddy kinetic energy currently exist in the oceanographic literature, although the work of Eden and Greatbatch (2008) and Eden et al. (2009) is moving in that direction. Still,

demonstrating an explicit connection between eddy diffusivity and kinetic energy, along with showing the consequences when the kinetic energy is **not** used, is a powerful and important result. It has been acknowledged as far back as Taylor (1921) that eddy diffusivity represents the correlation between time-evolving Lagrangian length and time scales, and despite previous efforts to connect these to quasi-static quantities such as deformation radius (e.g. Stammer, 1998), any diffusivity scaling must have this transience built in. Our connection with the eddy kinetic energy accomplishes this, but it shifts the onus onto how to properly write a local subgridscale energy balance. Such work is outside the scope of this thesis, and it may be some time before real headway is made on this topic.

Where the field of eddy parameterization goes from here remains an open question, for there are many aspects of the current GM90-Redi scheme that are suboptimal. Many of the shortcomings of GM90 in particular are listed in Section 1.6. Some of these likely will never be solved without moving on to a wholly new scheme[3] , and others perhaps should be addressed by adding a new parameterization, not altering an existing one.

In terms of modeling, exact representation of the subgridscale energy and tracer spectra is impossible, and perhaps unnecessary. In reality we simply need to budget for what we expect the subgridscale flow to contribute to the evolution of momentum (the Reynolds stresses), the thermodynamic state (the density/buoyancy fluxes), and the tracer fields (the tracer fluxes) at coarse resolution, and we do so by parameterizing processes that play leading order roles in the mean budgets. With regard to mesoscale turbulence, aside from the issue of boundary-layer tapering (Section 4.1.1) the physics of the GM90-Redi parameterization are well-justified and deserve no modification even as we look to smaller scales. However, the diffusivity coefficient κ provides the link between GM90 and Redi and therefore governs the total contribution of the parameterization to the mean tracer budget. In the author's point of view, the challenge now will be to develop

[3] For example, the vertically-integrated streamfunction of Ferrari et al. (2010) is spun off of GM90, but in reality is a completely unique concept. For example, one major difference between FGNV10 and GM90 is that FGNV10 does not have to provide a local sign-definite sink of potential energy, as has been found in eddy-resolving simulations (Wolfe et al., 2008).

a **scale-dependent** definition of κ, so that we will be able to represent the subgridscale budgets even as OGCM resolution continues to decrease.

One possibility mentioned in Fox-Kemper and Menemenlis (2008) would be to use a dynamical method for prescribing κ at each timestep of a simulation. To do so would require a method akin to the Germano et al. (1991) family of schemes prevalent in large-eddy simulations (Lilly, 1992; Meneveau et al., 1996; Meneveau and Katz, 2000), which adjusts the eddy viscosity locally according to the resolved turbulent Reynolds stresses. For models running at mesoscale resolution where we expect a direct enstrophy cascade, Fox-Kemper and Menemenlis (2008) propose such a method based on setting the eddy Prandtl number to one and employing Leith viscosity scaling. To the author's knowledge, no attempts have been made to try this experimentally. Another possibility would be to pursue a stochastic parameterization, wherein the subgridscale fluxes are represented according to their likelihood of occurrence given a particular background flow. Perhaps a next-generation parameterization could be both stochastic and dynamic, which is at once both an exciting and intimidating thought!

To conclude, for now it suffices to say that there is still much work to be done on mesoscale eddy parameterization and on turbulence parameterizations in general. Fortunately, these are not simply a numerical exercises to make our models behave better, for our attempts at parameterizing turbulence shed light on the complex interactions between numerics and physics. We will always be limited by model resolution and there will always be a need for more and better parameterizations. Hopefully, the tantalizing prospect of representing the global climate in its full, glorious, gory complexity will keep modelers engaged indefinitely!

Bibliography

Abernathey, R., Marshall, J., Mazloff, M. and Shuckburgh, E. (2010), "Enhancement of mesoscale eddy stirring at steering levels in the Southern Ocean", Journal of Physical Oceanography , Vol. 40, pp. 170–184.

Aiki, H., Jacobson, T. and Yamagata, T. (2004), "Parameterizing ocean eddy transports from surface to bottom", Geophysical Research Letters , Vol. 31, American Geophysical Union, p. L19302.

Allen, D. and Nakamura, N. (2001), "A seasonal climatology of effective diffusivity in the stratosphere", Journal of Geophysical Research , Vol. 106, pp. 7917–7935.

Andrews, D. (1983), "A finite-amplitude Eliassen-Palm theorem in isentropic coordinates", Journal of the Atmospheric Sciences , Vol. 40, pp. 1877–1883.

Andrews, D. (1987), "On the interpretation of the Eliassen-Palm flux divergence", Quarterly Journal of the Royal Meteorological Society , Vol. 113, Wiley Online Library, pp. 323–338.

Andrews, D., Holton, J. and Leovy, C. (1987), Middle Atmosphere Dynamics, International Geophysics Series, Academic Press.
URL: *http://books.google.com/books?id=N1oNurYZefAC*

Andrews, D. and McIntyre, M. (1976), "Planetary waves in horizontal and vertical shear: The generalized Eliassen-Palm relation and the mean zonal acceleration.", Journal of Atmospheric Sciences , Vol. 33, pp. 2031–2048.

Andrews, D. and McIntyre, M. (1978a), "An exact theory of nonlinear waves on a Lagrangian-mean flow", Journal of Fluid Mechanics , Vol. 89, Cambridge Univ Press, pp. 609–646.

Andrews, D. and McIntyre, M. (1978b), "Generalized Eliassen-Palm and Charney-Drazin theorems for waves oin axismmetric mean flows in compressible atmospheres", Journal of the Atmospheric Sciences , Vol. 35, pp. 175–185.

Arbic, B. and Flierl, G. (2004), "Baroclinically unstable geostrophic turbulence in the limits of strong and weak bottom Ekman friction: Application to midocean eddies", Journal of Physical Oceanography , Vol. 34, pp. 2257–2273.

Bachman, S. and Fox-Kemper, B. (submitted for review), "Eddy parameterization challenge suite. I: Eady spindown", Ocean Modelling .

Barton, E. and Hill, A. (1989), "Abyssal flow through the Amirante Trench (Western Indian Ocean)", Deep Sea Research Part A. Oceanographic Research Papers , Vol. 36, Elsevier, pp. 1121–1126.

Bauer, S., Swenson, M., Griffa, A., Mariano, A. and Owens, K. (1998), "Eddy–mean flow decomposition and eddy-diffusivity estimates in the tropical Pacific Ocean. I. Methodology", Journal of Geophysical Research , Vol. 103, American Geophysical Union, pp. 30855–30.

Berloff, P. and McWilliams, J. (1999), "Large-scale, low-frequency variability in wind-driven ocean gyres", Journal of Physical Oceanography , Vol. 29, pp. 1925–1949.

Böning, C. (1988), "Characteristics of particle dispersion in the North Atlantic: an alternative interpretation of SOFAR float results", Deep Sea Research Part A. Oceanographic Research Papers , Vol. 35, Elsevier, pp. 1379–1385.

Bratseth, A. (1998), "On the estimation of transport characteristics of atmospheric data sets", Tellus A , Vol. 50, Wiley Online Library, pp. 451–467.

Bretherton, F. (1966a), "Baroclinic instability and the short wavelength cut-off in terms of potential vorticity", Quarterly Journal of the Royal Meteorological Society , Vol. 92, Wiley Online Library, pp. 335–345.

Bretherton, F. (1966b), "Critical layer instability in baroclinic flows", Quarterly Journal of the Royal Meteorological Society , Vol. 92, Wiley Online Library, pp. 325–334.

Brink, K., Beardsley, R., Niiler, P., Abbott, M., Huyer, A., Ramp, S., Stanton, T. and Stuart, D. (1991), "Statistical properties of near surface currents in the California coastal transition zone", American Geophysical Union.

Bryan, F. (1987), "Parameter sensitivity of primitive equation ocean general circulation models", Journal of Physical Oceanography , Vol. 17, pp. 970–985.

Bryan, K. (1991), "Poleward heat transport in the ocean", Tellus B , Vol. 43, Wiley Online Library, pp. 104–115.

Bryan, K. and Cox, M. (1967), "A numerical investigation of the oceanic general circulation", Tellus , Vol. 19, Wiley Online Library, pp. 54–80.

Bryan, K., Dukowicz, J. and Smith, R. (1999), "On the mixing coefficient in the parameterization of bolus velocity", Journal of Physical Oceanography , Vol. 29, pp. 2442–2456.

Bryden, H. and Heath, R. (1985), "Energetic eddies at the northern edge of the Antarctic Circumpolar Current in the southwest Pacific", Progress in Oceanography , Vol. 14, Elsevier, pp. 65–87.

Buhler, O. (2009), Waves and mean flows, Cambridge University Press.

Burger, A. (1962), "O the non-existence of critical wavelengths in a continuous baroclinic stability problem.", Journal of Atmospheric Sciences , Vol. 19, pp. 31–38.

Charney, J. (1947), "The dynamics of long waves in a baroclinic westerly current", Journal of Meteorology , Vol. 4, pp. 135–161.

Charney, J. (1971), "Geostrophic turbulence.", Journal of Atmospheric Sciences , Vol. 28, pp. 1087–1094.

Charney, J. and Stern, M. (1962), "On the stability of internal baroclinic jets in a rotating atmosphere.", Journal of Atmospheric Sciences , Vol. 19, pp. 159–172.

Chelton, D., DeSzoeke, R., Schlax, M., El Naggar, K. and Siwertz, N. (1998), "Geographical variability of the first baroclinic Rossby radius of deformation", Journal of Physical Oceanography , Vol. 28, pp. 433–460.

Chelton, D., Schlax, M., Samelson, R. and de Szoeke, R. (2007), "Global observations of large oceanic eddies", Geophysical Research Letters , Vol. 34, American Geophysical Union, p. L15606.

Cox, M. (1987), "Isopycnal diffusion in a z-coordinate ocean model", Ocean Modelling , Vol. 74, p. 5.

Cushman-Roisin, B. and Beckers, J. (2011), Introduction to geophysical fluid dynamics: Physical and numerical aspects, Academic Press.

Danabasoglu, G. (2004), "A comparison of global ocean general circulation model solutions obtained with synchronous and accelerated integration methods", Ocean Modelling , Vol. 7, Elsevier, pp. 323–341.

Danabasoglu, G., Ferrari, R. and McWilliams, J. (2008), "Sensitivity of an ocean general circulation model to a parameterization of near-surface eddy fluxes", Journal of Climate , Vol. 21, pp. 1192–1208.

Danabasoglu, G. and Marshall, J. (2007), "Effects of vertical variations of thickness diffusivity in an ocean general circulation model", Ocean Modelling , Vol. 18, Elsevier, pp. 122–141.

Danabasoglu, G. and McWilliams, J. (1995), "Sensitivity of the global ocean circulation to parameterizations of mesoscale tracer transports", Journal of Climate , Vol. 8, pp. 2967–2987.

Danielsen, E. (1981), "An objective method for determining the generalized transport tensor for two-dimensional Eulerian models", Journal of Atmospheric Sciences , Vol. 38, pp. 1319–1339.

Danilov, S. and Gurarie, D. (2002), "Rhines scale and spectra of the β-plane turbulence with bottom drag", Physical Review E , Vol. 65, APS, p. 067301.

Danilov, S. and Gurarie, D. (2004), "Scaling, spectra and zonal jets in beta-plane turbulence", Physics of Fluids , Vol. 16, p. 2592.

Davis, R. (1991), "Observing the general circulation with floats", Deep Sea Research. Part A. Oceanographic Research Papers , Vol. 38, Pergamon, pp. S531–S571.

De Madron, X. and Weatherly, G. (1994), "Circulation, transport and bottom boundary layers of the deep currents in the Brazil Basin", Journal of Marine Research , Vol. 52, Sears Foundation for Marine Research, pp. 583–638.

de Szoeke, R. and Levine, M. (1981), "The advective flux of heat by mean geostrophic motions in the Southern Ocean", Deep Sea Research Part A. Oceanographic Research Papers , Vol. 28, Elsevier, pp. 1057–1085.

Dukowicz, J. and Greatbatch, R. (1999), "The bolus velocity in the stochastic theory of ocean turbulent tracer transport", Journal of Physical Oceanography , Vol. 29, pp. 2232–2239.

Dukowicz, J. and Smith, R. (1997), "Stochastic theory of compressible turbulent fluid transport", Physics of Fluids , Vol. 9, p. 3523.

Dunkerton, T. (1980), "A Lagrangian mean theory of wave, mean-flow interaction with applications to nonacceleration and its breakdown", Reviews of Geophysics , Vol. 18, American Geophysical Union, pp. 387–400.

Eady, E. (1949), "Long waves and cyclone waves", Tellus , Vol. 1, Wiley Online Library, pp. 33–52.

Eden, C. (2006), "Thickness diffusivity in the Southern Ocean", Geophysical Research Letters , Vol. 33, American Geophysical Union, p. L11606.

Eden, C. (2007), "Eddy length scales in the North Atlantic Ocean", Journal of Geophysical Research , Vol. 112, American Geophysical Union, p. C06004.

Eden, C. (2010a), "Anisotropic rotational and isotropic residual isopycnal mesoscale eddy fluxes", Journal of Physical Oceanography , Vol. 40, pp. 2511–2524.

Eden, C. (2010b), "Parameterising meso-scale eddy momentum fluxes based on potential vorticity mixing and a gauge term", Ocean Modelling , Vol. 32, Elsevier, pp. 58–71.

Eden, C. (2011), "A closure for mesoscale eddy fluxes based on linear instability theory", Ocean Modelling , Vol. 39, Elsevier, pp. 362–369.

Eden, C. (in press), "Relating Lagrangian, Residual, and Isopycnal Means", Journal of Physical Oceanography .

Eden, C. and Greatbatch, R. (2008), "Towards a mesoscale eddy closure", Ocean Modelling , Vol. 20, Elsevier, pp. 223–239.

Eden, C. and Greatbatch, R. (2009), "A diagnosis of isopycnal mixing by mesoscale eddies", Ocean Modelling , Vol. 27, Elsevier, pp. 98–106.

Eden, C., Greatbatch, R. and Olbers, D. (2007), "Interpreting eddy fluxes", Journal of Physical Oceanography , Vol. 37, pp. 1282–1296.

Eden, C., Greatbatch, R. and Willebrand, J. (2007), "A diagnosis of thickness fluxes in an eddy-resolving model", Journal of Physical Oceanography , Vol. 37, pp. 727–742.

Eden, C., Jochum, M. and Danabasoglu, G. (2009), "Effects of different closures for thickness diffusivity", Ocean Modelling , Vol. 26, Elsevier, pp. 47–59.

Eliassen, A. (1951), "Slow thermally or frictionally controlled meridional circulation in a circular vortex", Astrophysica Norvegica , Vol. 5, p. 19.

England, M. (1995), "The age of water and ventilation timescales in a global ocean model", Journal of Physical Oceanography , Vol. 25, [Boston, etc.,] American Meteorological Society, 1971-, pp. 2756–2777.

Fernández, C., Raimbault, P., Caniaux, G., Garcia, N. and Rimmelin, P. (2005), "Influence of mesoscale eddies on nitrate distribution during the POMME program in the northeast Atlantic Ocean", Journal of Marine Systems , Vol. 55, Elsevier, pp. 155–175.

Ferrari, R., Griffies, S., Nurser, A. and Vallis, G. (2010), "A boundary-value problem for the parameterized mesoscale eddy transport", Ocean Modelling , Vol. 32, Elsevier, pp. 143–156.

Ferrari, R., McWilliams, J., Canuto, V. and Dubovikov, M. (2008), "Parameterization of eddy fluxes near oceanic boundaries", Journal of Climate , Vol. 21, pp. 2770–2789.

Ferrari, R. and Nikurashin, M. (2010), "Suppression of eddy diffusivity across jets in the Southern Ocean", Journal of Physical Oceanography , Vol. 40, pp. 1501–1519.

Ferreira, D. and Marshall, J. (2006), "Formulation and implementation of a residual-mean ocean circulation model", Ocean Modelling , Vol. 13, Elsevier, pp. 86–107.

Ferreira, D., Marshall, J. and Heimbach, P. (2005), "Estimating eddy stresses by fitting dynamics to observations using a residual-mean ocean circulation model and its adjoint", Journal of Physical Oceanography , Vol. 35, pp. 1891–1910.

Flierl, G. and McWilliams, J. (1977), "On the sampling requirements for measuring moments of eddy variability", Journal of Marine Research , Vol. 35, pp. 797–820.

Fox-Kemper, B. (2004), "Wind-driven barotropic gyre II: Effects of eddies and low interior viscosity", Journal of Marine Research , Vol. 62, Sears Foundation for Marine Research, pp. 195–232.

Fox-Kemper, B. (2005), "Reevaluating the roles of eddies in multiple barotropic wind-driven gyres", Journal of Physical Oceanography , Vol. 35, pp. 1263–1278.

Fox-Kemper, B., Bryan, F. and Dennis, J. (2012), "Global diagnosis of the mesoscale eddy tracer flux-gradient relation", Ocean Modelling . In preparation.

Fox-Kemper, B. and Ferrari, R. (2009), "An eddifying Parsons model", Journal of Physical Oceanography , Vol. 39, pp. 3216–3227.

Fox-Kemper, B., Ferrari, R. and Hallberg, R. (2008), "Parameterization of mixed layer eddies. Part i: Theory and diagnosis", Journal of Physical Oceanography , Vol. 38, pp. 1145–1165.

Fox-Kemper, B., Ferrari, R. and Pedlosky, J. (2003), "On the indeterminacy of rotational and divergent eddy fluxes", Journal of Physical Oceanography , Vol. 33, pp. 478–483.

Fox-Kemper, B. and Menemenlis, D. (2008), "Can large eddy simulation techniques improve mesoscale rich ocean models", Ocean Modeling in an Eddying Regime, Geophys. Monogr. Ser , Vol. 177, pp. 319–338.

Fox-Kemper, B. and Pedlosky, J. (2004a), "Wind-driven barotropic gyre I: Circulation control by eddy vorticity fluxes to an enhanced removal region", Journal of Marine Research , Vol. 62, Sears Foundation for Marine Research, pp. 169–193.

Fox-Kemper, B. and Pedlosky, J. (2004b), "Wind-driven barotropic gyre I: Circulation control by eddy vorticity fluxes to an enhanced removal region", Journal of Marine Research , Vol. 62, Sears Foundation for Marine Research, pp. 169–193.

Fu, L. and Flierl, G. (1980), "Nonlinear energy and enstrophy transfers in a realistically stratified ocean", Dynamics of Atmospheres and Oceans , Vol. 4, Elsevier, pp. 219–246.

Ganachaud, A. and Wunsch, C. (2000), "Improved estimates of global ocean circulation, heat transport and mixing from hydrographic data", Nature , Vol. 408, Nature Publishing Group, pp. 453–457.

Garabato, A., Polzin, K., King, B., Heywood, K. and Visbeck, M. (2004), "Widespread intense turbulent mixing in the Southern Ocean", Science , Vol. 303, American Association for the Advancement of Science, pp. 210–213.

Garabato, A., Stevens, D., Watson, A. and Roether, W. (2007), "Short-circuiting of the overturning circulation in the Antarctic Circumpolar Current", Nature , Vol. 447, Nature Publishing Group, pp. 194–197.

Gardiner, C. (1983), 'Handbook of statistical methods'.

Gent, P. and McWilliams, J. (1990), "Isopycnal mixing in ocean circulation models", Journal of Physical Oceanography , Vol. 20, pp. 150–155.

Gent, P., Willebrand, J., McDougall, T. and McWilliams, J. (1995), "Parameterizing eddy-induced tracer transports in ocean circulation models", Journal of Physical Oceanography , Vol. 25, pp. 463–474.

Gerdes, R., Köberle, C. and Willebrand, J. (1991), "The influence of numerical advection schemes on the results of ocean general circulation models", Climate Dynamics , Vol. 5, Springer, pp. 211–226.

Germano, M., Piomelli, U., Moin, P. and Cabot, W. (1991), "A dynamic subgrid-scale eddy viscosity model", Physics of Fluids A: Fluid Dynamics , Vol. 3, p. 1760.

Gilbarg, D. and Trudinger, N. (2001), Elliptic partial differential equations of second order, Vol. 224, Springer Verlag.

Gill, A. (1982), Atmosphere-ocean dynamics, Vol. 30, Academic Press.

Gill, A., Green, J. and Simmons, A. (1974), Energy partition in the large-scale ocean circulation and the production of mid-ocean eddies, in 'Deep Sea Research and Oceanographic Abstracts', Vol. 21, Elsevier, pp. 499–528.

Gille, S. (2003), "Float observations of the Southern Ocean.Part II: Eddy fluxes", Journal of Physical Oceanography , Vol. 33, pp. 1182–1196.

Gille, S. and Davis, R. (1999), "The influence of mesoscale eddies on coarsely resolved density: An examination of subgrid-scale parameterization", Journal of Physical Oceanography , Vol. 29, pp. 1109–1123.

Gille, S., Speer, K., Ledwell, J. and Garabato, A. (2007), "Mixing and stirring in the Southern Ocean", EOS, Transactions American Geophysical Union , Vol. 88, American Geophysical Union, p. 382.

Gnanadesikan, A., Griffies, S. and Samuels, B. (2007), "Effects in a climate model of slope tapering in neutral physics schemes", Ocean Modelling , Vol. 16, Elsevier, pp. 1–16.

Gnanadesikan, A., Slater, R. and Samuels, B. (2003), "Sensitivity of water mass transformation and heat transport to subgridscale mixing in coarse-resolution ocean models", Geophysical Research Letters , Vol. 30, American Geophysical Union, p. 1967.

Gordon, A. and Owens, W. (1987), "Polar oceans", Reviews of Geophysics , Vol. 25, American Geophysical Union, pp. 227–233.

Gough, W. and Lin, C. (1995), "Isopycnal mixing and the Veronis effect in an ocean general circulation model", Journal of Marine Research , Vol. 53, Sears Foundation for Marine Research, pp. 189–199.

Gough, W. and Welch, W. (1994), "Parameter space exploration of an ocean general circulation model using an isopycnal mixing parameterization", Journal of Marine Research , Vol. 52, Sears Foundation for Marine Research, pp. 773–796.

Greatbatch, R. (1998), "Exploring the relationship between eddy-induced transport velocity, vertical momentum transfer, and the isopycnal flux of potential vorticity", Journal of Physical Oceanography , Vol. 28, pp. 422–432.

Greatbatch, R. and Lamb, K. (1990), "On parameterizing vertical mixing of momentum in non-eddy resolving ocean models", Journal of Physical Oceanography , Vol. 20, pp. 1634–1637.

Greatbatch, R., Zhai, X., Eden, C. and Olbers, D. (2007), "The possible role in the ocean heat budget of eddy-induced mixing due to air-sea interaction", Geophysical Research Letters , Vol. 34, American Geophysical Union, p. L07604.

Green, J. (1960), "A problem in baroclinic stability", Quarterly Journal of the Royal Meteorological Society , Vol. 86, Wiley Online Library, pp. 237–251.

Green, J. (1970), "Transfer properties of the large-scale eddies and the general circulation of the atmosphere", Quarterly Journal of the Royal Meteorological Society , Vol. 96, Wiley Online Library, pp. 157–185.

Griesel, A., Gille, S., Sprintall, J., McClean, J. and Maltrud, M. (2009), "Assessing eddy heat flux and its parameterization: A wavenumber perspective from a 1/10 ocean simulation", Ocean Modelling , Vol. 29, Elsevier, pp. 248–260.

Griffies, S. (1998), "The Gent-McWilliams skew flux", Journal of Physical Oceanography , Vol. 28, pp. 831–841.

Griffies, S. (2004), Fundamentals of ocean climate models, Vol. 518, Princeton University Press Princeton,, USA.

Griffies, S., Böning, C., Bryan, F., Chassignet, E., Gerdes, R., Hasumi, H., Hirst, A., Treguier, A. and Webb, D. (2000), "Developments in ocean climate modelling", Ocean Modelling , Vol. 2, Elsevier, pp. 123–192.

Griffies, S., Gnanadesikan, A., Dixon, K., Dunne, J., Gerdes, R., Harrison, M., Rosati, A., Russell, J., Samuels, B., Spelman, M. et al. (2005), "Formulation of an ocean model for global climate simulations", Ocean Science , Vol. 1, pp. 45–79.

Griffies, S., Gnanadesikan, A., Pacanowski, R., Larichev, V., Dukowicz, J. and Smith, R. (1998), "Isoneutral diffusion in a z-coordinate ocean model", Journal of Physical Oceanography , Vol. 28, pp. 805–830.

Grooms, I., Julien, K. and Fox-Kemper, B. (2011), "On the interactions between planetary geostrophy and mesoscale eddies", Dynamics of Atmospheres and Oceans , Vol. 51, Elsevier, pp. 109–136.

Haine, T. and Marshall, J. (1998), "Gravitational, symmetric, and baroclinic instability of the ocean mixed layer", Journal of Physical Oceanography , Vol. 28, pp. 634–658.

Hallberg, R. and Gnanadesikan, A. (2006), "The role of eddies in determining the structure and response of the wind-driven Southern Hemisphere overturning: Results from the Modeling Eddies in the Southern Ocean (MESO) project", Journal of Physical Oceanography , Vol. 36, pp. 2232–2252.

Haynes, P. and Shuckburgh, E. (2000), "Effective diffusivity as a diagnostic of atmospheric transport. I - Stratosphere", Journal of Geophysical Research , Vol. 105, p. 22.

Held, I. (1999), "The macroturbulence of the troposphere", Tellus B , Vol. 51, Wiley Online Library, pp. 59–70.

Held, I. and Larichev, V. (1995), "A scaling theory for horizontally homogeneous, baroclinically unstable flow on a beta-plane", arXiv preprint ao-sci/9503001 .

Henning, C. and Vallis, G. (2004), "The effects of mesoscale eddies on the main subtropical thermocline", Journal of Physical Oceanography , Vol. 34, pp. 2428–2443.

Henning, C. and Vallis, G. (2005), "The effects of mesoscale eddies on the stratification and transport of an ocean with a circumpolar channel", Journal of Physical Oceanography , Vol. 35, pp. 880–896.

Heywood, K., Naveira Garabato, A. and Stevens, D. (2002), High diapycnal eddy diffusivity in the abyssal Southern Ocean, in 'EGS General Assembly Conference Abstracts', Vol. 27, p. 4372.

Hogg, N., Biscaye, P., Gardner, W. and Schmitz Jr, W. (1982), "On the transport and modification of Antarctic Bottom Water in the Vema Channel", Journal of Marine Research , Vol. 40, pp. 231–263.

Holloway, G. (1986), "Estimation of oceanic eddy transports from satellite altimetry", Nature Publishing Group.

Holloway, G. (1992), "Representing topographic stress for large-scale ocean models", Journal of Physical Oceanography , Vol. 22, pp. 1033–1046.

Hoskins, B. (1975), "The geostrophic momentum approximation and the semi-geostrophic equations.", Journal of Atmospheric Sciences , Vol. 32, pp. 233–242.

Hoskins, B. and Bretherton, F. (1972), "Atmospheric frontogenesis models: Mathematical formulation and solution", Journal of the Atmospheric Sciences , Vol. 29, pp. 11–37.

Hoskins, B. and Draghici, I. (1977), "The forcing of ageostrophic motion according to the semi-geostrophic equations and in an isentropic coordinate model.", Journal of Atmospheric Sciences , Vol. 34, pp. 1859–1867.

Hoskins, B., Draghici, I. and Davies, H. (1978), "A new look at the ω-equation", Quarterly Journal of the Royal Meteorological Society , Vol. 104, Wiley Online Library, pp. 31–38.

Howells, I. (1960), "An approximate equation for the spectrum of a conserved scalar quantity in a turbulent fluid", Journal of Fluid Mechanics , Vol. 9, Cambridge Univ Press, pp. 104–106.

Im Sang Oh, V., Park, W. et al. (2000), "Estimating horizontal diffusivity in the East Sea (Sea of Japan) and the northwest Pacific from satellite-tracked drifter data", Journal of Geophysical Research , Vol. 105, American Geophysical Union, pp. 6483–6492.

Iselin, C. (1939), "The influence of vertical and lateral turbulence on the characteristics of the waters at mid-depths", Transcripts of the American Geophysical Union , Vol. 20, pp. 414–417.

Jochum, M. (1997), Eine ortsabhängige Parameterisierung von Wirbelflüssen, PhD thesis, Masters thesis, Institut für Meereskunde, Kiel.

Johnson, G. and Bryden, H. (1989), "On the size of the Antarctic Circumpolar Current", Deep Sea Research Part A. Oceanographic Research Papers , Vol. 36, Elsevier, pp. 39–53.

Karsten, R., Jones, H. and Marshall, J. (2002), "The role of eddy transfer in setting the stratification and transport of a circumpolar current", Journal of Physical Oceanography , Vol. 32, pp. 39–54.

Keffer, T. (1985), "The ventilation of the world's oceans: Maps of the potential vorticity field", Journal of Physical Oceanography , Vol. 15, pp. 509–523.

Keffer, T. and Holloway, G. (1988), "Estimating Southern Ocean eddy flux of heat and salt from satellite altimetry", Nature Publishing Group.

Killworth, P. (1997), "On the parameterization of eddy transfer Part I. Theory", Journal of Marine Research , Vol. 55, Sears Foundation for Marine Research, pp. 1171–1197.

Killworth, P. and Nurser, A. (2006), Implementing a nonlocal eddy parameterization into a global ocean model, in 'Geophysical Research Abstracts', Vol. 8, p. 088.

Klocher, A., Ferrari, R. and LaCasce, J. (2012, in press), "Estimating suppression of eddy mixing by mean flows", Journal of Physical Oceanography .

Kolmogorov, A. (1941), The local structure of turbulence in incompressible viscous fluid for very large Reynolds numbers, in 'Akademiia Nauk SSSR Doklady', Vol. 30, pp. 301–305.

Kostrykin, S. and Schmitz, G. (2006), "Effective diffusivity in the middle atmosphere based on general circulation model winds", Journal of Geophysical Research , Vol. 111, American Geophysical Union, p. D02304.

Kraichnan, R. (1967), "Inertial ranges in two-dimensional turbulence", Physics of fluids , Vol. 10, The American Institute of Physics, pp. 1417–1423.

Krauß, W. and Boning, C. (1987), "Lagrangian properties of eddy fields in the northern North Atlantic as deduced from satellite-tracked buoys", Journal of Marine Research , Vol. 45, Sears Foundation for Marine Research, pp. 259–291.

Kunze, E. and Sanford, T. (1996), "Abyssal mixing: Where it is not", Journal of Physical Oceanography , Vol. 26, American Meteorological Society, pp. 2286–2296.

Kuo, A., Plumb, R. and Marshall, J. (2005), "Transformed Eulerian-mean theory. Part II: Potential vorticity homogenization and the equilibrium of a wind-and buoyancy-driven zonal flow", Journal of Physical Oceanography , Vol. 35, pp. 175–187.

Kuo, H. (1952), "Three-dimensional disturbances in a baroclinic zonal current.", Journal of Atmospheric Sciences , Vol. 9, pp. 260–278.

LaCasce, J. (2008), "Statistics from Lagrangian observations", Progress in Oceanography , Vol. 77, Elsevier, pp. 1–29.

LaCasce, J. and Bower, A. (2000), "Relative dispersion in the subsurface North Atlantic", Journal of marine research , Vol. 58, Sears Foundation for Marine Research, pp. 863–894.

Large, W., Danabasoglu, G., Doney, S. and McWilliams, J. (1997), "Sensitivity to surface forcing and boundary layer mixing in a global ocean model: Annual-mean climatology", Journal of Physical Oceanography , Vol. 27, pp. 2418–2447.

Large, W., McWilliams, J. and Doney, S. (1994), "Oceanic vertical mixing: A review and a model with a nonlocal boundary layer parameterization", Reviews of Geophysics , Vol. 32, American Geophysical Union, pp. 363–403.

Large, W. and Yeager, S. (2004), Diurnal to decadal global forcing for ocean and sea-ice models: The data sets and flux climatologies, National Center for Atmospheric Research.

Larichev, V. and Held, I. (1995), "Eddy amplitudes and fluxes in a homogeneous model of fully developed baroclinic instability", Journal of Physical Oceanography , Vol. 25, pp. 2285–2297.

Lau, N. and Wallace, J. (1979), "On the distribution of horizontal transports by transient eddies in the Northern Hemisphere wintertime circulation", Journal of the Atmospheric Sciences , Vol. 36, pp. 1844–1861.

Ledwell, J., Montgomery, E., Polzin, K., St Laurent, L., Schmitt, R. and Toole, J. (2000), "Evidence for enhanced mixing over rough topography in the abyssal ocean", Nature , Vol. 403, pp. 179–182.

Ledwell, J., St. Laurent, L., Girton, J. and Toole, J. (2011), "Diapycnal mixing in the Antarctic Circumpolar Current", Journal of Physical Oceanography , Vol. 41, pp. 241–246.

Ledwell, J., Watson, A. and Law, C. (1993), "Evidence for slow mixing across the pycnocline from an open-ocean tracer-release experiment", Nature , Vol. 364, pp. 701–703.

Ledwell, J., Watson, A. and Law, C. (1998), "Mixing of a tracer in the pycnocline", Journal of Geophysical Research , Vol. 103, American Geophysical Union, pp. 21499–21.

Lee, M., Marshall, D. and Williams, R. (1997), "On the eddy transfer of tracers: Advective or diffusive?", Journal of Marine Research , Vol. 55, Sears Foundation for Marine Research, pp. 483–505.

Lee, M. and Nurser, A. (2006), The role of isopycnal heat fluxes in the overturning circulation of the Southern Ocean, in 'Geophysical Research Abstracts', Vol. 8, p. 09933.

Lilly, D. (1992), "A proposed modification of the Germano subgrid-scale closure method", Physics of Fluids , Vol. 4, pp. 633–635.

Lumpkin, R. and Flament, P. (2001), "Lagrangian statistics in the central North Pacific", Journal of Marine Systems , Vol. 29, Elsevier, pp. 141–155.

Lumpkin, R., Treguier, A. and Speer, K. (2002), "Lagrangian eddy scales in the northern Atlantic Ocean", Journal of Physical Oceanography , Vol. 32, pp. 2425–2440.

Mahadevan, A. (2006), "Modeling vertical motion at ocean fronts: Are nonhydrostatic effects relevant at submesoscales?", Ocean Modelling , Vol. 14, Elsevier, pp. 222–240.

Mantyla, A. and Reid, J. (1983), "Abyssal characteristics of the World Ocean waters", Deep Sea Research Part A. Oceanographic Research Papers , Vol. 30, Elsevier, pp. 805–833.

Marshall, D., Maddison, J. and Berloff, P. (2012), "A framework for parameterizing eddy potential vorticity fluxes", Journal of Physical Oceanography , Vol. 42, pp. 539–557.

Marshall, J. (1982), "The vorticity equilibrium of ocean gyres and vorticity boundary conditions", Ocean Modelling , Vol. 47, pp. 1–3.

Marshall, J., Adcroft, A., Hill, C., Perelman, L. and Heisey, C. (1997), "A finite-volume, incompressible Navier-Stokes model for studies of the ocean on parallel computers", Journal of Geophysical Research , Vol. 102, American Geophysical Union, pp. 5753–5766.

Marshall, J., Hill, C., Perelman, L. and Adcroft, A. (1997), "Hydrostatic, quasi-hydrostatic, and nonhydrostatic ocean modeling", Journal of Geophysical Research , Vol. 102, American Geophysical Union, pp. 5733–5752.

Marshall, J., Jones, H., Karsten, R. and Wardle, R. (2002), "Can eddies set ocean stratification?", Journal of Physical Oceanography , Vol. 32, pp. 26–38.

Marshall, J., Shuckburgh, E., Jones, H. and Hill, C. (2006), "Estimates and implications of surface eddy diffusivity in the Southern Ocean derived from tracer transport", Journal of Physical Oceanography , Vol. 36, pp. 1806–1821.

Marshall, J. and Shutts, G. (1981), "A note on rotational and divergent eddy fluxes", Journal of Physical Oceanography , Vol. 11, pp. 1677–1679.

Marshall, J. et al. (2005), "CLIMODE: A mode water dynamics experiment in support of CLIVAR", US Clivar Variations , Vol. 3, pp. 8–14.

Matsuno, T. (1980), "Lagrangian motion of air parcels in the stratosphere in the presence of planetary waves", Pure and Applied Geophysics , Vol. 118, Springer, pp. 189–216.

Mazloff, M. (2008), The Southern Ocean meridional overturning circulation as diagnosed from an eddy permitting state estimate, PhD thesis, Massachusetts Institute of Technology.

McCarthy, M., Talley, L. and Baringer, M. (1997), "Deep upwelling and diffusivity in the southern Central Indian Basin", Geophysical Research Letters , Vol. 24, American Geophysical Union, pp. 2801–2804.

McClean, J., Poulain, P., Pelton, J. and Maltrud, M. (2002), "Eulerian and Lagrangian statistics from surface drifters and a high-resolution POP simulation in the North Atlantic", Journal of Physical Oceanography , Vol. 32, pp. 2472–2491.

McDougall, T. (1987), "Neutral surfaces", Journal of Physical Oceanography , Vol. 17, pp. 1950–1964.

McDougall, T. and McIntosh, P. (1996), "The temporal-residual-mean velocity. Part I: Derivation and the scalar conservation equations", Journal of Physical Oceanography , Vol. 26, pp. 2653–2665.

McDougall, T. and McIntosh, P. (2001), "The temporal-residual-mean velocity. Part II: Isopycnal interpretation and the tracer and momentum equations", Journal of Physical Oceanography , Vol. 31, pp. 1222–1246.

McDowell, S., Rhines, P. and Keffer, T. (1982), "North Atlantic potential vorticity and its relation to the general circulation", Journal of Physical Oceanography , Vol. 12, pp. 1417–1436.

McWilliams, J. (1996), "Modeling the oceanic general circulation", Annual Review of Fluid Mechanics , Vol. 28, Annual Reviews 4139 El Camino Way, PO Box 10139, Palo Alto, CA 94303-0139, USA, pp. 215–248.

McWilliams, J. (2003), "Diagnostic force balance and its limits", Nonlinear Processes in Geophysical Fluid Dynamics , Kluwer, pp. 287–304.

McWilliams, J. and Chow, J. (1981), "Equilibrium geostrophic turbulence i: A reference solution in a β-plane channel", Journal of Physical Oceanography , Vol. 11, pp. 921–949.

McWilliams, J. and Chow, J. (1983), 'Coauthors, 1983: The local dynamics of eddies in the western North Atlantic'.

Medvedev, A. and Greatbatch, R. (2004), "On advection and diffusion in the mesosphere and lower thermosphere: The role of rotational fluxes", Journal of Geophysical Research , Vol. 109, American Geophysical Union, p. D07104.

Mellor, G. and Yamada, T. (1974), "A hierarchy of turbulence closure models for planetary boundary layers", Journal of the Atmospheric Sciences , Vol. 31, pp. 1791–1806.

Mellor, G. and Yamada, T. (1977), A turbulence model applied to geophysical fluid problems, in 'Symposium on Turbulent Shear Flows', Vol. 1, p. 6.

Mellor, G. and Yamada, T. (1982), "Development of a turbulence closure model for geophysical fluid problems", Reviews of Geophysics and Space Physics , Vol. 20, pp. 851–875.

Meneveau, C. and Katz, J. (2000), "Scale-invariance and turbulence models for large-eddy simulation", Annual Review of Fluid Mechanics , Vol. 32, Annual Reviews 4139 El Camino Way, PO Box 10139, Palo Alto, CA 94303-0139, USA, pp. 1–32.

Meneveau, C., Lund, T. and Cabot, W. (1996), "A Lagrangian dynamic subgrid-scale model of turbulence", Journal of Fluid Mechanics , Vol. 319, Cambridge Univ Press, pp. 353–385.

Miles, J. (1964), "Baroclinic instability of the zonal wind", Reviews of Geophysics , Vol. 2, American Geophysical Union, pp. 155–176.

Monin, A. and Yaglom, A. (1971), "Statistical fluid dynamics", Vol. I and II MIT Press, Cambridge .

Montgomery, R. (1940), "The present evidence on the importance of lateral mixing processes in the ocean", Bulletin of the American Meteorological Society , Vol. 21, pp. 87–94.

Morris, M., Hall, M., St. Laurent, L. and Hogg, N. (2001), "Abyssal mixing in the Brazil Basin", Journal of Physical Oceanography , Vol. 31, pp. 3331–3348.

Munk, W. (1950), "On the wind-driven ocean circulation", Journal of Meteorology , Vol. 7, pp. 79–93.

Munk, W. (1966), Abyssal recipes, in 'Deep Sea Research and Oceanographic Abstracts', Vol. 13, Elsevier, pp. 707–730.

Nakamura, M. and Chao, Y. (2000), "On the eddy isopycnal thickness diffusivity of the Gent-McWilliams subgrid mixing parameterization", Journal of Climate , Vol. 13, pp. 502–510.

Nakamura, N. (1996), "Two-dimensional mixing, edge formation, and permeability diagnosed in an area coordinate", Journal of the Atmospheric Sciences , Vol. 53, [Boston, etc.] American Meteorological Society., pp. 1524–1537.

Nowlin Jr., W. and Klinck, J. (1986), "The physics of the Antarctic circumpolar current", Reviews of Geophysics , Vol. 24, American Geophysical Union, pp. 469–491.

Nurser, A. and Lee, M. (2004), "Isopycnal averaging at constant height. Part I: The formulation and a case study", Journal of Physical Oceanography , Vol. 34, pp. 2721–2739.

O'Dwyer, J. and Williams, R. (1997), "The climatological distribution of potential vorticity over the abyssal ocean", Journal of Physical Oceanography , Vol. 27, pp. 2488–2506.

Olbers, D., Wenzel, M. and Willebrand, J. (1985), "The inference of North Atlantic circulation patterns from climatological hydrographic data", Reviews of Geophysics , Vol. 23, American Geophysical Union, pp. 313–356.

Olbers, D., Willebrand, J. and Eden, C. (2012), Ocean Dynamics, Springer Verlag Berlin, Berlin. **URL:** *http://www.springer.com/earth+sciences+and+geography/oceanography/book/978-3-642-23449-1*

Paduan, J. and Niiler, P. (1993), "Structure of velocity and temperature in the Northeast Pacific as measured with Lagrangian drifters in fall 1987", Journal of Physical Oceanography , Vol. 23, American Meteorological Society, pp. 585–600.

Pedlosky, J. (1982), "Geophysical Fluid Dynamics", New York and Berlin, Springer-Verlag, 1982. 636 p. , Vol. 1.

Pedlosky, J. (1984), "The equations for geostrophic motion in the ocean", Journal of Physical Oceanography , Vol. 14, American Meteorological Society, pp. 448–455.

Peterson, K. and Greatbatch, R. (2001), "Vorticity fluxes in shallow water ocean models", Atmosphere-Ocean , Vol. 39, Taylor & Francis, pp. 1–14.

Philander, S. (1990), El Niño, La Niña, and the Southern Oscillation, Vol. 46, Academic Press.

Phillips, H. and Rintoul, S. (2000), "Eddy variability and energetics from direct current measurements in the Antarctic Circumpolar Current south of Australia", Journal of Physical Oceanography , Vol. 30, pp. 3050–3076.

Plumb, R. (1979), "Eddy fluxes of conserved quantities by small-amplitude waves", Journal of the Atmospheric Sciences , Vol. 36, pp. 1699–1704.

Plumb, R. and Ferrari, R. (2005), "Transformed Eulerian-mean theory. Part I: Nonquasigeostrophic theory for eddies on a zonal-mean flow", Journal of Physical Oceanography , Vol. 35, pp. 165–174.

Plumb, R. and Mahlman, J. (1987), "The zonally averaged transport characteristics of the GFDL general circulation/transport model", Journal of the Atmospheric Sciences , Vol. 44, pp. 298–327.

Polzin, K., Speer, K., Toole, J. and Schmitt, R. (1996), "Intense mixing of Antarctic Bottom Water in the equatorial Atlantic Ocean", Nature Publishing Group.

Polzin, K., Toole, J., Ledwell, J. and Schmitt, R. (1997), "Spatial variability of turbulent mixing in the abyssal ocean", Science , Vol. 276, American Association for the Advancement of Science, pp. 93–96.

Pope, S. (2000), Turbulent flows, Cambridge University Press.

Poulain, P. and Niiler, P. (1989), "Statistical analysis of the surface circulation in the California Current System using satellite-tracked drifters", Journal of Physical Oceanography , Vol. 19, American Meteorological Society, pp. 1588–1603.

Prandtl, L. (1935), "The mechanics of viscous fluids", Springer.

Price, J. (1981), Upper ocean response to a hurricane, Woods Hole Oceanographic Institution.

Price, J. (2001), "Subduction", International Geophysics , Vol. 77, Elsevier, pp. 357–371.

Price, J., Weller, R. and Pinkel, R. (1986), "Diurnal cycling: Observations and models of the upper ocean response to diurnal heating, cooling, and wind mixing", Journal of Geophysical Research , Vol. 91, pp. 8411–8427.

Priest, E. (1982), "Solar magnetohydrodynamics", Reidel, Boston, MA.

Pyle, J. and Rogers, C. (1980), "Stratospheric transport by stationary planetary waves-the importance of chemical processes", Quarterly Journal of the Royal Meteorological Society , Vol. 106, Wiley Online Library, pp. 421–446.

Radko, T. and Marshall, J. (2004), "Eddy-induced diapycnal fluxes and their role in the maintenance of the thermocline", Journal of Physical Oceanography , Vol. 34, pp. 372–383.

Radko, T. and Marshall, J. (2006), "The Antarctic circumpolar current in three dimensions", Journal of Physical Oceanography , Vol. 36, pp. 651–669.

Randall, D. (2009), "Reynolds averaging", Unpublished manuscript .

Redi, M. (1982), "Oceanic isopycnal mixing by coordinate rotation", Journal of Physical Oceanography , Vol. 12, pp. 1154–1158.

Rhines, P. (1975), "Waves and turbulence on a beta-plane", Journal of Fluid Mechanics , Vol. 69, Cambridge University Press, pp. 417–443.

Rhines, P. and Holland, W. (1979), "A theoretical discussion of eddy-induced circulation", Dynamics of Atmospheres and Oceans , Vol. 3, pp. 285–325.

Rhines, P. and Holland, W. (1980), "An example of eddy-induced ocean circulation", Journal of Physical Oceanography , Vol. 10, pp. 1010–1031.

Rhines, P. and Young, W. (1982a), "Hornogenization of potential vorticity in planetary gyres", Journal of Fluid Mechanics , Vol. 122, pp. 347–367.

Rhines, P. and Young, W. (1982b), "A theory of the wind-driven circulation. I. Mid-ocean gyres", Journal of Marine Research , Vol. 40, pp. 559–596.

Rix, N. and Willebrand, J. (1996), "A note on the parameterisation of eddy-induced mixing from eddy-resolving model data", Journal of Physical Oceanography , Vol. 26, pp. 2281–2285.

Robbins, P., Price, J., Owens, W. and Jenkins, W. (2000), "The importance of lateral diffusion for the ventilation of the lower thermocline in the subtropical North Atlantic", Journal of Physical Oceanography , Vol. 30, pp. 67–89.

Roberts, M. and Marshall, D. (2000), "On the validity of downgradient eddy closures in ocean models", Journal of Geophysical Research , Vol. 105, pp. 28–613.

Robitaille, D. and Weaver, A. (1995), "Validation of sub-grid-scale mixing schemes using CFCs in a global ocean model", Geophysical Research Letters , Vol. 22, American Geophysical Union, pp. 2917–2920.

Roemmich, D. and Gilson, J. (2001), "Eddy transport of heat and thermocline waters in the North Pacific: A key to interannual/decadal climate variability?", Journal of Physical Oceanography , Vol. 31, pp. 675–687.

Roemmich, D., Hautala, S. and Rudnick, D. (1996), "Northward abyssal transport through the Samoan Passage and adjacent regions", Journal of Geophysical Research , Vol. 101, American Geophysical Union, pp. 14039–14.

Rossby, H., Riser, S. and Mariano, A. (1983), 'The western North Atlantica Lagrangian viewpoint'.

Ryaben'kii, V. and Tsynkov, S. (2006), A theoretical introduction to numerical analysis, Chapman & Hall/CRC.

Sallée, J., Speer, K., Morrow, R. and Lumpkin, R. (2008), "An estimate of Lagrangian eddy statistics and diffusion in the mixed layer of the Southern Ocean", Journal of Marine Research , Vol. 66, Sears Foundation for Marine Research, pp. 441–463.

Salmon, R. (1998), Lectures on geophysical fluid dynamics, Oxford University Press, USA.

Sarmiento, J. and Bryan, K. (1982), "An ocean transport model for the North Atlantic", Journal of Geophysical Research , Vol. 87, American Geophysical Union, pp. 394–408.

Saunders, P. (1987), "Currents, dispersion and light transmittance measurements on the Madeira Abyssal Plain", Institute of Oceanographic Sciences Deacon Laboratory.

Sawyer, J. and Sawyer, J. (1956), "The vertical circulation at meteorological fronts and its relation to frontogenesis", Proceedings of the Royal Society of London. Series A. Mathematical and Physical Sciences , Vol. 234, The Royal Society, pp. 346–362.

Schlösser, F. and Eden, C. (2007), "Diagnosing the energy cascade in a model of the North Atlantic", Geophysical Research Letters , Vol. 34, American Geophysical Union, p. L02604.

Schneider, T. and Walker, C. (2006), "Self-organization of atmospheric macroturbulence into critical states of weak nonlinear eddy-eddy interactions", Journal of the Atmospheric Sciences , Vol. 63, pp. 1569–1586.

Scott, R. and Straub, D. (1998), "Small viscosity behavior of a homogeneous, quasi-geostrophic, ocean circulation model", Journal of Marine Research , Vol. 56, Sears Foundation for Marine Research, pp. 1225–1258.

Scott, R. and Wang, F. (2005), "Direct evidence of an oceanic inverse kinetic energy cascade from satellite altimetry", Journal of Physical Oceanography , Vol. 35, pp. 1650–1666.

Shuckburgh, E. and Haynes, P. (2003), "Diagnosing transport and mixing using a tracer-based coordinate system", Physics of Fluids , Vol. 15, American Institute of Physics, pp. 3342–3357.

Shuckburgh, E., Jones, H., Marshall, J. and Hill, C. (2009), "Understanding the regional variability of eddy diffusivity in the Pacific sector of the Southern Ocean", Journal of Physical Oceanography , Vol. 39, pp. 2011–2023.

Shuckburgh, E., Maze, G., Ferreira, D., Marshall, J., Jones, H. and Hill, C. (2011), "Mixed layer lateral eddy fluxes mediated by air-sea interaction", Journal of Physical Oceanography , Vol. 41, pp. 130–144.

Smagorinsky, J. (1963), "General circulation experiments with the primitive equations", Monthly Weather Review , Vol. 91, pp. 99–164.

Smagorinsky, J. (1993), "Some historical remarks on the use of nonlinear viscosities", Large eddy simulation of complex engineering and geophysical flows , Vol. 1, Cambridge University Press, pp. 69–106.

Smith, K. (2007), "The geography of linear baroclinic instability in Earth's oceans", Journal of Marine Research , Vol. 65, Sears Foundation for Marine Research, pp. 655–683.

Smith, K., Boccaletti, G., Henning, C., Marinov, I., Tam, C., Held, I. and Vallis, G. (2002), "Turbulent diffusion in the geostrophic inverse cascade", Journal of Fluid Mechanics , Vol. 469, Cambridge Univ Press, pp. 13–48.

Smith, K. and Vallis, G. (2001), "The scales and equilibration of midocean eddies: Freely evolving flow", Journal of Physical Oceanography , Vol. 31, pp. 554–571.

Smith, R. and Gent, P. (2004), "Anisotropic Gent-McWilliams parameterization for ocean models", Journal of Physical Oceanography , Vol. 34, pp. 2541–2564.

Smith, R. and McWilliams, J. (2003), "Anisotropic horizontal viscosity for ocean models", Ocean Modelling , Vol. 5, Elsevier, pp. 129–156.

Solomon, H. (1971), "On the representation of isentropic mixing in ocean circulation models", Journal of Physical Oceanography , Vol. 1, pp. 233–234.

Solovev, M., Stone, P. and Malanotte-Rizzoli, P. (2002), "Assessment of mesoscale eddy parameterizations for a single-basin coarse-resolution ocean model", Journal of Geophysical Research , Vol. 107, American Geophysical Union, p. 3126.

Spall, M. (2000), "Generation of strong mesoscale eddies by weak ocean gyres", Journal of Marine Research , Vol. 58, Sears Foundation for Marine Research, pp. 97–116.

Spall, M., Richardson, P. and Price, J. (1993), "Advection and eddy mixing in the Mediterranean salt tongue", Journal of Marine Research , Vol. 51, Sears Foundation for Marine Research, pp. 797–818.

Stammer, D. (1997), "Global characteristics of ocean variability estimated from regional TOPEX/POSEIDON altimeter measurements", Journal of Physical Oceanography , Vol. 27, pp. 1743–1769.

Stammer, D. (1998), "On eddy characteristics, eddy transports, and mean flow properties", Journal of Physical Oceanography , Vol. 28, pp. 727–739.

Stammer, D., Wunsch, C. and Ueyoshi, K. (2006), "Temporal changes in ocean eddy transports", Journal of Physical Oceanography , Vol. 36, pp. 543–550.

Stone, P. (1972a), "On non-geostrophic baroclinic stability: Part III. The momentum and heat transports", Journal of the Atmospheric Sciences , Vol. 29, pp. 419–426.

Stone, P. (1972b), "A simplified radiative-dynamical model for the static stability of rotating atmospheres", Journal of the Atmospheric Sciences , Vol. 29, pp. 405–418.

Sukoriansky, S., Dikovskaya, N. and Galperin, B. (2007), "On the arrest of inverse energy cascade and the Rhines scale", Journal of the Atmospheric Sciences , Vol. 64, pp. 3312–3327.

Sundermeyer, M. and Price, J. (1998), "Lateral mixing and the North Atlantic Tracer Release Experiment: Observations and numerical simulations of Lagrangian particles and a passive tracer", Journal of Geophysical Research , Vol. 103, p. 21.

Swenson, M. and Niiler, P. (1996), "Statistical analysis of the surface circulation", Journal of Geophysical Research , Vol. 101, pp. 22–631.

Talley, L. (1988), "Potential vorticity distribution in the North Pacific", Journal of Physical Oceanography , Vol. 18, pp. 89–106.

Tandon, A. and Garrett, C. (1996), "On a recent parameterization of mesoscale eddies", Journal of Physical Oceanography , Vol. 26, pp. 406–416.

Taylor, G. (1921), "Diffusion by continuous movements", Proceedings of the London Mathematical Society , Vol. 20, pp. 196–211.

Thomas, L. (1949), "Elliptic problems in linear difference equations over a network", Watson Sci. Comput. Lab. Rept., Columbia University, New York .

Thomas, L. (2005), "Destruction of potential vorticity by winds", Journal of Physical Oceanography , Vol. 35, pp. 2457–2466.

Thomas, L. and Ferrari, R. (2008), "Friction, frontogenesis, and the stratification of the surface mixed layer", Journal of Physical Oceanography , Vol. 38, pp. 2501–2518.

Thomas, L. and Lee, C. (2005), "Intensification of ocean fronts by down-front winds", Journal of Physical Oceanography , Vol. 35, pp. 1086–1102.

Thomas, L., Tandon, A. and Mahadevan, A. (2008), "Submesoscale processes and dynamics", Ocean Modeling in an Eddying Regime, Geophys. Monogr. Ser , Vol. 177, pp. 17–38.

Thompson, A. and Young, W. (2006), "Scaling baroclinic eddy fluxes: Vortices and energy balance", Journal of Physical Oceanography , Vol. 36, pp. 720–738.

Thompson, A. and Young, W. (2007), "Two-layer baroclinic eddy heat fluxes: Zonal flows and energy balance", Journal of the Atmospheric Sciences , Vol. 64, pp. 3214–3231.

Toole, J., Schmitt, R., Polzin, K. et al. (1994), "Estimates of diapycnal mixing in the abyssal ocean.", Science (New York, NY) , Vol. 264, p. 1120.

Treguier, A. (1999), "Evaluating eddy mixing coefficients from eddy-resolving ocean models: A case study", Journal of Marine Research , Vol. 57, Sears Foundation for Marine Research, pp. 89–108.

Treguier, A., Held, I. and Larichev, V. (1997), "Parameterization of quasigeostrophic eddies in primitive equation ocean models", Journal of Physical Oceanography , Vol. 27, pp. 567–580.

Tulloch, R., Marshall, J., Hill, C. and Smith, K. (2011), "Scales, growth rates, and spectral fluxes of baroclinic instability in the ocean", Journal of Physical Oceanography , Vol. 41, pp. 1057–1076.

Tulloch, R., Marshall, J. and Smith, K. (2009), "Interpretation of the propagation of surface altimetric observations in terms of planetary waves and geostrophic turbulence", Journal of Geophysical Research , Vol. 114, American Geophysical Union, p. C02005.

Vallis, G. (2006), Atmospheric and oceanic fluid dynamics: fundamentals and large-scale circulation, Cambridge University Press.

Veronis, G. (1975), "The role of models in tracer studies", Numerical Models of Ocean Circulation , pp. 133–146.

Visbeck, M., Marshall, J., Haine, T. and Spall, M. (1997), "Specification of eddy transfer coefficients in coarse-resolution ocean circulation models*", Journal of Physical Oceanography , Vol. 27, pp. 381–402.

Wardle, R. and Marshall, J. (2000), "Representation of eddies in primitive equation models by a PV flux", Journal of Physical Oceanography , Vol. 30, pp. 2481–2503.

Webb, D. and Suginohara, N. (2001), "Oceanography: Vertical mixing in the ocean", Nature , Vol. 409, Nature Publishing Group, pp. 37–37.

Weller, R., Furey, P., Spall, M. and Davis, R. (2004), "The large-scale context for oceanic subduction in the Northeast Atlantic", Deep Sea Research Part I: Oceanographic Research Papers , Vol. 51, Elsevier, pp. 665–699.

Whitehead Jr., J. (1984), "Estimates of the relative roles of diapycnal, isopycnal and double-diffusive mixing in Antarctic Bottom Water in the North Atlantic", Journal of Geophysical Research , Vol. 89, pp. 10–479.

Whitehead Jr., J. and Worthington, L. (1982), "The flux and mixing rates of Antarctic Bottom Water within the North Atlantic", Journal of Geophysical Research , Vol. 87, American Geophysical Union, pp. 7903–7924.

Wilson, C. and Williams, R. (2006), "When are eddy tracer fluxes directed downgradient?", Journal of Physical Oceanography , Vol. 36, pp. 189–201.

Wolfe, C., Cessi, P., McClean, J. and Maltrud, M. (2008), "Vertical heat transport in eddying ocean models", Geophysical Research Letters , Vol. 35, American Geophysical Union, p. L23605.

Wunsch, C. (1996), The ocean circulation inverse problem, Cambridge University Press.

Wunsch, C. (1999), "Where do ocean eddy heat fluxes matter?", Journal of Geophysical Research , Vol. 104, American Geophysical Union, pp. 13235–13.

Wunsch, C. and Ferrari, R. (2004), "Vertical mixing, energy, and the general circulation of the oceans", Annual Reviews in Fluid Mechanics , Vol. 36, Annual Reviews, pp. 281–314.

Wyrtki, K., Magaard, L. and Hager, J. (1976), "Eddy energy in the oceans", Journal of Geophysical Research , Vol. 81, American Geophysical Union, pp. 2641–2646.

Young, W. (2012), "An exact thickness-weighted average formulation of the Boussinesq equations", Journal of Physical Oceanography , Vol. 42, pp. 692–707.

Zhao, R. and Vallis, G. (2008), "Parameterizing mesoscale eddies with residual and Eulerian schemes, and a comparison with eddy-permitting models", Ocean Modelling , Vol. 23, Elsevier, pp. 1–12.

Zhurbas, V., Oh, I. and Pyzhevich, M. (2003), "Maps of horizontal diffusivity and Lagrangian scales in the Pacific Ocean obtained from drifter data", Oceanology C/C of Okeanologikaa , Vol. 43, American Geophysical Union, pp. 622–631.

Zhurbas, V. et al. (2004), "Drifter-derived maps of lateral diffusivity in the Pacific and Atlantic Oceans in relation to surface circulation patterns", Journal of Geophysical Research , Vol. 109, American Geophysical Union, p. C05015.

Appendix A

Appendix A

This appendix contains the text of Bachman and Fox-Kemper (submitted for review), current as of November 21, 2012.

Appendix B

Appendix B

B.1 Reynolds Averaging of the Boussinesq Primitive Equations

Presented in this section is a detailed derivation of the mean and eddy components of the Reynolds averaged, Boussinesq, hydrostatic primitive equations. The dimensional governing equations for the system are as follows:

$$\frac{D\mathbf{u}}{Dt} + \mathbf{f} \times \mathbf{u} = -\nabla_z \phi$$
$$\frac{\partial \phi}{\partial z} = b$$
$$\frac{Db}{Dt} = 0$$
$$\nabla \cdot \mathbf{u} = 0.$$

The evolution equation for a conserved passive tracer τ is $\frac{D\tau}{Dt} = 0$.

The Reynolds averaging follows the same rules as were outlined in Section 1.3.1, so we decompose the dependent variables into mean and perturbation components under the following assumptions:

1. Commutes with differentiation
2. $\bar{\bar{a}} = \bar{a}$
3. $\bar{a'} = 0$
4. $a \bar{+} b = \bar{a} + \bar{b}$.

We proceed with the Reynolds decomposition explicitly in Cartesian coordinates, then summarize in vector notation at the end. The finalized equations appear in rectangular boxes.

B.1.1 The Mass Continuity Equation

Begin with the incompressible mass continuity equation, which arises by making the Boussinesq approximation:

$$\frac{\partial u}{\partial x} + \frac{\partial v}{\partial y} + \frac{\partial w}{\partial z} = 0.$$

Reynolds averaging gives

$$\frac{\partial(\bar{u} + u')}{\partial x} + \frac{\partial(\bar{v} + v')}{\partial y} + \frac{\partial(\bar{w} + w')}{\partial z} = 0.$$

Now take the mean of each term in the full averaged equation:

$$\frac{\partial\overline{(\bar{u} + u')}}{\partial x} + \frac{\partial\overline{(\bar{v} + v')}}{\partial y} + \frac{\partial\overline{(\bar{w} + w')}}{\partial z} = 0.$$

$$\boxed{\frac{\partial \bar{u}}{\partial x} + \frac{\partial \bar{v}}{\partial y} + \frac{\partial \bar{w}}{\partial z} = 0}$$

We subtract off this equation from the mass continuity equation for the total flow to find the continuity equation for the pertubation:

$$\frac{\partial u}{\partial x} + \frac{\partial v}{\partial y} + \frac{\partial w}{\partial z} - \frac{\partial \bar{u}}{\partial x} + \frac{\partial \bar{v}}{\partial y} + \frac{\partial \bar{w}}{\partial z} = 0$$
$$\frac{\partial(u - \bar{u})}{\partial x} + \frac{\partial(v - \bar{v})}{\partial y} + \frac{\partial(w - \bar{w})}{\partial z} = 0$$

$$\boxed{\frac{\partial u'}{\partial x} + \frac{\partial v'}{\partial y} + \frac{\partial w'}{\partial z} = 0}$$

B.1.2 The Momentum Equations

The zonal momentum equation for the mean flow is decomposed following the same procedure as for the continuity equation (the equation for the meridional velocity is derived similarly). Begin with the equation for the total flow:

$$\frac{\partial u}{\partial t} + u\frac{\partial u}{\partial x} + v\frac{\partial u}{\partial y} - fu = -\frac{\partial \phi}{\partial x}.$$

Reynolds averaging yields

$$\frac{\partial(\bar{u}+u')}{\partial t} + (\bar{u}+u')\frac{\partial(\bar{u}+u')}{\partial x} + (\bar{v}+v')\frac{\partial(\bar{u}+u')}{\partial y} - f(\bar{u}+u') = -\frac{\partial(\bar{\phi}+\phi')}{\partial x}.$$

Take the mean of the entire equation to obtain

$$\frac{\partial\overline{(\bar{u}+u')}}{\partial t} + \overline{(\bar{u}+u')\frac{\partial(\bar{u}+u')}{\partial x}} + \overline{(\bar{v}+v')\frac{\partial(\bar{u}+u')}{\partial y}} - \overline{f(\bar{u}+u')} = -\frac{\partial\overline{(\bar{\phi}+\phi')}}{\partial x}.$$

The decomposition for the nonlinear advection term can be treated by noting that

$$\begin{aligned}\overline{(\bar{u}+u')\cdot\frac{\partial(\bar{u}+u')}{\partial x}} &= \overline{\bar{u}\frac{\partial\bar{u}}{\partial x} + \bar{u}\frac{\partial u'}{\partial x} + u'\frac{\partial\bar{u}}{\partial x} + u'\frac{\partial u'}{\partial x}} \\ &= \bar{u}\frac{\partial\bar{u}}{\partial x} + \overline{u'\frac{\partial u'}{\partial x}} \\ &= \bar{u}\frac{\partial\bar{u}}{\partial x} + \frac{1}{2}\frac{\partial\overline{u'u'}}{\partial x}.\end{aligned}$$

because of the continuity equation. Then the final equation for the zonal mean flow becomes

$$\boxed{\frac{\partial\bar{u}}{\partial t} + \bar{u}\frac{\partial\bar{u}}{\partial x} + \bar{v}\frac{\partial\bar{u}}{\partial y} - f\bar{u} - \frac{1}{2}\frac{\partial\overline{u'u'}}{\partial x} - \frac{1}{2}\frac{\partial\overline{u'v'}}{\partial x} = -\frac{\partial\bar{\phi}}{\partial x}}$$

Subtract the zonal mean flow from the total flow to find the equation for the zonal perturbation. This can be done directly by subtracting the above equation from the total zonal momentum equation:

$$\frac{\partial(u-\bar{u})}{\partial t} + u\frac{\partial u}{\partial x} - \bar{u}\frac{\partial\bar{u}}{\partial x} + v\frac{\partial u}{\partial y} - \bar{v}\frac{\partial\bar{u}}{\partial x} - f(u-\bar{u}) - \frac{1}{2}\frac{\partial\overline{u'u'}}{\partial x} - \frac{1}{2}\frac{\partial\overline{u'v'}}{\partial x} = -\frac{\partial(\phi-\bar{\phi})}{\partial x}.$$

Decomposing the u terms above using $u = \bar{u} + u'$, we arrive at the perturbation equation

$$\boxed{\frac{\partial u'}{\partial t} + \bar{u}\frac{\partial u'}{\partial x} + \bar{v}\frac{\partial u'}{\partial y} + u'\frac{\partial\bar{u}}{\partial x} + v'\frac{\partial\bar{u}}{\partial y} + u'\frac{\partial u'}{\partial x} + v'\frac{\partial u'}{\partial y} - fu' = -\frac{\partial\phi'}{\partial x}}$$

B.1.3 Kinetic Energy and Variance

We can take the equation for the zonal mean momentum and multiply by $\bar{u}$ to obtain an equation for the kinetic energy of the mean zonal flow:

$$\bar{u}\left(\frac{\partial \bar{u}}{\partial t}+\bar{u}\frac{\partial \bar{u}}{\partial x}+\bar{v}\frac{\partial \bar{u}}{\partial y}-f\bar{u}-\frac{\partial \overline{u'u'}}{\partial x}-\frac{\partial \overline{u'v'}}{\partial x}\right)=-\bar{u}\frac{\partial \bar{\phi}}{\partial x}$$

$$\boxed{\frac{1}{2}\frac{\partial \bar{u}^2}{\partial t}+\frac{1}{2}\bar{u}\frac{\partial \bar{u}^2}{\partial x}+\frac{1}{2}\bar{v}\frac{\partial \bar{u}^2}{\partial y}-f\bar{u}^2-\bar{u}\frac{\partial \overline{u'u'}}{\partial x}-\bar{u}\frac{\partial \overline{u'v'}}{\partial x}=-\bar{u}\frac{\partial \bar{\phi}}{\partial x}}$$

In a similar vein, we can take the perturbation momentum equation, multiply by u', and take the mean of the result to get the eddy zonal velocity variance:

$$u'\left(\frac{\partial u'}{\partial t}+\bar{u}\frac{\partial u'}{\partial x}+\bar{v}\frac{\partial u'}{\partial y}+u'\frac{\partial \bar{u}}{\partial x}+v'\frac{\partial \bar{u}}{\partial y}+u'\frac{\partial u'}{\partial x}+v'\frac{\partial u'}{\partial y}-fu'\right)=-u'\frac{\partial \phi'}{\partial x}$$

$$\frac{1}{2}\frac{\partial u'^2}{\partial t}+\frac{1}{2}\bar{u}\frac{\partial u'^2}{\partial x}+\frac{1}{2}\bar{v}\frac{\partial u'^2}{\partial y}+u'^2\frac{\partial \bar{u}}{\partial x}+u'v'\frac{\partial \bar{u}}{\partial y}+\frac{1}{2}\frac{\partial u'u'u'}{\partial x}+\frac{1}{2}\frac{\partial u'^2v'}{\partial y}-fu'^2=-\frac{\partial u'\phi'}{\partial x}$$

$$\boxed{\frac{1}{2}\frac{\partial \overline{u'^2}}{\partial t}+\frac{1}{2}\bar{u}\frac{\partial \overline{u'^2}}{\partial x}+\frac{1}{2}\bar{v}\frac{\partial \overline{u'^2}}{\partial y}+\overline{u'^2}\frac{\partial \bar{u}}{\partial x}+\overline{u'v'}\frac{\partial \bar{u}}{\partial y}+\frac{1}{2}\frac{\partial \overline{u'u'u'}}{\partial x}+\frac{1}{2}\frac{\partial \overline{u'^2v'}}{\partial y}-f\overline{u'^2}=-\frac{\partial \overline{u'\phi'}}{\partial x}}$$

B.1.4 The Tracer Equation

We next perform the Reynolds decomposition on the conservation equation for a materially conserved tracer. Note that we have made no assumption about whether the tracer is passive or active, so in the quasigeostrophic Boussinesq approximation this derivation applies to both potential vorticity and buoyancy as well as passive tracers. Begin with the general conservation equation for a tracer τ, with no sources or sinks:

$$\frac{\partial \tau}{\partial t}+u\frac{\partial \tau}{\partial x}+v\frac{\partial \tau}{\partial y}+w\frac{\partial \tau}{\partial z}=0.$$

Perform the usual Reynolds decomposition to get

$$\frac{\partial(\bar{\tau}+\tau')}{\partial t}+(\bar{u}+u')\frac{\partial(\bar{\tau}+\tau')}{\partial x}+(\bar{v}+v')\frac{\partial(\bar{\tau}+\tau')}{\partial y}+(\bar{w}+w')\frac{\partial(\bar{\tau}+\tau')}{\partial z}=0.$$

Average the above equation in the same way as shown in the previous section to obtain

$$\frac{\partial \bar{\tau}}{\partial t} + \bar{u}\frac{\partial \bar{\tau}}{\partial x} + \bar{v}\frac{\partial \bar{\tau}}{\partial y} + \bar{w}\frac{\partial \bar{\tau}}{\partial z} + \frac{\partial \overline{u'\tau'}}{\partial x} + \frac{\partial \overline{v'\tau'}}{\partial y} + \frac{\partial \overline{w'\tau'}}{\partial z} = 0.$$

Subtract the mean equation from the full tracer conservation equation to obtain the eddy equation for the tracer evolution

$$\frac{\partial \tau'}{\partial t} + u'\frac{\partial \bar{\tau}}{\partial x} + v'\frac{\partial \bar{\tau}}{\partial y} + w'\frac{\partial \bar{\tau}}{\partial z} + \bar{u}\frac{\partial \tau'}{\partial x} + \bar{v}\frac{\partial \tau'}{\partial y} + \bar{w}\frac{\partial \tau'}{\partial z} + u'\frac{\partial \tau'}{\partial x} + v'\frac{\partial \tau'}{\partial y} + w'\frac{\partial \tau'}{\partial z} - \frac{\partial \overline{u'\tau'}}{\partial x} - \frac{\partial \overline{v'\tau'}}{\partial y} - \frac{\partial \overline{w'\tau'}}{\partial z} = 0.$$

Multiplying the mean tracer equation by $\bar{\tau}$ gives

$$\frac{1}{2}\frac{\partial \bar{\tau}^2}{\partial t} + \frac{1}{2}\bar{u}\frac{\partial \bar{\tau}^2}{\partial x} + \frac{1}{2}\bar{v}\frac{\partial \bar{\tau}^2}{\partial y} + \frac{1}{2}\bar{w}\frac{\partial \bar{\tau}^2}{\partial z} + \bar{\tau}\frac{\partial \overline{u'\tau'}}{\partial x} + \bar{\tau}\frac{\partial \overline{v'\tau'}}{\partial y} + \bar{\tau}\frac{\partial \overline{w'\tau'}}{\partial z} = 0.$$

Finally, multiplying the eddy tracer equation by τ' gives

$$\frac{1}{2}\frac{\partial \tau'^2}{\partial t} + u'\tau'\frac{\partial \bar{\tau}}{\partial x} + v'\tau'\frac{\partial \bar{\tau}}{\partial y} + w'\tau'\frac{\partial \bar{\tau}}{\partial z} + \frac{1}{2}\bar{u}\frac{\partial \tau'^2}{\partial x} + \frac{1}{2}\bar{v}\frac{\partial \tau'^2}{\partial y} + \frac{1}{2}\bar{w}\frac{\partial \tau'^2}{\partial z} + \frac{1}{2}\frac{\partial u'\tau'^2}{\partial x} + \frac{1}{2}\frac{\partial v'\tau'^2}{\partial y} + \frac{1}{2}\frac{\partial w'\tau'^2}{\partial z} - \tau'\frac{\partial \overline{u'\tau'}}{\partial x} - \tau'\frac{\partial \overline{v'\tau'}}{\partial y} - \tau'\frac{\partial \overline{w'\tau'}}{\partial z} = 0,$$

and we take the mean of this equation to obtain the tracer variance equation

$$\boxed{\frac{1}{2}\frac{\partial \overline{\tau'^2}}{\partial t} + \overline{u'\tau'}\frac{\partial \bar{\tau}}{\partial x} + \overline{v'\tau'}\frac{\partial \bar{\tau}}{\partial y} + \overline{w'\tau'}\frac{\partial \bar{\tau}}{\partial z} + \frac{1}{2}\bar{u}\frac{\partial \overline{\tau'^2}}{\partial x} + \frac{1}{2}\bar{v}\frac{\partial \overline{\tau'^2}}{\partial y} + \frac{1}{2}\bar{w}\frac{\partial \overline{\tau'^2}}{\partial z} + \frac{1}{2}\frac{\partial \overline{u'\tau'^2}}{\partial x} + \frac{1}{2}\frac{\partial \overline{v'\tau'^2}}{\partial y} + \frac{1}{2}\frac{\partial \overline{w'\tau'^2}}{\partial z} = 0.}$$

Similarly, we can return to the perturbation equation

$$\frac{\partial \tau'}{\partial t} + u'\frac{\partial \bar{\tau}}{\partial x} + v'\frac{\partial \bar{\tau}}{\partial y} + w'\frac{\partial \bar{\tau}}{\partial z} + \bar{u}\frac{\partial \tau'}{\partial x} + \bar{v}\frac{\partial \tau'}{\partial y} + \bar{w}\frac{\partial \tau'}{\partial z} + u'\frac{\partial \tau'}{\partial x} + v'\frac{\partial \tau'}{\partial y} + w'\frac{\partial \tau'}{\partial z} - \frac{\partial \overline{u'\tau'}}{\partial x} - \frac{\partial \overline{v'\tau'}}{\partial y} - \frac{\partial \overline{w'\tau'}}{\partial z} = 0$$

and multiply by some higher power of τ' to derive an equation for the higher moments of τ'. Consider multiplying by τ'^{n-1}, which gives us

$$\frac{1}{n}\frac{\partial \tau'^n}{\partial t} + u'\tau'^{n-1}\frac{\partial \bar{\tau}}{\partial x} + v'\tau'^{n-1}\frac{\partial \bar{\tau}}{\partial y} + w'\tau'^{n-1}\frac{\partial \bar{\tau}}{\partial z} + \frac{1}{n}\bar{u}\frac{\partial \tau'^n}{\partial x} + \frac{1}{n}\bar{v}\frac{\partial \tau'^n}{\partial y} + \frac{1}{n}\bar{w}\frac{\partial \tau'^n}{\partial z} + \frac{1}{n}\frac{\partial u'\tau'^n}{\partial x} + \frac{1}{n}\frac{\partial v'\tau'^n}{\partial y} + \frac{1}{n}\frac{\partial w'\tau'^n}{\partial z} - \tau'^{n-1}\frac{\partial \overline{u'\tau'}}{\partial x} - \tau'^{n-1}\frac{\partial \overline{v'\tau'}}{\partial y} - \tau'^{n-1}\frac{\partial \overline{w'\tau'}}{\partial z} = 0.$$

Multiplying by n, this equation is rewritten

$$\frac{\partial \tau'^n}{\partial t} + nu'\tau'^{n-1}\frac{\partial \bar{\tau}}{\partial x} + nv'\tau'^{n-1}\frac{\partial \bar{\tau}}{\partial y} + nw'\tau'^{n-1}\frac{\partial \bar{\tau}}{\partial z} + \bar{u}\frac{\partial \tau'^n}{\partial x} + \bar{v}\frac{\partial \tau'^n}{\partial y} + \bar{w}\frac{\partial \tau'^n}{\partial z} + \frac{\partial u'\tau'^n}{\partial x} + \frac{\partial v'\tau'^n}{\partial y} + \frac{\partial w'\tau'^n}{\partial z} - n\tau'^{n-1}\frac{\partial \overline{u'\tau'}}{\partial x} - n\tau'^{n-1}\frac{\partial \overline{v'\tau'}}{\partial y} - n\tau'^{n-1}\frac{\partial \overline{w'\tau'}}{\partial z} = 0.$$

We use the identity $\partial u'\tau'^n/\partial x = u'\partial\tau'^n/\partial x + \tau'^n\partial u'/\partial x$, along with the nondivergence of $\mathbf{u}'$, to rewrite this equation again as

$$\frac{\partial \tau'^n}{\partial t} + nu'\tau'^{n-1}\frac{\partial \bar{\tau}}{\partial x} + nv'\tau'^{n-1}\frac{\partial \bar{\tau}}{\partial y} + nw'\tau'^{n-1}\frac{\partial \bar{\tau}}{\partial z} + \bar{u}\frac{\partial \tau'^n}{\partial x} + \bar{v}\frac{\partial \tau'^n}{\partial y} + \bar{w}\frac{\partial \tau'^n}{\partial z} + u'\frac{\partial \tau'^n}{\partial x} + v'\frac{\partial \tau'^n}{\partial y} + w'\frac{\partial \tau'^n}{\partial z} - n\tau'^{n-1}\frac{\partial \overline{u'\tau'}}{\partial x} - n\tau'^{n-1}\frac{\partial \overline{v'\tau'}}{\partial y} - n\tau'^{n-1}\frac{\partial \overline{w'\tau'}}{\partial z} = 0.$$

Taking the mean of this equation, we have the equation for the nth tracer moment

$$\frac{\partial \overline{\tau'^n}}{\partial t} + n\overline{u'\tau'^{n-1}}\frac{\partial \bar{\tau}}{\partial x} + n\overline{v'\tau'^{n-1}}\frac{\partial \bar{\tau}}{\partial y} + n\overline{w'\tau'^{n-1}}\frac{\partial \bar{\tau}}{\partial z} + \bar{u}\frac{\partial \overline{\tau'^n}}{\partial x} + \bar{v}\frac{\partial \overline{\tau'^n}}{\partial y} + \bar{w}\frac{\partial \overline{\tau'^n}}{\partial z} + \overline{u'\frac{\partial \tau'^n}{\partial x}} + \overline{v'\frac{\partial \tau'^n}{\partial y}} + \overline{w'\frac{\partial \tau'^n}{\partial z}} - n\overline{\tau'^{n-1}}\frac{\partial \overline{u'\tau'}}{\partial x} - n\overline{\tau'^{n-1}}\frac{\partial \overline{v'\tau'}}{\partial y} - n\overline{\tau'^{n-1}}\frac{\partial \overline{w'\tau'}}{\partial z} = 0$$

This set of equations for the higher tracer moments forms the basis for a rotational flux closure proposed by Eden, Greatbatch and Olbers (2007), and is discussed further in Section 2.2.

B.1.5 The Tracer Flux Equations

We can write an evolution equation for the tracer fluxes $\overline{\mathbf{u}'\tau'}$ by first considering the "eddy" tracer equation

$$\frac{\partial \tau'}{\partial t} + u'\frac{\partial \bar{\tau}}{\partial x} + v'\frac{\partial \bar{\tau}}{\partial y} + w'\frac{\partial \bar{\tau}}{\partial z} + \bar{u}\frac{\partial \tau'}{\partial x} + \bar{v}\frac{\partial \tau'}{\partial y} + \bar{w}\frac{\partial \tau'}{\partial z} + u'\frac{\partial \tau'}{\partial x} + v'\frac{\partial \tau'}{\partial y} + w'\frac{\partial \tau'}{\partial z} - \frac{\partial \overline{u'\tau'}}{\partial x} - \frac{\partial \overline{v'\tau'}}{\partial y} - \frac{\partial \overline{w'\tau'}}{\partial z} = 0.$$

Without loss of generality, we will focus for now only on the zonal flux $\overline{u'\tau'}$, noting that our derivation can easily be extended to the $v-$ and $w-$ fluxes (later we will summarily write them all

in vector notation). Multiply the eddy tracer equation by u' to obtain

$$u'\frac{\partial\tau'}{\partial t} + u'^2\frac{\partial\bar{\tau}}{\partial x} + u'v'\frac{\partial\bar{\tau}}{\partial y} + u'w'\frac{\partial\bar{\tau}}{\partial z} + u'\bar{u}\frac{\partial\tau'}{\partial x} + u'\bar{v}\frac{\partial\tau'}{\partial y} + u'\bar{w}\frac{\partial\tau'}{\partial z} + u'^2\frac{\partial\tau'}{\partial x} + u'v'\frac{\partial\tau'}{\partial y} + u'w'\frac{\partial\tau'}{\partial z} - u'\frac{\partial\overline{u'\tau'}}{\partial x} - u'\frac{\partial\overline{v'\tau'}}{\partial y} - u'\frac{\partial\overline{w'\tau'}}{\partial z} = 0.$$

Noting that by the product rule

$$\frac{\partial(u'\tau')}{\partial\xi} = u'\frac{\partial\tau'}{\partial\xi} + \tau'\frac{\partial u'}{\partial\xi},$$

where we are writing ξ as a stand-in for any of the independent variables t, x, y, or z, we can consume the u' into the partial derivative operators and rewrite the above equation as

$$\frac{\partial u'\tau'}{\partial t} - \tau'\frac{\partial u'}{\partial t} + u'^2\frac{\partial\bar{\tau}}{\partial x} + u'v'\frac{\partial\bar{\tau}}{\partial y} + u'w'\frac{\partial\bar{\tau}}{\partial z} + \bar{u}\left(\frac{\partial u'\tau'}{\partial x} - \tau'\frac{\partial u'}{\partial x}\right) + \bar{v}\left(\frac{\partial u'\tau'}{\partial y} - \tau'\frac{\partial u'}{\partial y}\right) + \bar{w}\left(\frac{\partial u'\tau'}{\partial z} - \tau'\frac{\partial u'}{\partial z}\right) + u'^2\frac{\partial\tau'}{\partial x} + u'v'\frac{\partial\tau'}{\partial y} + u'w'\frac{\partial\tau'}{\partial z} - u'\frac{\partial\overline{u'\tau'}}{\partial x} - u'\frac{\partial\overline{v'\tau'}}{\partial y} - u'\frac{\partial\overline{w'\tau'}}{\partial z} = 0.$$

Taking the mean of this equation and grouping the time derivatives and advection operators into the material derivative D/Dt, the final tracer flux equation is

$$\frac{D\overline{u'\tau'}}{Dt} - \overline{\tau'\frac{Du'}{Dt}} + \overline{u'^2}\frac{\partial\bar{\tau}}{\partial x} + \overline{u'v'}\frac{\partial\bar{\tau}}{\partial y} + \overline{u'w'}\frac{\partial\bar{\tau}}{\partial z} + \overline{u'^2\frac{\partial\tau'}{\partial x}} + \overline{u'v'\frac{\partial\tau'}{\partial y}} + \overline{u'w'\frac{\partial\tau'}{\partial z}} = 0.$$

B.1.6 Vector Notation

In vector notation, the eddy/mean equations can be simplified to the following forms:

$$\frac{\partial \bar{\mathbf{u}}}{\partial t} + \bar{\mathbf{v}} \cdot \nabla \bar{\mathbf{u}} + \nabla \cdot \overline{\mathbf{v}'\mathbf{u}'} + \mathbf{f} \times \bar{\mathbf{u}} = -\nabla_z \bar{\phi}$$

$$\frac{\partial \mathbf{u}'}{\partial t} + \bar{\mathbf{v}} \cdot \nabla \mathbf{u}' + \mathbf{v}' \cdot \nabla \bar{\mathbf{u}} + \mathbf{v}' \cdot \nabla \mathbf{u}' - \mathbf{f} \times \mathbf{u}' - \nabla \cdot \overline{\mathbf{v}'\mathbf{u}'} = -\nabla_z \phi'$$

$$\frac{1}{2}\frac{\partial \bar{\mathbf{u}}^2}{\partial t} + \frac{1}{2}\bar{\mathbf{v}} \cdot \nabla \bar{\mathbf{u}}^2 + (\nabla \cdot \overline{\mathbf{v}'\mathbf{u}'})\bar{\mathbf{u}} + \mathbf{f} \times \bar{\mathbf{u}}^2 = -\bar{\mathbf{u}}\nabla_z \bar{\phi}$$

$$\frac{1}{2}\frac{\partial \overline{\mathbf{u}'^2}}{\partial t} + \bar{\mathbf{v}} \cdot \nabla \overline{\mathbf{u}'^2} + \overline{\mathbf{u}'\mathbf{v}'} \cdot \nabla \bar{\mathbf{u}} + \frac{1}{2}\nabla \cdot \overline{\mathbf{u}'^2\mathbf{v}'} - \mathbf{f} \times \mathbf{u}' = -\nabla_z \phi'$$

$$\frac{\partial \bar{\tau}}{\partial t} + \bar{\mathbf{u}} \cdot \nabla \bar{\tau} + \nabla \cdot \overline{\mathbf{u}'\tau'} = 0$$

$$\frac{\partial \tau'}{\partial t} + \mathbf{u}' \cdot \nabla \bar{\tau} + \bar{\mathbf{u}} \cdot \nabla \tau' + \mathbf{u}' \cdot \nabla \tau' - \nabla \cdot \overline{\mathbf{u}'\tau'} = 0$$

$$\frac{1}{2}\frac{\partial \bar{\tau}^2}{\partial t} + \frac{1}{2}\bar{\mathbf{u}} \cdot \nabla \bar{\tau}^2 + \bar{\tau}\nabla \cdot \overline{\mathbf{u}'\tau'} = 0$$

$$\frac{\partial \overline{\tau'^2}}{\partial t} + 2\overline{\mathbf{u}'\tau'} \cdot \nabla \bar{\tau} + \bar{\mathbf{u}} \cdot \nabla \overline{\tau'^2} + \nabla \cdot \overline{\mathbf{u}'\tau'^2} = 0$$

$$\frac{\partial \overline{\tau'^n}}{\partial t} + n\overline{\mathbf{u}\tau'^{n-1}} \cdot \nabla \bar{\tau} + \nabla \cdot \overline{\mathbf{u}\tau'^n} - n\overline{\tau'^{n-1}}\nabla \cdot \overline{\mathbf{u}'\tau'} = 0$$

$$\frac{D\overline{\mathbf{u}'\tau'}}{Dt} - \overline{\tau'\frac{D\mathbf{u}'}{Dt}} + \left(\mathbf{u}' \cdot \nabla \bar{\tau}\right)\mathbf{u}' + \overline{\left(\mathbf{u}' \cdot \nabla \tau'\right)\mathbf{u}'} = 0.$$

Appendix C

Appendix C

C.1 The Boussinesq Quasigeostrophic Equations

In this section we derive the quasigeostrophic potential vorticity equation beginning from the nondimensionalized Boussinesq primitive equations. The derivation herein closely follows that found in Chapter 5 of Vallis (2006).

Quasigeostrophy forms the foundation for the linear instability analysis performed in this research; specifically, a numerical solver based on layer-wise quasigeostrophy (Smith, 2007) is used to calculate growth rates and vertical structures of the linear baroclinic wave modes. The nondimensionalized form is useful because it makes clear the importance of the Lagrangian advection. Unlike planetary geostrophy, we do not scale this term out based on small Rossby number. Instead, we choose to keep it to make a first-order approximation to true geostrophy, which gives us the leverage to form the materially-conserved potential vorticity.

We begin with the non-dimensional primitive equations using the Boussinesq approximation:

$$\begin{aligned} Ro\frac{D\hat{\mathbf{u}}}{D\hat{t}} + \hat{\mathbf{f}} \times \hat{\mathbf{u}} &= -\nabla_z \hat{\phi} \\ \frac{\partial \hat{\phi}}{\partial \hat{z}} &= \hat{b} \\ \nabla_z \cdot \hat{\mathbf{u}} &= 0 \\ Ro\frac{D\hat{b}}{D\hat{t}} + \left(\frac{L_d}{L}\right)^2 \hat{w} &= 0. \end{aligned}$$

Expand the non-dimensional dependent variables in an asymptotic series in Rossby number, so

that

$$\hat{\mathbf{u}} = \hat{\mathbf{u}}_0 + Ro\ \hat{\mathbf{u}}_1 + ...$$

$$\hat{\phi} = \hat{\phi}_0 + Ro\ \hat{\phi}_1 + ...$$

$$\hat{b} = \hat{b}_0 + Ro\ \hat{b}_1 + ...$$

Taking $Ro \ll 1$, this implies that the lowest-order momentum equation is simply geostrophic balance

$$\hat{\mathbf{f}}_0 \times \hat{\mathbf{u}}_0 = -\nabla\hat{\phi}_0,$$

which in turn implies that the lowest-order horizontal velocity is nondivergent. Unfortunately, in this limit the relative vorticity is identically zero[1] , which is why we must go to higher order to get the potential vorticity. Then to first-order, the momentum and thermodynamic equations are

$$\frac{D_0\hat{\mathbf{u}}_0}{D\hat{t}} + \hat{\beta}\hat{y}\mathbf{k} \times \hat{\mathbf{u}}_0 + \hat{\mathbf{f}} \times \hat{\mathbf{u}}_1 = -\nabla\hat{\phi}_1$$

$$\frac{D_0\hat{b}_0}{D\hat{t}} + \hat{w}_1\left(\frac{L_d}{L}\right)^2 = 0,$$

where the operator $D_0/Dt = \partial/\partial\hat{t} + (\hat{\mathbf{u}}_0 \cdot \nabla)$.The first-order mass conservation equation is still the incompressibility condition.

We cross-differentiate the first-order momentum equation to get the vorticity equation

$$\frac{D_0\hat{\zeta}_0}{D\hat{t}} + (\hat{\mathbf{u}}_0 \cdot \nabla)\,\hat{\zeta}_0 + \hat{v}_0\beta = -f_0\nabla_z \cdot \hat{u}_1.$$

Use the incompressibility condition to obtain

$$\frac{D_0}{D\hat{t}}\left(\zeta_0 + \hat{f}\right) = \hat{f}_0\frac{\partial\hat{w}}{\partial z},$$

and combining this with the first-order thermodynamic equation gives

$$\frac{D_0}{D\hat{t}}\left(\zeta_0 + \hat{f}\right) = -\hat{f}_0\frac{\partial}{\partial\hat{z}}\left[\frac{D_0}{D\hat{t}}\left(F\hat{b}_0\right)\right],$$

[1] This can be seen by cross-differentiating the geostrophic momentum equations and subtracting them from each other.

where $F \equiv (L/L_d)^2$. Here we note that the right hand side is

$$\frac{\partial}{\partial \hat{z}}\left(\frac{D_0 \hat{b}_0}{D\hat{t}}\right) = \frac{D_0}{D\hat{t}}\left(\frac{\partial \hat{b}_0}{\partial \hat{z}}\right) + \frac{\partial \hat{\mathbf{u}}_0}{\partial \hat{z}} \cdot \nabla \hat{b}_0,$$

and that the second term here vanishes due to the thermal wind equation

$$\mathbf{k} \times \frac{\partial \hat{\mathbf{u}}_0}{\partial \hat{z}} = -\frac{1}{\hat{f}_0} \nabla \hat{b}_0.$$

Then the vorticity equation becomes, with the hydrostatic relation,

$$\frac{D_0}{D\hat{t}}\left[\hat{\zeta}_0 + \hat{f} + \hat{f}_0 \frac{\partial}{\partial \hat{z}}\left(F \frac{\partial \hat{\phi}_0}{\partial z}\right)\right] = 0.$$

Because the lowest order horizontal velocity is nondivergent, we can define a streamfunction $\hat{\psi}$ such that

$$\hat{u}_0 = -\frac{\partial \hat{\psi}}{\partial \hat{y}}, \qquad \hat{v}_0 = -\frac{\partial \hat{\psi}}{\partial \hat{x}},$$

where we have that $\phi_0 = \hat{f}_0 \psi$ and $\hat{\zeta}_0 = \nabla^2 \hat{\psi}$. The vorticity equation then becomes an equation of a single unknown

$$\frac{D_0}{D\hat{t}}\left[\nabla_h^2 \hat{\psi} + \hat{\beta}\hat{y} + \hat{f}_0^2 \frac{\partial}{\partial \hat{z}}\left(F \frac{\partial \hat{\psi}}{\partial z}\right)\right] = 0.$$

This is the nondimensional form of the quasigeostrophic (QG) potential vorticity equation, which reduces the full Navier-Stokes equations to a single nonlinear PDE in a single unknown. The equivalent dimensional form is

$$\boxed{\begin{gathered} \frac{Dq}{D\hat{t}} = 0 \\ q = \nabla_h^2 \psi + \beta y + \frac{f_0^2}{\tilde{\rho}} \frac{\partial}{\partial z}\left(\frac{\tilde{\rho}}{N^2} \frac{\partial \psi}{\partial z}\right) \end{gathered}}$$

It is important to note the in the derivation above the nondivergence of the geostrophic velocity forces the zeroth-order vertical velocity w to be zero[2] . However, in layer-wise quasigeostrophy this does not mean that the layers are not coupled - recall that we used the first-order velocity w_1 in our

[2] More specifically, it forces $\partial w_0/\partial z = 0$, but since it is assumed that $w = 0$ at the vertical boundaries, these are one and the same.

derivation. This essentially forced the vertical velocity to be slave to the zeroth-order buoyancy, so that vertical motion appears implicitly through the vortex stretching term (on the far right).

The Boussinesq approximation assumes that the mean stratification is horizontally constant and is much larger than any deviations away from it, so that

$$b = \bar{b}(z) + b'(x, y, z, t). \tag{C.1}$$

Then because the background stratification is unchanging in the horizontal, the QG streamfunction is affected only by the buoyancy **perturbations** through the relation $b' = f_0 \partial\psi/\partial z$. Quasigeostrophy thus is a natural framework in which to discuss large-scale fluid instability.

We perform our instability analysis by assuming that the QG approximation applies; that is, we are considering spatial scales larger than the deformation radius in a sufficiently stratified fluid. Specifically, we consider three cases: the classical Eady problem, a case with exponential stratification and shear, and a case with arbitrary (but smoothly varying) stratification and shear. For boundary conditions, we assume that the top and bottom of the domain are slippery, rigid, flat surfaces. Then here the vertical velocity is zero, so we can write the thermodynamic equation as

$$\frac{D_h b'}{Dt} = 0, \qquad b' = f_0 \frac{\partial \psi}{\partial z}.$$

This will act as our vertical boundary condition. Side boundary conditions require that $\psi = 0$ at x, $y = \pm L/2$.

With the QG equations in hand, we can now discuss the linear instability of the basic states used in the challenge suite.

C.2 Eady Linear Stability

The seminal work of Eady (1949) provided one of the first mathematical descriptions of baroclinic instability, and even today is perhaps the most elegant. A large part of its genius is the simplicity of the initial flow. Computationally, the Eady problem provides an excellent first test configuration for our tracer inversion method (Chapter 2).

Deriving the solution to the Eady problem begins with the Boussinesq quasigeostrophic potential vorticity equations

$$\frac{Dq}{Dt} = 0, \qquad 0 < z < H \tag{C.2}$$

$$q = \nabla^2\psi + \beta y + \frac{\partial}{\partial z}\left(F\frac{\partial \psi}{\partial z}\right), \tag{C.3}$$

where $F = f_0^2/N^2$, and the buoyancy equation

$$\frac{\partial b}{\partial t} + \mathbf{u}\cdot\nabla b = 0 \qquad\qquad z = 0, -H. \tag{C.4}$$

$$b = f_0\frac{\partial \psi}{\partial z}. \tag{C.5}$$

The simplest nontrivial solution for these equations is a purely zonal flow $\bar{\mathbf{u}} = U(y,z)\mathbf{i}$ with a corresponding density field in thermal wind balance. More generally, we could use any horizontally constant flow $\bar{\mathbf{u}} = U(y,z)\mathbf{i} + V(y,z)\mathbf{j}$ here, but we will restrict ourselves to a zonal flow to save time and space. For the Eady problem, we will assume a basic state streamfunction $\bar{\psi} = -\Lambda z y$, with $U = -\partial\bar{\psi}/\partial y$.. We will take the motion to be on the f-plane, so we let $\beta = 0$. Using the first baroclinic Rossby deformation radius, $L_d = NH/f_0$, the potential vorticity of this flow is then

$$Q = \nabla^2\bar{\psi} + \frac{\partial}{\partial z}\left(\frac{H^2}{L_d^2}\frac{\partial\bar{\psi}}{\partial z}\right) = 0. \tag{C.6}$$

We may now perform a Reynolds decomposition $\mathbf{u} = \bar{\mathbf{u}} + \mathbf{u}'$ on the streamfunction in C.3, treating the mean flow ("bar" variables) as the basic state. Because $Q = 0$, many of the "bar" terms in the expanded form of C.2 become zero, so the linearized potential vorticity equation for the interior becomes

$$\left(\frac{\partial}{\partial t} + \Lambda z\frac{\partial}{\partial x}\right)\left(\nabla^2\psi' + \frac{H^2}{L_d^2}\frac{\partial^2\psi'}{\partial z^2}\right) = 0. \tag{C.7}$$

In an x-periodic channel we seek solutions of the form

$$\psi'(x,y,z,t) = Re\ \tilde{\psi}(y,z)e^{ik(x-ct)}, \tag{C.8}$$

which gives

$$(\Lambda z - c)\left(\frac{\partial^2\tilde{\psi}}{\partial y^2} + \frac{H^2}{L_d^2}\frac{\partial^2\tilde{\psi}}{\partial z^2} - k^2\tilde{\psi}\right) = 0. \tag{C.9}$$

Sets of vertical and lateral boundary conditions must be satisfied. In our periodic channel, we impose $\psi = 0$ at the lateral boundaries $y = \pm L/2$ and seek solutions of the form

$$\psi'(x, y, z, t) = Re\ \Phi(z) \sin ly\ e^{ik(x-ct)}, \tag{C.10}$$

with $l = n\pi/L$ and n a positive integer. The vertical boundary conditions are given by the buoyancy equation (neglecting Ekman layers and bottom topography)

$$b'_t + J(\psi', b') + N^2 w = 0 \tag{C.11}$$

$$b' = f_0 \psi'_z. \tag{C.12}$$

We have that $w = 0$ at $z = 0$ and $z = H$, and thus the boundary condition reduces to

$$\left(\frac{\partial}{\partial t} + \Lambda z \frac{\partial}{\partial x}\right) \frac{\partial \psi'}{\partial z} - \Lambda \frac{\partial \psi'}{\partial x} = 0, \qquad z = 0, H \tag{C.13}$$

The interior potential vorticity equation is found by substituting C.10 into C.9, which gives

$$(\Lambda z - c)\left[\frac{H^2}{L_d^2}\frac{\partial^2 \Phi}{\partial z^2} - (k^2 + l^2)\Phi\right] = 0. \tag{C.14}$$

Substitute C.10 into C.13 to find the potential vorticity equations at the boundaries

$$c\frac{d\Phi}{dz} + \Lambda\Phi = 0, \qquad z = 0 \tag{C.15}$$

$$(c - \Lambda H)\frac{d\Phi}{dz} + \Lambda\Phi = 0, \qquad z = H. \tag{C.16}$$

If $\Lambda z \neq c$, then C.14 becomes

$$H^2 \frac{d^2\Phi}{dz^2} - \mu^2 \Phi = 0, \tag{C.17}$$

where $\mu^2 = L_d^2(k^2 + l^2)$. Solutions to this equation are of the form

$$\Phi(z) = A \cosh \mu\hat{z} + B \sinh \mu\hat{z}, \tag{C.18}$$

where $\hat{z} = z/H$. The boundary conditions are satisfied if

$$A[\Lambda H] + B[\mu c] = 0 \tag{C.19}$$

$$A[(c - \Lambda H)\mu \sinh \mu + \Lambda H \cosh \mu] + B[(c - \Lambda H)\mu \cosh \mu + \Lambda H \sinh \mu] = 0. \tag{C.20}$$

Non-trivial solutions to this system only exist if the determinant of the coupling matrix (formed by the terms in the square brackets) equals zero, which implies

$$c^2 - Uc + U^2(\mu^{-1}\coth\mu - \mu^{-2}) = 0, \tag{C.21}$$

where $U = \Lambda H$. The solution to this equation is

$$c = \frac{U}{2} \pm \frac{U}{\mu}\left[\left(\frac{\mu}{2} - \coth\frac{\mu}{2}\right)\left(\frac{\mu}{2} - \tanh\frac{\mu}{2}\right)\right]^{1/2}. \tag{C.22}$$

This implies that the waves will grow exponentially if c has an imaginary part. The growth rates are the imaginary part of c multiplied by the x-wavenumber, or

$$\sigma = kc_i = k\frac{U}{\mu}\left[\left(\frac{\mu}{2} - \coth\frac{\mu}{2}\right)\left(\frac{\mu}{2} - \tanh\frac{\mu}{2}\right)\right]^{1/2}. \tag{C.23}$$

Using the solution for c to solve for A and B in the boundary conditions gives us the vertical structure of the wave,

$$\Phi(\hat{z}) = \cosh\mu\hat{z} - \frac{Uc_r\sinh\mu\hat{z}}{\mu|c^2|} + \frac{iUc_i\sinh\mu\hat{z}}{\mu|c^2|}. \tag{C.24}$$

The vertical structure of ψ is that of the first baroclinic mode both in theory and in practice (Section 4.2.1). The fact that it has a closed analytical form allows us to evaluate the skill of the Ferrari et al. (2010) boundary value problem for diagnosing ψ during the course of our simulations.

C.3 Exponential Linear Stability

A second test case for our inversion method uses exponential stratification, where the density is tapered downward with an e-folding scale λ as in Chapter 4. This case is a reasonable approximation of true ocean stratification from the thermocline downward, and serves as an intermediate test between the highly idealized Eady (1949) problem and the "real ocean" profiles to be used in future work. It is also perhaps the most complex stratification we can work with analytically - more complicated vertical profiles must be dealt with by a numerical solver. This case differs from the classic Charney (1947) problem in that we take $\beta = 0$ for simplicity.

The derivations below are courtesy of Baylor Fox-Kemper; a β-plane version is presented in Pedlosky (1982). Again we begin with the Boussinesq quasigeostrophic potential vorticity equations

$$\frac{Dq}{Dt} = 0, \qquad 0 \ < \ z \ < \ H \tag{C.25}$$

$$q = \nabla^2\psi + \beta y + \frac{\partial}{\partial z}\left(F\frac{\partial \psi}{\partial z}\right), \tag{C.26}$$

where $F = f_0^2/N^2$, and the buoyancy equation

$$\frac{\partial b}{\partial t} + \mathbf{u}\cdot\nabla b = 0, \qquad z = 0, -H \tag{C.27}$$

$$b = f_0\frac{\partial \psi}{\partial z}. \tag{C.28}$$

As in the Eady case, the simplest nontrivial solution for these equations is a purely zonal flow $\mathbf{u} = U(y,z)\mathbf{i}$ with a corresponding density field in thermal wind balance. The potential vorticity of this flow is

$$Q = \beta y + \frac{\partial^2 \Psi}{\partial y^2} + \frac{\partial}{\partial z}\left(F\frac{\partial \Psi}{\partial z}\right), \tag{C.29}$$

with $U = -\partial\Psi/\partial y$. Assume motion on the f-plane and linearize C.25 about such a base state to get a potential vorticity equation for the interior

$$\frac{\partial q'}{\partial t} + U\frac{\partial q'}{\partial x} + \psi'_x\frac{\partial Q}{\partial y} = 0, \qquad -H \ < \ z \ < \ 0 \tag{C.30}$$

with $q' = \nabla^2\psi' + \frac{\partial}{\partial z}\left(F\frac{\partial \psi'}{\partial z}\right)$. Hereafter we drop the primes for ease of notation. The boundary conditions are given by the buoyancy equation (neglecting Ekman layers and bottom topography)

$$b_t + J(\psi, b) + N^2 w = 0 \tag{C.31}$$

$$b = \psi_z + \Psi_z, \tag{C.32}$$

or equivalently,

$$\psi_{zt} + J(\psi, \Psi_z) + J(\Psi, \psi_z) + N^2 w = 0 \tag{C.33}$$

We have that $w = 0$ at both the top and the bottom boundaries, thus the boundary condition C.27 reduces to

$$\left(\partial_t + U\partial_x\right)\psi_z - U_z\psi_x = 0 \tag{C.34}$$

The problem we consider is:

$$\frac{\rho}{\rho_0} = 1 - \alpha \left[T_0 + e^{z/\lambda} \left(\Delta T_v + \Delta T_h \frac{y - y_0}{L} \right) \right] \tag{C.35}$$

$$\Delta T_v \equiv \frac{T_L + T_R - 2T_0}{2} \tag{C.36}$$

$$\Delta T_h \equiv T_R - T_L, \tag{C.37}$$

where the constants are the temperature on the western boundary (T_L), temperature on the eastern boundary (T_R), bottom temperature (T_0), thermal expansion coefficient (α), center of channel (y_0), active channel width (L), and depth (H).

The background flow is geostrophic and the bottom velocity is considered to be zero (as it is set initially). The horizontal changes in temperature are small in comparison to the vertical, so the background density is independent of y (so drop the ΔT_h term above). Define new variables as follows:

$$S_0 \equiv \frac{g\alpha\Delta T_v}{\lambda f^2} \tag{C.38}$$

$$\Delta U \equiv \frac{g\lambda\alpha\Delta T_h}{fL} \tag{C.39}$$

$$U_0 \equiv \frac{g\lambda\alpha\Delta T_h}{fL} e^{-H/\lambda} \tag{C.40}$$

With the above variables, the parameters for the model are

$$\frac{\rho_s}{\rho_0} = 1 - \alpha[T_0 + \Delta T_v e^{z/\lambda}] \tag{C.41}$$

$$N^2 \equiv \frac{-g}{\rho_s}\rho_{s,z} = \frac{g\alpha\Delta T_v}{\lambda} e^{z/\lambda} \tag{C.42}$$

$$\frac{f^2}{N^2} = \frac{\lambda f^2}{g\alpha\Delta T_v} e^{-z/\lambda} = S_0^{-1} e^{-z/\lambda} \tag{C.43}$$

$$U_z = -\frac{g\rho_y}{f\rho_0} = \frac{g\alpha\Delta T_h}{fL} e^{z/\lambda} = \frac{\Delta U}{\lambda} e^{z/\lambda} \tag{C.44}$$

$$U = \frac{g\lambda\alpha\Delta T_h}{fL}(e^{z/\lambda} - e^{-H/\lambda}) = \Delta U e^{z/\lambda} - U_0 \tag{C.45}$$

$$Q = 0, \tag{C.46}$$

and the governing equations are:

$$\left[\partial_t + (\Delta U e^{z/\lambda} - U_0)\partial_x\right]\left(\nabla^2\psi + \frac{\partial_z e^{-z/\lambda}}{S_0}\partial_z\psi\right) = 0 \tag{C.47}$$

$$\psi_{zt} + (\Delta U - U_0)\psi_{xz} - \frac{\Delta U}{\lambda}\psi_x = 0, \qquad z = 0 \tag{C.48}$$

$$\psi_{zt} - \frac{\Delta U}{\lambda}e^{-H/\lambda}\psi_x = 0, \qquad z = -H \tag{C.49}$$

We assume the usual normal mode solution in x, and a discretized sine series in y:

$$\psi = \sum_{k,l}\phi(z)\sin(ly)e^{ik(x-ct)} \tag{C.50}$$

$$l = \frac{\pi}{L}\times\{0,1,2,3,\dots\} \tag{C.51}$$

Thus

$$(\Delta U e^{z/D} - U_0 - c)\left[\frac{\partial_z e^{-z/\lambda}\partial_z\phi}{S_0} - (k^2+l^2)\phi\right] = 0 \tag{C.52}$$

$$(\Delta U - U_0 - c)\phi_z - \frac{\Delta U}{\lambda}\phi = 0, \qquad z = 0 \tag{C.53}$$

$$c\phi_z + \frac{\Delta U}{\lambda}e^{-H/\lambda}\phi = 0, \qquad z = -H \tag{C.54}$$

Now perform the change of variables

$$\zeta \equiv e^{z/2\lambda} \tag{C.55}$$

$$\partial_z = \zeta_z\partial_\zeta = \frac{1}{2\lambda}\zeta\partial_\zeta \tag{C.56}$$

$$\zeta\varphi \equiv \phi \tag{C.57}$$

So now we have

$$(\Delta U\zeta^2 - U_0 - c)\left[\partial_\zeta(\zeta^{-1}(\partial_\zeta\zeta\varphi)) - (4\lambda^2 S_0)(k^2+l^2)\varphi\right] = 0. \tag{C.58}$$

With another change of variables $p = 2\lambda\sqrt{S_0(k^2+l^2)}$, and multiplying both sides by ζ^2 since ζ is never equal to 0, this becomes

$$(\Delta U\zeta^2 - U_0 - c)\left[\zeta^2\varphi_{\zeta\zeta} + \zeta\varphi_\zeta - (p^2\zeta^2+1)\varphi\right] = 0. \tag{C.59}$$

Finally, letting $\xi \equiv p\zeta$ we have

$$(\Delta U \xi^2 p^{-2} - U_0 - c)\left[\xi^2 \varphi_{\xi\xi} + \xi\varphi_\xi - (\xi^2+1)\varphi\right] = 0 \tag{C.60}$$

$$\partial_\xi \xi\varphi + \frac{2\Delta U}{U_0 + c - \Delta U}\varphi = 0, \qquad \xi = p \tag{C.61}$$

$$\partial_\xi \xi\varphi + \frac{2\Delta U}{c} e^{-H/\lambda}\varphi = 0, \qquad \xi = pe^{-H/2\lambda} \tag{C.62}$$

The solutions to this equation are the modified Bessel functions.

$$\varphi_1 = AI_1(\xi) + BK_1(\xi) \tag{C.63}$$

Using the property of the Bessel functions $\partial_\xi \xi I_1(\xi) = \xi I_0(\xi)$ the boundary conditions become

$$AI_0(p) + BK_0(p) + \frac{2\Delta U}{p(U_0 + c - \Delta U)}(AI_1(p) + BK_1(p)) = 0 \tag{C.64}$$

$$AI_0(pe^\zeta) + BK_0(pe^\zeta) + \frac{2\Delta U}{cp} e^\zeta (AI_1(pe^\zeta) + BK_1(pe^\zeta)) = 0, \tag{C.65}$$

where $\zeta = -H/2d$. Or, more clearly,

$$A\left(I_0(p) + \frac{2\Delta U}{p(U_0 + c - \Delta U)} I_1(p)\right) + B\left(K_0(p) + \frac{2\Delta U}{p(U_0 + c - \Delta U)} K_1(p)\right) = 0 \tag{C.66}$$

$$A\left(I_0(pe^\zeta) + \frac{2\Delta U}{cp} e^\zeta I_1(pe^\zeta)\right) + B\left(K_0(pe^\zeta) + \frac{2\Delta U}{cp} e^\zeta K_1(pe^\zeta)\right) = 0 \tag{C.67}$$

These boundary conditions have nontrivial solutions only if the determinant vanishes, which gives the dispersion relation:

$$\frac{(U_0 + c - \Delta U)pI_0(p) + 2\Delta U I_1(p)}{(U_0 + c - \Delta U)pK_0(p) + 2\Delta U K_1(p)} = \frac{cpI_0(pe^\zeta) + 2\Delta U e^\zeta I_1(pe^\zeta)}{cpK_0(pe^\zeta) + 2\Delta U e^\zeta K_1(pe^\zeta)} \tag{C.68}$$

This is a quadratic in c. There are growing modes when $b_1^2 < 4b_0$, and the imaginary part of c is

nonzero.

$$b_1 = U_0 - \Delta U + 2\Delta U(g(p,\zeta)\,[f(p,\zeta) + g(p,\zeta)] \tag{C.69}$$

$$b_0 = 2\Delta U\,[(U_0 - \Delta U)g(p,\zeta) + 2\Delta U h(p,\zeta)] \tag{C.70}$$

$$f(p,\zeta) = \frac{I_0(p)e^{\zeta}K_1(pe^{\zeta}) - K_0(p)e^{\zeta}I_1(pe^{\zeta})}{pI_0(p)K_0(pe^{\zeta}) - pK_0(p)I_0(pe^{\zeta})} \tag{C.71}$$

$$g(p,\zeta) = \frac{I_1(p)K_0(pe^{\zeta}) - K_1(p)I_0(pe^{\zeta})}{pI_0(p)K_0(pe^{\zeta}) - pK_0(p)I_0(pe^{\zeta})} \tag{C.72}$$

$$h(p,\zeta) = \frac{I_1(p)e^{\zeta}K_1(pe^{\zeta}) - K_1(p)e^{\zeta}I_1(pe^{\zeta})}{pI_0(p)K_0(pe^{\zeta}) - pK_0(p)I_0(pe^{\zeta})} \tag{C.73}$$

$$c_r = -b_1/2 \tag{C.74}$$

$$c_i = \pm\sqrt{b_0 - b_1^2/4} \tag{C.75}$$

where

$$p \equiv \frac{1}{f}\sqrt{2g\lambda\alpha(T_L + T_R - 2T_0)(k^2 + l^2)} \tag{C.76}$$

$$\zeta \equiv -H/2\lambda \tag{C.77}$$

$$l = \frac{\pi}{L}\{0, 1, 2, 3, ...\} \tag{C.78}$$

$$\Delta U \equiv \frac{g\lambda\alpha(T_R - T_L)}{fL} \tag{C.79}$$

$$U_0 \equiv \frac{g\lambda\alpha(T_R - T_L)}{fL}e^{2\lambda} \tag{C.80}$$

Then the final solutions are of the form:

$$\psi_{kn} = \Phi(z)\sin\left(\frac{\pi n y}{L}\right)e^{ik(x-ct)}, \tag{C.81}$$

with the vertical structure given by

$$\Phi(z) = \left[I_1\left(pe^{\frac{z}{2\lambda}}\right) - \frac{(U_0 + c - \Delta U)pI_0(p) + 2\Delta U I_1(p)}{(U_0 + c - \Delta U)pK_0(p) + 2\Delta U K_1(p)}K_1\left(pe^{\frac{z}{2\lambda}}\right)\right] \tag{C.82}$$

As with the linear Eady problem (Appendix C.2), the complex wave speed c_i can be used to inform our choice of grid resolution. Unlike in the Eady problem, the vertical structures found in the linear analysis are not applicable to the nonlinear problem - the inverse cascade will barotropize

the structure of ψ away from these modes. For this reason, sophisticated numerical schemes such as that of Ferrari et al. (2010) are called upon to parameterize $\psi(z)$ in OGCM's; evaluating the skill of such schemes is the primary purpose of the parameterization challenge suite (Chapter 4).

C.4 Linear Stability of an Arbitrary Profile

As can be deduced from Appendix C.3, even a stratification profile as simple as the exponential case can be extremely difficult to handle when conducting linear instability analysis. Therefore, it should not be surprising that we turn to numerical methods to work with more complicated cases than this, as are found in the real ocean. Below we discuss how to set up the quasigeostrophic eigenvalue problem in a layered model with an arbitrary stratification profile, from which a numerical eigenvalue solver can be constructed (Smith, 2007).

Begin with the Boussinesq quasigeostrophic potential vorticity equations

$$\frac{Dq}{Dt} = 0, \qquad 0 \ < \ z \ < \ H \tag{C.83}$$

$$q = \nabla^2\psi + \beta y + \frac{\partial}{\partial z}\left(F\frac{\partial \psi}{\partial z}\right), \tag{C.84}$$

where $F = f_0^2/N^2$.

A solution for these equations is a flow that is horizontally constant, $\bar{\mathbf{u}} = U(z)\hat{\mathbf{i}} + V(z)\hat{\mathbf{j}}$ with a corresponding density field in thermal wind balance. These assumptions can be taken as a proxy for a velocity field and stratification that are horizontally **local** and slowly varying, appropriate for the oceans at QG scales (Pedlosky, 1984). Performing a Reynolds decomposition $\psi = \mathbf{\Psi} + \psi'$, we define the mean streamfunction Ψ and eddy streamfunction ψ', whose relation to the buoyancy is given by

$$\bar{b} = f_0\frac{\partial \Psi}{\partial z} \tag{C.85}$$

$$b' = f_0\frac{\partial \psi'}{\partial z}, \tag{C.86}$$

and whose relation to the mean and eddy velocity fields is

$$\bar{u} = -\Psi_y \qquad \bar{v} = \Psi_x \tag{C.87}$$

$$u' = -\psi'_y \qquad v' = \psi'_x. \tag{C.88}$$

Linearizing C.83 about the mean state gives

$$q_t + \bar{\mathbf{u}} \cdot \nabla q + \mathbf{u}' \cdot \nabla Q = 0, \qquad -H < z < 0, \tag{C.89}$$

with boundary conditions

$$\psi'_{zt} + \bar{\mathbf{u}} \cdot \nabla \psi'_z + \mathbf{u}' \cdot \nabla \Psi_z = 0, \qquad z = -H, 0 \tag{C.90}$$

obtained by using the QG boundary conditions in the buoyancy b.

We will take the motion to be on the f-plane, so we let $\beta = 0$. The mean potential vorticity of this flow is then

$$Q = \frac{\partial}{\partial z}\left(\frac{f^2}{N^2}\frac{\partial \Psi}{\partial z}\right) = 0. \tag{C.91}$$

The horizontal gradient of Q is

$$\nabla Q = \frac{\partial}{\partial z}\left(\nabla\frac{f^2}{N^2}\frac{\partial \Psi}{\partial z} + \frac{f^2}{N^2}\frac{\partial \nabla\Psi}{\partial z}\right) \tag{C.92}$$

$$= \frac{\partial}{\partial z}\left(\frac{f^2}{N^2}\frac{\partial \nabla\Psi}{\partial z}\right). \tag{C.93}$$

Using the thermal wind identity

$$f\frac{\partial \bar{\mathbf{u}}}{\partial z} = \frac{g}{\rho_0}\nabla\bar{\rho} \tag{C.94}$$

and the Brunt-Vaisala frequency $N^2 = -\frac{g}{\rho_0}\frac{\partial \bar{\rho}}{\partial z}$, (C.93) becomes

$$\nabla Q = \frac{\partial}{\partial z}\left[f\frac{g\frac{\nabla\bar{\rho}}{\rho_0}}{-g\frac{\bar{\rho}_z}{\rho_0}}\right] \tag{C.95}$$

$$= \frac{\partial}{\partial z}\left(f\frac{-\nabla\bar{\rho}}{\bar{\rho}_z}\right), \tag{C.96}$$

so that ∇Q is proportional to the isopycnal slope vector $\nabla\bar{\rho}/\bar{\rho}_z$.

In earlier sections we assumed that the domain was periodic in x alone, which was convenient mathematically because it allowed us to shorten our analysis somewhat. This specification was arbitrary; it is just as reasonable to assume periodicity in both directions, which in this case is useful because we would like our numerical solver to handle perturbations in any horizontal direction. Then we assume that the domain is horizontally periodic in both x and y, so that we may substitute a plane-wave solution $\psi' = \Re\left(\hat{\psi}'(z)\exp\left[kx+ly-\omega t\right]\right)$ into (C.83) and (C.84) to obtain

$$(\mathbf{K}\cdot\bar{\mathbf{u}}-\omega)\left(\frac{f^2}{N^2}-|\mathbf{K}|^2\right)\hat{\psi}' = -\left(kQ_y - lQ_x\right)\hat{\psi}', \qquad -H<z<0 \tag{C.97}$$

$$(\mathbf{K}\cdot\bar{\mathbf{u}}-\omega)\,\hat{\psi}'_z = \left(k\bar{u}_z - l\bar{v}_z\right)\hat{\psi}' \qquad z=-H,0. \tag{C.98}$$

The discrete form of the vortex stretching operator $\Gamma_{nm} = f^2/N^2$ is

$$\Gamma_{nm}\psi'_m = \frac{f^2\rho_0}{g}\begin{cases} \frac{1}{\delta_1}\left(\frac{\psi'_2-\psi'_1}{\bar{\rho}_2-\bar{\rho}_1}\right) & n=1 \\ \frac{1}{\delta_n}\left(\frac{\psi'_{n-1}-\psi'_n}{\bar{\rho}_n-\bar{\rho}_{n-1}}-\frac{\psi'_n-\psi'_{n+1}}{\bar{\rho}_{n+1}-\bar{\rho}_n}\right) & n=2\ldots,N-1 \\ \frac{1}{\delta_N}\left(\frac{\psi'_{N-1}-\psi'_N}{\bar{\rho}_N-\bar{\rho}_{N-1}}\right) & n=N. \end{cases}, \tag{C.99}$$

where n is the density level, m is the eigenmode of the coupled system, and $\delta_n = (\Delta_{n-1}+\Delta_n)/2$ is the mean vertical distance between adjacent levels. A very similar discretization can be applied to form a discrete version of the horizontal potential vorticity gradient ∇Q_n. Then the discrete version of the generalized eigenvalue problem (C.97) and (C.98) becomes

$$M_{ij}\hat{\psi}'_j = \lambda_{ij}\hat{\psi}'_j \tag{C.100}$$

$$M_{ij} = \omega(\Gamma_{ij} - K^2\delta_{ij}) \tag{C.101}$$

$$\lambda_{ij} = (kQ^m_y - lQ^m_x)\delta_{ijm} + (kU^m + lV^m)\delta_{inm}M_{nj}, \tag{C.102}$$

where the Kronecker delta δ_{ijk} is

$$\delta_{ijk} = \begin{cases} 1 & i=j=k \\ 0 & \text{otherwise.} \end{cases} \tag{C.103}$$

For this research, a Python implementation of this eigenvalue problem is used to determine the vertical structure of each eigenmode $\hat{\psi'}_m$, which can then extrapolated to the vertical structure of ψ', b', v', etc. The Python QG instability calculator is also used to determine the growth rate of the fastest growing unstable mode, from which the horizontal grid spacing is determined.

Appendix D

Appendix D

D.1 Nondimensionalization

Research in geophysical fluid dynamics is aided greatly by the concept of dynamical similitude, wherein fluid flows of different spatial and temporal scales are geometrically, kinematically, and dynamically similar. This concept may seem strange at first - after all, how can we expect a flow on the planetary scale to be at all similar to one we can experiment with in a laboratory? The leverage we have in demonstrating this similarity is that both of these flows obey the same set of conservation equations[1] .

To see the similarity mathematically, we turn to a technique called **scaling**. This amounts to defining a set of characteristic scales (length, time, velocity, buoyancy, pressure, etc.) that we anticipate the flow to have[2] . We then write the dimensional variables in terms of their characteristic dimension multiplied by a nondimensional variable (so for example, $x = L\hat{x}$, where L is our chosen characteristic length). Substituting these terms into the conservation equations, we are left with equations written in terms of the nondimensional variables, with dimensional coefficients revealing the relative magnitudes of each term.

[1] The concept of flow similarity even extends to magnetized flows (Priest, 1982) as well. Conceivably, we could include every possible force, source, or sink in the conservation equations. The power of scaling and nondimensionalization is that any terms that do not significantly contribute to the equation balance will be clearly revealed. In effect, nondimensionalization is a means of filtering the equations to expose only the terms that truly matter to the force balance.

[2] For example, one might choose the characteristic length scale in a study of baroclinic instability to be the Rossby deformation radius. Intuitively, this choice makes sense, although it is understood that the turbulent scales of mesoscale baroclinic eddies will nearly always be larger than this. It is for this reason that we emphasize that we get to **choose** the characteristic scales, and there is no guarantee that our choice will be the best possible one, or even a physically correct one.

A simple example of this process is the rotating inviscid momentum equation

$$\frac{D\mathbf{u}}{Dt} + \mathbf{f} \times \mathbf{u} = -\nabla\phi. \tag{D.1}$$

Defining our scalings to be

$$\mathbf{x} = L\hat{\mathbf{x}} \tag{D.2}$$

$$\mathbf{u} = U\hat{\mathbf{u}} \tag{D.3}$$

$$\mathbf{f} = f\hat{\mathbf{f}} \tag{D.4}$$

$$t = \frac{L}{U}\hat{t} \tag{D.5}$$

$$\phi = U^2\hat{\phi}, \tag{D.6}$$

we may substitute each of them in to D.1 to obtain

$$\frac{U}{fL}\frac{D\hat{\mathbf{u}}}{D\hat{t}} + \hat{\mathbf{f}} \times \hat{\mathbf{u}} = -\nabla\hat{\phi}. \tag{D.7}$$

Here we may define the familiar Rossby number $Ro = U/fL$, which represents the relative strengths of the inertial force and Coriolis force. Based on the magnitude of Ro we can tell whether we may drop the inertial term D/Dt. In the process of nondimensionalizing (D.1) and grouping the dimensional terms together, we set all of the remaining terms to be of order unity; thus, if we impose $Ro \ll 1$, we are saying that the inertial term is much smaller than the others and may be dropped from the equation. Physically, this means that the Coriolis force dominates, and the resulting flow will be heavily constrained by the planetary rotation. Dropping the inertial term leaves us with

$$\mathbf{f} \times \mathbf{u} = -\nabla\phi, \tag{D.8}$$

the familiar equation for geostrophic balance.

Our research project on turbulent fluxes requires nondimensionalization for two reasons. The first is that both rotation and stratification affect the evolution of baroclinic turbulence, and as a result the turbulence may span an entire range of length scales. The second is that different

numerical models use different grid resolutions, and it would be naive to diagnose eddy diffusivities at one particular spatial scale and expect it to hold in every model and flow situation. Thus, nondimensionalization gives us a way out, in that we can explore turbulence in a wide variety of flow settings and unify the results through nondimensional parameters like the Rossby number.

D.1.1 Eady-like Stratification

We would like to use the same equations that our numerical model solves, so we begin with the Boussinesq momentum, mass, and buoyancy conservation equations. For the Eady problem, we nondimensionalize using the following scales:

$$\begin{aligned} x, y \sim L \qquad & \qquad z \sim H \\ \phi \sim \phi_0 = \max(UfL, U^2) \qquad & \qquad b \sim \frac{\phi_0}{H} \\ u, v \sim U \qquad & \qquad t \sim \frac{L}{U} \\ & w \sim \frac{\phi_0 U}{N^2 H L}. \end{aligned}$$

We seek to nondimensionalize the equations in terms of the parameters

$$Ro = \frac{U}{fL} \qquad Ri = \frac{N^2 f^2}{M^4} \qquad \lambda = \frac{\delta_N}{H}.$$

The Rossby number is as defined above. The Richardson number Ri expresses the importance of mechanical and density effects in the fluid, effectively acting as a stability parameter. At small Ri, the stratification is unimportant, and the flow may become unstable to shear instability. At high Ri, the opposite is true; the flow will be very stable to shear, but in a situation with tilted isopycnals there may be a tremendous amount of available potential energy to facilitate the growth of baroclinic instability. Finally, in the exponential stratification case the parameter λ tells us how quickly the stratification changes in relation to the fluid depth.

In the Eady problem the momentum equation nondimensionalizes as

$$\frac{\partial \mathbf{u}}{\partial t} + \mathbf{u}\cdot\nabla\mathbf{u} + w\frac{\partial \mathbf{u}}{\partial z} + \mathbf{f}\times\mathbf{u} = -\nabla\phi$$

$$\frac{U^2}{L}\frac{\partial \tilde{\mathbf{u}}}{\partial \tilde{t}} + \frac{U^2}{L}\tilde{\mathbf{u}}\cdot\tilde{\nabla}\tilde{\mathbf{u}} + \frac{U^2\phi_0}{H^2N^2L}\tilde{w}\frac{\partial \tilde{\mathbf{u}}}{\partial \tilde{z}} + fU\tilde{\mathbf{f}}\times\tilde{\mathbf{u}} = -\frac{\phi_0}{L}\tilde{\nabla}\tilde{\phi}$$

$$\frac{U}{fL}\frac{\partial \tilde{\mathbf{u}}}{\partial \tilde{t}} + \frac{U}{fL}\tilde{\mathbf{u}}\cdot\tilde{\nabla}\tilde{\mathbf{u}} + \frac{U}{fL}\frac{\max(UfL, U^2)}{H^2N^2}\tilde{w}\frac{\partial \tilde{\mathbf{u}}}{\partial \tilde{z}} + \tilde{\mathbf{f}}\times\tilde{\mathbf{u}} = -\max\left(1, \frac{U}{fL}\right)\tilde{\nabla}\tilde{\phi}$$

$$Ro\frac{\partial \tilde{\mathbf{u}}}{\partial \tilde{t}} + Ro\ \tilde{\mathbf{u}}\cdot\tilde{\nabla}\tilde{\mathbf{u}} + \frac{Ro}{Ri}\max\left(1, \frac{1}{Ro}\right)\tilde{w}\frac{\partial \tilde{\mathbf{u}}}{\partial \tilde{z}} + \tilde{\mathbf{f}}\times\tilde{\mathbf{u}} = -\max\left(1, Ro\right)\tilde{\nabla}\tilde{\phi}$$

$$\boxed{\frac{\partial \tilde{\mathbf{u}}}{\partial \tilde{t}} + \tilde{\mathbf{u}}\cdot\tilde{\nabla}\tilde{\mathbf{u}} + \frac{1}{Ri}\max\left(1, \frac{1}{Ro}\right)\tilde{w}\frac{\partial \tilde{\mathbf{u}}}{\partial \tilde{z}} + \frac{1}{Ro}\tilde{\mathbf{f}}\times\tilde{\mathbf{u}} = -\max\left(1, \frac{1}{Ro}\right)\tilde{\nabla}\tilde{\phi}.}$$

The buoyancy equation nondimensionalizes as

$$\frac{\partial b}{\partial t} + \mathbf{u}\cdot\nabla b + w\frac{\partial b}{\partial z} = 0$$

$$\frac{U\phi_0}{HL}\frac{\partial \tilde{b}}{\partial \tilde{t}} + \frac{U\phi_0}{HL}\tilde{\mathbf{u}}\cdot\tilde{\nabla}\tilde{b} + \frac{U\phi_0}{N^2HL}\frac{\phi_0}{H^2}\tilde{w}\frac{\partial \tilde{b}}{\partial \tilde{z}} = 0$$

$$\frac{\partial \tilde{b}}{\partial \tilde{t}} + \tilde{\mathbf{u}}\cdot\tilde{\nabla}\tilde{b} + \frac{\phi_0}{N^2H^2}\tilde{w}\frac{\partial \tilde{b}}{\partial \tilde{z}} = 0$$

$$\frac{\partial \tilde{b}}{\partial \tilde{t}} + \tilde{\mathbf{u}}\cdot\tilde{\nabla}\tilde{b} + \frac{\max\left(UfL, U^2\right)}{N^2H^2}\tilde{w}\frac{\partial \tilde{b}}{\partial \tilde{z}} = 0,$$

which simplifies to

$$\boxed{\frac{\partial \tilde{b}}{\partial \tilde{t}} + \tilde{\mathbf{u}}\cdot\tilde{\nabla}\tilde{b} + \frac{1}{Ri}\max\left(1, \frac{1}{Ro}\right)\tilde{w}\frac{\partial \tilde{b}}{\partial \tilde{z}} = 0.}$$

The mass conservation nondimensionalizes as

$$\mathbf{u}\cdot\nabla\mathbf{u}+\frac{\partial w}{\partial z}=0$$

$$\frac{U}{L}\tilde{\mathbf{u}}\cdot\tilde{\nabla}\tilde{\mathbf{u}}+\frac{\phi_0 U}{N^2H^2L}\frac{\partial\tilde{w}}{\partial\tilde{z}}=0$$

$$\tilde{\mathbf{u}}\cdot\tilde{\nabla}\tilde{\mathbf{u}}+\frac{\phi_0}{N^2H^2}\frac{\partial\tilde{w}}{\partial\tilde{z}}=0$$

$$\tilde{\mathbf{u}}\cdot\tilde{\nabla}\tilde{\mathbf{u}}+\max\left(\frac{UfL}{N^2H^2},\frac{U^2}{N^2H^2}\right)\frac{\partial\tilde{w}}{\partial\tilde{z}}=0$$

$$\boxed{\tilde{\mathbf{u}}\cdot\tilde{\nabla}\tilde{\mathbf{u}}+\frac{1}{Ri}\max\left(1,\frac{1}{Ro}\right)\frac{\partial\tilde{w}}{\partial\tilde{z}}=0.}$$

D.1.2 Exponential Stratification

We would like to consider two cases where the fluid is exponentially stratified with depth. Partition the density into the sum of a constant background state plus some variation that depends on depth, $\rho=\rho_0+\tilde{\rho}(z)$. Then we note that

$$\frac{\partial\rho}{\partial z}=\frac{\partial\tilde{\rho}}{\partial z}$$
$$-\frac{g}{\rho_0}\frac{\partial\rho}{\partial z}=-\frac{g}{\rho_0}\frac{\partial\tilde{\rho}}{\partial z}=\frac{\partial b}{\partial z}.$$

We define exponential stratification to mean that $\delta_N^{-1}=-\rho^{-1}\frac{\partial\rho}{\partial z}$, where δ_N is the density scale height. The corresponding buoyancy goes as $b=b_0e^{z/\delta_N}$, where $b_0=-g/\rho_0$. For the case with exponential shear and stratification (but no β-effect), retain the same scales but adopt the new buoyancy gradient scaling $\frac{\partial b}{\partial z}\sim\frac{\phi_0}{H\delta_N}$.

Because we have not changed any of the scalings used in the mass conservation equation, it nondimensionalizes identically to the Eady case. For exponential shear, we introduce the new shear scaling $\frac{\partial u}{\partial z} \sim \frac{U}{\delta_N}$. Then the momentum equation nondimensionalizes as

$$\frac{\partial \mathbf{u}}{\partial t} + \mathbf{u} \cdot \nabla \mathbf{u} + w \frac{\partial \mathbf{u}}{\partial z} + \mathbf{f} \times \mathbf{u} = -\nabla \phi$$

$$\frac{U^2}{L} \frac{\partial \tilde{\mathbf{u}}}{\partial \tilde{t}} + \frac{U^2}{L} \tilde{\mathbf{u}} \cdot \tilde{\nabla} \tilde{\mathbf{u}} + \frac{U^2 \phi_0}{H N^2 L \delta_N} \tilde{w} \frac{\partial \tilde{\mathbf{u}}}{\partial \tilde{z}} + f U \tilde{\mathbf{f}} \times \tilde{\mathbf{u}} = -\frac{\phi_0}{L} \tilde{\nabla} \tilde{\phi}$$

$$\frac{U}{fL} \frac{\partial \tilde{\mathbf{u}}}{\partial \tilde{t}} + \frac{U}{fL} \tilde{\mathbf{u}} \cdot \tilde{\nabla} \tilde{\mathbf{u}} + \frac{U}{fL} \frac{\max(UfL, U^2)}{H N^2 \delta_N} \tilde{w} \frac{\partial \tilde{\mathbf{u}}}{\partial \tilde{z}} + \tilde{\mathbf{f}} \times \tilde{\mathbf{u}} = -\max\left(1, \frac{U}{fL}\right) \tilde{\nabla} \tilde{\phi}$$

$$Ro \frac{\partial \tilde{\mathbf{u}}}{\partial \tilde{t}} + Ro\, \tilde{\mathbf{u}} \cdot \tilde{\nabla} \tilde{\mathbf{u}} + \frac{H}{\delta_N} \frac{Ro}{Ri} \max\left(1, \frac{1}{Ro}\right) \tilde{w} \frac{\partial \tilde{\mathbf{u}}}{\partial \tilde{z}} + \tilde{\mathbf{f}} \times \tilde{\mathbf{u}} = -\max\left(1, Ro\right) \tilde{\nabla} \tilde{\phi}$$

$$\boxed{\frac{\partial \tilde{\mathbf{u}}}{\partial \tilde{t}} + \tilde{\mathbf{u}} \cdot \tilde{\nabla} \tilde{\mathbf{u}} + \frac{\lambda}{Ri} \max\left(1, \frac{1}{Ro}\right) \tilde{w} \frac{\partial \tilde{\mathbf{u}}}{\partial \tilde{z}} + \frac{1}{Ro} \tilde{\mathbf{f}} \times \tilde{\mathbf{u}} = -\max\left(1, \frac{1}{Ro}\right) \tilde{\nabla} \tilde{\phi}.}$$

The buoyancy equation nondimensionalizes as

$$\frac{\partial b}{\partial t} + \mathbf{u} \cdot \nabla b + w \frac{\partial b}{\partial z} = 0$$

$$\frac{U\phi_0}{HL} \frac{\partial \tilde{b}}{\partial \tilde{t}} + \frac{U\phi_0}{HL} \tilde{\mathbf{u}} \cdot \tilde{\nabla} \tilde{b} + \frac{U\phi_0}{N^2 HL} \frac{\phi_0}{H\delta_N} \tilde{w} \frac{\partial \tilde{b}}{\partial \tilde{z}} = 0$$

$$\frac{\partial \tilde{b}}{\partial \tilde{t}} + \tilde{\mathbf{u}} \cdot \tilde{\nabla} \tilde{b} + \frac{\phi_0}{N^2 H \delta_N} \tilde{w} \frac{\partial \tilde{b}}{\partial \tilde{z}} = 0$$

$$\frac{\partial \tilde{b}}{\partial \tilde{t}} + \tilde{\mathbf{u}} \cdot \tilde{\nabla} \tilde{b} + \max\left(\frac{UfL}{N^2 H \delta_N}, \frac{U^2}{N^2 H \delta_N} \right) \tilde{w} \frac{\partial \tilde{b}}{\partial \tilde{z}} = 0$$

This can be reduced to

$$\boxed{\frac{\partial \tilde{b}}{\partial \tilde{t}} + \tilde{\mathbf{u}} \cdot \tilde{\nabla} \tilde{b} + \frac{\lambda}{Ri} \max\left(1, \frac{1}{Ro}\right) \tilde{w} \frac{\partial \tilde{b}}{\partial \tilde{z}} = 0.}$$

Using quasigeostrophic scaling, we naturally assume that the Rossby number is small enough for the flow to be in near-geostrophic balance. Therefore we can take $Ro < 1$, in which case the nondimensionalizations for each of the three cases is summarized as follows:

Eady

$$\frac{\partial \tilde{\mathbf{u}}}{\partial \tilde{t}} + \tilde{\mathbf{u}} \cdot \tilde{\nabla} \tilde{\mathbf{u}} + \frac{1}{Ro\, Ri} \tilde{w} \frac{\partial \tilde{\mathbf{u}}}{\partial \tilde{z}} + \frac{1}{Ro} \tilde{\mathbf{f}} \times \tilde{\mathbf{u}} = -\frac{1}{Ro} \tilde{\nabla} \tilde{\phi}$$

$$\frac{\partial \tilde{b}}{\partial \tilde{t}} + \tilde{\mathbf{u}} \cdot \tilde{\nabla} \tilde{b} + \frac{1}{Ro\, Ri} \tilde{w} \frac{\partial \tilde{b}}{\partial \tilde{z}} = 0$$

$$\tilde{\mathbf{u}} \cdot \tilde{\nabla} \tilde{\mathbf{u}} + \frac{1}{Ro\, Ri} \frac{\partial \tilde{w}}{\partial \tilde{z}} = 0$$

Exponentially-stratified

$$\frac{\partial \tilde{\mathbf{u}}}{\partial \tilde{t}} + \tilde{\mathbf{u}} \cdot \tilde{\nabla} \tilde{\mathbf{u}} + \frac{\lambda}{Ro\, Ri} \tilde{w} \frac{\partial \tilde{\mathbf{u}}}{\partial \tilde{z}} + \frac{1}{Ro} \tilde{\mathbf{f}} \times \tilde{\mathbf{u}} = -\frac{1}{Ro} \tilde{\nabla} \tilde{\phi}$$

$$\frac{\partial \tilde{b}}{\partial \tilde{t}} + \tilde{\mathbf{u}} \cdot \tilde{\nabla} \tilde{b} + \frac{\lambda}{Ro\, Ri} \tilde{w} \frac{\partial \tilde{b}}{\partial \tilde{z}} = 0$$

$$\tilde{\mathbf{u}} \cdot \tilde{\nabla} \tilde{\mathbf{u}} + \frac{1}{Ro\, Ri} \frac{\partial \tilde{w}}{\partial \tilde{z}} = 0$$

These respective forms of the nondimensionalization are revealing in a couple of ways. First, as the scaling ratio $\lambda = H/\delta_N$ approaches zero (which is the case as the stratification scaling δ_N goes to infinity), the exponential problem converges to a trivial form of the Eady problem. The buoyancy scaling we used for these cases implies that, in this limit, we converge toward a single-layer fluid of constant density (equivalent in the Boussinesq approximation to $N^2 = 0$). Our scaling assumptions for w then imply that the geostrophic velocity becomes horizontally non-divergent, and the system will essentially reduce to two-dimensional flow.

With the information above, we would anticipate that the strength of the turbulence would have to depend on some combination of the three parameters Ro, Ri, and λ (for the exponentially-stratified case only). These parameters allow us to compare model results regardless of the grid resolution, mean velocity, or stratification. Note that since the parameters are nondimensional there is no reason to believe that turbulence scalings would have to depend on **integer** powers - it is fully conceivable that decimal or fractional powers will appear in our scaling laws, so we must make sure to account for this possibility.